



POLITECNICO
MILANO 1863

SCHOOL OF CIVIL, ENVIRONMENTAL AND LAND MANAGEMENT ENGINEERING
Master's Degree in Civil Engineering – Track: Structures

**INTERACTION PROBLEMS IN
OUTRIGGERED STRUCTURAL SYSTEMS
SUBJECTED TO TORSION**

Advisor:

Prof. Ing. Franco Mola

Candidates:

Edoardo Copelli

Matr. 881265

Alfonso Tornisiello

Matr. 880837

ACADEMIC YEAR 2017/2018

INDEX

ABSTRACT	5
SOMMARIO	7
SOMMARIO ESTESO	9
1 AIMS AND RESEARCH SIGNIFICANCE	23
2 TALL BUILDINGS AND OUTRIGGER STRUCTURAL SYSTEMS	25
2.1 HISTORICAL NOTES	25
2.2 ITALIAN SCENARIO	27
2.3 TALL BUILDINGS STRUCTURAL SYSTEMS	31
2.4 CONCRETE FOR TALL BUILDINGS	35
2.5 OUTRIGGER STRUCTURAL SYSTEMS	36
2.5.1 <i>Deformation Reduction</i>	40
2.5.2 <i>Efficiency</i>	40
2.5.3 <i>Foundation Forces</i>	41
2.5.4 <i>Gravity Force Transfers</i>	41
2.5.5 <i>Torsional Stiffness</i>	41
2.5.6 <i>Disproportionate Collapse Resistance</i>	41
2.5.7 <i>Architectural Flexibility</i>	42
3 THIN-WALLED ELASTIC BEAMS	43
3.1 CALCULATION MODEL AND FUNDAMENTAL HYPOTHESES	44
3.1.1 <i>The Displacement Field</i>	46
3.1.2 <i>The Strain Field</i>	52
3.1.3 <i>Stress-Strain Relations</i>	52
3.1.4 <i>Equilibrium Equations in Principal Coordinates</i>	56
3.1.5 <i>Generalized Cross-Sectional Forces</i>	57
3.2 THE SOLUTION OF THE TORSION EQUATION	60
3.3 TORSION INDUCED BY A LONGITUDINAL FORCE TRANSMITTED THROUGH A RIGID ARM	63
3.4 BEAMS REINFORCED BY CLOSELY-SPACED STRIPS	67
3.4.1 <i>Diaphragms</i>	71
3.4.2 <i>Lintels</i>	74
4 STRUCTURAL ANALYSIS OF OUTRIGGER SYSTEMS	79
4.1 OUTRIGGER-THIN-WALLED CORE INTERACTION	79
4.1.1 <i>Green Function: Concentrated Axial Load P</i>	81
4.1.2 <i>Green Function: Concentrated Bending Moment M_x</i>	82
4.1.3 <i>Green Function: Concentrated Bending Moment M_y</i>	83
4.1.4 <i>Green Function: Concentrated Bimoment M_ω</i>	84
4.1.5 <i>Load Case 1: Uniform Load q_x or q_y</i>	87

4.1.6	<i>Load Case 2: Triangular Load with Maximum q_x or q_y at the Top</i>	90
4.1.7	<i>Load Case 3: Uniform Torque Load q_ω</i>	93
4.1.8	<i>Load Case 4: Triangular Torque Load with Maximum q_ω at the Top</i>	96
4.1.9	<i>Generalized Solution for Multiple Outrigger Structures</i>	100
5	CASE STUDY	103
5.1	CHARACTERIZATION OF THE STRUCTURE	103
5.2	CORE-OUTRIGGERS INTERACTION: BENDING BEHAVIOUR	110
5.2.1	<i>Structure with One Level of Outriggers</i>	110
5.2.2	<i>Structure with Two Levels of Outriggers</i>	112
5.2.3	<i>Results</i>	115
5.3	CORE-OUTRIGGERS INTERACTION: TORSIONAL BEHAVIOUR	117
5.3.1	<i>Structure with One Level of Outriggers</i>	117
5.3.2	<i>Structure with Two Levels of Outriggers</i>	119
5.3.3	<i>Results</i>	122
5.3.4	<i>Structural Behaviour in Presence of Diaphragms</i>	125
5.3.5	<i>Structural Behaviour in Presence of Lintels</i>	128
5.3.6	<i>Long-Term Behaviour</i>	135
5.4	BENDING – TORSION INTERACTION	147
5.5	NUMERICAL MODEL	155
5.5.1	<i>Midas GEN: Background</i>	155
5.5.2	<i>Numerical Model</i>	159
5.5.3	<i>Model I: Rigid Diaphragm Floors</i>	162
5.5.4	<i>Model II: Real Slabs</i>	164
5.5.5	<i>Model III: Core with Lintels</i>	167
5.5.6	<i>Bending – Torsion Interaction</i>	170
6	CONCLUSIONS AND FUTURE RESEARCH	175
	INDEX OF FIGURES	177
	INDEX OF TABLES	181
	BIBLIOGRAPHY	183

ABSTRACT

Outrigger systems are increasingly becoming a more common choice for tall buildings worldwide. The use of this kind of structural system to provide lateral stiffness and lateral load resistance to tall buildings has become more and more popular in the past decades because of its effectiveness and wide-ranging adaptability to evolving architectural needs. The use of outrigger systems is generally confined to the increase of lateral stiffness under bending actions for roughly height-wise regular structures; nevertheless, in modern architecture, they are also used in very complex new shapes, particularly buildings possessing a variation of the plan distribution of the vertical elements along the height of the building. These particular structural shapes, which generally include inclined peripheral columns, give way to torsional effects also under vertical loads. Another interesting fact regards the torsional properties of the central cores: in some cases, they can be idealized as thin-walled elements with open cross-sections. This fact introduces an additional deformation component, that is warping, in the compatibility equations between the core, the outriggers and the peripheral columns. In the present work, these problems will be discussed in detail and the analysis of outrigger systems in defining the structural response of tall buildings subjected to torsional effects will be addressed.

The Vlasov Theory will be recalled and generalized to account for the presence of a rigid arm connected to the core cross section, simulating the effect of outriggers on the structure. Both a theoretical and numerical approach will be applied to study different structural configurations characterized by the presence of one or two levels of outriggers and their interaction with transverse stiffeners, e.g. diaphragms and lintels.

In these conditions, the effects of the delayed deformation of concrete are of paramount importance for the design of the outriggers, thus the long-term behaviour of the structure will be analysed in special limit cases.

Finally, the interaction between flexural and torsional effects induced by an additional external eccentric volume will be investigated, as it represents an interesting case frequently present in modern tall buildings.

Keywords:

Outrigger systems, Tall Buildings, Torsional Effects, Deformation Component, Warping, Long-Term Behaviour, Creep, Bending-Torsion Interaction.

SOMMARIO

L'impiego dei sistemi outriggers sta diventando sempre più frequente nella realizzazione di edifici alti in tutto il mondo. Questo tipo di sistema strutturale fornisce infatti un'elevata rigidità e resistenza ai carichi laterali oltre che adattabilità a necessità architettoniche in continua evoluzione. Sebbene gli outriggers siano generalmente impiegati in strutture pressoché regolari in altezza, nell'ambito dell'architettura moderna sono di comune utilizzo anche in forme più complesse, caratterizzate da una variazione lungo l'altezza della distribuzione in pianta degli elementi verticali. Queste particolari forme strutturali danno origine ad effetti torsionali anche sotto la sola azione di carichi verticali. Un aspetto di grande importanza connesso a tali effetti riguarda le proprietà dei nuclei centrali: in alcuni casi essi possono infatti essere idealizzati come elementi in parete sottile a sezione aperta. A seguito di ciò, nelle equazioni di congruenza tra nucleo, outriggers e colonne perimetrali viene ad aggiungersi una componente addizionale di deformazione: l'ingobbamento.

Nel presente lavoro si analizza questo problema nel dettaglio focalizzando l'attenzione sulla risposta strutturale di sistemi nucleo-outriggers in edifici alti soggetti ad azioni torcenti.

A tal proposito la teoria di Vlasov verrà richiamata e generalizzata per considerare la presenza di appendici rigide connesse alla sezione trasversale del nucleo, atte a simulare gli effetti degli outriggers.

Mediante analisi teorica e numerica, si procederà ad analizzare una serie di configurazioni strutturali caratterizzate dalla presenza di uno o due livelli di outriggers e la loro interazione con altri elementi di irrigidimento, quali diaframmi e/o architravi.

Data l'importanza degli effetti differiti del calcestruzzo, sarà analizzato il comportamento a lungo termine della struttura in casi limite significativi.

Infine, si valuteranno gli effetti interattivi di flesso-torsionale indotti dalla presenza di volumi eccentrici, caso frequente nell'architettura moderna.

Parole chiave:

Outrigger, Edifici Alti, Effetti Torsionali, Deformabilità, Ingobbamento, Comportamento a lungo termine, Viscosità, Effetti Interattivi Flesso-Torsionali.

SOMMARIO ESTESO

La necessità di contenere gli spostamenti laterali agli stati limite d'esercizio congiunta con quella di garantire un adeguato livello di sicurezza agli stati limite ultimi, ha da sempre rappresentato il problema fondamentale del progetto di edifici alti. Di conseguenza, si è resa necessaria la definizione di sistemi strutturali con una morfologia ben delineata e tesa ad incrementare l'efficienza globale degli edifici. Ad oggi, la letteratura tecnica elenca un vasto numero di possibili soluzioni, tra cui i cosiddetti sistemi con outriggers, essenzialmente caratterizzati da uno o più nuclei disposti entro i limiti delle solette di piano, la stabilità dei quali, sotto l'applicazione di carichi laterali, è aumentata dalla presenza di elementi a mensola di notevole rigidezza, vincolati verticalmente dalle colonne perimetrali.

Sistemi di questo tipo sono largamente utilizzati nella loro configurazione piana come riduttori degli spostamenti laterali indotti da carichi flessionali. Poiché l'efficienza degli outriggers è influenzata sia dalla rigidezza assiale delle colonne che dalla loro rigidezza flessionale e quella del nucleo, sono stati condotti studi estesi ed esaustivi che permettono di avere a disposizione mezzi sufficienti per poter stabilire quale sia la posizione ottimale degli outriggers al fine di potenziare al massimo i loro effetti e, quindi, la risposta globale della struttura.

Nella pratica moderna, tuttavia, forme architettoniche di crescente complessità, spesso caratterizzate da variazioni marcate delle proprietà geometriche lungo l'altezza, stanno diventando sempre più frequenti, dando luogo a una risposta strutturale di non immediata analisi. Un caso particolare è quello di strutture che presentano irregolarità in elevazione, situazione che porta, generalmente, ad includere nel progetto la presenza di colonne perimetrali inclinate rispetto alla verticale. Ne consegue che la struttura può trovarsi soggetta ad effetti torsionali anche in presenza dei soli carichi verticali.

È bene osservare che l'effetto degli outriggers è tanto più pronunciato quanto più i loro spostamenti verticali, generati dalla deformazione flessionale del nucleo a cui sono connessi, sono elevati. In presenza di torsione, gli spostamenti verticali negli outriggers sono una conseguenza diretta dell'ingobbamento della sezione trasversale del nucleo. Dunque, è immediato constatare come la presenza di outriggers sia di maggiore rilevanza allorché il nucleo abbia una sezione trasversale aperta e di piccolo spessore, mentre, per contro, gli effetti benefici ad essi associati possono ritenersi trascurabili quando il nucleo presenta una sezione trasversale chiusa o, comunque, essenzialmente tale.

Un altro aspetto significativo concerne le deformazioni differite che sono indotte negli elementi in calcestruzzo da azioni con caratteristica di permanenza nel tempo. Per tenerne conto in maniera approssimata ma comunque soddisfacente, si può fare riferimento ad una formulazione algebrica in grado di descrivere la disomogeneità reologica tramite modelli viscoelastici in situazioni limite per le parti della struttura aventi età maggiore rispetto alle altre. In questo modo è possibile valutare l'evoluzione temporale degli stati di sforzo e deformazione negli elementi resistenti della struttura.

L'obiettivo della tesi consiste nello studio dettagliato del comportamento di strutture con uno o più livelli di outriggers, allorché siano soggetti, oltre che a sollecitazioni flessionali, anche ad effetti torsionali.

La tesi si sviluppa su 6 capitoli i cui argomenti sono sommariamente illustrati nel prosieguo.

Nel *Capitolo 1* vengono fissati gli obiettivi del presente lavoro.

Nel *Capitolo 2*, è mostrata, in breve, la storia degli edifici alti, che si estende dalle prime iconiche realizzazioni quali l'*Empire State Building* di New York fino alle più recenti quali l'attuale grattacielo più alto del mondo, il *Burj Khalifa* di Dubai. Specifico riguardo è dedicato allo sviluppo degli edifici alti in Italia, in particolare nelle città di Milano e Torino.

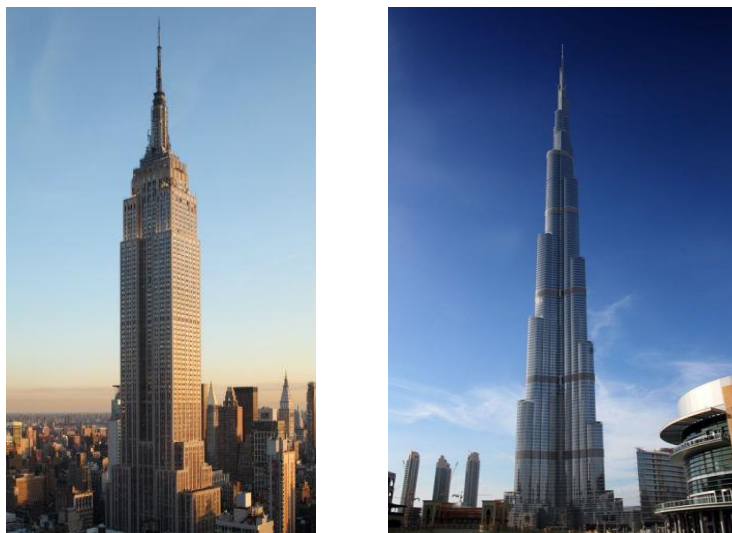


Figura S.1: *Empire State Building, NY (1931); Burj Khalifa, Dubai (2010)*

L'attenzione è stata anche focalizzata sull'evoluzione delle tipologie strutturali e dei materiali da costruzione, in particolare del calcestruzzo armato, divenuto elemento fondamentale nella realizzazione degli edifici alti, dato l'elevato rapporto prestazioni/prezzo dei moderni calcestruzzi, in grado di raggiungere resistenze caratteristiche superiori ai 90 MPa (si veda figura S.2).

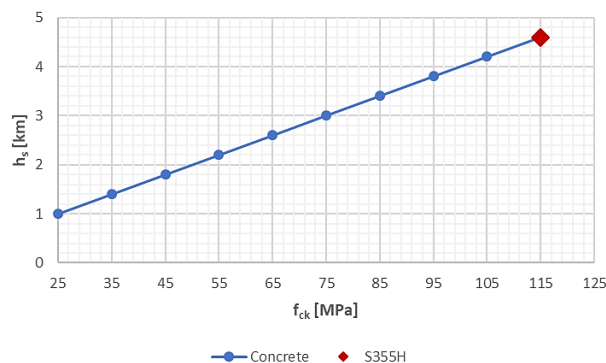


Figura S.2: Efficienza del calcestruzzo

Infine, si sono analizzati i sistemi outriggers. La loro presenza comporta notevoli vantaggi, ad esempio la riduzione degli spostamenti laterali del nucleo, la riduzione del momento ribaltante, la riduzione delle forze agenti sulla fondazione del nucleo, l'incremento della rigidità torsionale, la riduzione degli accorciamenti differenziali tra colonne, o tra colonne e nucleo, e la presenza di percorsi di carico alternativi in caso di collassi parziali.

Il principio di funzionamento a flessione dei sistemi outriggers è illustrato in Figura. S.3 e da essa si evince che una porzione del momento ribaltante agente sul nucleo viene trasferita agli outriggers, generando forze di trazione nelle colonne sopravvento e compressione in quelle sottovento.

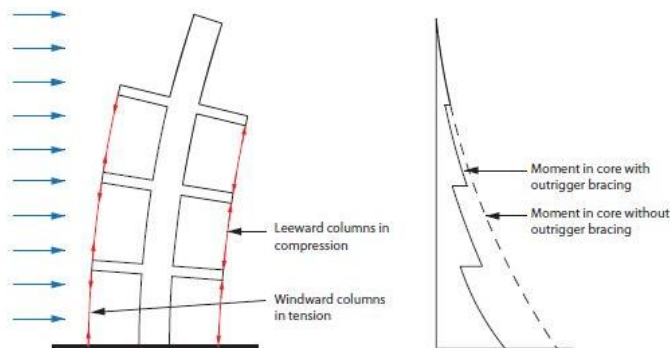


Figura S.3: Interazione nucleo-outriggers a flessione

Allo stesso modo, in strutture soggette a torsione, aventi nuclei in parete sottile e sezione aperta, i sistemi outriggers riducono la rotazione torsionale del nucleo inducendo forze di compressione e trazione nelle colonne conseguenti all'ingobbamento del nucleo.

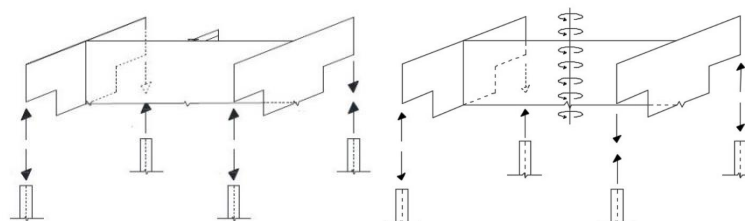


Figura S.4: Forze di interazione outriggers-colonne nel caso di flessione e di torsione

Nel *Capitolo 3* è richiamata la trattazione teorica del comportamento torsionale di elementi a parete sottile e sezione aperta secondo la teoria di Vlasov, generalizzata per tener conto degli spostamenti verticali presenti in appendici connesse alla sezione trasversale. Come noto, la teoria di Vlasov richiede che siano soddisfatte le seguenti disequaglianze:

$$\frac{\delta}{d} \leq 0.1; \quad \frac{d}{L} \leq 0.1$$

le quali sono riscontrabili negli impianti strutturali degli edifici alti.

Le equazioni di equilibrio di un elemento in parete sottile a sezione aperta soggetto a carichi trasversali flettenti (q_x, q_y) e torcenti (q_ω) con riferimento al sistema di coordinate principali della sezione, si scrivono:

$$\begin{aligned} EA w'' &= 0 \\ EI_{xx} u^{IV} &= q_x \\ EI_{yy} v^{IV} &= q_y \\ EI_{\omega\omega} \theta^{IV} - GI_d \theta'' &= q_\omega \end{aligned}$$

La soluzione della quarta equazione, governante il problema torsionale, dipende dal parametro k , avente formula:

$$k = L \sqrt{\frac{GI_d}{EI_{\omega\omega}}}$$

dove I_d è la rigidità torsionale per pura torsione, $I_{\omega\omega}$ è la rigidità torsionale di ingobbamento e L è la lunghezza della trave.

Bassi valori di k si hanno allorché la rigidità torsionale di ingobbamento prevalga su quella per torsione pura. Al contrario, per elevati valori di k la torsione primaria prevale su quella di ingobbamento, circostanza che può verificarsi sia quando la rigidità torsionale per pura torsione è maggiore di quella per ingobbamento sia quando si ha a che fare con lunghezze L elevate. Si osservi come L sia determinante nella definizione di k , la cui influenza sugli effetti torsionali è illustrata in Figura S.5 per elemento soggetto a carico torcente uniformemente distribuito sull'altezza.

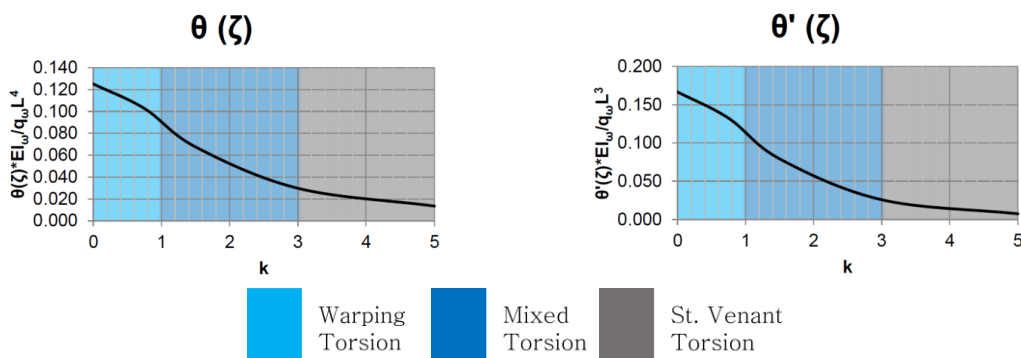


Figura S.5: Effetti torsionali al variare del parametro k per una mensola sottoposta a carico torcente uniforme

Sulla base delle precedenti considerazioni, l'effetto statico di più outriggers applicati alla medesima quota, può così esprimersi:

$$N = \sum_m P_i; \quad M_x = \sum_m P_i \cdot x_{oi}; \quad M_y = - \sum_m P_i \cdot y_{oi}; \quad M_\omega = \sum_m P_i \cdot \omega_{oi}$$

Si evince pertanto che le forze di interazione outriggers-colonne portano all'insorgenza nel nucleo, oltre che di uno sforzo assiale e due momenti flettenti, anche di un bimomento.

Poiché la modellazione del nucleo quale profilo in parete sottile a sezione aperta rappresenta una semplificazione, si è proceduto a studiare gli effetti dati da irrigidimenti trasversali quali diaframmi ed architravi. Per tenere conto di questi effetti, è sufficiente introdurre nell'equazione governante un valore variato di k , esprimibile come:

$$k_{var} = L \sqrt{\frac{G(I_d + \bar{I}_d)}{EI_{\omega\omega}}}$$

dove \bar{I}_d rappresenta il contributo aggiuntivo di rigidità per torsione pura dato dallo specifico irrigidimento trasversale.

Nel caso di diaframmi, chiamando Ω il doppio dell'area racchiusa dalla linea media della sezione trasversale del nucleo, h lo spessore del diaframma e b il passo dei diaframmi, la componente aggiuntiva di rigidità torsionale per pura torsione risulta:

$$\bar{I}_d = \frac{h^3 \Omega}{6b}$$

Nel caso di architravi, invece, definendo a , I_{br} ed A_{br} rispettivamente la lunghezza, il momento d'inerzia e l'area della sezione trasversale dell'architrave, la componente aggiuntiva di rigidità torsionale per pura torsione risulta essere:

$$\bar{I}_d = \frac{\Omega^2}{ab} \cdot \frac{1}{\left(\frac{\alpha^2 G}{12EI_{br}} + \frac{1.2}{A_{br}} \right)}$$

Si evince dunque che all'aumentare degli irrigidimenti trasversali, il parametro k aumenta, la torsione pura finisce per prevalere su quella non uniforme, riducendo le potenzialità torsionali degli outriggers.

Nel *Capitolo 4* il problema dell'interazione nucleo-outrigger è stato affrontato nella sua veste generale. Considerando un nucleo in parete sottile e sezione aperta di forma generica, soggetto ad una distribuzione qualunque di outriggers, il problema conduce alla risoluzione di un sistema di $(n \times m)$ equazioni di congruenza, dove n rappresenta il numero di livelli di outriggers mentre m è il numero di outriggers presenti a ciascun livello.

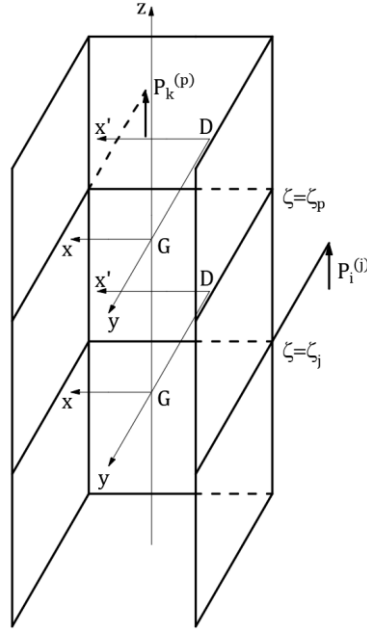


Figura S.6: Schema base per l'analisi strutturale

Le equazioni di congruenza si scrivono come segue:

$$\begin{aligned}
 & \sum_{i=1}^m \sum_{j=1}^n P_i^{(j)} \left[w_h(\zeta_p, \zeta_j) + x_i^{(j)} x_k^{(p)} u'_h(\zeta_p, \zeta_j) \right] + \\
 & - \sum_{i=1}^m \sum_{j=1}^n P_i^{(j)} \left[y_i^{(j)} y_k^{(p)} v'_h(\zeta_p, \zeta_j) + \omega_i^{(j)} \omega_k^{(p)} \theta'_h(\zeta_p, \zeta_j) \right] + \\
 & \quad + \frac{P_k^{(p)} \left(e_k^{(p)} \right)^3}{3EI_k^{(p)}} + \\
 & - u'_0(\zeta_p) x_k^{(p)} - v'_0(\zeta_p) y_k^{(p)} - \theta'_0(\zeta_p) \omega_k^{(p)} \\
 & = \\
 & - \left[\sum_{r=1}^p P_k^{(r)} \frac{L\zeta^{(r)}}{(EA)_k} + \sum_{r=p+1}^n P_k^{(r)} \frac{L\zeta^{(p)}}{(EA)_k} \right]
 \end{aligned}$$

con $h = 1$ for $j \leq p$, $h = 2$ for $j \geq p + 1$, ($k = 1, 2, \dots, m$), ($p = 1, 2, \dots, n$), $\zeta = \frac{z}{L}$

Nell'equazione riportata, $P_i^{(j)}$ rappresenta l'azione longitudinale applicata dalla i -esima colonna esterna all' i -esimo outrigger all'ascissa ζ_j e $P_k^{(p)}$ l'azione applicata dalla k -esima colonna esterna al k -esimo outrigger all'ascissa ζ_p . I termini $I_k^{(p)}$ ed $(EA)_k$ rappresentano rispettivamente il momento d'inerzia dell'outrigger a cui è applicata la forza $P_k^{(p)}$ e la rigidezza assiale della colonna associata. I termini $u_0(\zeta_p)$, $v_0(\zeta_p)$ e $\theta_0(\zeta_p)$ rappresentano gli

spostamenti prodotti dai carichi esterni, mentre i termini $u'_h(\zeta_p, \zeta_j)$, $v'_h(\zeta_p, \zeta_j)$ e $\theta'_h(\zeta_p, \zeta_j)$ rappresentano rispettivamente le *Funzioni di Green* di rotazione ed ingobbamento per un carico concentrato applicato a quota ζ_j .

Per i casi di carico flettente uniforme e triangolare, gli spostamenti dati dai carichi esterni sono stati ricavati risolvendo le rispettive linee elastiche con le opportune condizioni al contorno. Per i carichi torcenti, uniforme e triangolare, si è invece adottato il metodo dei parametri iniziali. Per quanto concerne gli effetti concentrati associati alla presenza di outriggers, si è fatto riferimento alle *Funzioni di Green*.

Risolvendo le $(n \times m)$ equazioni di compatibilità, è dunque possibile ricavare le $(n \times m)$ azioni assiali nelle colonne $P_K^{(p)}$ e, applicando il principio di sovrapposizione degli effetti, è stato possibile ottenere le azioni interne e gli spostamenti del nucleo.

Nel *Capitolo 5* si è applicata la trattazione sviluppata nei capitoli precedenti per studiare il comportamento di una struttura di 170 m di altezza, avente 40 piani con un'altezza di interpiano pari a 4.25 m . La particolarità della struttura è costituita da due volumi prismatici triangolari aventi base in sommità e disposti in maniera antisimmetrica rispetto agli assi x e y . A seguito dei carichi verticali ad essi applicati e dell'inclinazione delle colonne perimetrali che li sorreggono, la struttura si trova ad essere sollecitata da un carico torcente distribuito triangolarmente con valore massimo q_ω in sommità. Oltre ad esso, si è considerata un'azione laterale, anch'essa distribuita triangolarmente ed agente nella direzione positiva di y , atta a simulare gli effetti del vento sulla struttura.

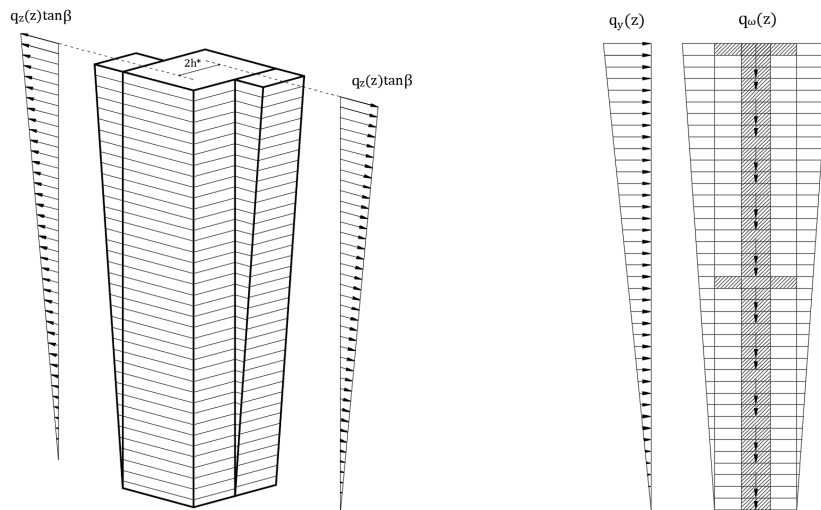


Figura S.7: Effetti torsionali indotti dai volumi sporgenti; Carico flessionale e torcente

Il nucleo presenta una sezione ad I di spessore $t = 0.45\text{ m}$. La struttura viene studiata considerando due livelli di 4 outriggers per livello, uno in sommità ed uno a mezza altezza, sorretti da megacolonne in calcestruzzo di forma circolare.

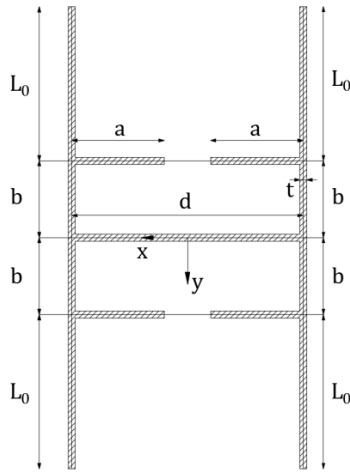


Figura S.8: Sezione trasversale sistema nucleo-outriggers.

Nucleo Centrale			
Ali:	$2b$	10	[m]
Anima:	d	15	[m]
Flange:	a	6	[m]
Spessore:	t	45	[cm]

Outriggers (Sezione Rettangolare)			
Base:	$t_0 = t$	45	[cm]
Altezza:	$h_0 = l$	425	[cm]
Campata:	$L_0 = 2b$	10	[m]
Numero per piano:	m	4	[-]
Diametro delle megacolonne:	D	160	[cm]
Posizione in elevazione:	Piani 19 – 20		[-]
	Piani 39 – 40		[-]

Dopo l'individuazione delle caratteristiche geometriche flessionali e torsionali del problema, vale a dire i momenti d'inerzia del nucleo, il diagramma delle aree settoriali nucleo-outriggers, la rigidità torsionale per pura torsione e quella per ingobbamento, si è proceduto a studiare, oltre alla struttura con solo nucleo, i due seguenti casi fondamentali:

- Struttura con un solo livello di outriggers, in sommità;
- Struttura con due livelli di outriggers, uno in sommità ed uno a mezza altezza.

Data la doppia simmetria del sistema nucleo-outriggers è stato possibile studiare il comportamento flessionale separatamente da quello torsionale, applicando al caso in esame la formula generale riportata nel *Capitolo 4*.

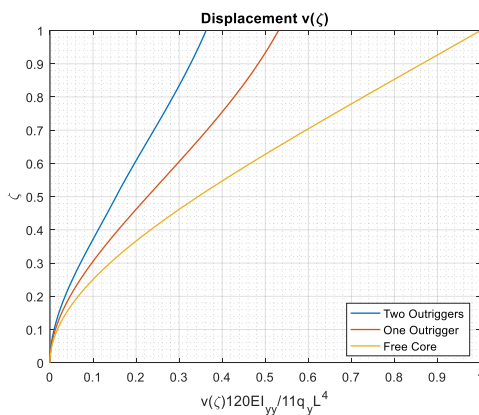


Figura S.9: Andamento sull'altezza dello spostamento laterale indotto dal carico flettente triangolare

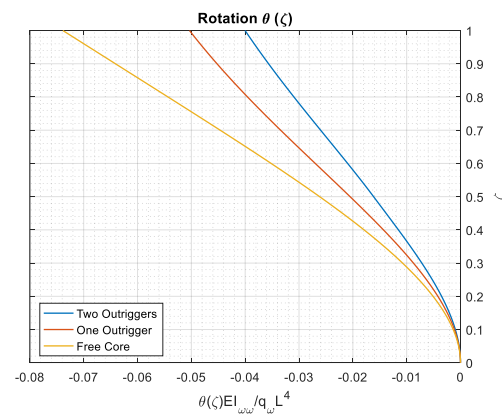


Figura S.10: Andamento sull'altezza della rotazione torsionale indotta dal carico torcente triangolare

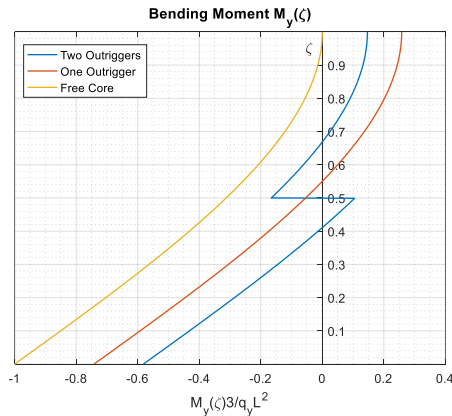


Figura S.11: Andamento sull'altezza del momento flettente indotto dal carico flettente triangolare.

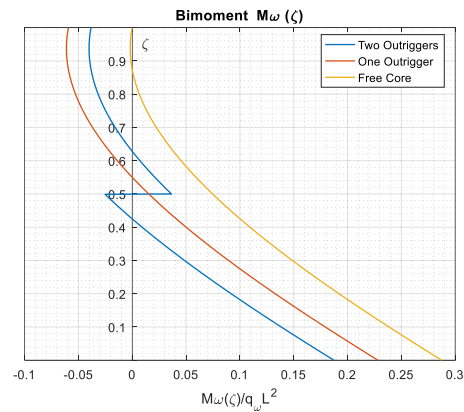


Figura S.12: Andamento sull'altezza del bimomento indotto dal carico torcente triangolare.

Come si evince da Figura S.9, gli outriggers sono di notevole efficacia nella riduzione degli effetti indotti dal carico flessionale, permettendo una riduzione dello spostamento laterale in sommità rispetto al caso di solo nucleo del 47% e del 64% a seconda che siano disposti outriggers solo in sommità od in sommità ed a mezza altezza. Analogamente, per quanto concerne le rotazioni torsionali, facendo riferimento a Figura. S. 10, la presenza di outriggers ne riduce l'importanza rispettivamente del 32% e del 51% a seconda che siano inseriti uno o due livelli di outriggers. Considerazioni analoghe possono essere fatte per momento flettente e bimomento, rotazione e ingobbamento.

Gli effetti riduttivi dell'efficienza degli outriggers indotti dalla presenza di diaframmi e/o architravi sono invece mostrati in Figura S.13, Figura S.14, Figura S.15 e Figura S.16.

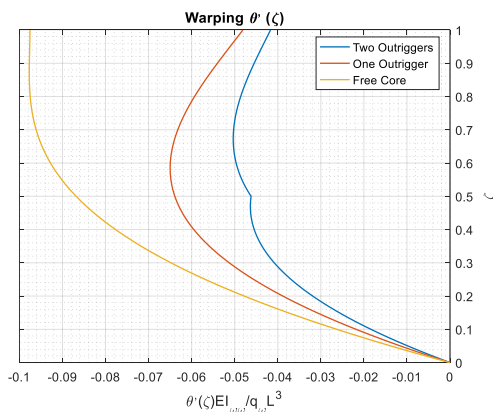


Figura S.13: Andamento sull'altezza dell'ingobbamento nel caso di nucleo con diaframmi, nucleo con diaframmi ed uno livello di outriggers, nucleo con diaframmi e due livelli di outriggers.

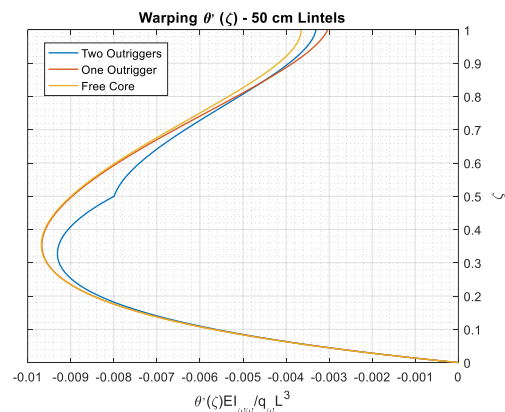


Figura S.14: Andamento sull'altezza dell'ingobbamento nel caso di nucleo con architravi di 50 cm, nucleo con architravi di 50 cm ed uno livello di outriggers, nucleo con architravi di 50 cm e due livelli di outriggers.

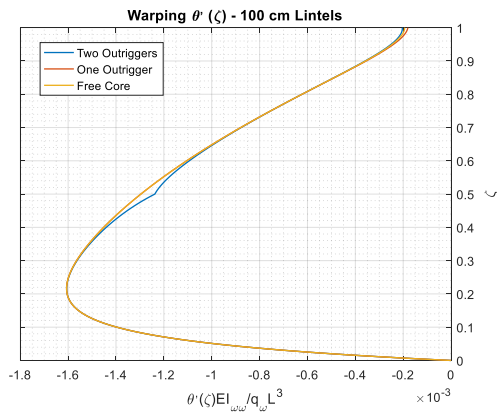


Figura S.15: Andamento sull'altezza dell'ingobbamento nel caso di nucleo con architravi di 100 cm, nucleo con architravi di 100 cm ed uno livello di outriggers, nucleo con architravi di 100 cm e due livelli di outriggers

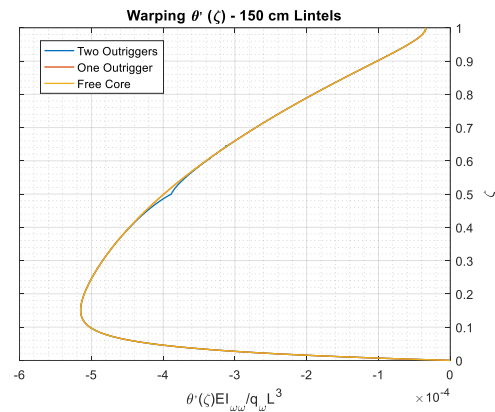


Figura S.16: Andamento sull'altezza dell'ingobbamento nel caso di nucleo con architravi di 150 cm, nucleo con architravi di 150 cm ed uno livello di outriggers, nucleo con architravi di 150 cm e due livelli di outriggers

Gli effetti a lungo termine, espressi mediante formulazione algebrica approssimata, conducono alle seguenti espressioni:

- Struttura Omogenea:

$$S(t) = S_e$$

$$s(t) = s_e \cdot [1 + \varphi(t, t_0)]$$

dove $S(t)$ rappresenta un'azione interna al tempo t mentre S_e il corrispondente valore elastico. Allo stesso modo $s(t)$ ed s_e sono gli spostamenti al tempo t ed il corrispettivo elastico.

- Struttura Non Omogenea:

$$S(t) = S_e^{(1)}(t) \cdot (1 - \mu) + \mu \cdot S_e$$

$$s(t) = s_e^{(1)}(t) \cdot (1 - \mu) + \mu \cdot s_e$$

dove $S_e^{(1)}$ ed $s_e^{(1)}$ sono le quantità elastiche valutate assumendo, per le parti viscoelastiche, un modulo elastico variato definito dalla seguente relazione:

$$E' = \frac{E}{1 + \chi\varphi}$$

essendo χ il coefficiente d'invecchiamento. Assumendo $\chi = 0.8$, il coefficiente di miscelazione μ è immediatamente definito come:

$$\mu = -\frac{1 - \chi}{\chi}$$

Considerando gli outriggers come elementi reologicamente disomogenei rispetto al resto della struttura, si sono considerati i due seguenti casi limite di analisi:

- Caso a): Nucleo-colonne viscoelastiche ed outriggers elastici
- Caso b): Nucleo-colonne elastiche ed outriggers viscoelastici.

In Figura S.17 e Figura S.18 si riportano, a titolo di esempio, i risultati in termini di rotazione torsionale in entrambi i casi a) e b).

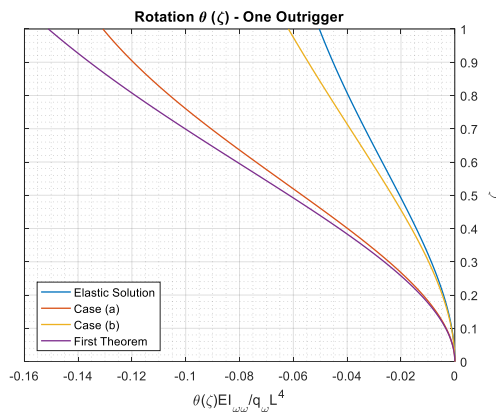


Figura S.17: Andamento sull'altezza della rotazione torsionale per nucleo con un solo livello di outriggers, in sommità, nei casi di struttura elastica, caso a), caso b) e struttura viscoelastica.

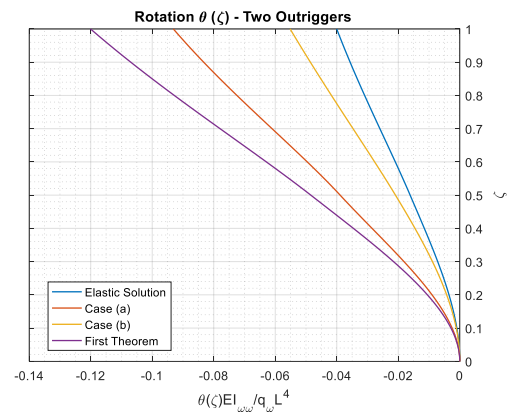


Figura S.18: Andamento sull'altezza della rotazione torsionale per nucleo con due livelli di outriggers, in sommità ed a mezza altezza, nei casi di struttura elastica, caso a), caso b) e struttura viscoelastica.

Per valutare gli effetti interattivi di flessione-torsione, si sono indagate diverse situazioni variando lungo un lato dell'edificio la posizione di un volume prismatico triangolare con base in sommità, come mostrato in Figura S.19.

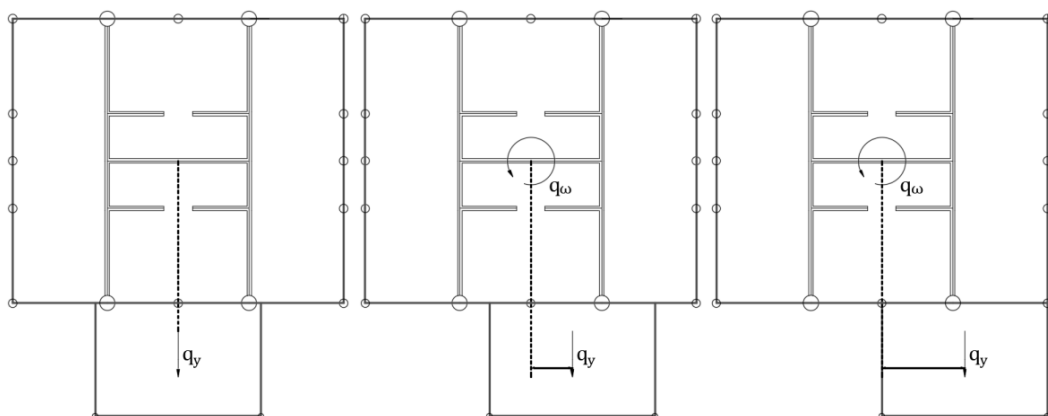


Figura S.19: Schema per lo studio dell'interazione flessione-torsione

Definendo $q_y(z)$ il carico flessionale indotto dal volume sulla struttura e $q_\omega(z) = e \cdot q_y(z)$ l'effetto torcente correlato, la trattazione viene a dipendere linearmente dall'eccentricità e

tra il baricentro del volume e il baricentro del nucleo. Risolvendo le equazioni di congruenza, è possibile ricavare le forze di interazione outriggers-colonne e, tramite le *Funzioni di Green* per forza assiale, gli spostamenti verticali nelle colonne:

Spostamento per flessione

$$w_1(\zeta, \bar{\zeta}) = P_{1y} \frac{L}{EA} \cdot \zeta$$

$$w_2(\zeta, \bar{\zeta}) = P_{1y} \frac{L}{EA} \cdot \bar{\zeta}$$

Spostamento per torsione

$$w_1(\zeta, \bar{\zeta}) = P_{1\omega} \frac{L}{EA} \cdot \zeta \quad 0 \leq \zeta \leq \bar{\zeta}$$

$$w_2(\zeta, \bar{\zeta}) = P_{1\omega} \frac{L}{EA} \cdot \bar{\zeta} \quad \bar{\zeta} \leq \zeta \leq 1$$

La trattazione è stata svolta per un solo livello di outriggers, in sommità.

In figura S.20 sono riportati, in forma adimensionale, gli andamenti degli spostamenti in sommità delle megacolonne al variare di e .

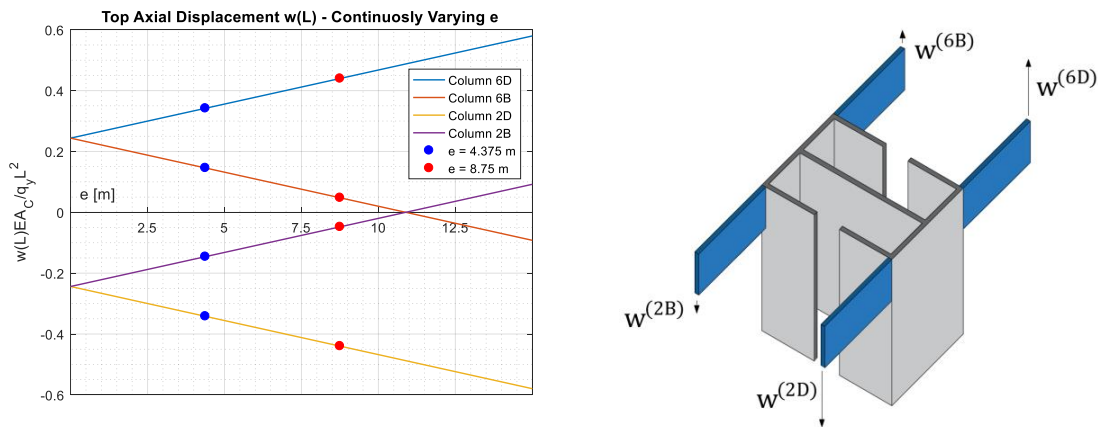


Figura S.20: Variazione dello spostamento in sommità delle megacolonne al variare di e ; Spostamenti ad $e=8.75$ m

L'analisi strutturale è stata svolta attraverso modellazione numerica mediante il software MidasGen onde verificare la concordanza fra i risultati numerici e quelli teorici. Usando piastre sottili per il nucleo, gli outriggers e le solette di piano, ed elementi tipo trave di Eulero-Bernoulli per le colonne, si è analizzata la risposta strutturale implementando tutti i casi teorici sopra riportati. Per verificare il comportamento del solo nucleo con uno o due livelli di outriggers, si è imposta l'indeformabilità nel proprio piano della sua sezione trasversale, alla base della teoria di Vlasov, tramite l'imposizione di *rigid diaphragms* ogni 4.25 m di altezza. Confrontando i risultati di Figura S.21 e Figura S.22 si riscontra una pressoché totale sovrapposibilità, mentre confrontando Figura S.23 e Figura S.24, relative rispettivamente al caso di risposta teorica con diaframmi di irrigidimento e risposta numerica con solette di piano deformabili, in quest'ultima si osserva una rotazione torsionale marcatamente minore rispetto a quanto predetto. Ne consegue una ridotta efficienza degli outriggers, i quali, nel caso di uno e due livelli, permettono di ridurre solamente del 6% e del 13% la rotazione rispetto al caso di solo nucleo (Figura S.24).

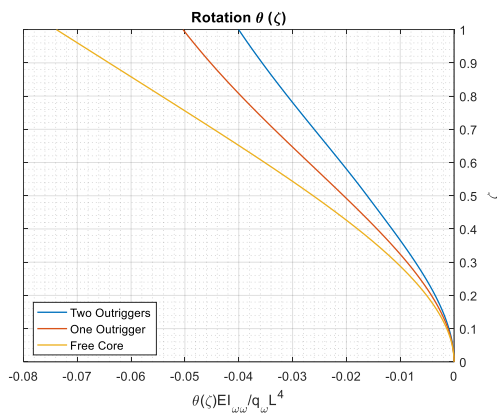


Figura S.21: Andamento sull'altezza della rotazione torsionale per nucleo alla Vlasov - Soluzione teorica

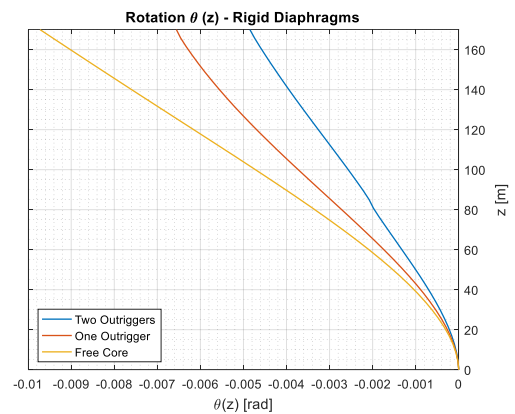


Figura S.22: Andamento sull'altezza della rotazione torsionale per nucleo alla Vlasov - Soluzione numerica

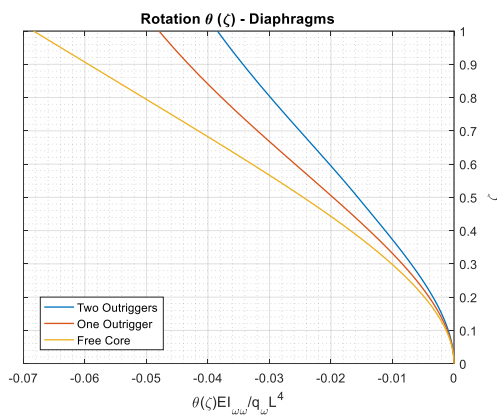


Figura S.23: Andamento sull'altezza della rotazione torsionale per nucleo con diaframmi - Soluzione teorica

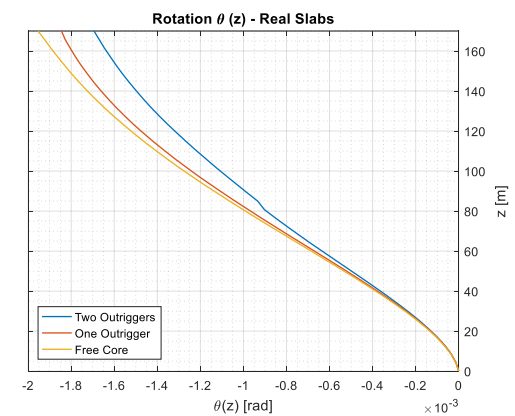


Figura S.24: Andamento sull'altezza della rotazione torsionale per nucleo con diaframmi - Soluzione numerica

Nel capitolo 6 sono riportate le considerazioni finali relative ai risultati ottenuti ed illustrate in breve possibili ricerche future.

1 AIMS AND RESEARCH SIGNIFICANCE

Outrigger systems are a convenient solution to ensure an adequate transverse stiffness of shear-resistant elements in tall buildings. The use of such systems, in spatial configurations, has been extensively studied in literature, by analysing the static interaction between outriggers, peripheral columns and cores subjected to displacement states deriving from biaxial bending. In complex architectural configurations, the rotational effects deriving from the warping generated by the application of torsional moments to the core, increases the vertical displacements of the outriggers which, in addition to their primary function of limiting flexural displacements, also act as torsional rotation reducers. This prerequisite is even more pronounced when the core warping deformations are higher, as occurs in case of cores having a thin-walled open section.

The aim of the present work is to analyse the outrigger systems in defining the structural response of tall buildings subjected to torsional effects.

After a brief discussion on tall buildings development, in which special care will be given to the evolution of structural systems and the importance of concrete as a suitable construction material to build high, the analysis will be focused on outrigger structural systems. Their behaviour in reducing flexural and torsional deformations and the benefits they provide to the whole building will be addressed.

Because of the relevance of the torsional problem in thin-walled open sections, the Vlasov Theory will be applied for both the cases of simple thin-walled elastic beams and thin-walled elastic beams transversally reinforced. After that, the solution for the structural problem of outrigger-core interaction will be treated in the form of a system of compatibility equations matching the vertical displacements of the outriggers with those of the supporting megacolumns.

Given the background to the problem, we will have all the tools to analyse how outrigger systems work in a real structure, by applying both a theoretical and numerical approach. In doing so, we will set the goal in understanding whether outriggers systems work effectively in reducing torsional rotations and how they are going to behave in different structural configurations, accounting for the presence of floor slabs and reinforcing systems like lintels. In addition, the long-term behaviour of the structure will also be analysed in special limit cases, in order to detect the role of outriggers in counteracting delayed deformations.

Finally, the interaction between flexural and torsional effects induced by an additional external eccentric volume will be investigate, as it represents an interesting case frequently present in modern tall buildings.

2 TALL BUILDINGS AND OUTRIGGER STRUCTURAL SYSTEMS

2.1 HISTORICAL NOTES

Starting from the beginning of the XX century high-rise buildings became part of the construction's history and their presence, initially confined into the urban fabric of United States, increased gradually into cities around the world. There are different reasons behind the development of tall buildings, started from a height of almost 50 m until the today 800 m, with an average annual increase of 6.8 m/year. However, building's height didn't develop gradually in time but there are significant accelerations during history, due to different factors, particularly the progress in structural and material engineering, and also construction technologies.

From the urbanistic and architectural point of view, tall buildings developed in time because of the need for more available volumes with limited buildable surfaces as well as the necessity to have a characterising element in the city landscape. Referring to this, the Eiffel Tower case is significant: built as interim structure for the 1889 Paris Expo, was hardly wanted by citizens as permanent building, becoming the first city landmark. In the same way, the Chrysler Building and the Empire State Building, both built between the end of '20s and the beginning of '30s, became unmistakable landmark in New York urban fabric.



Figure 2.1: *Tour Eiffel, Paris (1889); Chrysler Building, NY (1930); Empire State Building, NY (1931)*

The first reinforced concrete tall building is the Ingalls Building, built in Cincinnati, Ohio, between 1902 and 1903 by Elzner and Anderson. At that time the reinforced concrete technology takes the first steps, therefore the construction of 16 floors structure, with 67m height, was seen as a hazard by the public opinion. However, the building was a success and it is still successfully working. Despite the Elzner and Anderson success, the rapid increase in tall buildings height was possible thanks to the structural steel only, because that time concrete strength and technology was not enough to reach those heights. This happened during the so called First New York Era, from which the Woolworth Building is the major representation, with its 241.4 m height.



Figure 2.2: *Ingalls Building, Cincinnati (1903); Woolworth Building, NY (1913)*

Similarly, until the end of '30s, during the so called Second New York Era, the concrete technology wasn't still developed sufficiently, so structural steel was fundamental to realize construction as the Chrysler Building, the Empire State Building and the Ge Building in Rockefeller Centre. During this period the maximum height was fixed at 381 m, record for tall buildings fixed for almost 43 years, until 1973.

The usage of concrete as structural material in high-rise buildings began almost at the end of '50s, when the technology and transport technique of this material allowed to realize sufficiently strength cross sections, with reduced dimensions. In the following 50 years, reinforced concrete was widely used, also for really high construction, for example the Petronas Twin Towers, which was the highest building at the realization time, with a 451,9 m height. Finally, also the current highest tall building, the Burj Khalifa, with its 829,8 m height, has a main concrete bearing structure.

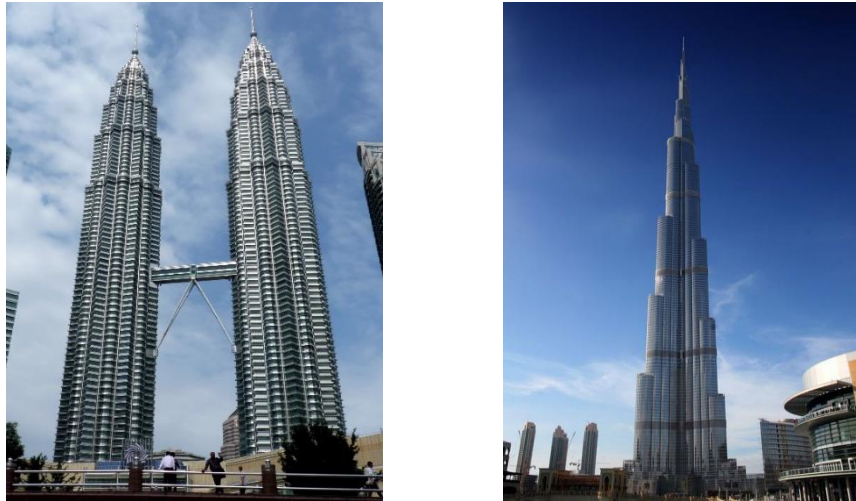


Figure 2.3: *Petronas Twin Towers, Kuala Lumpur (1996); Burj Khalifa, Dubai (2010)*

These brief historical notes have allowed to highlight the long path of concrete, which had led this material from the high mistruth of the Ingalls Building to the today high quality and reliability, becoming the main construction material of high-rise buildings structure.

2.2 ITALIAN SCENARIO

In Italy there are not buildings with height as the others mentioned in the previous sub-chapter, however there are a lot of structures higher than 100 m. From a chronological point of view, the first of them is Piacentini Tower, built in Genova during 1940, designed by the architect Marcello Piacentini and the engineer Angelo Invernizzi. This tower, realized in reinforced concrete, was also the tallest of Europe at that time, until 1958, when Velasca Tower was realized. With its 106 m height, it is characterized by the distinctive increase of plane surface at the 18th floor, thanks to inclined columns realized outside the building.

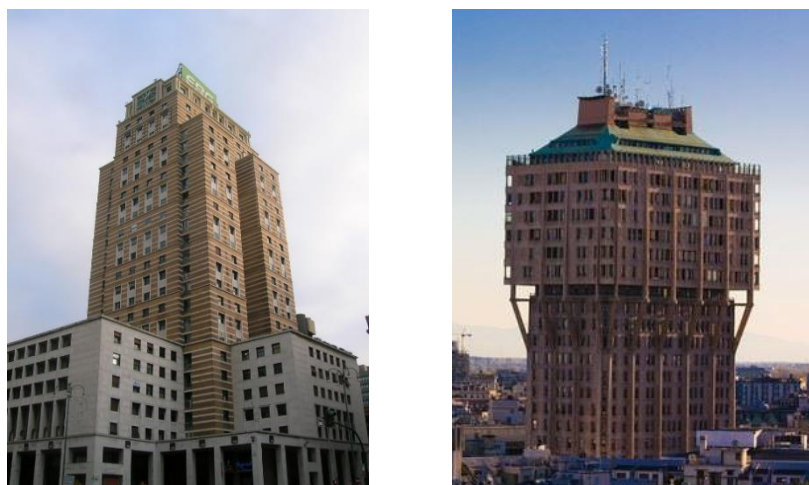


Figure 2.4: *Piacentini Tower, Genova (1940); Velasca Tower, Milan (1958)*

In 1960 Pirelli Tower became the highest reinforced concrete building, with its 127.1 m. The structure is composed by 4 pillars having 2 m width section (reduced to 50 cm at the top) connected by horizontal beams, which are the bearing elements for the slabs of each floor. The plant is 75.5 long and 20.5 large, for a total surface of 1900 m². For the construction 30000 m³ of concrete were used and the total weight of the building is almost 70000 tons, with a total volume of 125324 m³. This means a specific weight higher than 0.5 t/m³, which is a quite high value nowadays. Probably, it is due to the lower quality of that time concrete and to the different safety measurement used. Pirelli Tower is for sure one of the main landmarks of Milan and it has been the highest tall building of the city for almost 50 years, until the construction of Palazzo Lombardia in 2010.

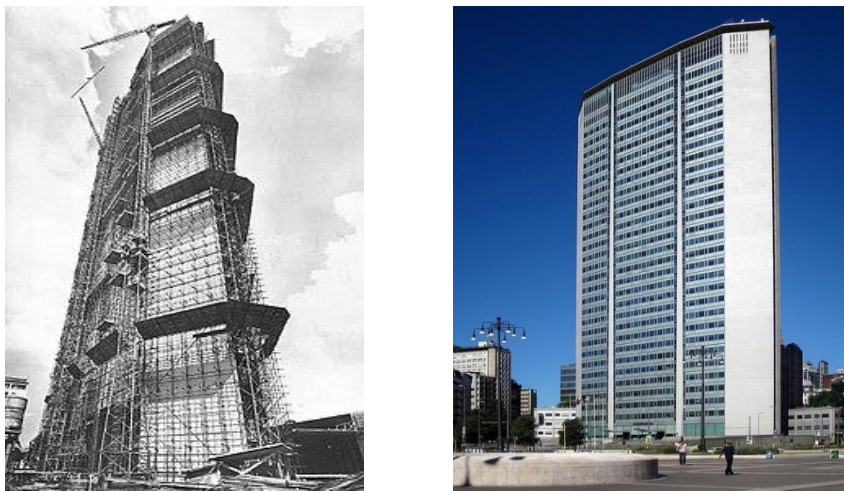


Figure 2.5: Pirelli Tower, Milan (1960)

Palazzo Lombardia is a building complex part of the Garibaldi-Repubblica redevelopment plan. The main building is a tower with a core structure, having a 161.3 m height which was the tallest to the roof in Italy until 2015, exceeded by Isozaki Tower.

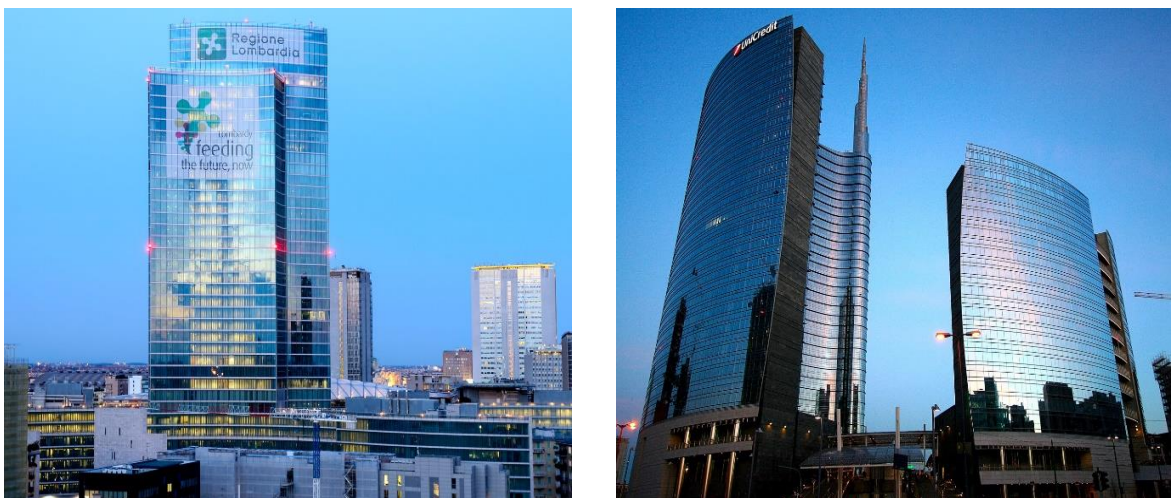


Figure 2.6: Palazzo Lombardia, Milan (2010); Unicredit Tower, Milan (2012)

Going up with the height there is a progressive reduction of beam and column cross section as well as localized reductions of the building plant. The structure is completely realized in reinforced concrete except for the last floors at the top of the building, the so called “Velario”. In the same area there is also the current highest tall building of Italy (taking into account the antenna), the Unicredit Tower, with its 231 m.

In Milan there are also other two redevelopment project: City Life and Porta Nuova. With the ending of these two big programmes, Milan landscape will be the first of Italy for variety and total amount of towers.

City Life is a residential, commercial and business district under construction situated a short distance from the old city centre of Milan; it has an area of 36.6 ha. The development is being carried out by a company controlled by Generali Group that won the international tender for the redevelopment of the historic neighbourhood of Fiera Milano. The project involves the construction of three skyscrapers:

- Il Dritto (The Straight One): designed by the Japanese architect Arata Isozaki, completed in 2015, it is the tallest to the roof building in Italy, with its 209.2 m (249 m with broadcast antenna). The stiffening system of the structure is composed by two r.c. core connected by two belt-trusses, forming a great portal. In addition, there are also four external diagonals connected to viscous damper which contribute to control the comfort in the building.
- Lo Storto (The Twisted One): completed in 2017, it reaches a height of 185 m (including Generali logo at the top). Designed by the Anglo-Iraqi architect Zaha Hadid, its geometry is that of a warping shape, where both the floors dimension and their orientation vary along the tower axis. The structure is concrete and composite, and it has a central core acting as main horizontal stiffening and resisting element. In order to resist the main torsional effects due to the warped column arrangement, the core lintels above main doors feature composite solutions with a mixed use of steel elements, rebar and concrete.
- Il Curvo (The Curved One): designed by the American architect Daniel Libeskind, it will be completed in 2019. It will reach a height of 175 m, with 28 floors and a total floor area of about 76 000 square meters.



Figure 2.7: *City Life neighbourhood, Milan*



Figure 2.8: *Il Dritto, Milan (2015); Lo Storto, Milan (2017); Il Curvo, Milan (2019)*

Porta Nuova project is a wide redevelopment plan of the business neighbourhood of Milan, which includes the area from the railway station Milano Porta Garibaldi to Piazza Della Repubblica, from Porta Nuova to Palazzo Lombardia, through Via Melchiorre Gioia. In this area it is planned the construction of almost ten skyscrapers, with height ranged from 94 to 161 m. Between them, the most relevant are: Solaria Tower (143 m), Diamond Tower (140 m), Bosco Verticale (111.15 m).

There also tall buildings in Turin: Regione Piemonte Skyscraper, designed by the Italian architect Massimiliano Fuksas, it will be completed in 2019 reaching 209 m height; Intesa Sanpaolo Skyscraper, completed in 2015, it reaches 167.25 m.



Figure 2.9: *Intesa Sanpaolo Skyscraper, Turin (2015); Regione Piemonte Skyscraper, Turin (2019)*

2.3 TALL BUILDINGS STRUCTURAL SYSTEMS

In tall buildings, the structure must sustain not only usual gravitational loads like self-weight, permanent and variable loads, but also horizontal actions, like wind and earthquakes, which are much more relevant with respect to normal buildings. For this reason, bracing systems must be realized to contain inter-story drifts, total displacements and reduce acceleration, in order to guarantee welfare of costumers and maximize usable areas.

Tall buildings can have different designated use: defensive (towers), communicative (bell tower), engineering usage (chimneys or antennas), residential, for service sector, or as landmark (e.g. the Eiffel Tower). Nowadays, the most relevant usage is certainly for residencies and offices, therefore we will focus our attention on these.

Because of the importance played by the cooperation between structural and architectural parts, in tall buildings it is possible to recognize two main kinds of mutually interacting systems:

- Structural systems realized to bear gravitational loads (i.e. slabs, columns and walls);
- Structural systems realized to sustain horizontal actions (bracing systems) which are the more relevant the higher the structure, influencing sometimes also the architectural shape.

From the point of view of the construction material used to realize the structural system, it is possible to divide tall buildings in:

- Steel Structures: supertall buildings are generally made of steel because of its high mechanical properties, lightness and ease of assembly.
- Reinforced Concrete Structures: the majority of tall buildings is made of reinforced concrete because cheaper than other materials but with really good properties (especially high-performance concrete).
- Hybrid Concrete-Steel Structures: the advantage in this case is the possibility to realize very stiff elements (columns or walls) with reduced dimensions, fundamental property to maximize available surfaces.

Furthermore, depending on the involved bracing system, another classification is also possible:

- Semi-rigid frames: columns, beams and, partially, connections are all involved to bear horizontal actions. In this way, however, the height is limited and a maximum of 10 stories can be reached.
- Rigid frames: columns and beams are rigidly connected; therefore, horizontal actions are sustained through the flexural deformation of the frame. Thus, higher heights are possible, allowing to reach until 30 stories.
- Rigid frames with bracing systems: in this case horizontal actions are sustained both by frame and shear walls (in case of R.C. structures) or diagonal bracing systems (in case of steel structures). 50 stories can be suitably reached in this way, even using slender widely spaced (6-9 m) columns.
- Frames with belt-trusses and/or outriggers: the bearing system is given by a frame, a core and horizontal cantilevers placed at suitable locations throughout the height of the building, connecting the core with the external columns. In this way, under the action of horizontal forces, the structure benefits from the stiffening contribution given by the columns' reaction, allowing to reach heights of the order of even 80 stories.
- Exterior framed tubes: constituted by a bracing external box structure connected with an internal frame bearing only gravitational loads. Buildings from 40 to 100 stories can be obtained, with the possibility of an interspacing until 20 m for internal columns.
- Exterior diagonalized tubes: constituted by a bracing external box structure composed of beams, columns and mega-diagonals, bearing both horizontal and gravitational actions. Thanks to this, no inner columns are needed, allowing for wide free internal spaces.

- Space truss structures: constituted by a main truss structure system, usually realized with steel, bearing both horizontal and vertical forces. They allow to realize really high buildings (70-150 stories).
- Diagrid systems: with their efficiency as a varied version of tubular systems, diagrid structures are emerging as a new aesthetic trend for tall buildings in this era of pluralistic styles. While the structural importance of diagonals was well recognized since early designs, the aesthetic potential of them has been appreciated only in recent era since they were considered obstructive for viewing the outdoors. They efficiently resist lateral shear by axial forces in the diagonal members but the joints need to be carefully designed.
- Super frame structures: they assume the form of a portal which is provided on the exterior of the building. The frame resists all wind forces as an exterior tubular structure. The portal frame is composed of vertical legs in each corner of the building which are linked by horizontal elements at about 12 to 14 floors. Since the vertical elements are concentrated in the corner areas of the building, maximum efficiency is obtained for resisting wind forces. This kind of systems can be used for ultrahigh-rise buildings, up to 160 stories.
- Structures with Y-shaped footprint and central core: used in modern buildings, they give the possibility to achieve reduced slenderness and inner space for usage.

In the following, a chart and a list of images are reported to briefly summarize the various typologies of structural systems discussed so far:

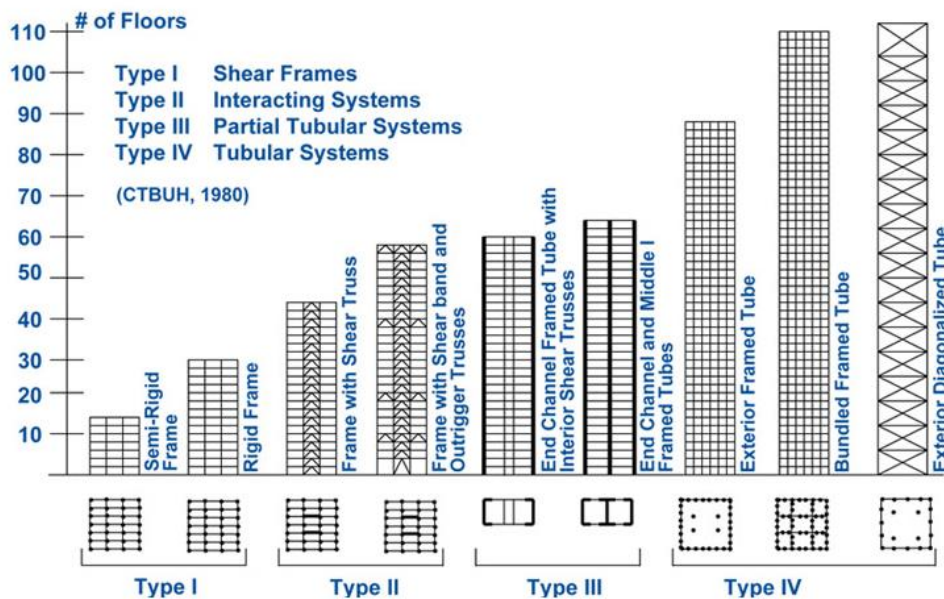


Figure 2.10: High-rise buildings and their evolution



Figure 2.11: *Lever House (Rigid Frame); North Riverside (Shear Walls); World Trade Centre (Outriggers)*

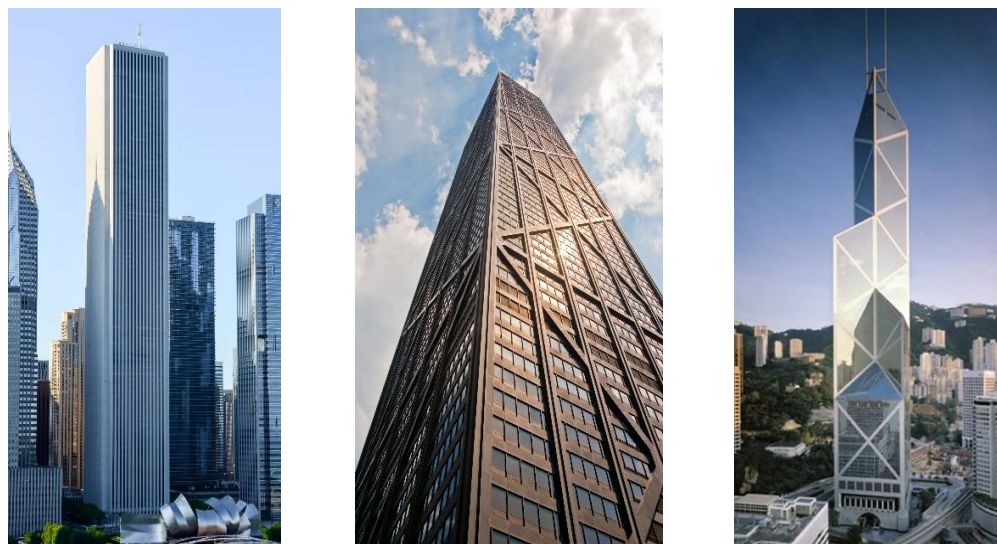


Figure 2.12: *Aon Centre (Framed Tube); Hancock Centre (Trussed Tube); Bank of China (Space Truss)*



Figure 2.13: *Hearst Tower (Diagrid systems); Burj Khalifa plant (Y footprint structure)*

2.4 CONCRETE FOR TALL BUILDINGS

The use of concrete in high-rise buildings is widely increased for many reasons. First, it is far cheaper than other structural materials, like steel, so it allows to reduce a lot the construction cost. Then, thanks to modern building technologies, based on industrialized formworks quickly movable after pouring concrete, it is possible to drive down construction time, reducing also costs directly connected to it.

From a historical point of view, the need of high performance was initially focused on compression strength, because the main aim was to use concrete for big structures, like tall buildings and long span bridges. Indeed, for both applications, a high strength/weight ratio is fundamental. For skyscrapers, high-strength concrete is needed to reduce cross section's dimensions of vertical elements, in order to have more available surface. For this kind of structures, the demand for high strength is often associated with other requirements related to mechanical and physical characteristic. For example, in the case of Burj Khalifa Tower it was necessary to use a self-compacting and self-levelling concrete with 60 MPa strength pumped up to 600 m height. In this case it is necessary to satisfy not only strength demand, but also special requirements like workability at high altitude.

High strength concrete can be obtained only by an accurate combination of components. It is necessary to use high quality cement, super-fluidizers to reduce water/cement ratio, fine materials with pozzolanic characteristic and to select accurately the granulometric curve. This allow to reduce the total porosity, increasing the quality of the hydration process products, obtaining also a higher durability. Finally, implementation of concrete is guaranteed thanks to self-compacting materials which do not need vibration and flow easily also through very congested rebar configurations, without segregation phenomena.

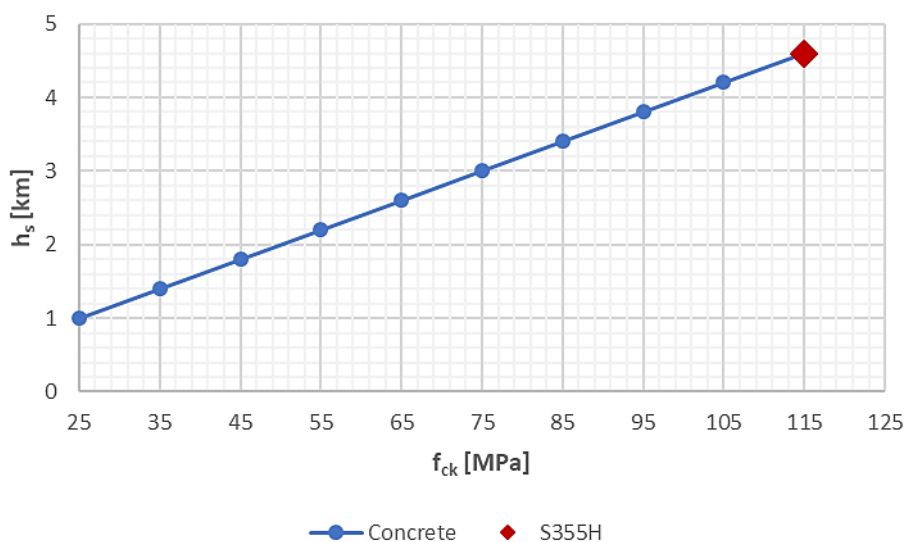


Figure 2.14: Concrete static efficiency

Nowadays, concrete compressive strength has reached a really high level, such that its static efficiency is comparable with structural steel, filling completely that gap which in the past led to prefer steel as structural material for tall buildings.

For what concerns vertical element, an interesting measurement of the bearing capacity is the static efficiency h_s , given by the ratio f_{ck}/ρ_c , where f_{ck} is the cylindrical compressive strength of concrete and ρ_c its density.

It is expressed in km and basically it represents the height of one column to have acting stress due to sole self-weight equal to the strength in the base cross section. As we can see from Figure 2.14, for ordinary concrete ($f_{ck} = 55$ MPa) the static efficiency is almost 2.2 km, much lower than the steel one (red mark). Therefore, comparing these two materials, steel is the only one suitable for high-rise buildings. On the contrary, if we consider high strength concrete ($f_{ck} = 90$ MPa), the static efficiency grows up to 3.6 km, almost like the 4.5 of structural steel. Taking into account that steel sections are subjected also to instability phenomena and in real cases static efficiency is never completely reached, concrete materials with compressive strengths of the order of 75-80 MPa are sufficient for supertall buildings, e.g. the Burj Khalifa in Dubai.

2.5 OUTRIGGER STRUCTURAL SYSTEMS

The ability to guarantee an efficient behaviour under lateral actions, both in the ultimate and serviceability limit states, is the basic characteristic of the structural systems in tall buildings. For what concerns ultimate limit states, the required performance is related to the resistance, in particular the ability to counteract lateral actions in extreme situations. On the other hand, the essential requirement for a structural system in the serviceability limit state consists in its ability to adequately develop reduced lateral displacements when subjected to lateral actions, applied in their most unfavourable combinations. This requirement is inherently connected to further effects, which are related to specific performance aspects of the structural system during its service life. The most common among these is the stiffness, which not only reduces lateral displacements, both total and relative between consecutive floors, but also by making vibrational effects acceptable, such as not to limit the comfort of the users. A second aspect of great importance regards the ability to ensure acceptable relative displacements between the load-bearing structure and non-structural elements, without undergoing significant damages. This aspect is particularly important for buildings whose façades are made from glass due to their restrictive displacement tolerances, where their damage can result in substantial economic consequences.

The need to ensure reduced lateral displacements, associated with that of guaranteeing an adequate safety level in the ultimate limit state, has always represented the fundamental problem of the structural design of tall buildings. The solution of the problem has led to the

definition of systems with well-known morphology, whose performance have been continuously improved, aimed at increasing the efficiency of the structural system, as the height of the buildings increases. Various systems have been illustrated and discussed in detail for this purpose in technical literature, among these are the so-called “Outrigger Systems”.

Outriggers are rigid horizontal structures designed to improve building overturning stiffness and strength by connecting the building core or spine to distant columns. Outriggers have been used in tall, narrow buildings for nearly half a century, but the design principle has been used for millennia. The oldest “outriggers” are horizontal beams connecting the main canoe-shaped hulls of Polynesian oceangoing boats to outer stabilizing floats or “amas” (see Figure 2.15).



Figure 2.15: *Samoan outrigger canoe*

A rustic contemporary version of this vessel type illustrates key points about building outrigger systems:

- A narrow boat hull can capsize or overturn when tossed by unexpected waves, but a small amount of *ama* flotation (upward resistance) or weight (downward resistance) acting through outrigger leverage is sufficient to avoid overturning. In the same manner, building outriggers connected to perimeter columns capable of resisting upward and downward forces can greatly improve the building’s overturning resistance.
- Even though a boat may be ballasted to resist overturning, it can still experience uncomfortable long-period roll. Outrigger-connected *amas* greatly reduce that behaviour and shorten the period of the movement. Similarly, building outriggers can greatly reduce overall lateral drift, story drifts, and building periods.
- Boats can have outriggers and *amas* on both sides or on one side. Buildings can have a centrally located core with outriggers extending to both sides, or a core located on one side of the building with outriggers extending to building columns on the opposite side.

The explanation of building outrigger behaviour is simple: because outriggers act as stiff arms engaging outer columns, when a central core tries to tilt, its rotation at the outrigger level induces a tension-compression couple in the outer columns, acting in opposition to that movement. The result is a type of restoring moment acting on the core at that level. Similarly, in case of thin-walled cores, due to torsion the section core warps creating tension-compression on the corner opposite columns, acting against the warping of the section. The result is, once again, a restoring bi-moment acting on the core at the outrigger level.

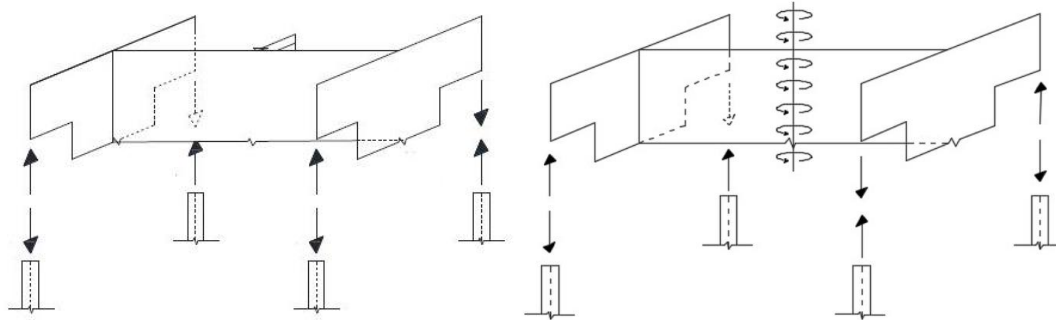


Figure 2.16: *Bending and torsional effects of outriggers*

Analysis and design of a complete core-and-outrigger system is not that simple: distribution of forces between the core and the outrigger system depends on the relative stiffness of each element. One cannot arbitrarily assign overturning and torsional forces to the core and the outrigger columns. However, it is certain that bringing perimeter structural elements together with the core as one resisting system will reduce core overturning moment and bi-moment (see Figure 2.17), but not core horizontal story shear forces. In fact, shear in the core can actually increase (and change direction) at outrigger stories, due to the outrigger horizontal force couples acting on it.

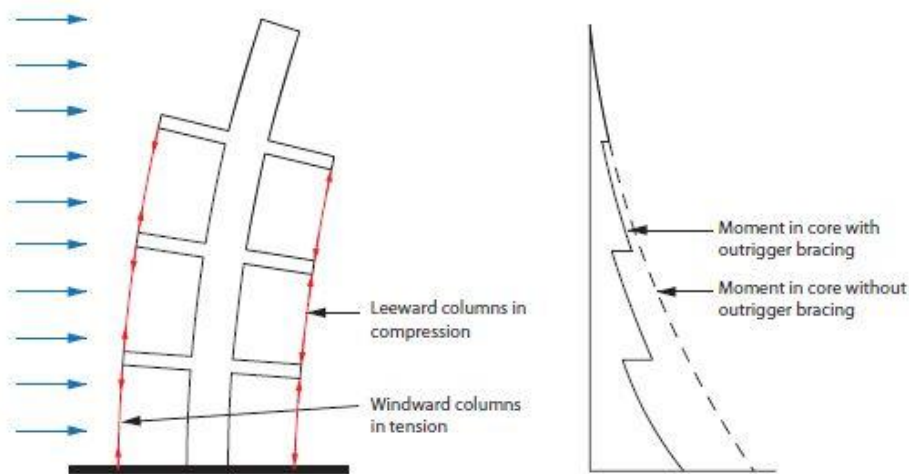


Figure 2.17: *Interaction of core and outrigger*

Belts, such as trusses or walls encircling the building, add further complexity. Belts can improve lateral system efficiency. For towers with outriggers engaging individual megacolumns, belts can direct more gravity load to the megacolumns. This minimizes net uplift, the amount of reinforcement or column splices required to resist tension and reduce stiffness associated with concrete in net tension. For towers with external tube systems, belts reduce the shear-lag effect of the external tube, more effectively engage axial stiffness contributions of multiple columns, and more evenly distribute across multiple columns the large vertical forces applied by outriggers. For both megacolumn and tube buildings, belts can further enhance overall building stiffness, through virtual or indirect outrigger behaviour provided by high in-plane shear stiffness, as well as increasing tower torsional stiffness. Belts working with megacolumns can also create a secondary lateral load-resisting system, in seismic engineering terminology.

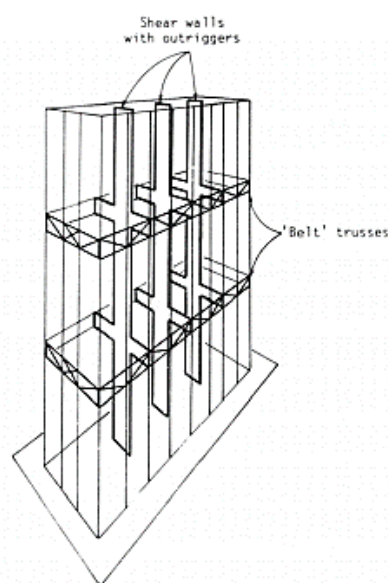


Figure 2.18: *Resisting system with belts*

It is worth noticing that the effect of the outrigger is more pronounced the more its vertical displacements increase. A core-and-outrigger system is frequently selected for the lateral load-resisting system of tall or slender buildings, where overturning moment is large compared to shear, and where overall building flexural deformations are major contributors to lateral deflections such as story drift. In such situations, outriggers reduce building drift and core wind moments. In addition, we shall consider that in modern structures the geometric configurations of buildings are increasing in complexity and are often characterized by marked variations along the height, giving torsion on the structure just with self-weight. In the presence of torsion, the generation of vertical displacements is a direct consequence of the warping in the cross section of the core, therefore vertical displacements are of greater importance as the warping of the core becomes more pronounced. It follows from these considerations that the presence of an outrigger becomes of significant

importance in the presence of cores whose cross section is open and of small thickness, while this effect tends to vanish in the case of virtually closed cross sections. Situations of this type occur in buildings of moderate height, for which the outrigger system is very efficient, both to reduce the torsional effects and the bending one. In addition, because of the increased stiffness they provide, outrigger systems are very efficient and cost-effective solutions to reduce building accelerations, which improves occupant comfort during high winds. In the following, some other benefits related to outriggers systems are briefly illustrated.

2.5.1 Deformation Reduction

In a building with a central core braced frame or shear walls, an outrigger system engages perimeter columns to efficiently reduce building deformations from overturning moments and the resulting lateral displacements at upper floors. A tall building structure that incorporates an outrigger system can experience a reduction in core overturning moment up to 40% compared to a free cantilever, as well as a significant reduction in drift, depending on the relative rigidities of the core and the outrigger system. For supertall towers with perimeter megacolumns sized for drift control, reduction in core overturning can be up to 60%. In case of open thin-walled cores, an outrigger system also reduces the torsional rotation and the warping of the cross section, particularly when the value of the parameter k as given by equation (3.47) is low. The system works by applying forces on the core that partially counteract rotation from overturning and vertical displacements from warping. These forces are provided by perimeter columns and delivered to the core through direct outrigger trusses or walls, or indirect or “virtual” outrigger action from belt trusses and diaphragms.

2.5.2 Efficiency

For systems with belt trusses that engage all perimeter columns, those columns already sized for gravity loads may be capable of resisting outrigger forces with minimal change in size or reinforcement, as different load factors apply to design combinations with and without lateral loads. In the event that additional overall flexural or torsional stiffness is required, the greater lever arm at outrigger columns makes additional material more effective than in the core. Outriggers may also permit optimization of the overall building system, using techniques to identify the best location for additional material. By significantly decreasing the fraction of building overturning that must be resisted by the core, wall, or column, material quantities in the core can be reduced, while outrigger, perimeter belt and column quantities are slightly increased. Lower limits on core required strength and stiffness may be defined by amount of story shear resisted by the core alone between outrigger levels, special loading condition that exist at outrigger stories, or short short-term capacity and stability if outrigger connections are delayed during construction.

2.5.3 Foundation Forces

A separate but related advantage is force reduction at core foundations. Outrigger systems help to effectively distribute overturning loads on foundations. Even where a foundation mat is extended over the full tower footprint, a core-only lateral system applying large local forces from overturning can generate such large mat shear and flexural demands, as well as net tension in piles or loss of bearing, that the design becomes uneconomical or impractical. Reducing core overturning and involving perimeter-column axial forces to help resist overturning from lateral loads reduces mat shear demand, flexural demand and net uplift conditions by spreading overturning loads across the tower footprint. Reducing lateral-load variations in sub-grade stresses or pile loads under the core will reduce foundation rotations that can contribute to overall and inter-story drifts. Having an outrigger system may or may not change other aspects of foundation design, such as governing pile loads and footing or mat bearing pressures.

2.5.4 Gravity Force Transfers

Outriggers and belt trusses can help reduce differential vertical shortening between columns or between a column and the core. This can reduce floor slopes between those elements that may occur from creep, shrinkage, or thermal changes. The reduction is achieved by force transfers between adjacent columns through belt trusses, or between the columns and core through outriggers. This is a secondary benefit at best and is a two-edged sword: force transfers can become quite large and costly to achieve. Balancing potential benefits and costs requires a solid understanding of the phenomenon as well as proper application of details and construction strategies to manage its effects.

2.5.5 Torsional Stiffness

Belt trusses can provide a different secondary benefit: improved torsional stiffness. A core-only tower can have low torsional stiffness compared to a perimeter-framed tower, due to the much smaller distance between resisting elements. A core-and-outrigger building can have similarly low torsional stiffness. Belt trusses can force perimeter columns to act as fibers of a perimeter tube that, while not as stiff as a continuous framed tube, still provides significant additional torsional stiffness.

2.5.6 Disproportionate Collapse Resistance

Another potential benefit related to force transfer capability is progressive disproportionate collapse resistance. On projects which require considering sudden loss of local member or connection capacity, outriggers can provide alternate load paths. For example, where perimeter columns are engaged by belt trusses, loads from floors above a failed perimeter column could “hang” from the upper column, acting in tension, and then be transferred

through upper belt trusses to adjacent undamaged columns. Where outriggers are present without belt trusses, it may be possible to hang upper floor loads from outriggers that load the core, but massive outrigger columns may be too heavily loaded for this load path to be practical. In a braced-frame-core building, loads from floors above a failed column could be shared by perimeter members through outriggers. Of course, the design must be checked to confirm that alternate load paths can accept the resulting forces rather than leading to further failures. For disproportionate collapse checks, load factors are often smaller and capacities considered are often large than those used for the basic design, so the effect of these conditions on the building design may be minimal, depending on the considered scenario.

2.5.7 Architectural Flexibility

Core-and-outrigger systems permit design variations in exterior column spacing to satisfy aesthetic goals and, in some cases, specific functional requirements. Internal or direct outriggers need not affect the buildings perimeter framing or appearance compared with other floors. Supertall buildings with outriggers may have a few exterior mega-columns on each face, which opens up the façade system for flexible aesthetic and architectural expression. This overcomes a primary disadvantage of closed-form tubular systems used in tall buildings. The quantity and location of mega-columns have impacts on typical floor framing. Plans featuring widely-separated columns and column-free corners may require deep and heavy spandrels for the strength, deflection control, and vibration control requirements of long spans and cantilevers. The core-and-outrigger approach is scalable, with potential applicability to buildings 150 stories tall or higher.

3 THIN-WALLED ELASTIC BEAMS

In the general field of modern structural engineering, basic elements can be divided according to their spatial character into four classes:

- massive bodies;
- plates and shells;
- solid beams;
- thin-walled beams.

The first class comprises bodies whose three dimensions are comparable, such as a sphere, a cube, a parallelepiped, an elastic continuum filling all space or a half-space, as well as various structural or machine parts, that are subject to local loads or thermal stresses. Problems concerning the determination of stresses and deformations in solid bodies, and methods for their exact solution are dealt with in the mathematical theory of elasticity.

The second class comprises bodies having one dimension (width) small compared with the other two (height and length) which are of the same order of magnitude. Examples of such bodies are plates, thin slabs, shells and, in general, most of the thin-walled structural members so widely used in structural engineering aviation, ship building, instrumental building, and other fields of engineering.

The general theory of plates and shells is based on geometrical hypotheses, valid for thin deformable bodies within a certain degree of approximation. The exact and approximated methods of calculation for plates and shells form the subject of an extensive separate field of modern structural engineering, which can be called the structural engineering of thin-walled three-dimensional systems.

The third class comprises bodies characterized in that two of their dimensions are of the same order of magnitude and very small compared with the third dimension. We call such bodies solid beams. In investigations of the phenomena of flexure and of tension in solid beams, their particular form allows to introduce a number of geometrical hypotheses which simplify calculations. On the basis of such hypotheses, in the case of a beam deformed by transverse bending and longitudinal extension, of the six components of the strain tensor only one is preserved, corresponding to the elongation in the direction parallel to beam axis. The other five components of the strain tensor are taken to vanish. The law of plane sections, which forms the basis of the elementary theory of the bending of beams, is a consequence

of these geometrical hypotheses. This law states that any cross section of a beam which is initially plane stays plane even after deformation.

When investigating the phenomenon of torsion, we assume the so-called theory of pure torsion to be valid. This theory is based on the hypotheses that there is no extension or shearing strain in the plane of the cross section, and furthermore that there is no longitudinal extension. Thus, this theory allows to determine only the tangential stresses arising in the cross sections of the beam.

The elementary theory of extension (compression), flexure and pure torsion is included in the general engineering theory of solid beams, which is essentially based on the application of the Saint-Venant's principle. According to this principle and the adopted hypotheses, the internal forces acting on the cross section of the beam (within the elastic limits) lead to one resultant, which is given as a vector in a 6-dimensional space of the three force components and the three components of the moment. This resultant may be replaced by an equivalent system of statically equipollent forces without changing the state of stress and strain on the mathematical model adopted for the solid beam.

Elements of the third class comprise all beam systems (plane, three dimensional, statically determinate or indeterminate) whose elements are beams that in bending obey the law of plane sections and undergo the torsion according to the law of pure torsion, i.e., mainly solid beams.

The fourth class of structural elements comprises bodies which have the form of long prismatic shells. These bodies are characterized by the fact that their three dimensions are all of different order of magnitude. The thickness of the shell is small compared with any characteristic dimension of the cross section, and the cross sectional dimensions are small compared with the length of the shell. These bodies are called thin-walled beams.

The distinctive feature of thin-walled beams is that they can undergo longitudinal extension as a result of torsion. Consequently, longitudinal normal stresses proportional to these strains are created, which lead to an internal equilibrium of the longitudinal forces in each cross section. These complementary longitudinal normal stresses, which arise as a result of the relative warping of the section and which are not examined in the theory of pure torsion, can attain very large values in thin-walled beams with open (rigid or flexible) cross-sections and also in beams with closed flexible cross sections.

3.1 CALCULATION MODEL AND FUNDAMENTAL HYPOTHESES

To introduce the general theory of elastic thin-walled beams with open cross-section we shall examine a thin-walled structure of a cylindrical or prismatic shell type, having an arbitrary cross section and consisting of a finite number of thin (flat or curved) narrow plates. We shall assume that the component plates of such a shell are rigidly connected along their lines

of contact so that no plate is free to move with respect to its neighbour at any point of the joint. Let δ be the thickness of the shell, d any characteristic dimension of the cross section (its width or height), and L its length. When the proportions satisfy the relations:

$$\frac{\delta}{d} \leq 0.1; \quad \frac{d}{L} \leq 0.1 \quad (3.1)$$

we can classify the given structures as long prismatic shells or, in other words, as thin-walled beams.

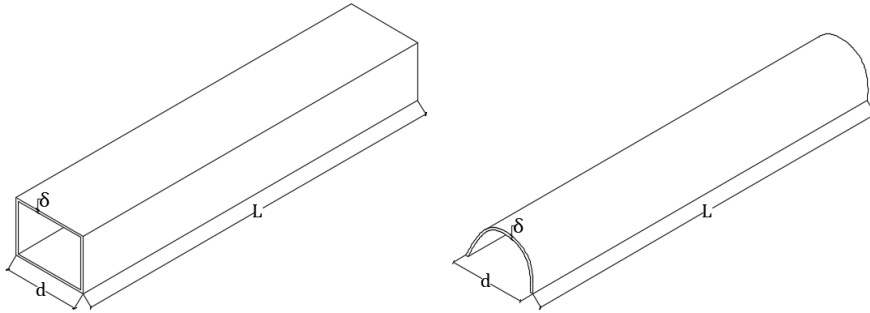


Figure 3.1: Example of thin-walled beams

In the theory of thin-walled beams (as in general shell theory) an important role is played by the so-called middle surface of the beam, i.e. the surface lying midway through the plates composing the beam. Straight lines lying on the middle surface and parallel to the beam axis are the generators of this surface. The intersection of the middle surface with a plane P normal to the generators is called the profile line or contour line.

Adopting a generator and a profile line as coordinate lines, we have an orthogonal coordinate system in which the position of any point on the middle surface is uniquely specified. Henceforward we shall denote the coordinates of any point M along the generator and profile line by z and s respectively. Any plane perpendicular to the beam axis (or to a generator) can be taken as the origin of the coordinate z . We shall usually use the terminal plane of the beam. The direction from this plane to the observer is taken as the positive direction of the coordinate z . Any generator can be taken as the origin of the coordinate s . We shall usually use as origin a generator which lies in a symmetry plane (in the case of symmetrical cross sections), or the generator coinciding with the lengthwise edge of any element of the beam profile.

Given this, according to Vlasov, the theory of beams of open section can be based on the following two geometrical hypotheses:

- a thin walled beam of open section can be considered as a shell of rigid (undeformable) cross section;
- the shearing deformation of the middle surface (characterizing the change in the angle between the coordinate lines $z = const$ and $s = const$) can be assumed to vanish.

In the theory of strength of materials, the line of centroids of the cross-sections is usually called axis of the beam. In the following, each line in space parallel to this axis shall be called arbitrary axis of the beam.

Let an arbitrary axis of the beam intersect the plane of the cross-section $z = \text{const}$ at the point O . The cross section of the beam forms part of a rectangular coordinate system Oxy with the origin at O (Figure 3.2). The Ox and Oy axes are oriented to form, together with the positive direction of the third axis Oz , a left-handed system of coordinates¹. The coordinates x and y of an arbitrary point M on the profile line of a thin-walled beam are well defined functions of the argument s , i.e. $x = x(s)$ and $y = y(s)$.

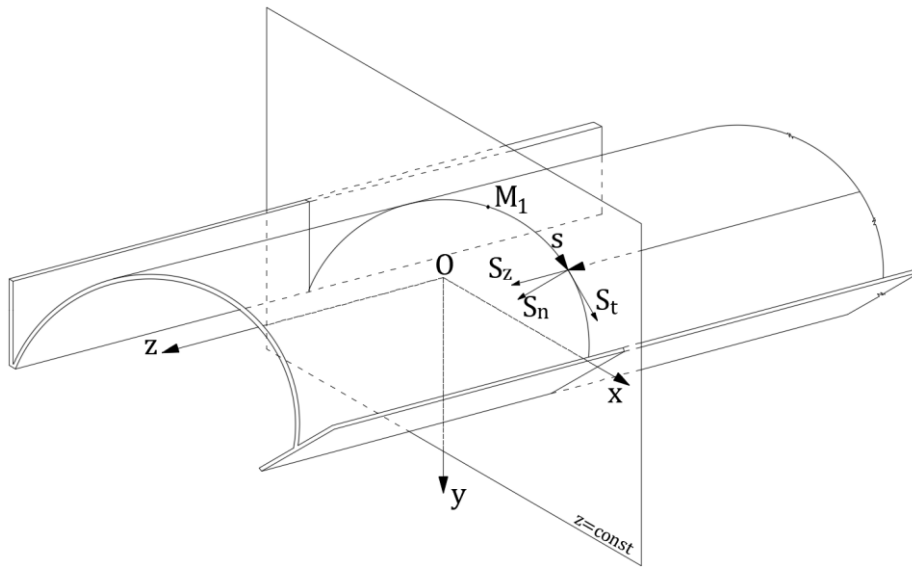


Figure 3.2: Geometrical characterization of the problem

3.1.1 *The Displacement Field*

Let the thin beam undergo some deformation. As a result of this deformation, any point M of the middle surface of the beam comes to occupy a new position in space. Our problem is now to determine the displacement of points of the middle surface, since the strained state of the beam is characterized by these displacements.

According to the geometrical hypothesis of rigid cross sections, the transverse displacement of the points of the section $z = \text{const}$ shall be given by the displacement of some chosen point A which lies in the cross section, and by the angle of rotation of the whole section about this point. If the point A does not belong to the profile line, we assume it to be rigidly connected to it.

¹ A coordinate system is called left-handed if, for an observer facing the Oxy plane from the z -positive side, clockwise rotation through 90° is necessary to make Ox coincide with Oy .

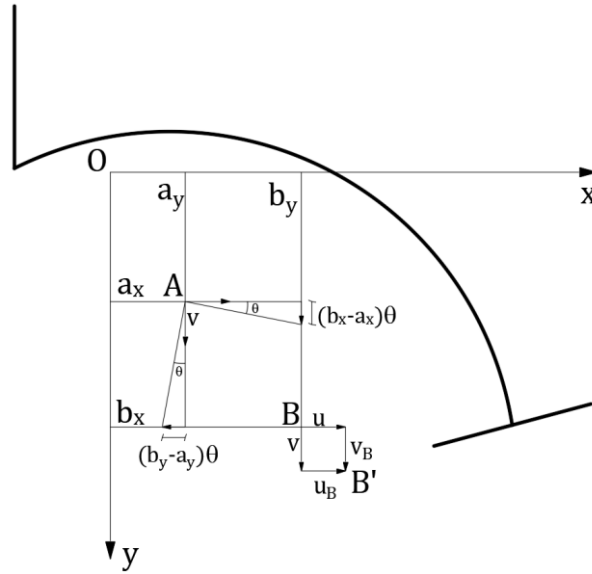


Figure 3.3: *In-plane displacements*

Let a_x and a_y be the coordinates of the point A , $u(z)$ and $v(z)$ the corresponding projections on the Ox and Oy axes of the displacement of the point A . Let $\theta(z)$ be the angle of rotation of the section $z = \text{const}$ in the Oxy plane about the same point A . As a function of z , this angle determines the torsional angle along the beam. We shall consider the torsional angle positive for clockwise rotation of the section $z = \text{const}$ as observed from the positive part of the Oz axis.

Thus, the displacements of any point B of the cross section of the beam can be computed according to the following expressions:

$$\begin{cases} u_B = u - (b_y - a_y)\theta \\ v_B = v + (b_x - a_x)\theta \end{cases} \quad (3.2)$$

where b_x and b_y are the coordinates of the point B .

For small values of $u(z)$, $v(z)$ and $\theta(z)$, the displacement of the cross section of the beam in its own plane can be regarded as rotation about a certain point, called the instantaneous centre of rotation. The position of this centre in the Oxy plane is determined by the condition that it is the one point that is fixed. Identifying the arbitrary point B with the instantaneous centre of rotation thus amounts to putting the displacements u_B and v_B of this point equal to zero.

From (3.2) we obtain the coordinates of the instantaneous centre of rotation as:

$$b_x = a_x - \frac{v}{\theta}; \quad b_y = a_y + \frac{u}{\theta} \quad (3.3)$$

In the following we shall call the instantaneous centre of rotation the torsion centre.

The full displacement of an arbitrary point M of the middle surface of a thin-walled beam is, naturally, a vector determined by three space components. For these components we take:

- The longitudinal displacement S_z ; this displacement shall be considered positive if it is in the direction of increasing z .
- The transverse tangential displacement S_t , directed along the tangent to the profile line. It is positive when the displacement is in the direction of increasing s .
- The transverse normal displacement S_n . The positive direction of this displacement is determined by the condition that the positive directions of the displacements S_z , S_t and S_n form a left-handed coordinate system (see Figure 3.2).

In the general case, all these displacements will be functions of the two independent variables z and s .

We shall now see how to determine the transverse displacements S_t and S_n . They are easily obtained from equation (3.2), which assumes the form:

$$\begin{cases} u_s = u - (y - a_y)\theta \\ v_s = v + (x - a_x)\theta \end{cases} \quad (3.4)$$

for an arbitrary point M of the profile line with the coordinates x and y . Here u_s and v_s are the displacements of the point M in the direction of the Ox and Oy axes.

Denoting by α the angle that the tangent to the profile line at the point M makes with the Ox axis and projecting u_s and v_s on this tangent as shown in Figure 3.4, we obtain for the transverse tangential displacement $v(z, s)$ the expression:

$$S_t(z, s) = u_s \cos \alpha + v_s \sin \alpha \quad (3.5)$$

Analogously we obtain the expression for the normal component $S_n(z, s)$ of the total displacement:

$$S_n(z, s) = v_s \cos \alpha - u_s \sin \alpha \quad (3.6)$$

Substituting in equations (3.5) and (3.6) the values of u_s and v_s from equations (3.4), we have:

$$\begin{aligned} S_t(z, s) &= u \cos \alpha + v \sin \alpha + [(x - a_x) \sin \alpha - (y - a_y) \cos \alpha] \theta \\ S_n(z, s) &= -u \sin \alpha + v \cos \alpha + [(x - a_x) \cos \alpha + (y - a_y) \sin \alpha] \theta \end{aligned} \quad (3.7)$$

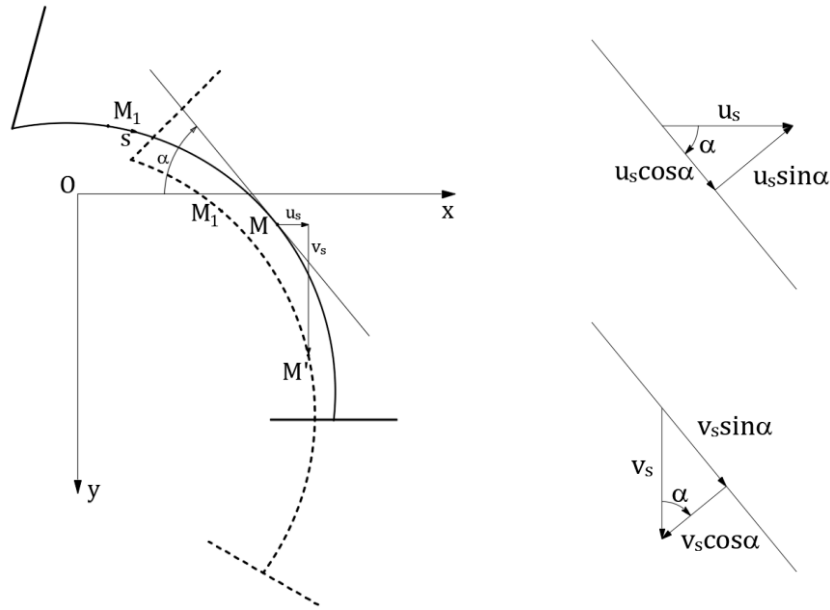


Figure 3.4: Geometrical characterization for the transverse tangent displacement

From Figure 3.5 it is seen that:

$$\begin{aligned} h(s) &= (x - a_x) \sin \alpha - (y - a_y) \cos \alpha \\ t(s) &= (x - a_x) \cos \alpha + (y - a_y) \sin \alpha \end{aligned} \quad (3.8)$$

where $h(s)$ and $t(s)$ are, respectively, the lengths of the perpendiculars from the point A to the tangent and normal of the profile line at M .

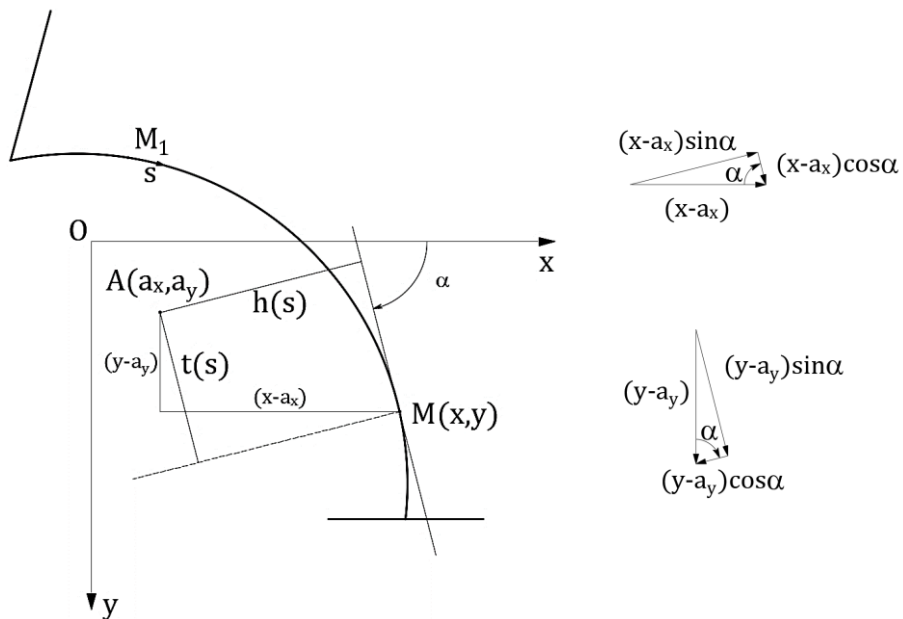


Figure 3.5: Geometrical characterization for the perpendiculars $h(s)$ and $t(s)$

Equations (3.8) can be used to give to the expressions for $v(z, s)$ and $w(z, s)$ a more compact form:

$$S_t(z, s) = u(z)\cos\alpha(s) + v(z)\sin\alpha(s) + \theta(z)h(s) \quad (3.9)$$

$$S_n(z, s) = -u(z)\sin\alpha(s) + v(z)\cos\alpha(s) + \theta(z)t(s) \quad (3.10)$$

We now determine the longitudinal displacement $S_z(z, s)$ of the point M . This is due to the deformation of the middle surface and is directed across the plane of the cross section. We can find this displacement by means of the second hypothesis concerning the absence of shearing strain between the coordinate lines $s = \text{const}$ and $z = \text{const}$.

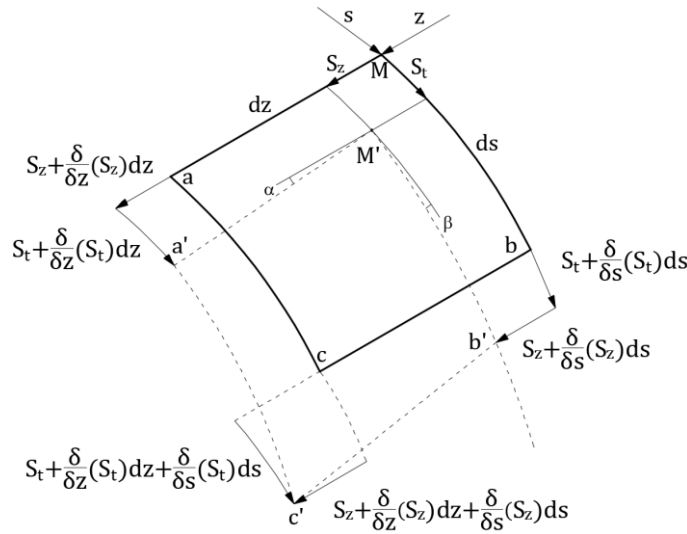


Figure 3.6: Tangential displacements of an elementary rectangle

Figure 3.6 shows the tangential displacements (occurring in appropriate tangent planes) of the four vertices M , a , b and c of an elementary rectangle. A knowledge of the displacements of all four vertices allows us to determine the desired shearing strain. This strain at the point M is, by definition, equal to the sum of the angles α and β , through which the sides Ma and Mb of the elementary rectangle rotate during deformation. Denoting the shearing strain by γ , we have:

$$\gamma_{zs} = \frac{\partial S_z}{\partial s} + \frac{\partial S_t}{\partial z} \quad (3.11)$$

Assuming that the shearing strain vanishes for a thin-walled beam of open cross section, we may set equation (3.11) equal to zero. Therefore, solving for the desired function $S_z(z, s)$, we have:

$$S_z(z, s) = w(z) - \int_{M_1}^M \frac{\partial S_t}{\partial z} ds \quad (3.12)$$

Here $w(z)$ is an arbitrary function, depending on z only, which describes the longitudinal displacement of the point M_1 , which serves as the origin of the coordinate s .

Differentiating (3.9) with respect to the variable z and multiplying both sides by ds , we obtain:

$$\frac{\partial S_t}{\partial z} ds = u'(z) \cos \alpha(s) ds + v'(z) \sin \alpha(s) ds + \theta'(z) h(s) ds \quad (3.13)$$

From Figure 3.7 we have:

$$\cos \alpha(s) ds = dx; \quad \sin \alpha(s) ds = dy; \quad h(s) ds = d\omega \quad (3.14)$$

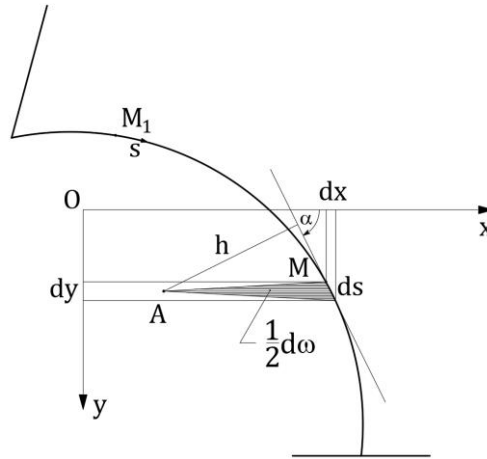


Figure 3.7: Geometrical characterization for the longitudinal displacement

Substituting (3.13) and (3.14) in the right-hand side of (3.12) and performing the integration, we obtain:

$$S_z(z, s) = w(z) - u'(z)x(s) - v'(z)y(s) - \theta'(z)\omega(s) \quad (3.15)$$

where $x(s)$ and $y(s)$ are the Cartesian coordinates of the point M and $\omega(s)$ is twice the area of the sector enclosed between the arc M_1M of the profile line and the two lines AM_1 and AM , joining the ends of this segment with A (Figure 3.8). According to Vlasov, this area is called sectorial area.

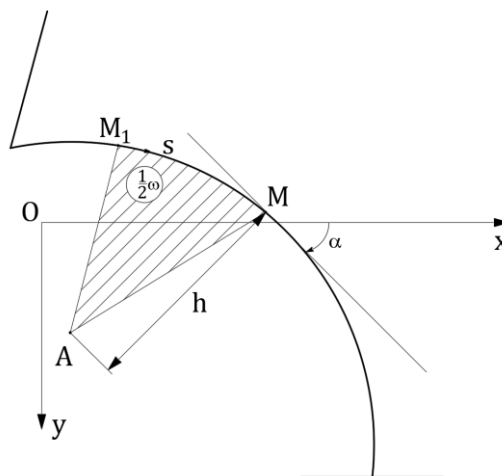


Figure 3.8: Definition of sectorial area

We call the point A the pole of the sectorial areas and the point M_1 the sectorial origin. The line AM_1 , which serves as initial ray for the sectorial areas and which connects the pole A with a chosen point M_1 on the profile line, may be called fixed radius vector. The line AM , which connects the pole A with the variable point M , i.e. with the point for which we calculated the area $\omega(s)$, shall be called mobile radius vector. We shall consider the sectorial area positive if the mobile radius vector AM moves clockwise when observed from the negative z direction. On straight flange-parts of the profile line the sectorial areas have always rectilinear (in the general case trapezoidal) diagrams, since the area $\omega(s)$ in this case is always a linear function of the coordinate s .

3.1.2 *The Strain Field*

Knowing the displacements of the points of the middle surface of the beam, we can now also find the deformation of this surface at any point M . In the following we shall be interested in the longitudinal deformation $\varepsilon = \varepsilon(z, s)$, which is given as the relative extension of the linear element dz which passes through the point M of the surface and lies parallel to its generators. This extension is defined as the ratio of the difference between the longitudinal displacements $S_z + \frac{\partial S_z}{\partial z} dz$ and S_z of two neighbouring points a and M , to the length of the element dz of the original (undeformed) surface (see Figure 3.6):

$$\varepsilon = \frac{S_z + \frac{\partial S_z}{\partial z} dz - S_z}{dz} = \frac{\partial S_z}{\partial z} \quad (3.16)$$

Differentiating with respect to z the longitudinal displacement $u(z, s)$ expressed by equation (3.15) and using (3.16), we obtain a general equation (which also has four terms) for the relative longitudinal extension:

$$\varepsilon(z, s) = w'(z) - u''(z)x(s) - v''(z)y(s) - \theta''(z)\omega(s) \quad (3.17)$$

Equation (3.17) shows that the relative longitudinal extensions $\varepsilon(z, s)$ at the profile line $z = \text{const}$ are made up of extensions linear in the coordinates $x(s)$ and $y(s)$ of the point on this line and obeying the law of plane sections, and extensions distributed along the profile line according to the law of sectorial areas which arise as a result of the warping of the section.

3.1.3 *Stress-Strain Relations*

Equation (3.17) does not fully determine the strain ε , since the functions $w(z)$, $u(z)$, $v(z)$ and $\theta(z)$ are unknown. This kinematical indeterminacy is due to our not having used all the static conditions, namely, the conditions of equilibrium for an elastic body which undergoes a definite deformation.

When the beam is deformed, internal elastic forces arise in it. These forces represent normal and tangential stresses in the cross section $z = \text{const}$. The tangential and normal stresses $\tau(z, s)$ and $\sigma(z, s)$ are considered as functions of the two variables z and s . The torsional moments per unit section (which depend on the difference of the tangential stresses at the extreme points of the wall) are replaced by a distribution of torsional moments $T_{DS}(z)$ over the cross-section. These moments will be functions of the variable z only.

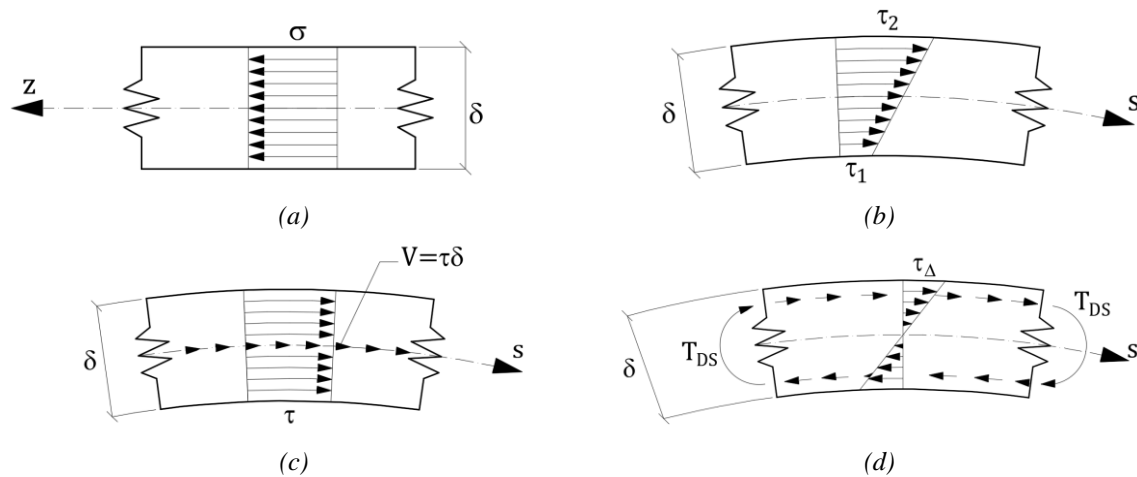


Figure 3.9: (a) normal stresses, (b) tangential stresses, (c) shear force, (d) pure torsional moments

We now agree on the signs of these quantities. An elementary area of the cross section shall be positive if its normal points in the direction of positive z (Figure 3.10). We shall consider the stresses acting on any point of this area as positive if they are in the direction of increasing coordinates for the point of the middle surface of the shell. We shall consider the torsional moment as positive if it causes the cross section to rotate clockwise when viewed from the positive side of the area.

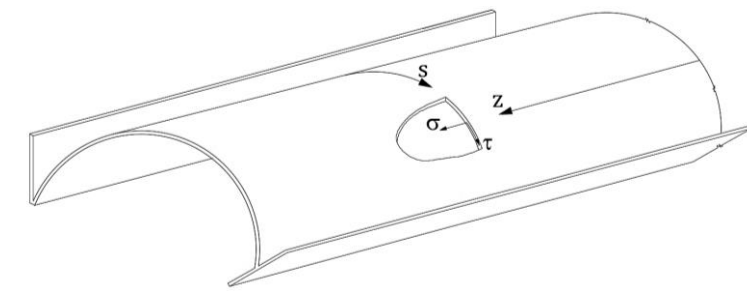


Figure 3.10: Sign convention for the stress components

By using the physical relation between the stresses and strains in the beam we can now find the stresses σ , τ and the moments T_{DS} from the strains. Hooke's law gives for the relative extensions of an element of the middle surface of the beam in two perpendicular directions:

$$\varepsilon = \frac{1}{E}(\sigma - \nu\sigma_1); \quad \varepsilon_1 = \frac{1}{E}(\sigma_1 - \nu\sigma) \quad (3.18)$$

where ε and ε_1 are the relative extensions of the beam in the longitudinal and transverse directions, σ and σ_1 the normal stresses in the longitudinal and transverse directions respectively, E the Young's modulus and ν the Poisson's ratio.

According to the supposed inflexibility of the contour, the extension ε_1 of the contour arc is equal to zero and thus $\sigma_1 = \nu\sigma$. Introducing this result into the first of equations (3.18) and solving for σ , we obtain:

$$\sigma = E_1 \varepsilon \quad (3.19)$$

where E_1 is the reduced Young's modulus of longitudinal elongation:

$$E_1 = \frac{E}{1 - \nu^2} \quad (3.20)$$

In the following we shall consider the quantity ν^2 negligible compared with unity and take $E = E_1$. Substituting the expression for ε from equation (3.17) in equation (3.19), we obtain the general law for the distribution of normal stresses $\sigma = \sigma(z, s)$:

$$\sigma = E(w' - u''x - v''y - \theta''\omega) \quad (3.21)$$

We now determine the torsional moment T_{DS} , arising as a result of the nonuniform distribution of the tangential stresses over the thickness of the wall of the beam. In the theory of pure torsion, we have for this term, the following expression:

$$T_{DS} = GI_d \theta' \quad (3.22)$$

where G is the shear modulus and I_d is the moment of inertia for pure torsion as calculated for a thin-walled folded cross section according to the equation:

$$I_d = \frac{\alpha}{3} \sum d\delta^3 \quad (3.23)$$

where d and δ are, respectively, the width and thickness of the plates which make up the beam and α is an empirical coefficient close to unity.

It now remains to determine the tangential stresses. These stresses are determined statically in the same way as in the elementary theory of bending.

By equilibrium in the direction of a generator of all the forces, we have (see Figure 3.11):

$$d(\sigma\delta)ds + d(\tau\delta)dz + p_z dz ds = 0 \quad (3.24)$$

where $p_z = p_z(z, s)$ is the projection of the external surface load on the axis z . In general, this projection depends on the variables z and s .

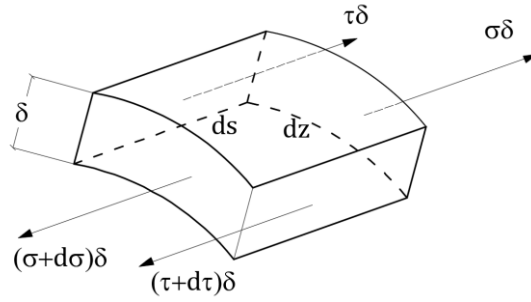


Figure 3.11: *Equilibrium in the longitudinal direction*

Dividing equation (3.24) by $dzds$, and solving it with respect to the tangential stresses τ (realizing that the thickness of the wall δ does not depend on z) we find:

$$\tau(z, s) = \frac{1}{\delta} \left[S_0(z) - \int_0^s p_z ds - \int_0^s \frac{\partial \sigma}{\partial z} \delta ds \right] \quad (3.25)$$

Here $S_0(z)$ is an arbitrary function which depends on the variable z , giving the shear stresses $\tau\delta$ which act on the longitudinal section $s = 0$.

Substituting (3.21) for σ in the right-hand side of (3.25) and denoting the differential of the section area δds by dA , we find:

$$\tau = \frac{1}{\delta} S_0 - \frac{1}{\delta} \int_0^s p_z ds - Ew'' \frac{A(s)}{\delta} + Eu''' \frac{S_y(s)}{\delta} + Ev''' \frac{S_x(s)}{\delta} + E\theta''' \frac{S_\omega(s)}{\delta} \quad (3.26)$$

where $A(s)$, $S_x(s)$ and $S_y(s)$ are respectively the area and the static moments with respect to the x and y axes, given by equations:

$$A(s) = \int_0^s 1 dA; \quad S_x(s) = \int_0^s y dA; \quad S_y(s) = \int_0^s x dA; \quad S_\omega(s) = \int_0^s \omega dA \quad (3.27)$$

$S_\omega(s)$ is reminiscent of the equation for a static moment, the only difference is that the moment arm in the latter equation is replaced here by a sectorial area ω . According to this, we shall henceforth call $S_\omega(s)$ the sectorial static moment.

If there is no longitudinal load distribution on the lateral edges or sides, equation (3.26) assumes the following simpler form:

$$\tau(z, s) = \frac{E}{\delta(s)} \left[-w''(z)A(s) + u'''(z)S_y(s) + v'''(z)S_x(s) + \theta'''(z)S_\omega(s) \right] \quad (3.28)$$

3.1.4 Equilibrium Equations in Principal Coordinates

It is seen from equations (3.21), (3.22) and (3.26) that the stresses σ , τ and the moment T_{DS} , which determine the state of the internal stresses of the shell in the cross section $z = \text{const}$, depend on the functions $w(z)$, $u(z)$, $v(z)$ and $\theta(z)$. These functions are unknown as yet. We have to apply the equilibrium conditions (which still have not been used) in order to determine them.

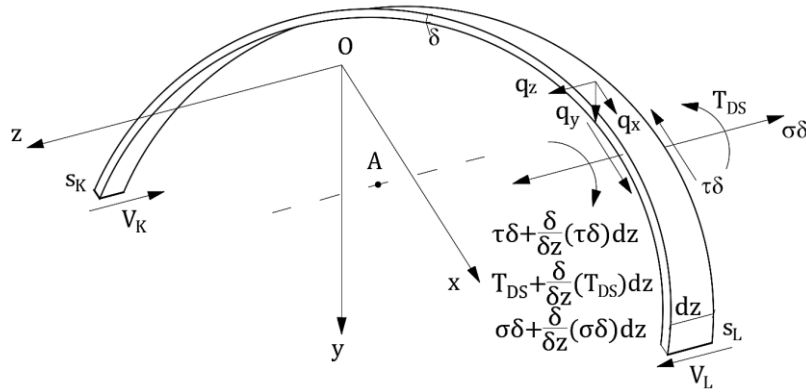


Figure 3.12: Forces on an elementary transverse strip

For an elementary transverse strip under the application of a transverse load, eccentric with respect to the shear centre A , and shear forces applied along the lateral edges, the equilibrium equations in principal coordinates (neglecting higher order infinitesimals) can be given in the following form:

$$\begin{aligned}
 EA w'' &= -q_z + V_K - V_L \\
 EI_{yy} u^{IV} &= q_x + V_L' x_L - V_K' x_K \\
 EI_{xx} v^{IV} &= q_y + V_L' y_L - V_K' y_K \\
 EI_{\omega\omega} \theta^{IV} - GI_d \theta^{II} &= q_\omega + V_L' \omega_L - V_K' \omega_K
 \end{aligned} \tag{3.29}$$

In this way, four separate equations can be obtained and if the lateral edges of the beam are free from shear forces and the external load is composed only of transverse specific forces $q_x = q_x(z)$, $q_y = q_y(z)$ and a moment $q_\omega = q_\omega(z)$ (the case common in practice), the equations assume even a simpler form:

$$\begin{aligned}
 EA w'' &= 0 \\
 EI_{yy} u^{IV} &= q_x \\
 EI_{xx} v^{IV} &= q_y \\
 EI_{\omega\omega} \theta^{IV} - GI_d \theta'' &= q_\omega
 \end{aligned} \tag{3.30}$$

The first of equations (3.30) determines the longitudinal displacement, $w(z)$, due to a longitudinal tension or compression which is applied to the ends of the beam and uniformly

distributed over the section. The second and third equations refer to the transverse bending of the beam and determine the displacements $u(z)$ and $v(z)$ for the shear centre A , that is that point of the cross section with respect to which the sectorial area function $\omega(s)$ is orthogonal to the functions $x(s)$ and $y(s)$. The fourth equation refers to the torsion of the beam under the action of a transverse load which creates a torsional moment, $q_\omega(z)$, with respect to the shear centre A .

We shall choose the basic functions 1 , $x(s)$, $y(s)$ and $\omega(s)$ so that they will be orthogonal. Orthogonality means the vanishing of all integrals of pair-products of these functions (but not their squares) taken over the entire section A , that is:

$$\begin{aligned} S_x &= \int_A 1y dA = 0 & S_\omega &= \int_A 1\omega dA = 0 \\ S_y &= \int_A 1x dA = 0 & I_{\omega x} &= \int_A x\omega dA = 0 \\ I_{xy} &= \int_A xy dA = 0 & I_{\omega y} &= \int_A y\omega dA = 0 \end{aligned} \quad (3.31)$$

We call the functions 1 , $x(s)$, $y(s)$ and $\omega(s)$, which satisfy the conditions of orthogonality (3.31) the principal generalized coordinates of the cross section of a thin-walled beam.

3.1.5 Generalized Cross-Sectional Forces

Solving the differential equations (3.29) for the case when $q_z = V_L = V_K = 0$, we determine the functions $w(z)$, $u(z)$, $v(z)$ and $\theta(z)$ for given boundary conditions. Knowing these functions, we are able to find the normal and tangential stresses, and also the torsional moments which appear in the cross section of the beam. For the case of a beam under transverse load ($q_z = V_L = V_K = 0$)², we had:

$$\begin{aligned} \sigma &= E(w' - u''x - v''y - \theta''\omega) \\ \tau &= E \left[u''' \frac{S_y(s)}{\delta} + v''' \frac{S_x(s)}{\delta} + \theta''' \frac{S_\omega(s)}{\delta} \right] \\ T_{DS} &= GI_d \theta' \end{aligned} \quad (3.32)$$

Starting from the notion of virtual work, we can determine the generalized longitudinal forces as the work of all the elementary longitudinal forces σdA in each of the admissible longitudinal generalized displacements $w(z)$, $u(z)$, $u'(z)$, $v(z)$, $v'(z)$, $\theta(z)$ and $\theta'(z)$ and put the work equal to unity.

² In this case, in virtue of the first equation (3.29), $w'' = 0$.

If we assume consecutively that in equation (3.15) $w = 1$, $u' = -1$, $v' = -1$ and $\theta' = -1$ (and the remaining three variables vanish), we obtain the four elementary states of longitudinal displacement $u(z, s)$ in the section $z = \text{const}$: 1, x , y and ω . If we then multiply the elementary longitudinal force, σdA , successively by each of the functions 1, x , y and ω and we integrate over the whole area of the section, we obtain for the generalized longitudinal forces which correspond to these states the following equations:

$$N = \int_A \sigma 1 dA; \quad M_x = \int_A \sigma y dA; \quad M_y = - \int_A \sigma x dA; \quad M_\omega = \int_A \sigma \omega dA \quad (3.33)$$

According to our sign convention, if a positive normal force σdA acts on an element of the section area in the first quadrant of the Oxy plane, a positive moment with respect to the Ox -axis and a negative moment with respect to the Oy -axis are produced (Figure 3.13). The fourth equation determines the so-called bimoment. In contrast to the moment, the bimoment is a generalized balanced force system, i.e. a force system statically equivalent to zero.

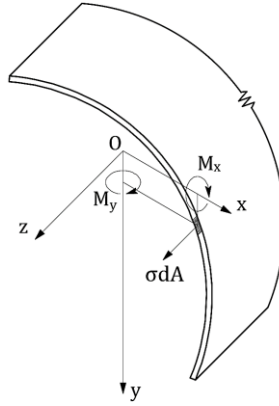


Figure 3.13: Bending moments induced by a positive elementary force (left-hand side rule)

Substituting in (3.33) the first of equations (3.32) and remembering that we are dealing with the principal generalized coordinates (1, x , y and ω) which satisfy the conditions of orthogonality, we obtain:

$$N = EA w'; \quad M_y = EI_{yy} u''; \quad M_x = -EI_{xx} v''; \quad M_\omega = -EI_{\omega\omega} \theta'' \quad (3.34)$$

or:

$$w' = \frac{N}{EA}; \quad u'' = \frac{M_y}{EI_{yy}}; \quad v'' = -\frac{M_x}{EI_{xx}}; \quad \theta'' = -\frac{M_\omega}{EI_{\omega\omega}} \quad (3.35)$$

Substituting expressions (3.35) in the first of equations (3.33), we obtain:

$$\sigma = \frac{N}{A} - \frac{M_y}{I_{yy}} x + \frac{M_x}{I_{xx}} y - \frac{M_\omega}{I_{\omega\omega}} \omega \quad (3.36)$$

We shall call the quantity $EI_{\omega\omega}$, which characterizes the stiffness of the beam for those cases of torsion when normal stresses $\sigma_{\omega} = \frac{M_{\omega}}{I_{\omega\omega}} \omega$ distributed according to the law of sectorial areas arise in the cross section, the sectorial warping rigidity of the beam (in analogy with the theory of bending).

Similarly, we can express the functions, which characterize the variation of the tangential stresses τ through the variable z , by statical factors, to wit, forces. We determine these forces as the work of the elementary contour tractions $(\tau\delta)ds$ in each of the possible unit displacements $u = 1$, $v = 1$, $\theta = 1$ of the section contour in the plane $z = \text{const}$. From equations (3.7) and (3.14) we can determine them in the following way:

$$V_x = \int_A (\tau\delta)dx; \quad V_y = \int_A (\tau\delta)dy; \quad T_{\omega} = \int_A (\tau\delta)d\omega = \int_A (\tau\delta)hds \quad (3.37)$$

Substituting the stresses τ , determined by the second of equations (3.32) in (3.37), and taking into consideration the orthogonality of the principal coordinates x , y and ω , the following relations are valid:

$$V_x = -EI_{yy}u'''; \quad V_y = -EI_{xx}v'''; \quad T_{\omega} = -EI_{\omega\omega}\theta''' \quad (3.38)$$

or:

$$u''' = -\frac{1}{EI_{yy}}V_x; \quad v''' = -\frac{1}{EI_{xx}}V_y; \quad \theta''' = -\frac{1}{EI_{\omega\omega}}T_{\omega} \quad (3.39)$$

By substituting the values found in (3.39) in equation (3.32) we obtain the following expression for the axial tangential stresses:

$$\tau = -\frac{1}{\delta} \left[\frac{V_x}{I_{yy}} S_y(s) + \frac{V_y}{I_{xx}} S_x(s) + \frac{T_{\omega}}{I_{\omega\omega}} S_{\omega}(s) \right] \quad (3.40)$$

By differentiating and eliminating the derivatives of the displacements, we obtain from equations (3.35) and (3.39) the relations:

$$V_x = -M'_y; \quad V_y = M'_x; \quad T_{\omega} = M'_{\omega} \quad (3.41)$$

These relations, which are a generalization of the Jourawski's theorem known from the theory of strength of materials, are valid only for the case of action of transverse loads on the beam.

The sum of the moments T_{ω} and T_{DS} gives the total torsional moment, which we shall denote by T :

$$T = T_{\omega} + T_{DS} = -EI_{\omega\omega}\theta''' + GI_d\theta' \quad (3.42)$$

3.2 THE SOLUTION OF THE TORSION EQUATION

It was established that thin-walled beams of rigid cross-section undergo not only bending but also torsion when subjected to a transverse load which does not pass through the shear centre. Here, we shall omit all that refers to the bending of beams based on the hypothesis of plane sections and concentrate on the study of torsion in a thin-walled beam, which in the general cases is produced by a transverse load. The last of equations (3.30) gives the following differential equation for the torsional angle $\theta(z)$, in case only a transverse load is acting:

$$EI_{\omega\omega}\theta^{IV} - GI_d\theta'' = q_\omega \quad (3.43)$$

where q_ω denotes the free term, which represents the external torsional couple per unit length of the beam in the case of purely transverse loading.

Dividing equation (3.43) by the coefficient of θ^{IV} and introducing the notation (L is the span length of the beam-shell along the generator):

$$k^2 = L^2 \frac{GI_d}{EI_{\omega\omega}}; \quad f(z) = \frac{1}{EI_{\omega\omega}} q_\omega \quad (3.44)$$

Equation (3.43) is simplified into:

$$\theta^{IV} - \frac{k^2}{L^2}\theta'' = f(z) \quad (3.45)$$

In the case when $q_\omega \neq 0$, (3.45) is a linear and inhomogeneous differential equation with constant coefficients. The general integral of such an equation can be written in the form:

$$\theta(z) = C_1 + C_2z + C_3\sinh\left(\frac{k}{L}z\right) + C_4\cosh\left(\frac{k}{L}z\right) + \bar{\theta}(z) \quad (3.46)$$

Here, C_1 , C_2 , C_3 and C_4 are arbitrary constants, obtained from integration of the homogeneous differential equation, $\bar{\theta}(z)$ is any particular solution of the inhomogeneous equation (3.45); k is a dimensionless characteristic number, determined by the first of equations (3.44):

$$k = L \sqrt{\frac{GI_d}{EI_{\omega\omega}}} \quad (3.47)$$

As we see, k depends on the ratio of the pure torsion GI_d , understood in the sense of Saint-Venant's theory, and the sectorial rigidity $EI_{\omega\omega}$ (i.e. the torsional rigidity of the beam which is associated with the appearance of normal stresses in the cross sections) and proportional to the span-length, L , of the beam. Performing the first, second and third order derivatives of the function $\theta(z)$ with respect to the variable z and introducing them into equations (3.34)

and (3.42), we obtain the general integrals of the four basic design quantities (two kinematical: the torsion angle θ and the warping θ' ; two statical: the bimoment M_ω and the total torsional moment T)³:

$$\begin{aligned}
 \theta(z) &= C_1 + C_2 z + C_3 \sinh\left(\frac{k}{L}z\right) + C_4 \cosh\left(\frac{k}{L}z\right) + \bar{\theta}(z) \\
 \theta'(z) &= C_2 + C_3 \frac{k}{L} \cosh\left(\frac{k}{L}z\right) + C_4 \frac{k}{L} \sinh\left(\frac{k}{L}z\right) + \bar{\theta}'(z) \\
 M_\omega(z) &= -GI_d \left[C_3 \sinh\left(\frac{k}{L}z\right) + C_4 \cosh\left(\frac{k}{L}z\right) + \frac{L^2}{k^2} \bar{\theta}''(z) \right] \\
 T(z) &= GI_d \left[C_2 + \bar{\theta}'(z) - \frac{L^2}{k^2} \bar{\theta}'''(z) \right]
 \end{aligned} \tag{3.48}$$

General methods for finding particular integrals of an inhomogeneous equation are discussed in the theory of differential equations. Thus, for example, knowing the general integral of a homogenous equation, it is possible to find the particular integral of the inhomogeneous by the method of variation of constants, which is generally applicable to linear equations with constant and variable coefficients.

For the most common cases of loading, we have:

- *Concentrated torsional moment* (due to the action of a concentrated transverse load which does not pass through the shear centre):

$$\theta^{IV} - \frac{k^2}{L^2} \theta'' = 0 \quad \rightarrow \quad \bar{\theta}(z) = 0 \tag{3.49}$$

- *Evenly distributed torsional moment* (due to the action of a transverse load of constant magnitude q and moment arm about the shear centre e):

$$\theta^{IV} - \frac{k^2}{L^2} \theta'' = \frac{qe}{EI_{\omega\omega}} \quad \rightarrow \quad \bar{\theta}(z) = -\frac{qe}{2EI_{\omega\omega}} \cdot \frac{L^2}{k^2} z^2 \tag{3.50}$$

- *Torsional moment for a trapezoidal distribution* (due to the action of a trapezoidal load given by the function $q_0 + \frac{q_1}{L}z$, applied along a line parallel to the generator and having an arm e about the shear centre):

³ It is worth observing that in (3.48) M_ω and T_ω are given in function of GI_d , while in (3.42) and (3.34) they are multiplied by $EI_{\omega\omega}$. In virtue of the relation $EI_{\omega\omega} = GI_d \frac{L^2}{k^2}$, the two expressions are equivalent.

$$\theta^{IV} - \frac{k^2}{L^2} \theta'' = \frac{e \left(q_0 + \frac{q_1}{L} z \right)}{EI_{\omega\omega}} \quad \rightarrow \quad \bar{\theta}(z) = -\frac{e \left(q_0 + \frac{q_1}{L} z \right)}{2EI_{\omega\omega}} \cdot \frac{L^2}{k^2} z^2 \quad (3.51)$$

Substituting for the case of interest, the particular solution in equations (3.48), it is possible to obtain the general integrals of the four basic design quantities as functions of four arbitrary integration constants. To determine these constants, the boundary conditions at the ends of the beam need to be imposed. Since there are four arbitrary constants, we must set two conditions at each end of the beam. The principal forms of the boundary conditions which we are likely to encounter can be divided into the following types:

- *Clamped end* (the section is fixed so as to prevent displacements in the plane of the section (no torsional angle) and away from this plane (no warping)). These are purely kinematical boundary conditions and can be written as:

$$\theta = 0; \quad \theta' = 0 \quad (3.52)$$

- *Hinged end* (the section is fixed so as to prevent rotation about the z axis (no torsional angle) but can freely deform out of its plane (no sectorial longitudinal forces in the section)). Here, one condition is kinematical, the other statical:

$$\theta = 0; \quad M_{\omega} = 0 \quad (3.53)$$

- *Free end* (there are no statical factors at the considered end (absence of longitudinal sectorial forces and total torsional moment)). Consequently, at the free end of a beam we have purely statical boundary conditions:

$$M_{\omega} = 0; \quad T = 0 \quad (3.54)$$

Given this general overview, there are simpler and faster methods for obtaining the particular integral for various particular forms of loads. In the applications of §5, we will intend to solve the differential equation of torsion by using the method of initial parameters.

3.3 TORSION INDUCED BY A LONGITUDINAL FORCE TRANSMITTED THROUGH A RIGID ARM

Because of the importance played in what will be discussed in the case study, we examine now the case of a longitudinal force applied outside the section of the beam and transmitted to it through a rigid arm fixed at some point D of the contour (Figure 3.14 (a)).

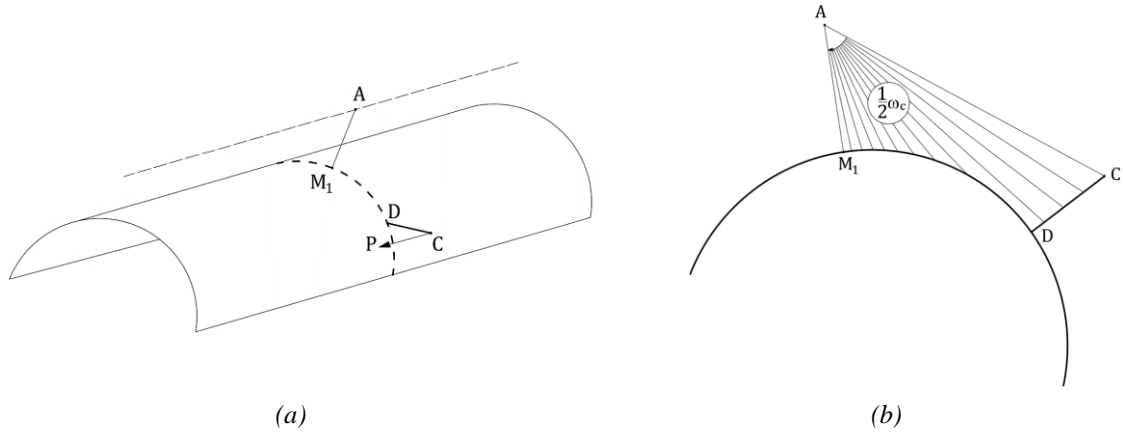


Figure 3.14: Section under a longitudinal force transmitted to it through a rigid arm

We shall, first of all, prove the following theorem:

If a rigid arm CD is fixed at some point D , at a right angle to the generator of a thin-walled beam whose cross section has a nondeformable contour and does not undergo shear deformation, the longitudinal displacements at the free end of the arm (the point C), in the most general deformation of the beam, consist of deformations determined by the law of plane sections and of a displacement which is proportional to the sectorial area ω_c . The line M_1DC , M_1 being the origin of the principal sectorial areas, serves as the basis for this sectorial area and its pole is situated in the shear centre A (Figure 3.14 (b)).

The longitudinal displacement of the end of the arm (the point C , Figure 3.15) is composed of the longitudinal displacement u_D of the base of the arm (the point D) and the relative longitudinal displacement $S_{z,CD}$ of the point C with respect to the point D , which appears as a result of the rotation of the arm CD , with respect to the line $n - n$, in the plane P of the cross section $\bar{z} = \text{const}$ and which passes through the point D at right angles to the arm CD :

$$S_{z,C} = S_{z,D} + S_{z,CD} \quad (3.55)$$

Since the point D lies on the middle surface of the beam, u_D is determined by equation (3.15):

$$S_{z,D} = w - u'x_D - v'y_D - \theta'\omega_D \quad (3.56)$$

where x_D , y_D and ω_D are the principal linear and sectorial coordinates of the point D .

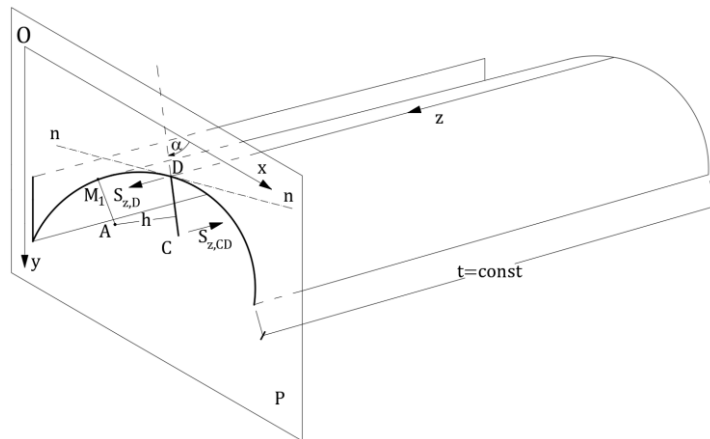


Figure 3.15: Involved longitudinal displacements

By denoting the angle formed by the direction of the arm CD with the axis x by α and the length of the perpendicular from the shear centre to the direction of the arm by h , we can determine from (3.9) the projection of the displacement of the point D on the direction of the arm:

$$S_{z,D} = u \cos \alpha + v \sin \alpha + \theta h \quad (3.57)$$

We draw a plane P through the generator of the beam, passing through the point D and the arm CD (Figure 3.16).

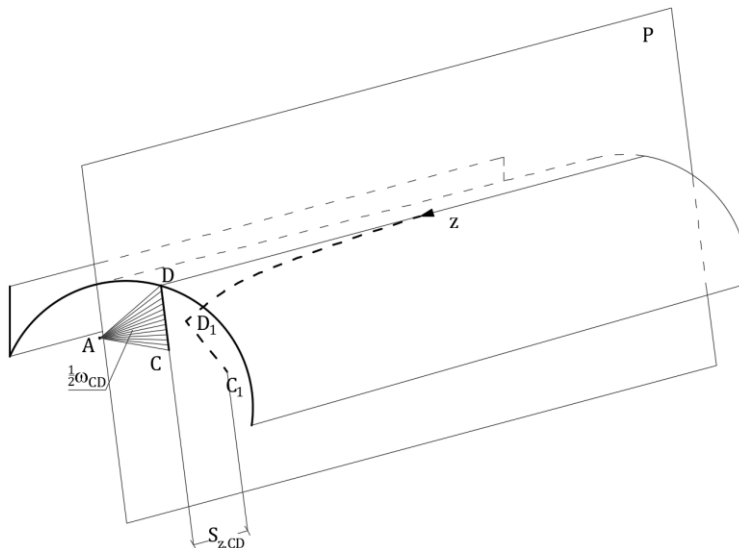


Figure 3.16: Rotation of the rigid arm

Since according to the given condition the arm CD is rigidly fixed to the contour at a right angle to the generator, it will rotate in the longitudinal plane after the deformation through a certain angle, whose tangent is given, up to second order terms, by the derivative of the displacement $S_{z,D}$ with respect to z :

$$\frac{S_{z,D}(z + dz) - S_{z,D}(z)}{dz} = \frac{dS_{z,D}}{dz} = S'_{z,D}$$

Multiplying $S'_{z,D}$ by the length of the arm CD (denoted by S_{CD}) we obtain the value of the longitudinal displacement $S_{z,CD}$ of the point C as a result of the indicated rotation of the arm CD after deformation:

$$S_{z,CD} = -S'_{z,D}S_{CD} \quad (3.58)$$

The minus sign is easily explained from Figure 3.16.

Introducing expression (3.57) in (3.58), differentiating once with respect to z , and noting that:

$$S_{CD}\cos\alpha = x_C - x_D; \quad S_{CD}\sin\alpha = y_C - y_D; \quad S_{CD}h = \omega_{CD}$$

we obtain:

$$S_{z,CD} = -u'(x_C - x_D) - v'(y_C - y_D) - \theta'\omega_{CD} \quad (3.59)$$

where x_C and y_C are the principal coordinates of the point C and ω_{CD} is twice the area of the triangle whose base is the length of the arm CD and whose height passes through the shear centre.

Introducing expressions (3.56) and (3.59) in equation (3.55) and noting that:

$$\omega_C = \omega_D + \omega_{CD} \quad (3.60)$$

we obtain:

$$S_{z,C} = w - u'x_C - v'y_C - \theta'\omega_C \quad (3.61)$$

which proves the theorem.

It is now possible to extend the concept of generalized external forces \bar{N} , \bar{M}_x , \bar{M}_y and \bar{M}_ω , which are the equivalent of the given force P in the sense of virtual work done in the displacements from the plane of the section $\bar{z} = const$, to embrace the case where the force is applied outside the contour of the cross section and transmitted to the section through a rigid arm. For these generalized forces, the equations will be:

$$\bar{N} = P \cdot 1; \quad \bar{M}_x = P \cdot y_C; \quad \bar{M}_y = -P \cdot x_C; \quad \bar{M}_\omega = P \cdot \omega_C \quad (3.62)$$

We can directly obtain the last of equations (3.67) from the following theorem:

If a longitudinal force applied outside the beam section is transmitted to the section through a rigid arm fixed at the contour point D (Figure 3.17) and if this force lies in a cross-sectional plane, the force will cause a bimoment equal to the product of the force P and twice the sectorial area AM_1DC , bounded by the two radius-vectors drawn from the shear

centre A to the origin of the contour M_1 and to the point C where the force P is applied, and by the section contour and the axis of the arm.

Let e stand for the length of the arm. We transfer the force P to the point D . In addition to the force P , we should apply a moment Pe at the point D . It is possible, in this case, to replace the longitudinal force P by statically equivalent quantities, since we are at the limits of the rigid arm (the longitudinal displacements of the arm obey the law of plane sections).

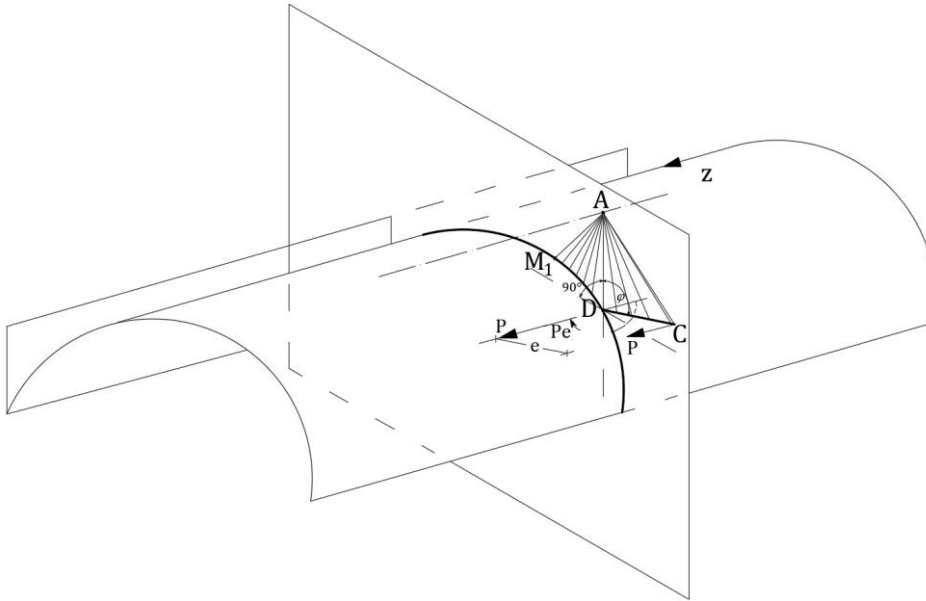


Figure 3.17: *Bimoment induced by a longitudinal force applied outside the section*

The force P , applied at a point D of the profile line, causes a bimoment $P\omega_D$, where ω_D is twice the area AM_1D . We resolve the moment at the fixed point D , equal to Pe and acting in the place of the arm, into two components; one actin in the plane of the radius-vector AD , and the other in the plane perpendicular to AD . Since its plane of action passes through the shear centre, the first moment does not cause torsion. The second moment, $Pe \sin\varphi$, causes a bimoment equal to $\overline{AD} \cdot Pe \sin\varphi$, where $\overline{AD} \sin\varphi$ is twice the area of ΔADC . Adding the two bimoments, we obtain:

$$\overline{M}_\omega = P\omega_D + P\omega_{\Delta ADC} = P\omega_C$$

where ω_C is twice the area of AM_1DC . The theorem is proved.

3.4 BEAMS REINFORCED BY CLOSELY-SPACED STRIPS

We shall now examine the problem of thin-walled beams reinforced in any longitudinal plane by transverse connections (strips, diaphragms etc). We assume that these transverse connections are closely spaced along the beam, which in this case has a channel cross-section (Figure 3.18 (a)). We shall consider such a structure as a composite spatial system consisting of a thin-walled beam and of an elastic reduced orthotropic plate equivalent in its mechanical properties to transverse connections (Figure 3.18 (b)).

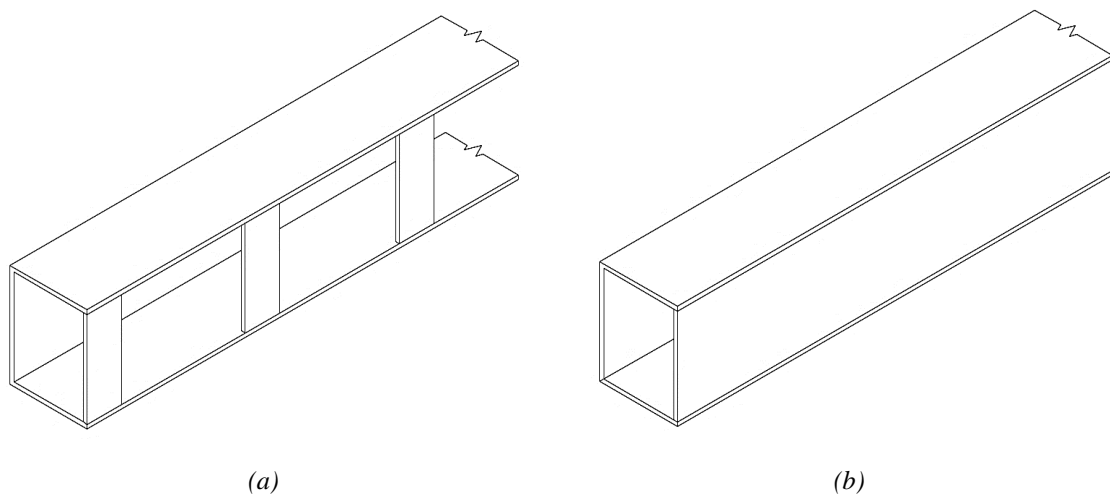


Figure 3.18: Elastic reduced orthotropic plate equivalent to the transverse connections

In our case, the orthotropy manifests itself by the plate being only able to sustain shear stresses and not tensile stresses. Making an imaginary cut along the line connecting the reduced plate to the beam, we must simulate by shear forces the action of this plate on the beam (Figure 3.19 (a)). We denote the shear forces per unit length by $V(z)$.

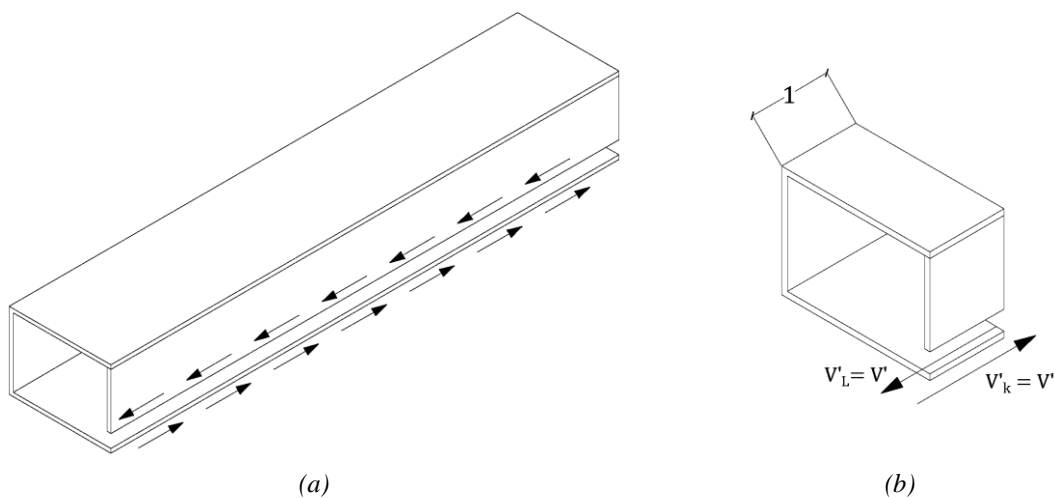


Figure 3.19: Analysis model for the transverse connections

To illustrate the problem, we write the equilibrium equations in principal coordinates for the case of only a transverse load distribution and shear forces, applied along the lateral edges:

$$\begin{aligned}
 EA w'' &= V_K - V_L \\
 EI_{yy} u^{IV} &= q_x + V'_L x_L - V'_K x_k \\
 EI_{xx} v^{IV} &= q_y + V'_L y_L - V'_K y_k \\
 EI_{\omega\omega} \theta^{IV} - GI_d \theta^{II} &= q_\omega + V'_L \omega_L - V'_K \omega_K
 \end{aligned} \tag{3.63}$$

We cut from the beam along the section $z = \text{const}$, an elementary transverse strip of unit width (Figure 3.19 (b)). On the cut we obviously have:

$$V(z) = V_K(z) = V_L(z) \tag{3.64}$$

Let Ω represents twice the area of the closed contour formed in the cross section of the contour line of the beam and the conditioning plate. Using (3.64), we write the differential equations of equilibrium (3.63), corresponding to our case, in the following form:

$$\begin{aligned}
 EA w'' &= 0 \\
 EI_{yy} u^{IV} &= q_x \\
 EI_{xx} v^{IV} &= q_y \\
 EI_{\omega\omega} \theta^{IV} - GI_d \theta^{II} &= q_\omega + V' \Omega
 \end{aligned} \tag{3.65}$$

As we can see, the presence of the conditioning elastic plate affects only the fourth equation of the system, which refers to the torsional behaviour of the beam, by means of the additional term $V' \Omega$. For a beam of closed section, this term represents the complementary torsional moment $q_{\omega V}$ due to the shear forces $V = V(z)$, uniformly distributed in the cross section $z = \text{const}$ on the contour line. We now have to express the torsional deformation of a thin-walled closed section induced by the uniform shear force V . To solve this problem, we shall start from the elasticity equation:

$$\frac{\partial S_z}{\partial s} + \frac{\partial S_t}{\partial z} = \frac{V}{G\delta} \tag{3.66}$$

Equation (3.66) for a beam-shell with a rigid cross section, takes the form:

$$\frac{\partial S_z}{\partial s} = \frac{V}{G\delta} - h\theta' \tag{3.67}$$

From this equation we find:

$$S_z = \int_0^s \frac{V}{G\delta} ds - \theta' \omega(s) + U_0(z) \tag{3.68}$$

where $U_0(z)$ is an arbitrary integration function which represents the longitudinal displacement of the origin of the coordinate s and of the sectorial area $\omega(s)$. Since the longitudinal displacement u should satisfy the condition of continuity, in all points of a closed cross section, we obtain the equation:

$$\oint \frac{V}{G\delta} ds - \theta'\Omega = 0 \quad (3.69)$$

where the integral is taken over the entire closed contour. Considering, in this equation, $V = V(z)$ not to depend on s , we obtain:

$$\delta_V V = \theta'\Omega \quad (3.70)$$

The coefficient δ_V represents here the relative longitudinal displacement of the ends of an elementary transverse strip, cut out of the shell, under the action of a unit shear force in this cut.

In the case of a closed shell, we obtain for this coefficient the equation:

$$\delta_V = \frac{1}{G} \oint \frac{ds}{\delta} \quad (3.71)$$

In the case of the composite system we examine here, having a closed cross section consisting of a shell and a reduced orthotropic plate, the coefficient δ_V can be computed by the equation:

$$\delta_V = \frac{1}{G} \oint \frac{ds}{\delta} + \delta_{pl} \quad (3.72)$$

Here, the integral in the first term is a definite integral taken over that part of the section which belongs to the thin-walled beam itself; δ_{pl} is the longitudinal relative displacement due to a force $V = 1$, which occurs as a result of the elastic flexibility of the reduced orthotropic plate only. Considering the thin-walled beam to be free of shear, i.e. assuming $G = \infty$ in equation (3.72), we obtain:

$$\delta_V = \delta_{pl} \quad (3.73)$$

Thus, the relative longitudinal displacement of the ends of the transverse strip occurs as a result of the fact that only one elastic orthotropic plate is subjected to shear.

From equation (3.70), we can get the following expression for the shear force:

$$V(z) = \frac{\Omega}{\delta_V} \theta'(z) \quad (3.74)$$

In this equation Ω and δ_V do not depend on the coordinate z . Therefore, the derivative of the shear force V with respect to z , appearing in the fourth equation of the system (3.65) can be given in the form:

$$V'(z) = \frac{\Omega}{\delta_V} \theta''(z) \quad (3.75)$$

and, consequently:

$$\Omega V'(z) = \frac{\Omega^2}{\delta_V} \theta''(z) \quad (3.76)$$

We introduce the notation:

$$\bar{I}_d = \frac{\Omega^2}{\delta_V G} \quad (3.77)$$

so that, equation (3.76) will take the form:

$$\Omega V' = G \bar{I}_d \theta''(z) \quad (3.78)$$

Using the last expression, we rewrite the differential equation of equilibrium for the torsion of the system (3.65) in the following form:

$$EI_{\omega\omega} \theta^{IV} - G(I_d + \bar{I}_d) \theta'' = q_\omega \quad (3.79)$$

We can see that equation (3.79) is identical with the usual differential equilibrium equation and, therefore, everything referring to the solution of such equation for an open section can be used for the solution of analogous problems, which refer to a thin-walled beam reinforced by transverse connections. For this purpose, it is necessary to replace the moment of inertia for a thin-walled beam in pure torsion, I_d , in all equations by the sum $I_d + \bar{I}_d$, where \bar{I}_d , as calculated by (3.77), can be called in analogy with I_d the torsional moment of inertia of a thin-walled beam with transverse connections. In particular. For the characteristic parameter k it is necessary to apply now the equation:

$$k_{var} = L \sqrt{\frac{G(I_d + \bar{I}_d)}{EI_{\omega\omega}}} \quad (3.80)$$

Moreover, instead of the equation for the torsional moment T_{DS} which appears in pure torsion, it is necessary to use the equation:

$$T_{DS} = G(I_d + \bar{I}_d) \theta' \quad (3.81)$$

Now it is necessary to compute the coefficient δ_V to define \bar{I}_d .

In the following, we consider the cases in which the transverse connection is represented by lintels and by diaphragms, since they will have a direct application when dealing with the torsional behaviour of thin-walled open cores.

3.4.1 Diaphragms

We now derive the equations which account for the influence of stiffening plates, like diaphragms, on the behaviour of a thin-walled beam. In deriving the equations, we are interested only in the torsion of the beam associated with the warping of the section.

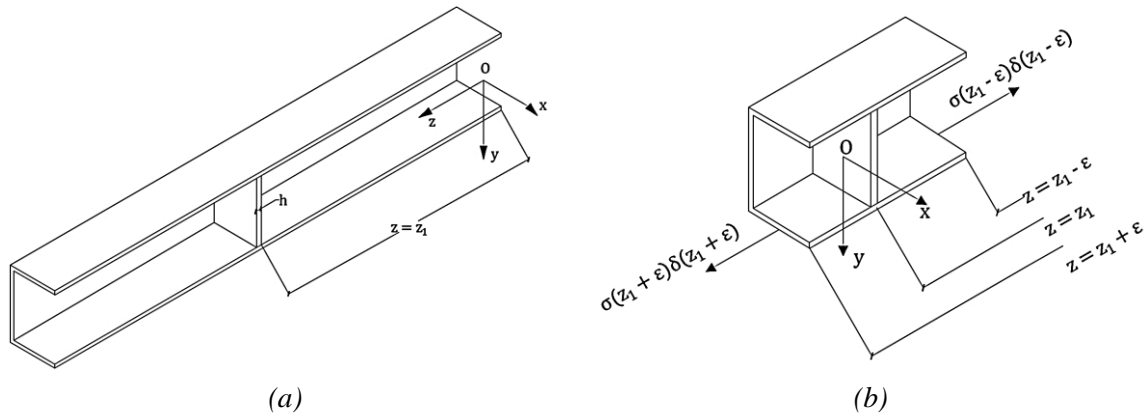


Figure 3.20: Structural scheme for diaphragms

Let's consider an elastic transverse plate of thickness h , connected to the beam in the section situated at $z = z_1$ from the initial section (Figure 3.20 (a)).

We shall solve the given contact problem by the variational method according to the principle of virtual displacements. Taking two cross sections $z = z_1 - \epsilon$ and $z = z_1 + \epsilon$, we isolate from the thin-walled beam an elementary strip which includes the plate, which we relate to the cross section $z = z_1$ (Figure 3.20 (b)), and we write for this strip the equation of virtual work. As the virtual displacement we take the longitudinal displacements $S_z(z, s)$. However, since we are interested only in the part of the displacements connected with the warping of the section, we can assume:

$$S_z(z, s) = -\theta'(z)\omega(s) \quad (3.82)$$

The displacements $w(x, y)$ away from the plane of the plate, directed along the axis Oz and appearing in the pure torsion of this plate, will be considered admissible.

From the condition of compatibility of deformation, it is obvious that the following conditions should be satisfied at the connection of the plate to the beam:

$$S_z(z_1, s) = w(x, y) \quad (3.83)$$

By equating to zero the work of external and internal forces in the corresponding virtual displacements, we obtain:

$$-\int (\sigma_1 \delta) S_z(z_1, s) ds + \int (\sigma_2 \delta) S_z(z_1, s) ds + \iint 2D(1-\nu) \left(\frac{\partial^2 w}{\partial x \partial y} \right)^2 dx dy = 0 \quad (3.84)$$

The last term, a double integral evaluated over the whole surface of the plate, expresses the work of the external forces, i.e. of the torsional moments, in the corresponding torsional deformations. This term is obtained as follows.

It is known from the theory of plates that the torsional moments are determined by the equation:

$$T_x = T_y = -D(1-\nu) \left(\frac{\partial^2 w}{\partial x \partial y} \right) \quad (3.85)$$

where $D = \frac{Eh^3}{12(1-\nu^2)}$ is the cylindrical rigidity of the plate, h is the thickness, ν is the Poisson's ratio. Each torsional moment T_x and T_y does work to produce the torsional curvature $\frac{\partial^2 w}{\partial x \partial y}$. Since the torsional moments and the torsional deformation have different signs and the work of the internal forces is taken as negative, we obtain the last term of equation (3.84) by integrating the work done by the torsional moments over the whole area of the plate.

The first two terms, expressed by integrals taken over the cross section of the thin-walled beam, refer to the work of the external forces with respect to our strip in the virtual longitudinal displacements $S_z(z_1, s)$. Such forces will be the longitudinal normal forces of the cross section $(\sigma \delta)$ for the isolated element of the beam. Here δ is the thickness of the thin-walled beam and σ the longitudinal normal stress which we denote by $(\sigma_1 \delta)$ for the section $z = z_1 - \varepsilon$ and by $(\sigma_2 \delta)$ for the section $z = z_1 + \varepsilon$.

We present these integrals in another form. Assuming $\delta ds = dA$ and using equation (3.82), we obtain:

$$\int (\sigma \delta) S_z(z_1, s) ds = -\theta'(z_1) \int \sigma w(s) dA \quad (3.86)$$

Since, by definition, $\int \sigma \omega dA = M_\omega$ represents the bimoment, we have:

$$\int (\sigma \delta) S_z(z_1, s) ds = -\theta'(z_1) M_\omega \quad (3.87)$$

Consequently, the first two terms can be replaced by:

$$(3.88)$$

$$\theta'(z_1 - \varepsilon)M_{\omega_1} - \theta'(z_1 + \varepsilon)M_{\omega_2}$$

where:

$$M_{\omega_1} = \int \sigma_1 \omega dA \qquad M_{\omega_2} = \int \sigma_2 \omega dA$$

and the integrals are evaluated over the whole area of the cross section of the beam.

It is possible to state the following regarding the bimoment M_{ω_1} and M_{ω_2} : for $\varepsilon \rightarrow 0$, i.e. for these two sections being infinitely close and in the absence of a plate, we have in the limit $M_{\omega_2} - M_{\omega_1} = 0$. With a plate M_{ω_2} will differ from M_{ω_1} by a certain value M_ω , equal to the bimoment which describes the influence of the plate on the beam.

Thus, to the two terms in the expression (3.84), written in the form of (3.88), can be given the following form in the limit for $\varepsilon \rightarrow 0$ and with a diaphragm in the section $z = z_1$:

$$[\theta'(z_1 - \varepsilon)M_{\omega_1} - \theta'(z_1 + \varepsilon)M_{\omega_2}]_{\varepsilon \rightarrow 0} = -\theta'(z_1)M_\omega \qquad (3.89)$$

where M_ω stands for the bimoment simulating the influence of the diaphragm on the beam. Considering (3.89), we can now write (for $\varepsilon \rightarrow 0$) equation (3.84) in the following form:

$$-\theta'(z_1)M_\omega + \iint 2D(1 - \nu) \left(\frac{\partial^2 w}{\partial x \partial y} \right)^2 dx dy = 0 \qquad (3.90)$$

We shall turn now to the calculation of the double integral in equation (3.90). It is known from the theory of plates that in the case of pure torsion of a plate the deflection w is determined by the equation:

$$w = Cxy \qquad (3.91)$$

where C is a constant determined by the relevant boundary conditions.

On the other hand, the bimoment due to an arbitrary balanced longitudinal load, whether distributed continuously or over the section consisting of concentrated forces, does not depend on the shear centre and on the origin of the sectorial area. Since the effect of the plate on the beam is expressed by such a balanced system of forces, we may place the pole of the sectorial areas to suit the calculation of the sectorial area $\omega(s)$ in equation (3.82).

If, in particular, we place the pole of the sectorial areas at the centre of the plate and let the axes of the coordinates pass through this centre (Figure 3.20 (b)), we obtain for $\omega(s)$ the equation:

$$\omega(s) = xy \qquad (3.92)$$

where x and y are the coordinates of the corresponding point on the contour line of the beam.

We can now write equation (3.82) for the virtual longitudinal displacement in the following form:

$$S_z(z, s) = -\theta'(z_1)xy \quad (3.93)$$

Since the compatibility conditions should be satisfied on the intersection of the contour line with the plane of the plate, we find by comparing (3.93) with (3.91) that:

$$C = -\theta'(z_1)$$

and, therefore, we have for the displacement w of the plate:

$$w(z, s) = -\theta'(z_1)xy \quad (3.94)$$

Introducing (3.94) in expression (3.90) and noting that $\frac{\partial^2 w}{\partial x \partial y} = -\theta'(z_1)$, and $\iint dx dy = A$, we obtain after reduction by $\theta'(z_1)$:

$$M_\omega = D(1 - \nu)\Omega\theta'(z_1) \quad (3.95)$$

where as usual Ω is twice the area of the plate.

Introducing the cylindrical rigidity D we can rewrite equation (3.95) in another form:

$$M_\omega = \frac{Eh^3\Omega}{12(1 + \nu)}\theta'(z_1) \quad (3.96)$$

This is the equation of the bimoment which replaces the effect of the plate on the beam. As seen from this formula, the bimoment is proportional to the relative warping of the beam in the cross section of the diaphragm. The proportionality coefficient depends on the physical characteristics and the dimensions of the diaphragm.

Comparing equation (3.96) with the usual expression of the torsional moment $GI_d\theta'$ and assuming the diaphragms as uniformly distributed at distance b , it is possible to define the torsional stiffness \bar{I}_d as follows:

$$\bar{I}_d = \frac{h^3\Omega}{6b} \quad (3.97)$$

3.4.2 Lintels

Lintels can be considered as transverse connections having the form of transverse braces of rectangular section, uniformly spaced along the span (Figure 3.21 (a)) and being subjected not only to shear but also to bending away from the plane of the cross section.

As a matter of fact, when dealing with thin-walled beams with an open section reinforced by braces, as they represent an intermediate situation between thin-walled beams of open cross

section and closed thin-walled beams, we shall proceed from the following two initial assumptions:

- The beam has, as before, a rigid section contour and shear deformations are neglected;
- The braces are deformable in their plane and their shear deformations are taken into consideration.

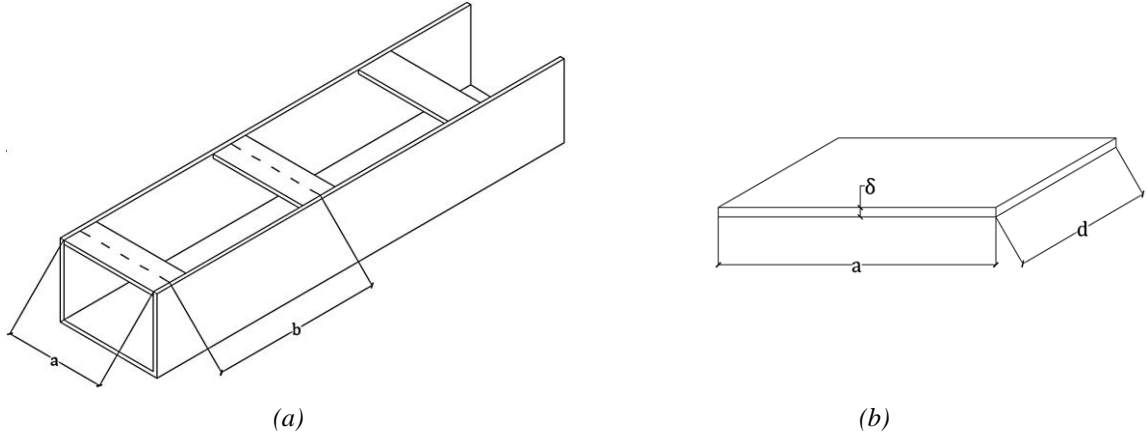


Figure 3.21: *Lintels geometry*

To compute δ_V in the case of lintels as transverse braces, we should refer to the general case of a thin-walled beam of open section, reinforced by n braces, assumed to be rigidly connected to the beam itself. Such a beam can be regarded as a composite three-dimensional structure, consisting of a cylindrical shell and a plane beam system of the Vierendeel type. If we take into consideration that the contour of the beam is considered to be nondeformable (and, therefore, the axial (longitudinal) deformations of the braces equal zero), and that, since the braces are rigidly connected with the beam, the diagram of the moments, when the braces are subjected to bending, will have the form of a skew symmetrical trapezium (Figure 3.22 (a)) with a zero point at the middle of the brace, we obtain, upon cutting the braces in the middle, a system of n equations as the fundamental system:

$$\left\{ \begin{array}{l} (\delta_{11} + \bar{\delta}_{11})Z_1 + \delta_{12}Z_2 + \dots + \delta_{1n}Z_n + \delta_{1q} = 0 \\ \delta_{21}Z_1 + (\delta_{22} + \bar{\delta}_{22})Z_2 + \dots + \delta_{2n}Z_n + \delta_{2q} = 0 \\ \dots \\ \delta_{n1}Z_1 + \delta_{n2}Z_2 + \dots + (\delta_{nn} + \bar{\delta}_{nn})Z_n + \delta_{nq} = 0 \end{array} \right. \quad (3.98)$$

The transverse forces $Z_1, Z_2, \dots, Z_i, \dots, Z_n$ which appear in the braces (Figure 3.22 (b)), are taken as the unknowns. The coefficients of these equations have the following physical meaning:

- δ_{ik} is the relative displacement of the ends of the i -th brace due to a unit force $Z_i = 1$ applied to the k -th brace. Such a displacement is in the direction of the acting forces and is determined without taking the deformations of the braces into account, since it results only from the warping of the beam.
- $\bar{\delta}_{ii}$ is the relative displacement of the ends of the i -th brace in the direction of the acting force, due to a unit force resulting from the deformation of the brace in its plane. It is determined by taking into account the shear deformation of the brace.
- δ_{iq} is the relative displacement, in the same direction, of the ends of the i -th brace, due to the given external load.

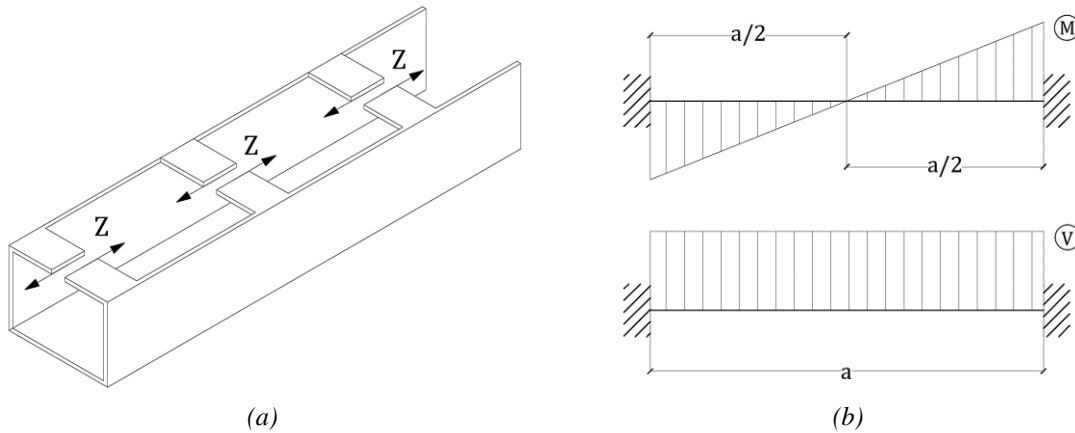


Figure 3.22: Structural scheme for lintels; Internal actions in lintels

For a single lintel, the coefficient which must be computed to define \bar{I}_d is $\bar{\delta}_{ii}$. This coefficient can be computed through the principle of virtual work by the following equation:

$$\bar{\delta}_{ii} = 2 \left(\int_0^{\frac{a}{2}} \frac{M^2}{EI} ds + \chi_V \int_0^{\frac{a}{2}} \frac{V^2}{GA} ds \right) \quad (3.99)$$

where a is the length of the brace; $I = \frac{\delta d^3}{12}$ is the moment of inertia of the brace; $A = \delta d$ is the area of the cross section of the brace; χ_V is the shear coefficient, depending on the form of the brace (for a rectangular brace $\chi_V = 1.2$). By using the diagrams of M and V shown in Figure 3.22 (b), we get:

$$\bar{\delta}_{ii} = \frac{a^3}{12EI} + \frac{1.2a}{GA} \quad (3.100)$$

Introducing the factor b , representing the step of the braces, we can transform discrete transverse connections into a conventional continuous elastic plate for which the

displacement δ_V will obviously be b times larger than for a continuous elastic plate whose cross section is equal to the longitudinal section of the brace.

Therefore, δ_V turns to have the following expression:

$$\delta_T = \frac{ab}{G} \left(\frac{a^2 G}{12EI_{br}} + \frac{1.2}{A_{br}} \right) \quad (3.101)$$

The resulting moment of inertia \bar{I}_d will be:

$$\bar{I}_d = \frac{\Omega^2}{\delta_T G} = \frac{\Omega^2}{ab} \cdot \frac{1}{\left(\frac{a^2 G}{12EI_{br}} + \frac{1.2}{A_{br}} \right)} \quad (3.102)$$

4 STRUCTURAL ANALYSIS OF OUTRIGGER SYSTEMS

4.1 OUTRIGGER-THIN-WALLED CORE INTERACTION

Let us consider a thin-walled core with an open cross-section as shown in Figure 4.1, where the abscissa \bar{z} is rigidly connected to the outrigger CO , supporting the vertical force P at the point O . The two reference systems of orthogonal axes are indicated with Gxy and $Dx'y'$, the first coinciding with the principal axes with origin in the centroid G of the section and the second with the x' , y' axes parallel to x and y , and with origin in the shear centre D .

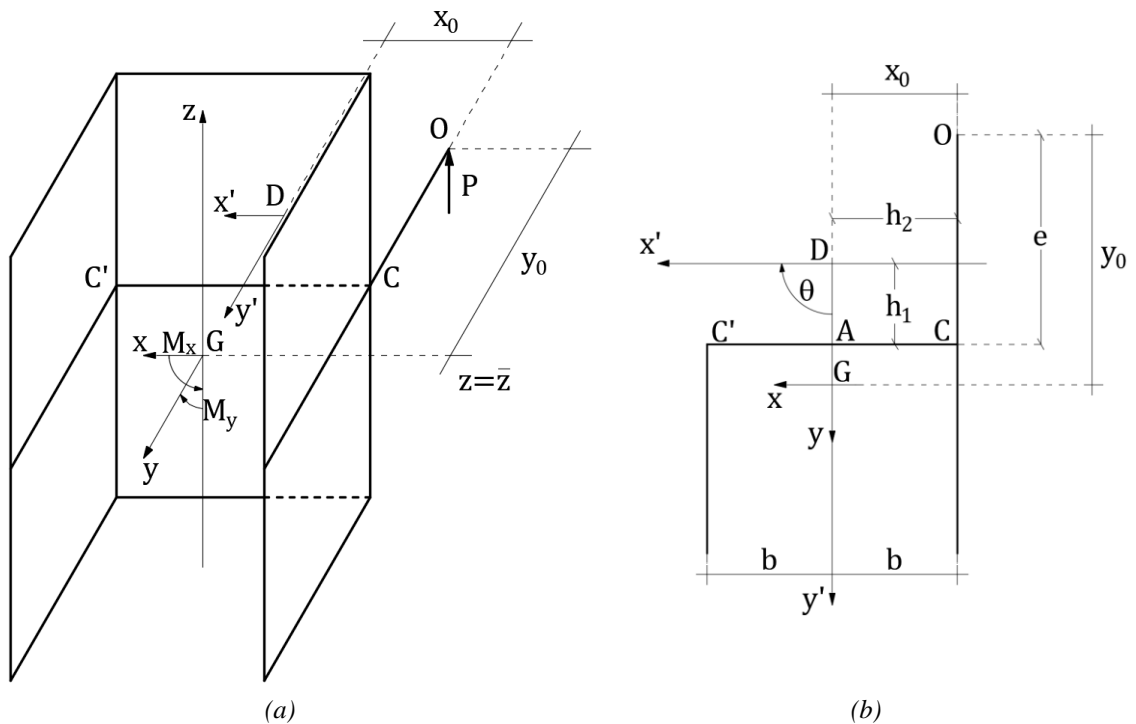


Figure 4.1: Outrigger-thin-walled core and reference axes

According to the theory of torsion discussed in §3, the structural effects induced by the load P are as given by equations (3.62):

$$N = P; \quad M_x = P \cdot x_0; \quad M_y = -P \cdot y_0; \quad M_\omega = P \cdot \omega_0 \quad (4.1)$$

According to Vlasov's theory, with reference to Figure 4.1 (b), the sectorial area ω_o referred to O can be defined as the sum of two contributions:

$$\omega_o = \omega_c + \omega_{cO} \quad (4.2)$$

Assuming the origin of the curvilinear abscissa s coinciding with A , ω_c and ω_{cO} are defined by the following expressions:

$$\omega_c = h_1 \cdot AC; \quad \omega_{cO} = h_2 \cdot CO \quad (4.3)$$

Assuming $\overline{AC} = b$ and $\overline{CO} = e$, we can rewrite (4.2) and get:

$$\omega_o = h_1 \cdot b + h_2 \cdot e = h_1 \cdot b \cdot \left(1 + \frac{h_2}{h_1} \cdot \frac{e}{b}\right) \quad (4.4)$$

When m outriggers are present, equations (4.1) can be generalized as follows:

$$N = \sum_m P_i; \quad M_x = \sum_m P_i \cdot x_{oi}; \quad M_y = -\sum_m P_i \cdot y_{oi}; \quad M_\omega = \sum_m P_i \cdot \omega_{oi} \quad (4.5)$$

Equations (4.5) represent the most general expression of the static effects induced in the core by a set of outriggers acting at abscissa \bar{z} .

The displacements u , v , w along the axes x , y , z respectively and the rotation θ around the shear centre D can be computed by means of the *Green Functions*, expressing the displacements for a unitary external force factor, applied at level \bar{z} . These functions allow to derive, by applying the principle of superimposition, the displacements induced by a general distribution of outriggers. When applying a unit longitudinal load, the equilibrium equations of the core, expressed in differential form, are given by equations (3.30) where the right-hand side terms q_x , q_y and q_ω are set equal to zero:

$$EAw'' = 0 \quad (4.6)$$

$$EI_{xx}u^{IV} = 0 \quad (4.7)$$

$$EI_{yy}v^{IV} = 0 \quad (4.8)$$

$$EI_{\omega\omega}\theta^{IV} - GI_d\theta'' = 0 \quad (4.9)$$

where A , I_{xx} , I_{yy} , $I_{\omega\omega}$ and I_d respectively represent the area, the inertia moments around the axis y , x , the warping moment of inertia and the pure torsion moment of inertia.

In other words, equations (4.6), (4.7), (4.8) and (4.9) represent the axial, bending (with respect to x , y axes) and torsional elastic lines respectively.

It must be observed that differently to what was assumed in developing the theory for thin-walled beams of open cross section, in the following we will denote by M_x and M_y the bending moments in the Gxz and Gyz planes respectively. Moreover, we use the following notation for the inertia moments:

$$I_{yy} = \int_A y^2 dA; \quad I_{xx} = \int_A x^2 dA;$$

4.1.1 Green Function: Concentrated Axial Load P

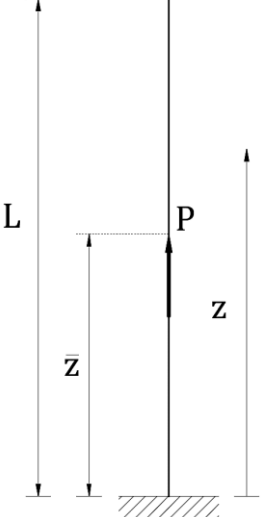
	<p>Differential equilibrium equation $EAw'' = 0$</p> <p>By integration $EAw'_i = A_i$ $EAw_i = A_i z + B_i$ with $i = 1,2$</p> <hr/> <p>Boundary conditions</p> <p>For $z = 0$ $w_1 = 0$</p> <p>For $z = \bar{z}$ $w_1 = w_2$ $EAw'_1 + EAw'_2 = P$</p> <p>For $z = L$ $EAw'_2 = 0$</p>
--	--

Table 4.1: Green Functions – Axial load P

Integrating the differential equations with the boundary conditions reported in Table 4.1, it is possible to find the four constants A_1, B_1, A_2, B_2 :

$$A_1 = P; \quad A_2 = 0; \quad B_1 = 0; \quad B_2 = P \cdot \bar{z} \quad (4.10)$$

Introducing the nondimensional abscissa $\zeta = \frac{z}{L}$, assuming $P = 1$ and replacing the constants (4.10) into the doubly integrated form of the differential equilibrium equation, it is possible to define the *Green Functions* for the axial displacement as follows:

$$\begin{aligned} w_1(\zeta, \bar{\zeta}) &= \frac{L}{EA} \cdot \zeta & 0 \leq \zeta \leq \bar{\zeta} \\ w_2(\zeta, \bar{\zeta}) &= \frac{L}{EA} \cdot \bar{\zeta} & \bar{\zeta} \leq \zeta \leq 1 \end{aligned} \quad (4.11)$$

4.1.2 Green Function: Concentrated Bending Moment M_x

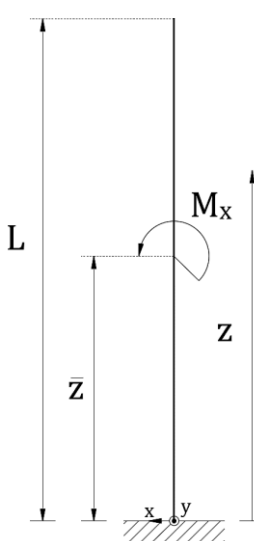
	<p>Differential equilibrium equation</p> $EI_{xx}u^{IV} = 0$ <p>By integration</p> $EI_{xx}u_i''' = A_i$ $EI_{xx}u_i'' = A_i z + B_i \quad \text{with } i = 1,2$ $EI_{xx}u_i' = A_i \frac{z^2}{2} + B_i z + C_i$ $EI_{xx}u_i = A_i \frac{z^3}{6} + B_i \frac{z^2}{2} + C_i z + D_i$ <hr/> <p>Boundary conditions</p> <p>For $z = 0$ $u_1 = 0$ $u_1' = 0$</p> <p>For $z = \bar{z}$ $u_1 = u_2$ $u_1' = u_2'$</p> $EI_{xx}u_1'' + EI_{xx}u_2'' = M_x$ $EI_{xx}u_1''' = -EI_{xx}u_2'''$ <p>For $z = L$ $EI_{xx}u_2'' = 0$</p> $EI_{xx}u_2''' = 0$
--	--

Table 4.2: Green Functions – Bending Moment M_x

Integrating the differential equations with the boundary conditions reported in Table 4.2, it is possible to find the eight constants $A_1, B_1, C_1, D_1, A_2, B_2, C_2, D_2$:

$$\begin{aligned}
 A_1 = 0; \quad B_1 = M_x; \quad C_1 = 0; \quad D_1 = 0 \\
 A_2 = 0; \quad B_2 = 0; \quad C_2 = M_x \cdot \bar{z}; \quad D_2 = -M_x \cdot \frac{\bar{z}^2}{2}
 \end{aligned}
 \tag{4.12}$$

Introducing the nondimensional abscissa $\zeta = \frac{z}{L}$, assuming $M_x = 1$ and replacing the constants (4.12) into the differential equilibrium equation integrated four times, it is possible to define the *Green Functions* for the displacement u as follows:

$$\begin{aligned}
 u_1(\zeta, \bar{\zeta}) &= \frac{L^2}{2EI_{xx}} \cdot \zeta^2 & 0 \leq \zeta \leq \bar{\zeta} \\
 u_2(\zeta, \bar{\zeta}) &= \frac{L^2 \cdot (2\zeta - \bar{\zeta}) \cdot \bar{\zeta}}{2EI_{xx}} & \bar{\zeta} \leq \zeta \leq 1
 \end{aligned}
 \tag{4.13}$$

4.1.3 Green Function: Concentrated Bending Moment M_y

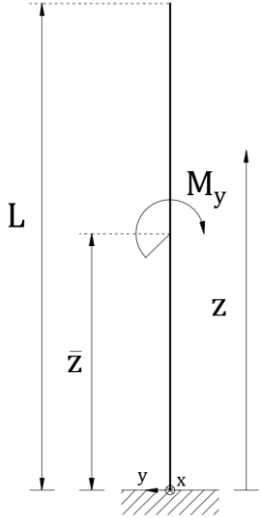
	<p>Differential equilibrium equation</p> $EI_{yy}v^{IV} = 0$ <p>By integration</p> $EI_{yy}v_i''' = A_i$ $EI_{yy}v_i'' = A_i z + B_i \quad \text{with } i = 1, 2$ $EI_{yy}v_i' = A_i \frac{z^2}{2} + B_i z + C_i$ $EI_{yy}v_i = A_i \frac{z^3}{6} + B_i \frac{z^2}{2} + C_i z + D_i$ <hr/> <p>Boundary conditions</p> <p>For $z = 0$ $v_1 = 0$ $v_1' = 0$</p> <p>For $z = \bar{z}$ $v_1 = v_2$ $v_1' = v_2'$ $EI_{yy}v_1'' + EI_{yy}v_2'' = M_y$ $EI_{yy}v_1''' = -EI_{yy}v_2'''$</p> <p>For $z = L$ $EI_{yy}v_2'' = 0$ $EI_{yy}v_2''' = 0$</p>
--	---

Table 4.3: Green Functions – Bending Moment M_y

Integrating the differential equations with the boundary conditions reported in Table 4.3, it is possible to find the eight constants $A_1, B_1, C_1, D_1, A_2, B_2, C_2, D_2$:

$$\begin{aligned}
 A_1 = 0; \quad B_1 = -M_y; \quad C_1 = 0; \quad D_1 = 0 \\
 A_2 = 0; \quad B_2 = 0; \quad C_2 = -M_y \cdot \bar{z}; \quad D_2 = M_y \cdot \frac{\bar{z}^2}{2}
 \end{aligned}
 \tag{4.14}$$

Introducing the nondimensional abscissa $\zeta = \frac{z}{L}$, assuming $M_y = 1$ and replacing the constants (4.14) into the differential equilibrium equation integrated four times, it is possible to define the *Green Functions* for the displacement v as follows:

$$\begin{aligned}
 v_1(\zeta, \bar{\zeta}) &= -\frac{L^2}{2EI_{yy}} \cdot \zeta^2 & 0 \leq \zeta \leq \bar{\zeta} \\
 v_2(\zeta, \bar{\zeta}) &= -\frac{L^2 \cdot (2\zeta - \bar{\zeta}) \cdot \bar{\zeta}}{2EI_{yy}} & \bar{\zeta} \leq \zeta \leq 1
 \end{aligned}
 \tag{4.15}$$

4.1.4 Green Function: Concentrated Bimoment M_{ω}

The problem will be solved by means of the *Method of Initial Parameters*.

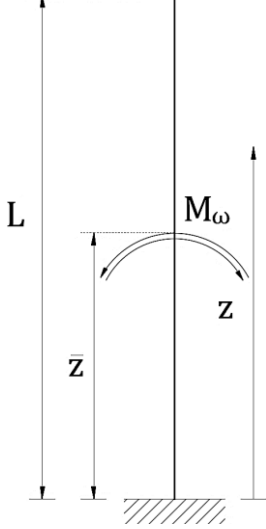
	<p>We place the origin of the z axis at the end of the core where it is fixed to the ground, consequently, the following boundary conditions at the two extremities of the core can be given:</p> <p>For $z = 0$ $\theta(0) = 0$ $\theta'(0) = 0$</p> <p>For $z = L$ $M_{\omega}(L) = 0$ $T(L) = 0$</p>
---	--

Table 4.4: Green Functions – Bimoment M_{ω} – Method of initial parameters

It is possible to write the following equations for the variation with z of the basic flexural-torsional factors:

$$\begin{aligned}
 \theta(z) &= \theta_0 + \frac{L}{k} \theta'_0 \sinh\left(\frac{k}{L}z\right) - \frac{1}{GI_d} M_{\omega 0} \left[\cosh\left(\frac{k}{L}z\right) - 1 \right] + \frac{1}{GI_d} T_0 \left[z - \frac{L}{k} \sinh\left(\frac{k}{L}z\right) \right] \\
 \theta'(z) &= \theta'_0 \cosh\left(\frac{k}{L}z\right) - \frac{k}{L} \frac{1}{GI_d} M_{\omega 0} \sinh\left(\frac{k}{L}z\right) + \frac{1}{GI_d} T_0 \left[1 - \cosh\left(\frac{k}{L}z\right) \right] \\
 T(z) &= T_0
 \end{aligned} \tag{4.16}$$

$$M_{\omega}(z) = -\frac{L}{k} GI_d \theta'_0 \sinh\left(\frac{k}{L}z\right) + M_{\omega 0} \cosh\left(\frac{k}{L}z\right) + \frac{L}{k} T_0 \sinh\left(\frac{k}{L}z\right) - \overline{M}_{\omega} \cosh\left(\frac{k}{L}(z - \bar{z})\right)$$

where θ_0 , θ'_0 , T_0 and $M_{\omega 0}$ are the initial parameters.

Introducing the boundary conditions in equations (4.16), the initial parameters turn out to be:

$$\theta_0 = 0; \quad \theta'_0 = 0; \quad T_0 = 0; \quad M_{\omega 0} = \frac{\overline{M}_{\omega} \cosh\left(\frac{k}{L}(L - \bar{z})\right)}{\cosh(k)} \tag{4.17}$$

By introducing expressions (4.17) into equations (4.16), one can completely determine the four design flexural-torsional factors for the considered case. In particular, recalling that:

$$k^2 = L^2 \frac{GI_d}{EI_{\omega\omega}}; \quad GI_d = k^2 \frac{EI_{\omega\omega}}{L^2} \rightarrow \frac{1}{GI_d} = \frac{L^2}{k^2 EI_{\omega\omega}}$$

and introducing the nondimensional abscissa $\zeta = \frac{z}{L}$, assuming $\overline{M_\omega} = 1$, the following *Green Functions* are obtained for the torsional angle θ :

$$\begin{aligned} \theta_1(\zeta, \bar{\zeta}) &= \frac{L^2}{k^2 EI_{\omega\omega}} \frac{\cosh(k) \cosh(k\bar{\zeta}) + N}{\cosh(k)} [1 - \cosh(k\zeta)] & 0 \leq \zeta \leq \bar{\zeta} \\ \theta_2(\zeta, \bar{\zeta}) &= \frac{L^2}{k^2 EI_{\omega\omega}} \left\{ \frac{M + N + Q + R}{\cosh(k)} \right\} & \bar{\zeta} \leq \zeta \leq 1 \end{aligned} \quad (4.18)$$

where M , N , Q and R are functions defined by the following equations:

$$\begin{aligned} M &= \cosh(k) [\cosh(k\bar{\zeta}) - 1]; & N &= -\sinh(k) \cdot \sinh(k\bar{\zeta}) \\ Q &= \sinh(k) \cdot \sinh(k\bar{\zeta}) \cdot \cosh(k\zeta); & R &= -\cosh(k) \cdot \sinh(k\bar{\zeta}) \cdot \sinh(k\zeta) \end{aligned} \quad (4.19)$$

For the sake of clearness, Table 4.5 lists all the *Green Functions* derived so far and that will have direct application in the case study.

Using the *Green Functions* of Table 4.5, the displacements induced by a generic distribution of outriggers can be evaluate in order to write the compatibility equations of the problem.

However, to do so it is still necessary to derive the displacement functions to account for the effects of given external loads.

In particular, introducing the generic distribution of loads $-q_z(z)$, $q_x(z)$, $q_y(z)$ and $q_\omega(z)$ in the second member of equations (4.6), (4.7), (4.8) and (4.9), we shall now solve the following equilibrium differential equations:

$$EAw'' = -q_z(z) \quad (4.20)$$

$$EI_{xx}u^{IV} = q_x(z) \quad (4.21)$$

$$EI_{yy}v^{IV} = q_y(z) \quad (4.22)$$

$$EI_{\omega\omega}\theta^{IV} - GI_d\theta'' = q_\omega(z) \quad (4.23)$$

Neglecting the axial load (i.e. $q_z(z) = 0$), we will consider two loading cases of q_x and q_y , constant or linear with maximum value at the top, obtaining u and v describing the flexural behaviour of the core. For what concerns the torsional problem, we will consider a distributed torque q_ω , obtaining θ due to this loading condition.

	Axial load P at $z = \bar{z}$	Bending Moment M_x at $z = \bar{z}$	Bending Moment M_y at $z = \bar{z}$
$0 \leq \zeta \leq \bar{\zeta}$	$w_1(\zeta, \bar{\zeta}) = \frac{L}{EA} \cdot \zeta$	$u_1(\zeta, \bar{\zeta}) = \frac{L^2}{2EI_{xx}} \cdot \zeta^2$	$v_1(\zeta, \bar{\zeta}) = -\frac{L^2}{2EI_{yy}} \cdot \zeta^2$
$\bar{\zeta} \leq \zeta \leq 1$	$w_2(\zeta, \bar{\zeta}) = \frac{L}{EA} \cdot \bar{\zeta}$	$u_2(\zeta, \bar{\zeta}) = \frac{L^2 \cdot (2\bar{\zeta} - \zeta) \cdot \bar{\zeta}}{2EI_{xx}}$	$v_2(\zeta, \bar{\zeta}) = -\frac{L^2 \cdot (2\bar{\zeta} - \zeta) \cdot \bar{\zeta}}{2EI_{yy}}$
Bimoment M_ω at $z = \bar{z} - \theta_1$ holds for $0 \leq \zeta \leq \bar{\zeta}$ while θ_2 for $\bar{\zeta} \leq \zeta \leq 1$			
$\theta_1(\zeta, \bar{\zeta}) = \frac{L^2}{k^2 EI_{\omega\omega}} \frac{\cosh(k) \cosh(k\bar{\xi}) - \sinh(k) \sinh(k\bar{\xi})}{\cosh(k)} [1 - \cosh(k\xi)]$			
$\theta_2(\zeta, \bar{\zeta}) = \frac{L^2}{k^2 EI_{\omega\omega}} \left\{ \frac{\cosh(k) [\cosh(k\bar{\xi}) - 1] - \sinh(k) \sinh(k\bar{\xi}) + \sinh(k) \sinh(k\bar{\xi}) \cosh(k\bar{\xi}) - \cosh(k) \sinh(k\bar{\xi}) \sinh(k\bar{\xi})}{\cosh(k)} \right\}$			

Table 4.5: Green Functions

4.1.5 Load Case 1: Uniform Load q_x or q_y

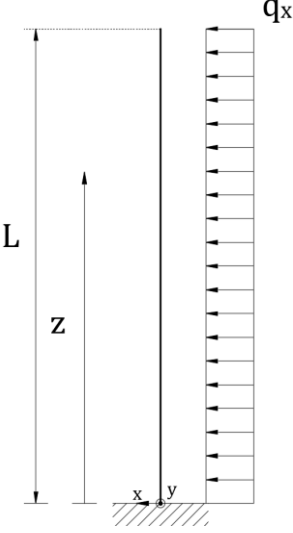
	<p>Differential equilibrium equation</p> $EI_{xx}u^{IV} = q_x$ <p>By integration</p> $EI_{xx}u''' = A + q_x z$ $EI_{xx}u'' = Az + B + q_x \frac{z^2}{2}$ $EI_{xx}u' = A \frac{z^2}{2} + Bz + C + q_x \frac{z^3}{6}$ $EI_{xx}u = A \frac{z^3}{6} + B \frac{z^2}{2} + Cz + D + q_x \frac{z^4}{24}$ <hr/> <p>Boundary conditions</p> <p>For $z = 0$ $u = 0$; $u' = 0$</p> <p>For $z = L$ $EI_{xx}u'' = 0$; $EI_{xx}u''' = 0$</p>
---	---

Table 4.6: External load effects – distributed load q_x

Integrating the differential equation with the boundary conditions reported in Table 4.6, it is possible to find the four constants A , B , C , D :

$$A = -q_x L; \quad B = \frac{q_x L^2}{2}; \quad C = 0; \quad D = 0 \quad (4.24)$$

Recalling that $-EI_{xx}u''(z) = M_x$ and $-EI_{xx}u'''(z) = V_x$, by means of constants (4.24) and introducing the nondimensional abscissa $\zeta = \frac{z}{L}$, it is possible to define the displacement u and all the basic design quantities as follows:

$$u(\zeta) = \frac{q_x L^4}{8EI_{xx}} \cdot \left(\frac{1}{3}\zeta^4 - \frac{4}{3}\zeta^3 + 2\zeta^2 \right); \quad u'(\zeta) = \frac{q_x L^3}{6EI_{xx}} \cdot (\zeta^3 - 3\zeta^2 + 3\zeta) \quad (4.25)$$

$$M_x(\zeta) = -\frac{q_x L^2}{2} \cdot (\zeta^2 - 2\zeta + 1); \quad V_x(\zeta) = -q_x L \cdot (\zeta - 1)$$

Similarly, for a uniformly distributed load q_y , we can obtain the displacement v and all the design quantities as:

$$v(\zeta) = \frac{q_y L^4}{8EI_{yy}} \cdot \left(\frac{1}{3}\zeta^4 - \frac{4}{3}\zeta^3 + 2\zeta^2 \right); \quad v'(\zeta) = \frac{q_y L^3}{6EI_{yy}} \cdot (\zeta^3 - 3\zeta^2 + 3\zeta) \quad (4.26)$$

$$M_y(\zeta) = -\frac{q_y L^2}{2} \cdot (\zeta^2 - 2\zeta + 1); \quad V_y(\zeta) = -q_y L \cdot (\zeta - 1)$$

The graphical representations of equations (4.25) are reported in the following. Clearly, these are valid also for equations (4.26).

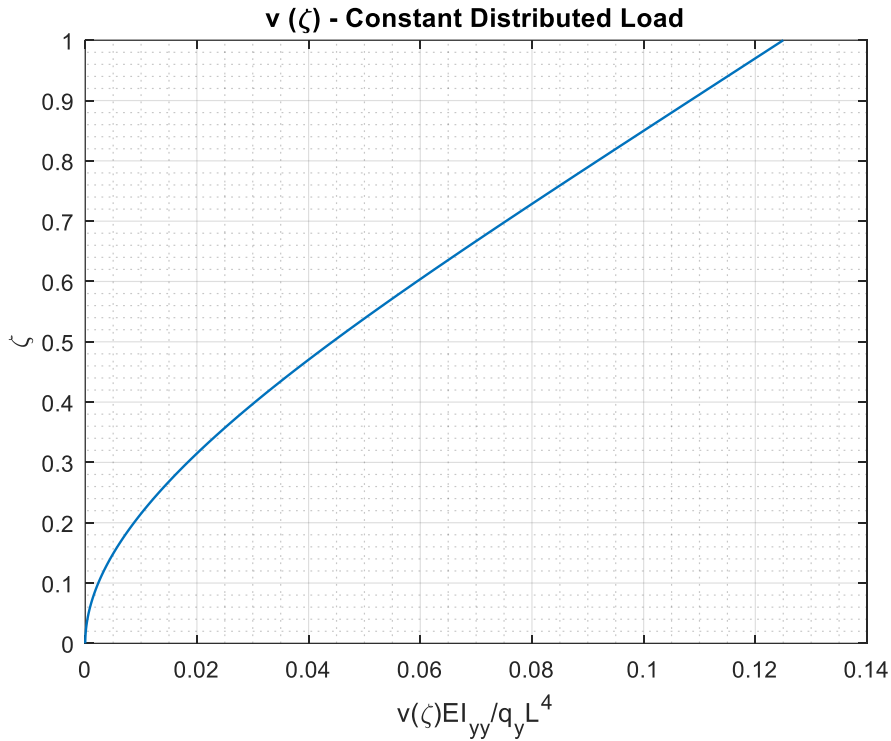


Figure 4.2: Displacement induced by a uniformly distributed load q_x

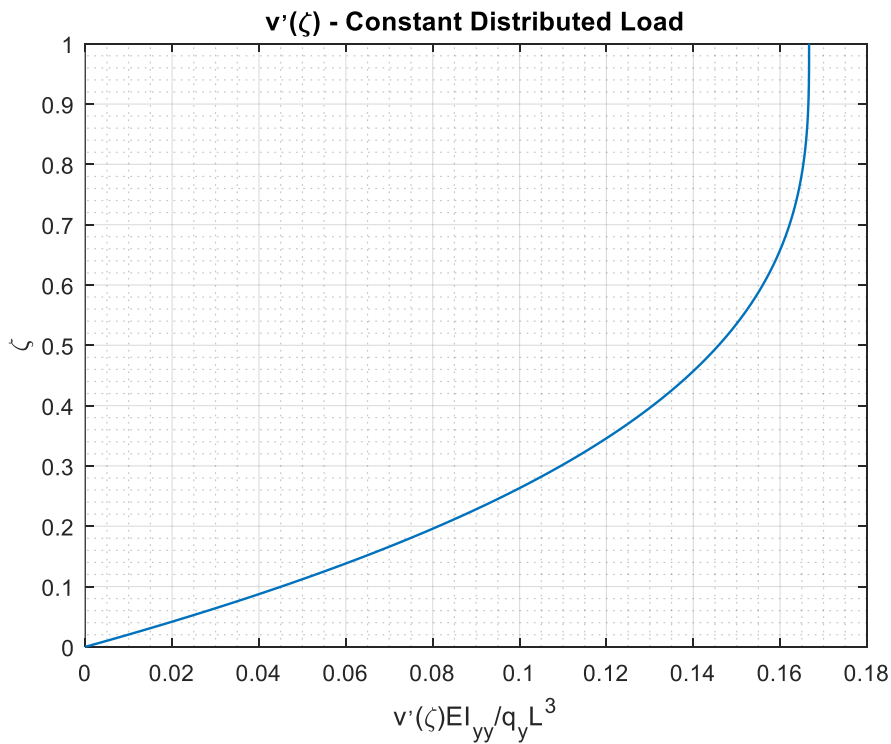


Figure 4.3: Rotation induced by a uniformly distributed load q_x

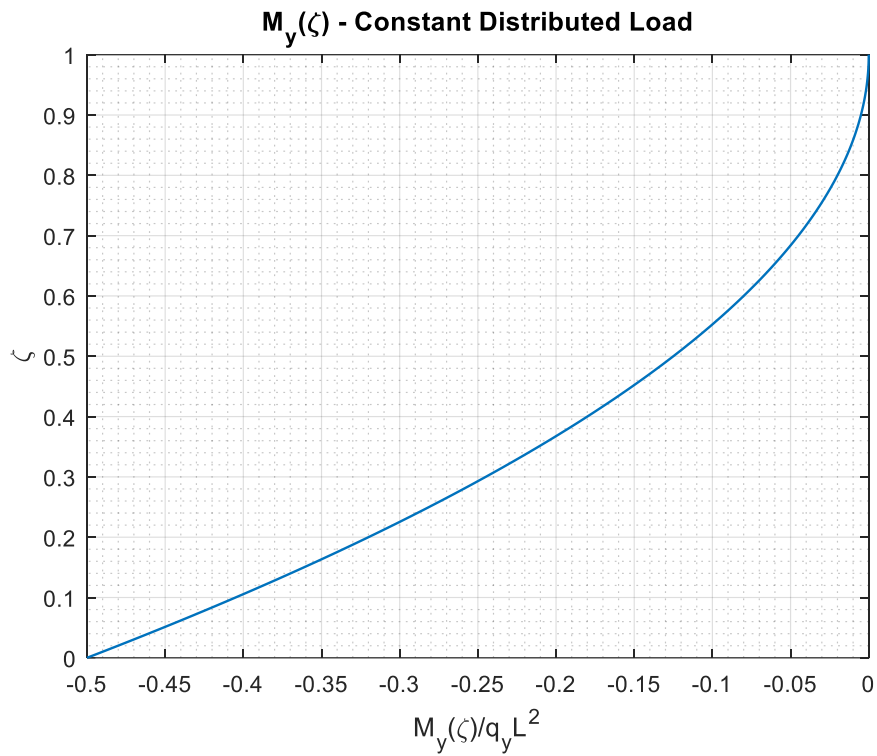


Figure 4.4: Bending moment induced by a uniformly distributed load q_x

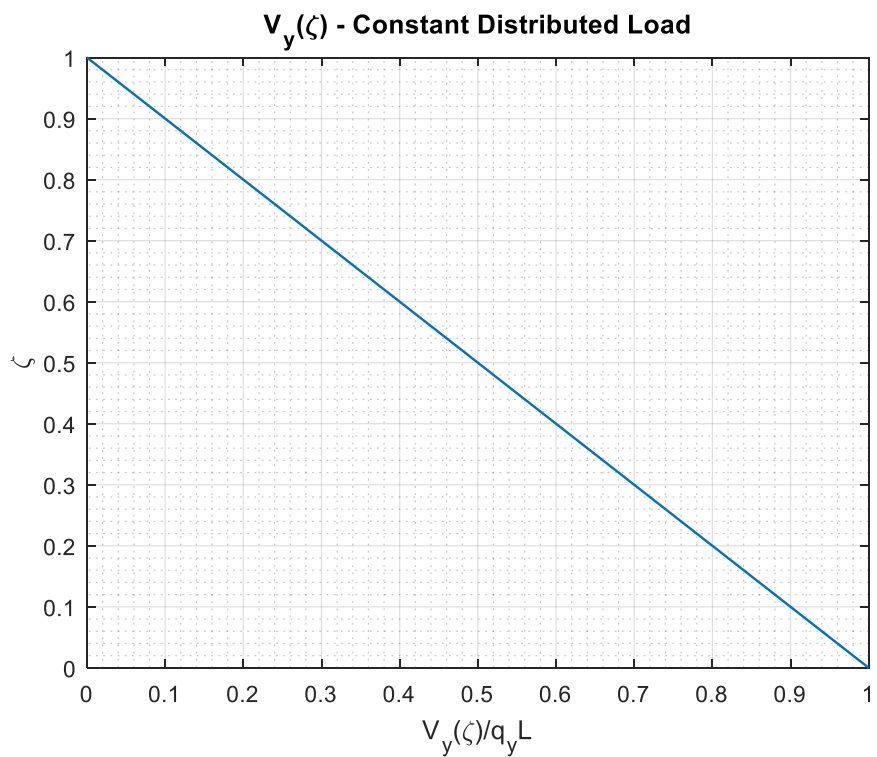


Figure 4.5: Shear force induced by a uniformly distributed load q_x

4.1.6 Load Case 2: Triangular Load with Maximum q_x or q_y at the Top

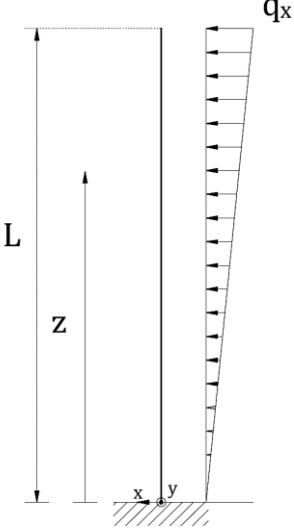
	<p>Differential equilibrium equation</p> $EI_{xx}u^{IV} = \frac{q_x z}{L}$ <p>By integration</p> $EI_{xx}u''' = A + q_x \frac{z^2}{2L}$ $EI_{xx}u'' = Az + B + q_x \frac{z^3}{6L}$ $EI_{xx}u' = A \frac{z^2}{2} + Bz + C + q_x \frac{z^4}{24L}$ $EI_{xx}u = A \frac{z^3}{6} + B \frac{z^2}{2} + Cz + D + q_x \frac{z^5}{120L}$ <hr/> <p>Boundary conditions</p> <p>For $z = 0$ $u = 0$; $u' = 0$</p> <p>For $z = L$ $EI_{xx}u'' = 0$; $EI_{xx}u''' = 0$</p>
---	---

Table 4.7: External load effects – Linearly distributed load with maximum value q_x at the top

Integrating the differential equations with the boundary conditions reported in Table 4.7 it is possible to find the four constants A , B , C , D :

$$A = -\frac{q_x L}{2}; \quad B = \frac{q_x L^2}{3}; \quad C = 0; \quad D = 0 \quad (4.27)$$

Recalling that $-EI_{xx}u''(z) = M_x$ and $-EI_{xx}u'''(z) = V_x$, by means of constants (4.27) and introducing the nondimensional abscissa $\zeta = \frac{z}{L}$, it is possible to define the displacement u and all the basic design quantities as follows:

$$u(\zeta) = \frac{11q_x L^4}{120EI_{xx}} \cdot \left(\frac{1}{11}\zeta^5 - \frac{10}{11}\zeta^3 + \frac{20}{11}\zeta^2 \right); \quad u'(\zeta) = \frac{q_x L^3}{8EI_{xx}} \cdot \left(\frac{1}{3}\zeta^4 - 2\zeta^2 + \frac{8}{3}\zeta \right) \quad (4.28)$$

$$M_x(\zeta) = -\frac{q_x L^2}{3} \cdot \left(\frac{1}{2}\zeta^3 - \frac{3}{2}\zeta + 1 \right); \quad V_x(\zeta) = -\frac{q_x L}{2} \cdot (\zeta^2 - 1)$$

Similarly, for a triangularly distributed load q_y , we can obtain the displacement v and all design quantities as:

$$v(\zeta) = \frac{11q_y L^4}{120EI_{yy}} \cdot \left(\frac{1}{11}\zeta^5 - \frac{10}{11}\zeta^3 + \frac{20}{11}\zeta^2 \right); \quad v'(\zeta) = \frac{q_y L^3}{8EI_{yy}} \cdot \left(\frac{1}{3}\zeta^4 - 2\zeta^2 + \frac{8}{3}\zeta \right) \quad (4.29)$$

$$M_y(\zeta) = -\frac{q_y L^2}{3} \cdot \left(\frac{1}{2}\zeta^3 - \frac{3}{2}\zeta + 1 \right); \quad V_y(\zeta) = -\frac{q_y L}{2} \cdot (\zeta^2 - 1)$$

The graphical representations of equations (4.28) are reported in the following. Clearly, these are valid also for equations (4.29).

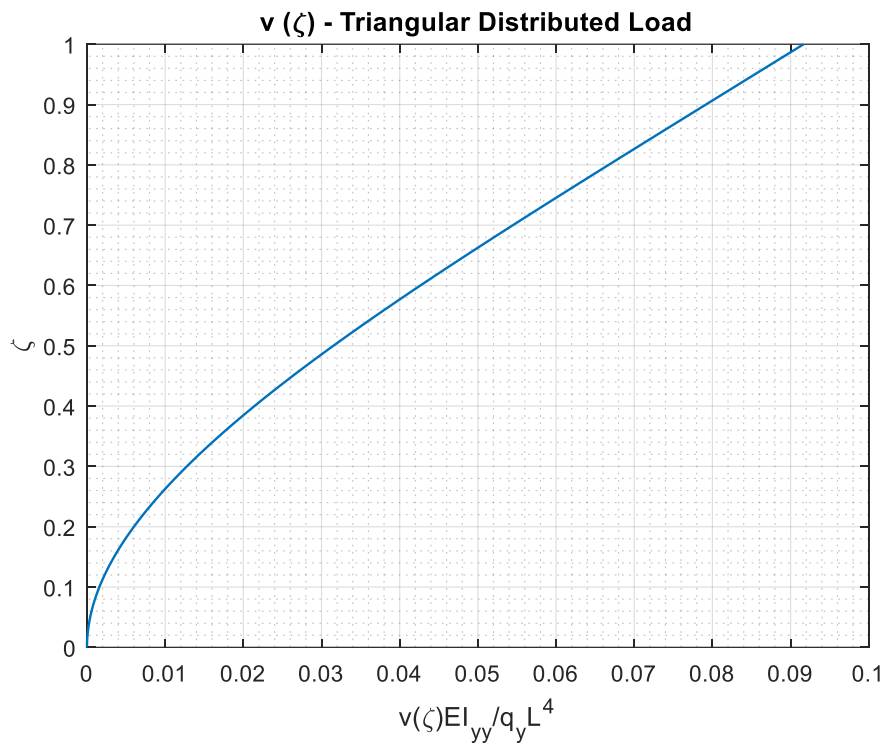


Figure 4.6: Displacement induced by a triangular load with maximum value q_x at the top

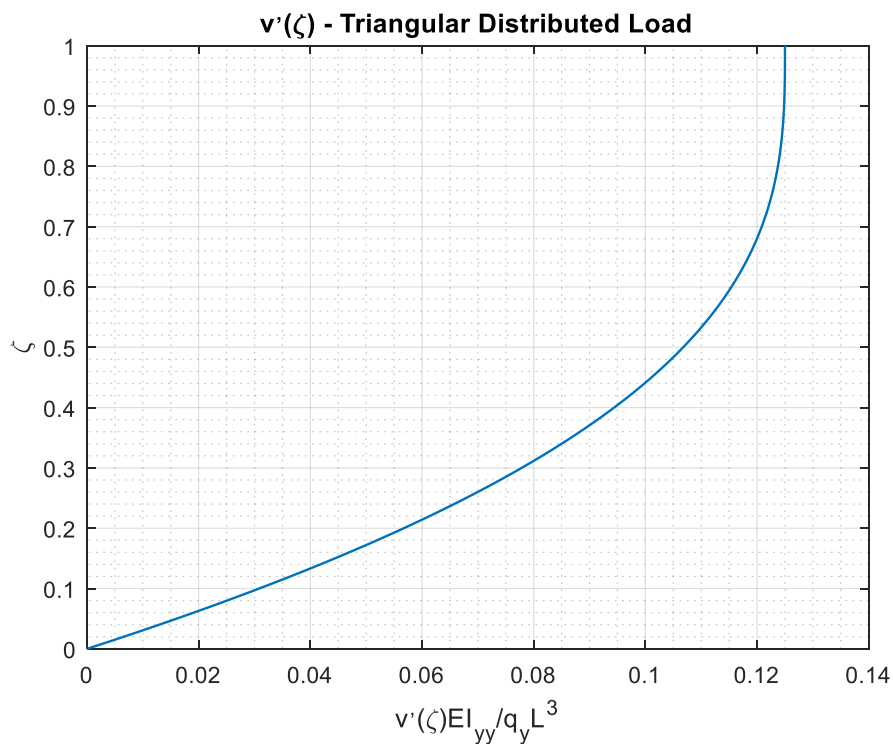


Figure 4.7: Rotation induced by a triangular load with maximum value q_x at the top

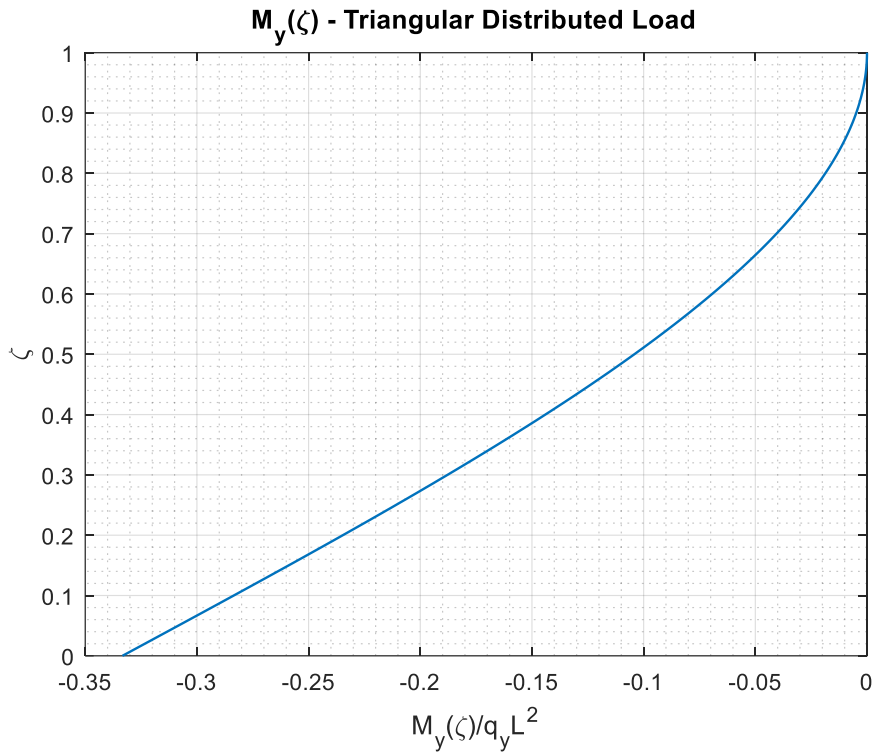


Figure 4.8: Bending moment induced by a triangular load with maximum value q_x at the top

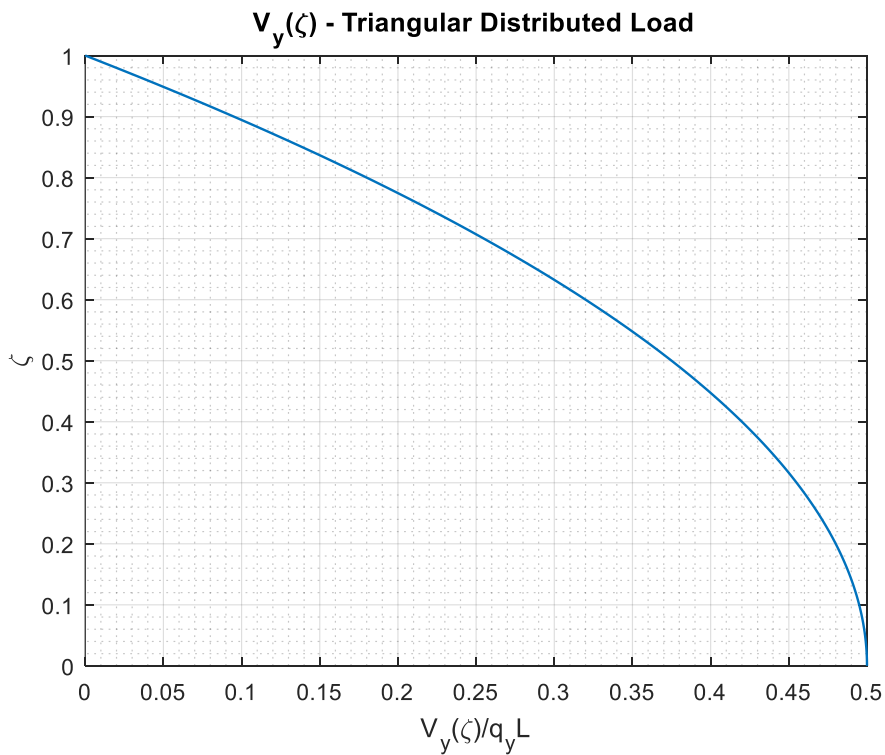


Figure 4.9: Shear force induced by a triangular load with maximum value q_x at the top

4.1.7 Load Case 3: Uniform Torque Load q_ω

The problem will be solved by means of the *Method of Initial Parameters*.

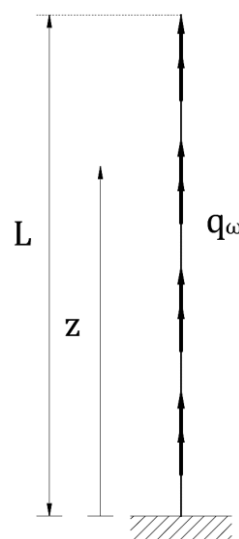
	<p>We place the origin of the z axis at the end of the core where it is fixed to the ground, consequently, the following boundary conditions at the two extremities of the core can be given:</p> <p>For $z = 0$ $\theta(0) = 0$ $\theta'(0) = 0$</p> <p>For $z = L$ $M_\omega(L) = 0$ $T(L) = 0$</p>
---	--

Table 4.8: Green Functions – Bimoment M_ω – Method of initial parameters

Considering $\bar{z}_1 = 0$ and $\bar{z}_2 = L$, the general equations for the basic flexural-torsional factors $\theta(z)$, $\theta'(z)$, $T(z)$ and $M_\omega(z)$ are given by the following equations:

$$\begin{aligned}
 \theta(z) &= \theta_0 + \theta'_0 \frac{L}{K} \sinh\left(\frac{k}{L}z\right) + \frac{M_{\omega 0}}{GI_d} \left[1 - \cosh\left(\frac{k}{L}z\right)\right] + \frac{T_0}{GI_d} \left[z - \frac{L}{k} \sinh\left(\frac{k}{L}z\right)\right] \\
 &\quad - \frac{q_\omega}{GI_d} \left\{ \frac{z^2}{2} - \frac{L^2}{k^2} \left[1 - \cosh\left(\frac{k}{L}z\right)\right] \right\} \\
 \theta'(z) &= \theta'_0 \cosh\left(\frac{k}{L}z\right) - \frac{M_{\omega 0}}{GI_d} \frac{k}{L} \sinh\left(\frac{k}{L}z\right) + \frac{T_0}{GI_d} \left[1 - \cosh\left(\frac{k}{L}z\right)\right] \\
 &\quad + \frac{q_\omega}{GI_d} \left\{ -z + \frac{L}{k} \sinh\left(\frac{k}{L}z\right) \right\} \\
 M_\omega(z) &= -GI_d \theta'_0 \sinh\left(\frac{k}{L}z\right) + M_{\omega 0} \cosh\left(\frac{k}{L}z\right) + T_0 \frac{L}{K} \sinh\left(\frac{k}{L}z\right) \\
 &\quad - q_\omega \frac{L^2}{k^2} \left\{ -1 + \cosh\left(\frac{k}{L}z\right) \right\} \\
 T(z) &= T_0 - q_\omega z
 \end{aligned} \tag{4.30}$$

where θ_0 , θ'_0 , T_0 and $M_{\omega 0}$ are the initial parameters.

Introducing the boundary conditions in equations (4.30), the initial parameters become:

$$\theta_0 = 0; \quad \theta'_0 = 0; \quad T_0 = q_\omega L; \quad M_{\omega 0} = \frac{q_\omega}{\cosh(k)} \left[\frac{L^2}{k^2} (\cosh(k) - 1) - \frac{L^2}{k} \sinh(k) \right] \tag{4.31}$$

By introducing expressions (4.31) into equations (4.30), one can completely determine the four design flexural-torsional factors for the considered case.

Introducing the nondimensional abscissa $\zeta = \frac{z}{L}$, they are:

$$\begin{aligned}
 \theta(\zeta) &= \frac{q_\omega L^4}{k^4 EI_{\omega\omega}} \left[\frac{1 + k \sinh(k)}{\cosh(k)} (\cosh(k\zeta) - 1) - k \sinh(k\zeta) + k^2 \zeta - \frac{k^2}{2} \zeta^2 \right] \\
 \theta'(\zeta) &= \frac{q_\omega L^3}{k^3 EI_{\omega\omega}} \left[\frac{1 + k \sinh(k)}{\cosh(k)} \sinh(k\zeta) - k \cosh(k\zeta) + k - k\zeta \right] \\
 M_\omega(\zeta) &= -\frac{q_\omega L^2}{k^2} \left[\frac{1 + k \sinh(k)}{\cosh(k)} \cosh(k\zeta) - k \sinh(k\zeta) - 1 \right] \\
 T_{DS}(\zeta) &= GI_d \theta' = q_\omega \frac{L}{k} \left[\frac{1 + k \sinh(k)}{\cosh(k)} \sinh(k\zeta) - k \cosh(k\zeta) + k - k\zeta \right] \\
 T_\omega(\zeta) &= -EI_{\omega\omega} \theta''' = -q_\omega \frac{L}{k} \left[\frac{1 + k \sinh(k)}{\cosh(k)} \sinh(k\zeta) - k \cosh(k\zeta) \right] \\
 T(\zeta) &= T_{DS} + T_\omega = q_\omega L (1 - \zeta)
 \end{aligned} \tag{4.32}$$

The graphical representation of equations (4.32) are reported in the following, for different values of the fundamental parameter k .

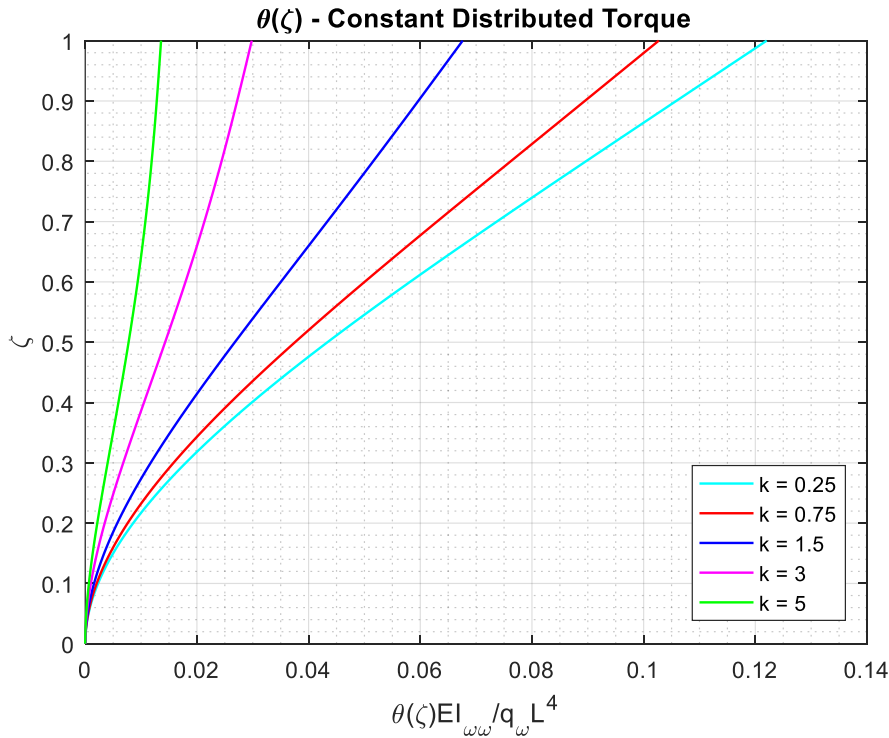


Figure 4.10: Torsional rotation for a uniform torque load q_ω

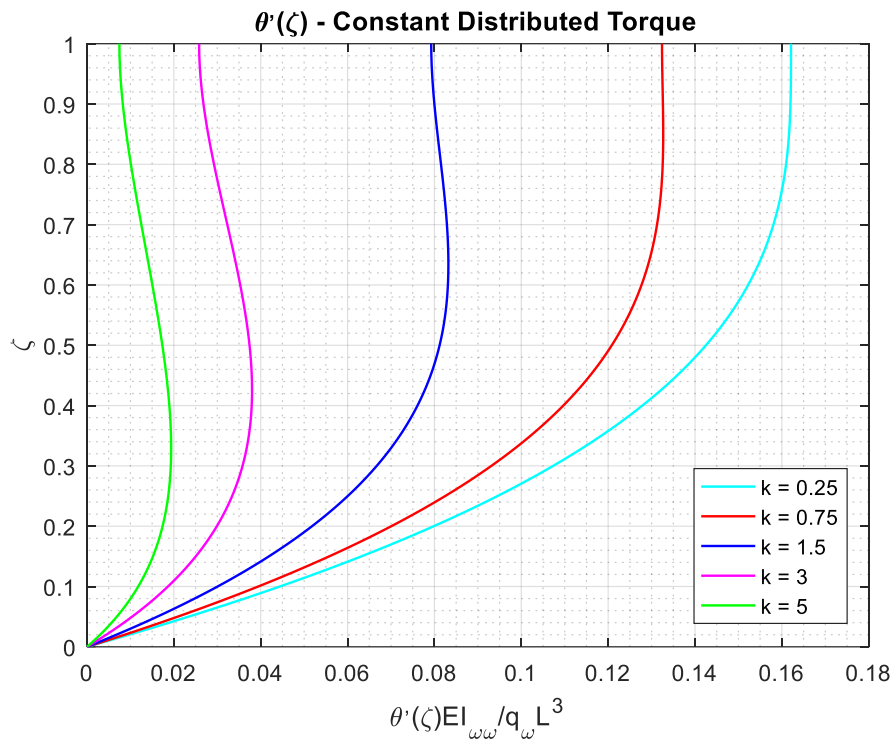


Figure 4.11: *Warping for a uniform torque load q_{ω}*

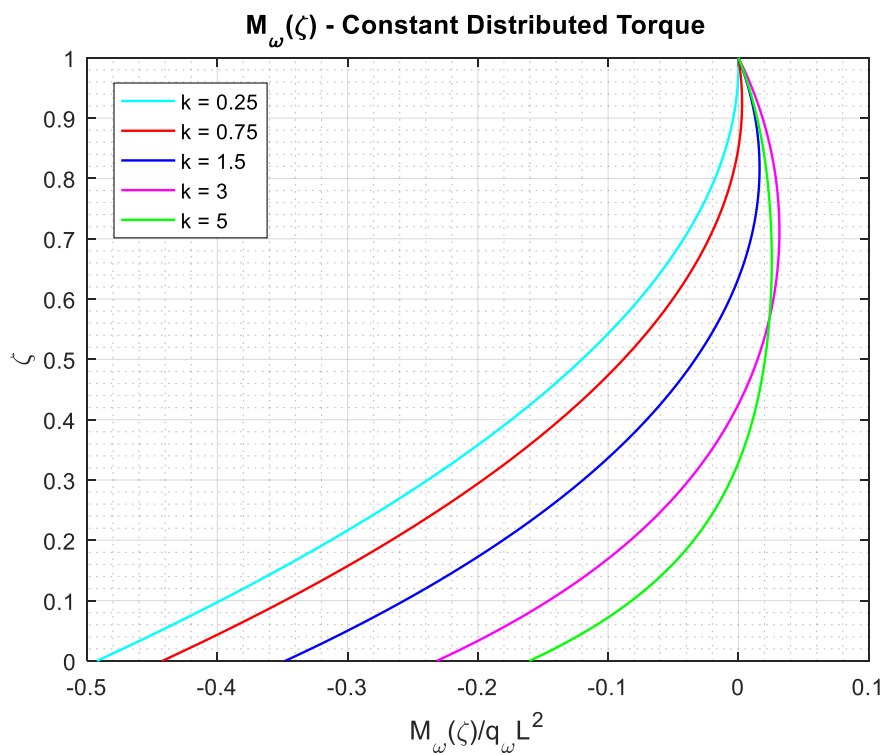


Figure 4.12: *Bimoment for a uniform torque load q_{ω}*

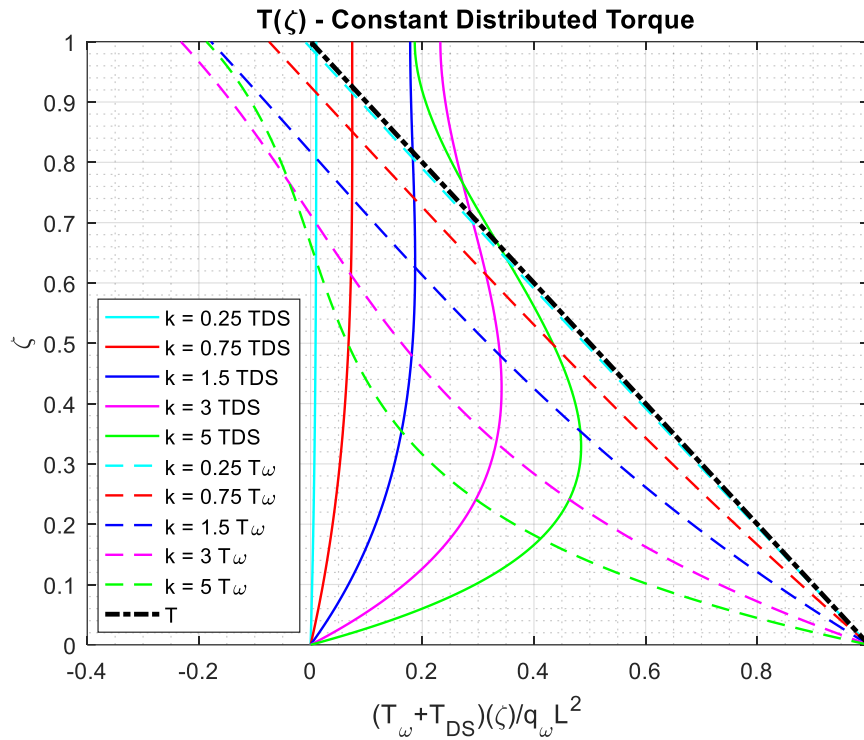


Figure 4.13: Torsional moments for a uniform torque load q_ω

For $k \rightarrow 0$, the terms in brackets of equations (4.32) assume the same form as those in equations (4.25), while for $k \rightarrow \infty$, the warping contributions T_ω and M_ω vanish. This fact aligns with the initial hypothesis of the outrigger efficiency being significant only for small values of k , i.e. when there are thin-walled open cross-sections.

4.1.8 Load Case 4: Triangular Torque Load with Maximum q_ω at the Top

As before, the problem will be solved by means of the *Method of Initial Parameters*. The only thing changing from the previous case is the term depending on the load, here computed according to the following equations:

$$\begin{aligned}
 \theta(z) &= -\frac{1}{GI_d} \int_{\bar{z}=0}^{\bar{z}=z} q_\omega \frac{\bar{z}}{L} K_{\theta T}(\bar{z}) d\bar{z} \\
 \theta'(z) &= -\frac{1}{GI_d} \int_{\bar{z}=0}^{\bar{z}=z} q_\omega \frac{\bar{z}}{L} (\bar{z}) K_{\theta' T}(\bar{z}) d\bar{z} \\
 \frac{1}{GI_d} M_\omega(z) &= -\frac{1}{GI_d} \int_{\bar{z}=0}^{\bar{z}=z} q_\omega \frac{\bar{z}}{L} (\bar{z}) K_{M_\omega T}(\bar{z}) d\bar{z} \\
 \frac{1}{GI_d} T(z) &= -\frac{1}{GI_d} \int_{\bar{z}=0}^{\bar{z}=z} q_\omega \frac{\bar{z}}{L} K_{TT}(\bar{z}) d\bar{z}
 \end{aligned} \tag{4.33}$$

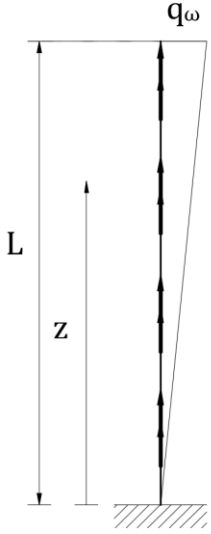
	<p>We place the origin of the z axis at the end of the core where it is fixed to the ground, consequently, the following boundary conditions at the two extremities of the core can be given:</p> <p>For $z = 0$ $\theta(0) = 0$ $\theta'(0) = 0$</p> <p>For $z = L$ $M_\omega(L) = 0$ $T(L) = 0$</p>
---	--

Table 4.9: Green Functions – Bimoment M_ω – Method of initial parameters

By following the same passages already shown for the case of a uniformly distributed torque load, the following initial parameters are obtained:

$$\theta_0 = \theta'_0 = 0; \quad T_0 = q_\omega L; \quad M_{\omega 0} = \frac{q_\omega}{\cosh(k)} \left[\frac{L^2}{k^2} \cosh(k) - \frac{L^2}{k^3} \sinh(k) - \frac{L^2}{2k} \sinh(k) \right] \quad (4.34)$$

From expressions (4.34) one can completely determine the four design flexural-torsional factors for the considered case. Introducing the nondimensional abscissa $\zeta = \frac{z}{L}$, they are:

$$\begin{aligned} \theta(\zeta) &= \frac{q_\omega L^4}{k^5 EI_{\omega\omega}} \left[F(k) \cdot (\cosh(k\zeta) - 1) - \left(\frac{k^2}{2} - 1 \right) \sinh(k\zeta) + \left(\frac{k^3}{2} - k \right) \zeta - \frac{k^3}{6} \zeta^3 \right] \\ \theta'(\zeta) &= \frac{q_\omega L^3}{k^4 EI_{\omega\omega}} \left[F(k) \cdot \sinh(k\zeta) - \left(\frac{k^2}{2} - 1 \right) \cosh(k\zeta) + \left(\frac{k^2}{2} - 1 \right) - \frac{k^2}{2} \zeta^2 \right] \\ M_\omega(\zeta) &= -\frac{q_\omega L^2}{k^3} \left[F(k) \cdot \cosh(k\zeta) - \left(\frac{k^2}{2} - 1 \right) \sinh(k\zeta) - k\zeta \right] \\ T_{DS}(\zeta) &= GI_d \theta' = q_\omega \frac{L}{k^2} \left[F(k) \cdot \sinh(k\zeta) - \left(\frac{k^2}{2} - 1 \right) \cosh(k\zeta) + \left(\frac{k^2}{2} - 1 \right) - \frac{k^2}{2} \zeta^2 \right] \\ T_\omega(\zeta) &= -EI_{\omega\omega} \theta'''' = -q_\omega \frac{L}{k^2} \left[F(k) \cdot \sinh(k\zeta) - \left(\frac{k^2}{2} - 1 \right) \cosh(k\zeta) - 1 \right] \end{aligned} \quad (4.35)$$

$$T(\zeta) = T_{DS} + T_\omega$$

where:

$$F(k) = \frac{k^2 \sinh(k) - 2 \sinh(k) + 2k}{2 \cosh(k)}$$

The graphical representations of equations (4.35) are reported in the following, for different values of the fundamental parameter k .

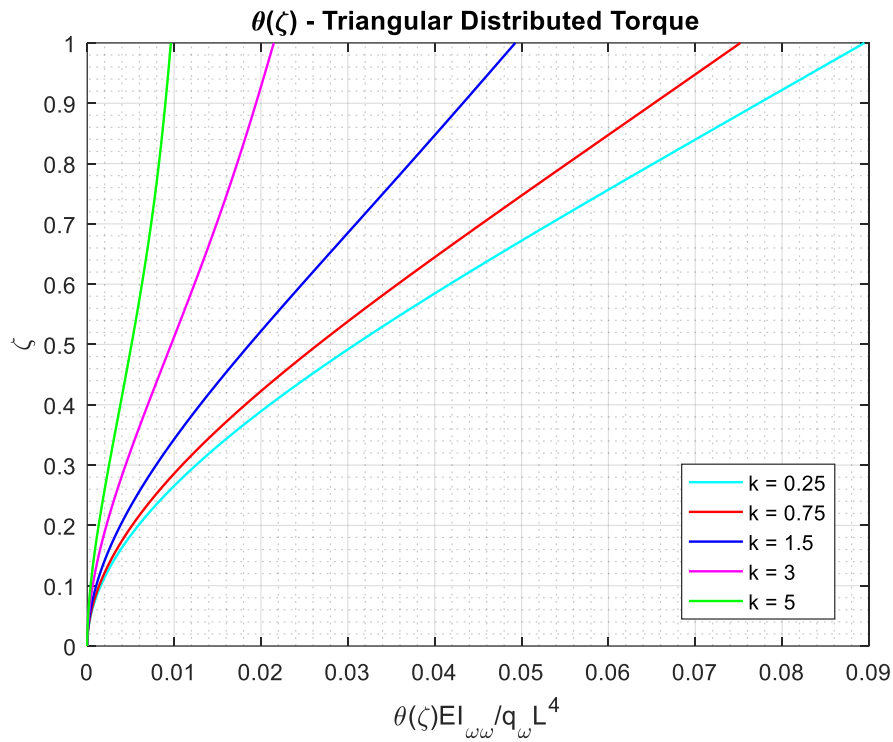


Figure 4.14: Torsional rotation for a triangular torque load q_ω

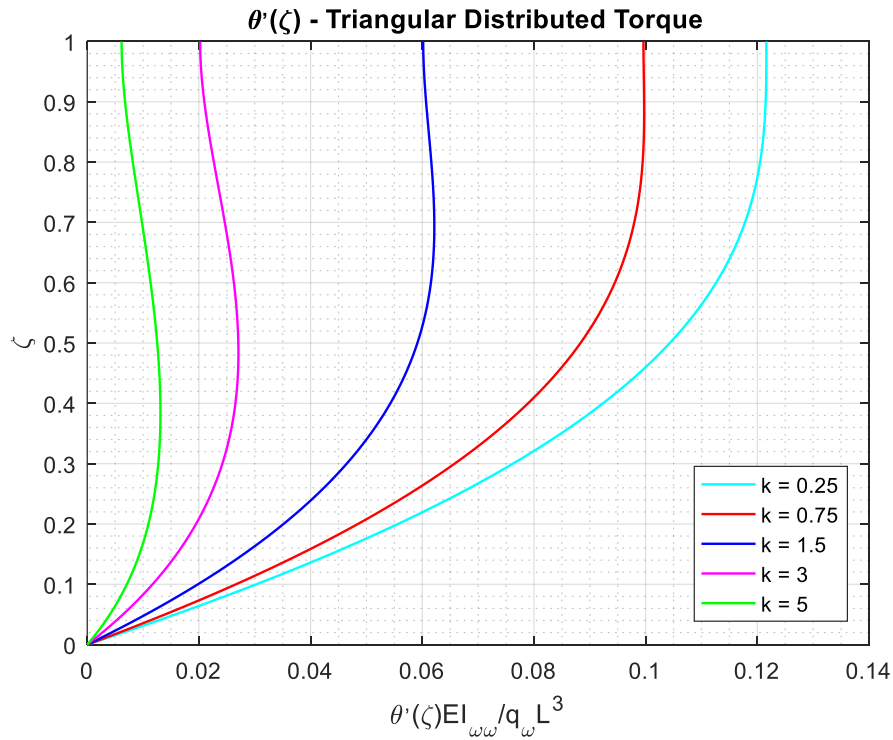


Figure 4.15: Warping for a triangular torque load q_ω

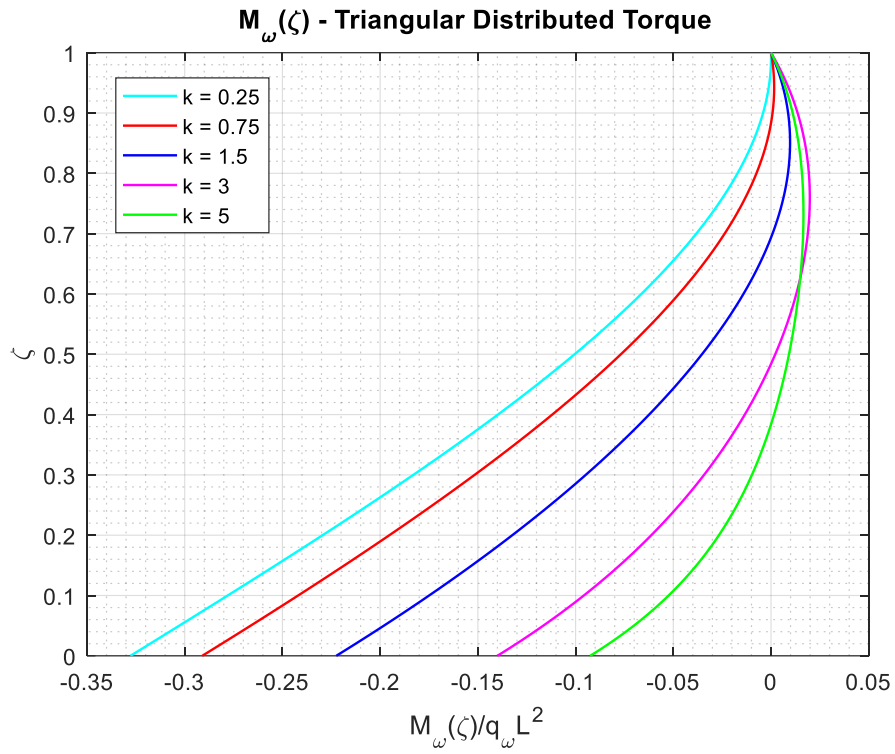


Figure 4.16: Bimoment for a triangular torque load q_ω

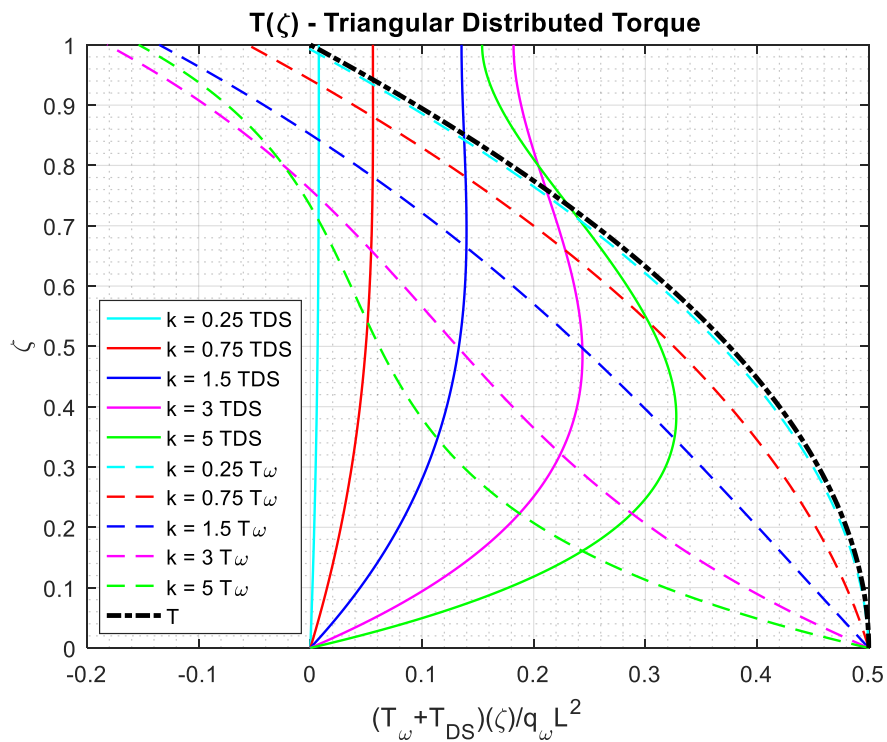


Figure 4.17: Torsional moments for a triangular torque load q_ω

4.1.9 Generalized Solution for Multiple Outrigger Structures

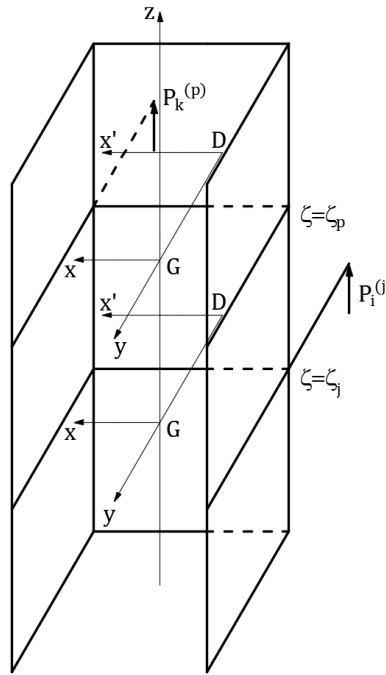


Figure 4.18: Scheme for structural analysis

Making reference to Figure 4.18, indicating by n the number of floors where outrigger systems are introduced and by m the number of outriggers present at each floor, the compatibility of longitudinal displacements between the outriggers and the columns, using the derived *Green Functions*, can be written in the subsequent way:

$$\begin{aligned}
 & \sum_{i=1}^m \sum_{j=1}^n P_i^{(j)} \left[w_h(\zeta_p, \zeta_j) + x_i^{(j)} x_k^{(p)} u'_h(\zeta_p, \zeta_j) \right] + \\
 & - \sum_{i=1}^m \sum_{j=1}^n P_i^{(j)} \left[y_i^{(j)} y_k^{(p)} v'_h(\zeta_p, \zeta_j) + \omega_i^{(j)} \omega_k^{(p)} \theta'_h(\zeta_p, \zeta_j) \right] + \\
 & \quad + \frac{P_k^{(p)} \left(e_k^{(p)} \right)^3}{3EI_k^{(p)}} + \\
 & - u'_0(\zeta_p) x_k^{(p)} - v'_0(\zeta_p) y_k^{(p)} - \theta'_0(\zeta_p) \omega_k^{(p)} \\
 & = \\
 & - \left[\sum_{r=1}^p P_k^{(r)} \frac{L\zeta^{(r)}}{(EA)_k} + \sum_{r=p+1}^n P_k^{(r)} \frac{L\zeta^{(p)}}{(EA)_k} \right]
 \end{aligned} \tag{4.36}$$

with $h = 1$ for $j \leq p$, $h = 2$ for $j \geq p + 1$, ($k = 1, 2, \dots, m$), ($p = 1, 2, \dots, n$)

We indicate by $P_i^{(j)}$ the longitudinal action applied by the i^{th} external column to the i^{th} outrigger at abscissa ζ_j and by $P_k^{(p)}$ the action exerted by the k^{th} column at abscissa ζ_p . $I_K^{(p)}$ and $(EA)_k$ represent respectively the inertia moment of the outrigger to which the force $P_k^{(p)}$ is applied and the axial rigidity of the related column while u_0, v_0, θ_0 are the core displacements produced by external loads, computed respectively by means of equations (4.25) and (4.26) in case of a uniformly distributed load, equations (4.28) and (4.29) in case of triangularly distributed load and equations (4.32) and (4.35) in case of a uniformly of triangularly distributed torque load.

Equations (4.36) consist of an algebraic system involving (mxn) unknowns represented by the axial loads $P_K^{(p)}$. By solving equations (4.36), we can compute the total state of stress and deformation of the core by summing to the effect of external loads the internal actions due to the unknowns $P_k^{(p)}$, which can be expressed by means of equations (4.5).

It is noteworthy to derive from equations (4.36) some interesting cases. We start observing that for structures symmetric with respect y we can study separately the effects produced by the axial load N and the bending moment M_y as they become independent with respect to the ones produced by M_x and M_ω . Therefore, equations (4.36) can be subdivided in two sub-systems everyone containing one half of the total unknowns. Furtherly, when the problem is doubly symmetric with respect x, y equations (4.36) become uncoupled, so that the effects of external loads can be studied in a separate way.

By analysing Figure 4.19, which shows the variation of the torsional rotation θ and the warping θ' for different values of the fundamental parameter k , in the case of a uniform torque load applied on a vertical cantilever. As it can be observed, the lower k , the higher the warping θ' of the section and thus the higher the outrigger's efficiency to counteract warping deformations. The most convenient situation in outriggers is when $0 < k < 1$, for $1 < k < 3$ the outrigger's efficiency significantly reduces while for $k > 3$ the outrigger contribution in reducing torsional displacements can be neglected.

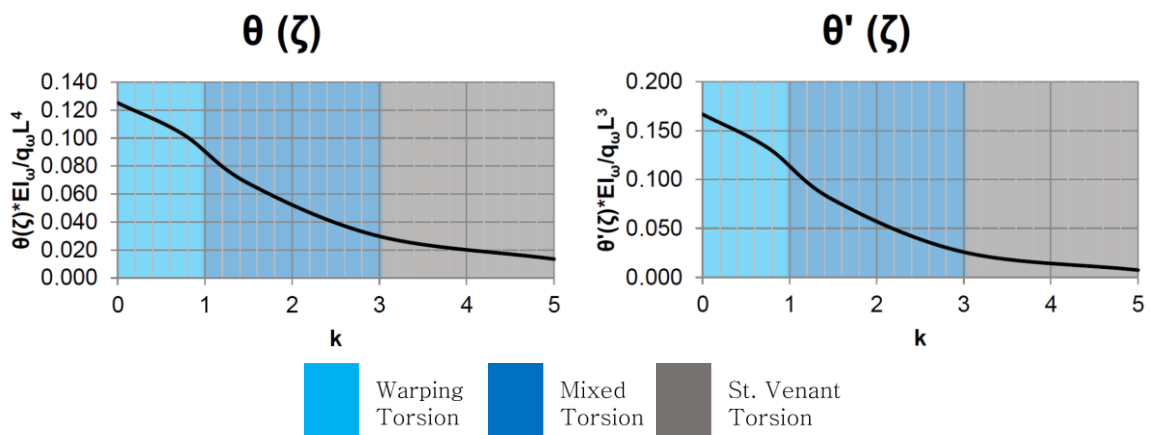


Figure 4.19: Torsional rotation and warping due to a constant distributed torque in free core

To conclude, another interesting property can be stated considering the *Green Functions* of the torsional problem of cores presenting small values of St-Venant torsional rigidity for which we can assume $GI_d = 0$, obtaining $k = 0$. Introducing $k = 0$ in equations (4.36), after some analytical passages to remove indeterminate forms, we get:

$$\begin{aligned} \theta_{10}(\zeta, \bar{\zeta}) &= -\frac{L^2}{2EI_{\omega\omega}} \cdot \zeta^2 & 0 \leq \zeta \leq \bar{\zeta} \\ \theta_{20}(\zeta, \bar{\zeta}) &= -\frac{L^2 \cdot (2\zeta - \bar{\zeta}) \cdot \bar{\zeta}}{2EI_{\omega\omega}} & \bar{\zeta} \leq \zeta \leq 1 \end{aligned} \quad (4.37)$$

As we can see, the *Green Functions* of the torsional problem become similar to the ones governing the bending behaviour. This property, which is often satisfied in practice, allows to highly simplify the problem as in this case only the Green Functions related to axial load and bending moments are necessary to obtain the general solution. Moreover, taking into account that the axial deformability of the core is generally negligible, we can assume $w_h = 0$, therefore for $k = 0$ only the bending Green Functions are needed to solve the bending-torsion interaction.

5 CASE STUDY

5.1 CHARACTERIZATION OF THE STRUCTURE

The previously discussed general procedure has been applied to study the structural behaviour of the high-rise building illustrated in Figure 5.1. The building, consisting of 40 storeys, is 170 m tall, with an interstorey height of 4.25 m.

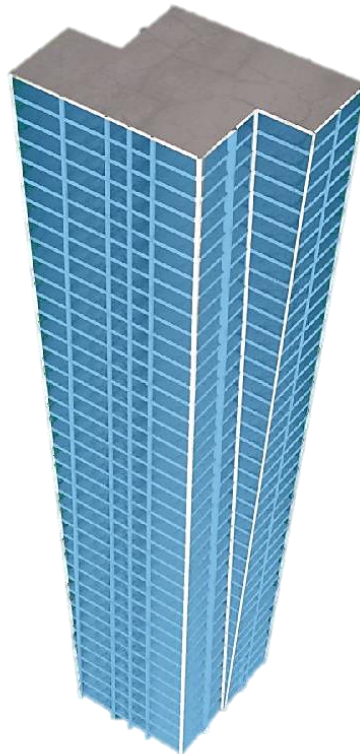


Figure 5.1: Case Study – General 3D view

The central core consists of an element with I-shaped section of maximum dimensions $d \times 2b = 15 \text{ m} \times 10 \text{ m}$, $a = 6 \text{ m}$ and constant thickness $t = 45 \text{ cm}$. Since the dimensions of the core are such that proportions (3.1) are satisfied, then the central core can be considered as an element of the thin-walled type. At the top and at mid height of the building, four outriggers with rectangular section $45 \text{ cm} \times 425 \text{ cm}$ are disposed parallel to the y -axis. The span of the outriggers is $L_0 = 2b = 10 \text{ m}$ and at their exterior edge they are connected to four circular columns having a 160 cm diameter.

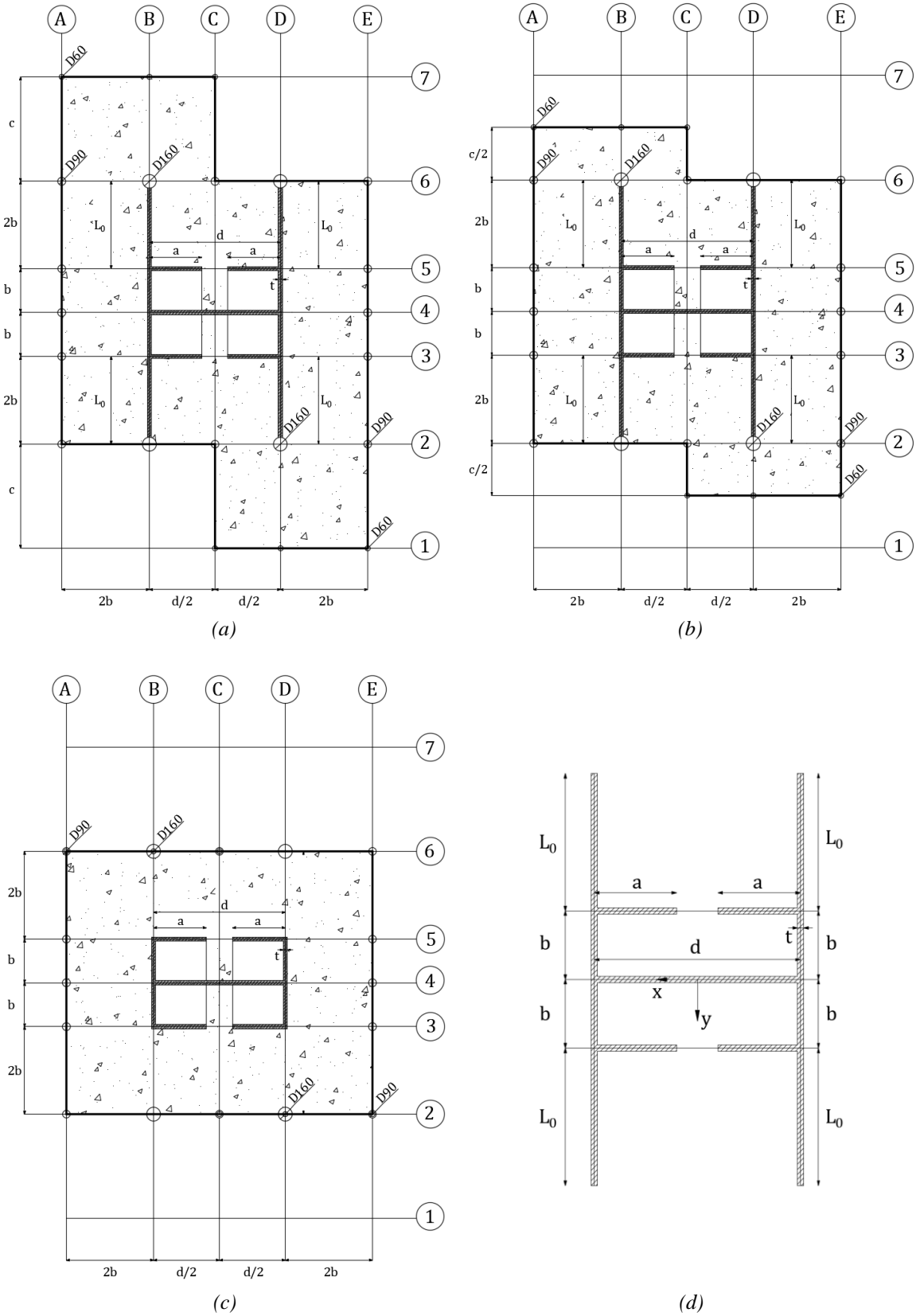


Figure 5.2: (a) Top floor; (b) Mid-height floor; (c) Mid-height floor; (d) Core-Outriggers system

On sides 2 and 6 of the building (see Figure 5.2), two triangular prismatic parts with base at the top are present, supported by concrete columns inclined by an angle $\beta = 4^\circ$ with respect to the vertical axis. The dimensions of these additional parts are $c \times (2b + d/2) = 11.90 \text{ m} \times 15 \text{ m}$ at the top and their weight per floor is indicated by $q_z(z)$. Due to the inclination of the columns, this weight can only be transferred to the ground according to an inclined pattern, this leading to two additional distributions of lateral forces $q_y(z) = q_z(z) \cdot \tan\beta$, necessary to maintain equilibrium (see Figure 5.3 (a)).

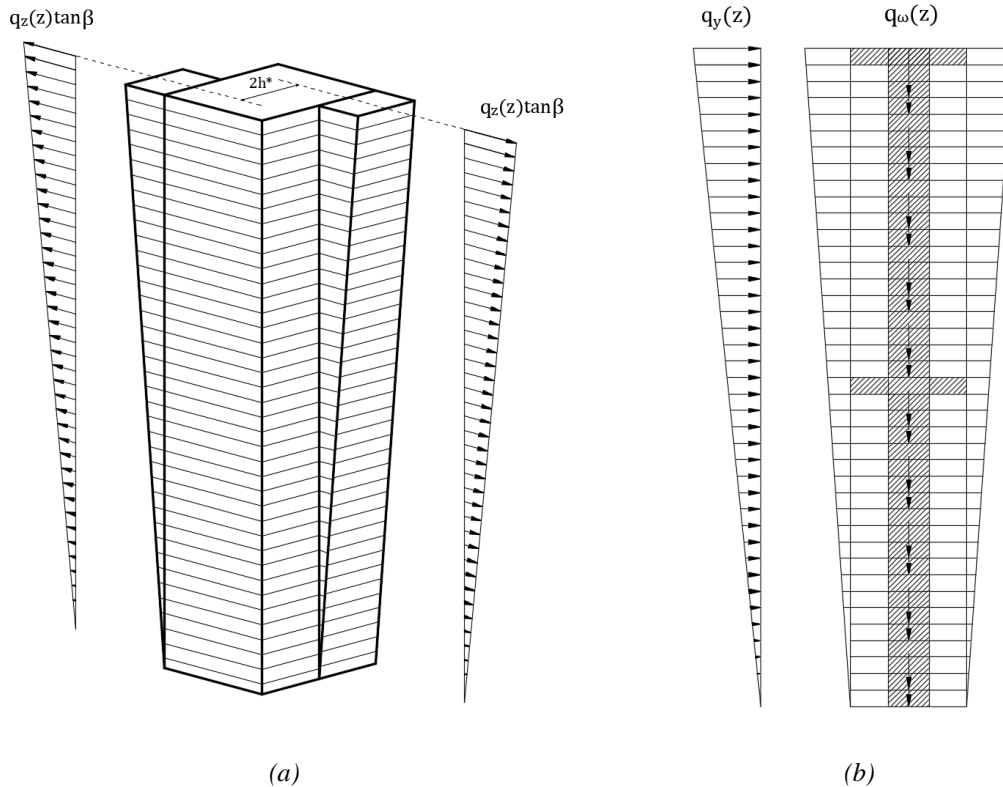


Figure 5.3: (a) Horizontal actions due to the inclined volumes; (b) Acting loads

Multiplying $q_y(z) = q_z(z) \cdot \tan\beta$ by their lever arm $2h^*$, a negative triangularly distributed torque load with maximum value at the top is produced, having expression given by:

$$q_\omega(z) = q_y(z)2h^* = \frac{q_z(L) \cdot \tan\beta \cdot 2h^*}{L} \cdot z \quad (5.1)$$

where:

$$h^* = \frac{1}{2} \left(2b + \frac{d}{2} \right) \quad (5.2)$$

Obviously, the overall resultant in the y -direction of forces $q_y(z)$ is zero.

On sides 6 and 7, the structure is also assumed to be under the action of a wind load, blowing in the positive direction of the y -axis. Since the aim of the present work is to put in evidence

the torsional behaviour of the structure, the wind load is now modelled in a simplified way by assuming a triangular distribution, with maximum value at the top. The loads acting on the structure are reported in Figure 5.3 (b).

For the sake of clearness, the geometrical features of the structure are now summarized in the following tables:

General Data

Total Height:	L	170	[m]
Interstorey Height:	l	4.25	[m]
Number of Floors:	n	40	[–]
Concrete:	C45/55		[–]

Table 5.1: General data of the building

Central Core

Flange:	$2b$	10	[m]
Web:	d	15	[m]
Lips:	a	6	[m]
Thickness:	t	45	[cm]

Table 5.2: Central core's properties

Outriggers (Rectangular Cross Section)

Width:	$t_0 = t$	45	[cm]
Height:	$h_0 = l$	425	[cm]
Span:	$L_0 = 2b$	10	[m]
Number per floor:	m	4	[–]
Diameter of supporting columns:	D	160	[cm]
Location in elevation:		Floors 19 – 20	[–]
		Floors 39 – 40	[–]

Table 5.3: Outriggers' properties

Triangular Prismatic Volumes

(Properties at the top – Top-to-Bottom variation with height: Linear)

Sides along x :	CE-1 AC-7	$2b + \frac{d}{2}$	15	[m]
Sides along y :	E-12 & C-12 A-67 & C-67	c	11.90	[m]
Angle with respect to the vertical axis:	–	β	4	[°]

Table 5.4: Triangular prismatic volumes' properties

Lastly, since they will be used in the following discussion, the values of the basic factors influencing the flexural and torsional behaviour, i.e. the inertia moments, the graph of sectorial areas, the moment of inertia for pure torsion and the sectorial moment of inertia, are now computed.

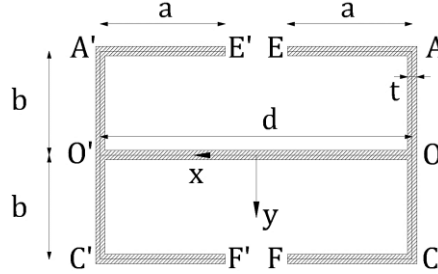


Figure 5.4: Scheme for the computation of the inertia moments

Reducing the core's cross section to its mid-line, the inertia moments can be computed by means of a piece-wise subdivision of the core through expressions:

$$I_{yy} = \int_A y^2 dA; \quad I_{xx} = \int_A x^2 dA; \quad I_G = I_{G'} + Ad^2 \quad (5.3)$$

where the last of equations (5.3) needs to be used only when the centroid G' of the considered core's trait of area A has a distance d with respect to the centroid G of the whole core.

Referring to Figure 5.4, by piece-wise subdivision the inertia moments of each trait are:

$$\begin{aligned} I_{yy}^{A'E'} &= I_{yy}^{C'F'} = I_{yy}^{AE} = I_{yy}^{CF} = ta(b)^2; \\ I_{yy}^{O'O} &= 0; \quad I_{yy}^{A'C'} = I_{yy}^{AC} = \frac{2tb^3}{3} \\ I_{xx}^{A'E'} &= I_{xx}^{C'F'} = I_{xx}^{AE} = I_{xx}^{CF} = t \frac{a^3}{12} + ta \left(\frac{d-a}{2} \right)^2 \\ I_{xx}^{O'O} &= t \frac{d^3}{12}; \quad I_{xx}^{A'C'} = I_{xx}^{AC} = 2bt \left(\frac{d}{2} \right)^2 \end{aligned} \quad (5.4)$$

By summing the contributions (5.4), the inertia moments of the core turn out to be:

$$I_{yy} = t \left[2 \frac{(2b)^3}{12} + 4ab^2 \right] = 345 m^4 \quad (5.5)$$

$$I_{xx} = t \left\{ \frac{d^3}{12} + 2b \frac{d^2}{2} + 4 \left[\frac{a^3}{12} + a \left(\frac{d-a}{2} \right)^2 \right] \right\} = 884 m^4 \quad (5.6)$$

On the other hand, the inertia moment of the outriggers is:

$$I_0 = \frac{t_0 h_0^3}{12} = 2.88 m^4 \quad (5.7)$$

For what concerns the diagram of sectorial areas, reference can be made to Figure 5.5:

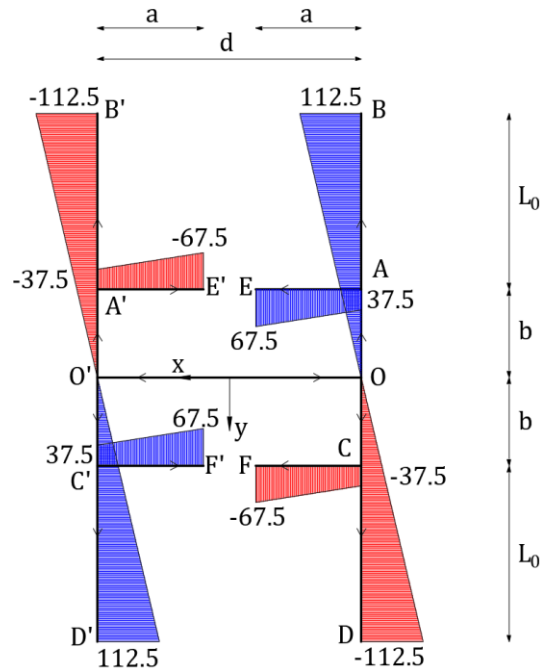


Figure 5.5: Diagram of sectorial areas - Blue: positive; Red: negative - Dimensions: m^2

where the sectorial areas of each segment composing the core-outriggers system can be computed by integration over the considered segment of the last of equations (3.14):

$$\omega(s) = \int_{b_1}^{b_2} h(s) ds \quad (5.8)$$

Here, s is the curvilinear abscissa moving along the mid-line of the core-outriggers cross section, $h(s)$ is the distance from the shear centre, here located in the origin of the reference axes x and y , of the mid-line of the considered segment, b_1 and b_2 are the extremities of the segment for which the sectorial area is computed.

According to this, the following sectorial areas are obtained:

$$\begin{aligned} \omega^O &= \omega^{O'} = 0 \\ \omega^A &= \omega^C = -\omega^{A'} = -\omega^{C'} = \frac{db}{2} \\ \omega^E &= \omega^{F'} = -\omega^{E'} = -\omega^{F'} = \frac{db}{2} + ab \\ \omega^B &= \omega^{D'} = -\omega^{B'} = -\omega^{D'} = \frac{db}{2} + \frac{dL_0}{2} \end{aligned} \quad (5.9)$$

As it can be observed, the diagram of sectorial areas of the core-outriggers system is skew-symmetric with respect to the symmetry axes and described by a linear function of s .

Using the values reported in the diagram of sectorial areas it is possible to derive the sectorial moment of inertia of the core:

$$\begin{aligned}
 I_{\omega\omega} &= \int_A \omega^2 dA = t \left[4 \int_0^b [(\omega^{OA}(s))]^2 ds + 4 \int_0^b [(\omega^{AE}(s))]^2 ds \right] = \\
 &= 4t \left(\frac{d^2 b^3}{12} + \frac{d^2 b^2}{4} a + \frac{db^2 a^2}{2} + \frac{b^2 a^3}{3} \right) = 34796.25 m^6
 \end{aligned} \tag{5.10}$$

where $\omega^{OA}(s)$ and $\omega^{AE}(s)$ are linear functions between the values computed in Figure 5.5:

$$\omega^{OA}(s) = \frac{d}{2}s; \quad \omega^{AE}(s) = \frac{db}{2} + bs \tag{5.11}$$

From equation (3.23), the moment of inertia for pure torsion is:

$$I_d = \frac{1}{3} \sum_{i=1}^n t_i^3 b_i = \frac{1}{3} t^3 [4a + 4b + d] = 1.79 m^4 \tag{5.12}$$

From the obtained values, it is finally possible to compute the value of the fundamental parameter k . Assuming a Poisson's ratio $\nu = 0.2$, we obtain $G/E = 0.417$ and therefore; according to equation (3.47):

$$k = L \sqrt{\frac{GI_d}{EI_{\omega\omega}}} = 0.787 \tag{5.13}$$

As it is possible to observe, the value of k for the present structure is lower than one, meaning that the core-outriggers system is expected to effectively reduce warping deformations when subjected to torsion, as shown in Figure 4.19.

Completed the geometrical description of the structure, from Figure 5.2 (d) it is possible to realize that the analysed core-outriggers system is symmetric with respect to both x and y axes. Therefore, the analysis of the bending and torsional behaviours of the system can be made separating the effects, since, as specified in §4.1.9, they are decoupled. To study them, two main cases will be considered in the following:

- Structure with one level of outriggers at the top;
- Structure with two levels of outriggers, at the top and at mid-height;

Moreover, when dealing with the torsional behaviour of the structure, in addition to the study of the simple core-outriggers system behaviour, the analysis will be extended to include the effects of both diaphragms and lintels of different dimensions as transverse bracings.

5.2 CORE-OUTRIGGERS INTERACTION: BENDING BEHAVIOUR

5.2.1 *Structure with One Level of Outriggers*

Indicating by P_{1y} the interaction forces between the outrigger and the column generated by the load q_y , the system of equations (4.36) turns now into a single compatibility equation with the only P_{1y} as unknown, having the form:

$$P_{1y} \left[-4v'_1(\bar{\zeta})y_0^2 + \frac{L_0^3}{3EI_0} + \bar{\zeta} \frac{L}{EA_C} \right] = v'_0(\bar{\zeta})y_0 \quad (5.14)$$

where $\bar{\zeta} = 1$ represents the level of the outriggers, that is, in this case, the top of the structure.

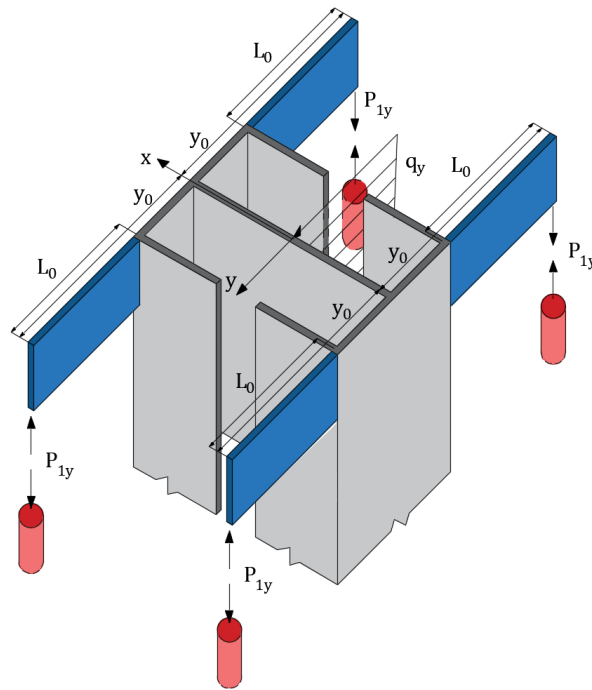


Figure 5.6: Core-outriggers interaction flexural forces - Case: One level of outriggers

In equation (5.14) it is possible to recognize 4 different contributions:

- $4 \cdot P_{1y} \cdot v'_1(\bar{\zeta})y_0^2$ represents the displacement in the column due to the rotation of the core given by the unknown bending moment $P_{1y} \cdot y_0$, assuming the outrigger as rigid. The factor 4 is due to the presence of 4 outriggers at the outriggers' level.
- $P_{1y} \cdot L_0^3/3EI_0$ is the displacement contribution given by the flexural deformability of the outrigger, assumed as a horizontal cantilever subjected to a vertical force at the free end.
- $P_{1y} \cdot \bar{\zeta} \cdot L/EA_C$ is the displacement due to axial deformability of the column.

- $v'_0(\bar{\zeta})y_0$ is the displacement in the column due to the external triangular load.

Computing the rotation $v'_1(\bar{\zeta})$ by deriving the corresponding *Green Function* of Table 4.5 and $v'_0(\bar{\zeta})$ according to the second of equations (4.29), it is possible to explicit all the contributions of equation (5.14) as:

$$\begin{aligned}
 -4P_{1y}v'_1(\bar{\zeta})y_0^2 &= 4P_{1y}\frac{L}{EI_{yy}}y_0^2 \\
 P_{1y}\frac{L_0^3}{3EI_0} &= P_{1y}\frac{L_0^3}{3EI_0} \\
 P_{1y}\bar{\zeta}\frac{L}{EA_C} &= P_{1y}\frac{L}{EA_C} \\
 v'_0(\bar{\zeta})y_0 &= \frac{q_yL^3}{8EI_{yy}}y_0
 \end{aligned} \tag{5.15}$$

Substituting equations (5.15) in the compatibility equation (5.14), yields the unknown P_{1y} with the following expression:

$$P_{1y} = q_yL \cdot \frac{3(y_0/L)}{96(y_0/L)^2 + 8(L_0/L)^3 \cdot I_{yy}/I_0 + 24(I_{yy}/L^2A_C)} \tag{5.16}$$

From the numerical data, P_{1y} and the related bending moment M_{1y} acting on the core are:

$$\begin{aligned}
 P_{1y} &= 0.2438 \cdot q_yL \\
 M_{1y} &= 4P_{1y}L \cdot \frac{y_0}{L} = 0.0860 \cdot q_yL^2
 \end{aligned} \tag{5.17}$$

Once we know these quantities, it is possible to define the displacement v of the core by applying the principle of superposition between the displacement $v_0(\zeta)$ due to the external load and the displacement $v_1^{M_{1y}}(\zeta, 1)$ due to the reaction of the column:

$$v(\zeta, \bar{\zeta}) = v_0(\zeta) + v_1^{M_{1y}}(\zeta) \tag{5.18}$$

In particular, $v_0(\zeta)$ is defined by equation (4.29) while $v_1^{M_{1y}}(\zeta, 1)$ is obtained by multiplying $v_1(\zeta)$ in Table 4.5 by M_{1y} defined by equation (5.17).

Given this, the rotation $v'(\zeta, \bar{\zeta})$ and the bending moment $M_y(\zeta, \bar{\zeta})$ can be defined by following the same path of reasoning, reading:

$$v'(\zeta, \bar{\zeta}) = v'_0(\zeta) + v'_1^{M_{1y}}(\zeta) \tag{5.19}$$

$$M_y(\zeta, \bar{\zeta}) = M_{0y}(\zeta) + M_{1y} \tag{5.20}$$

5.2.2 *Structure with Two Levels of Outriggers*

Differently to the previous case, here we have two unknown axial forces, therefore two compatibility equations are needed, one for each level of outriggers. It is important to highlight that in this case the two equations are coupled because the effects of one level of outriggers are present on the other, and vice versa. This means that it is necessary to solve a system of two coupled equations in the unknowns P_{1y} and P_{2y} :

$$\begin{aligned} P_{1y} \left[-4v'_1(\bar{\zeta}_1, \bar{\zeta}_1)y_0^2 + \frac{L_0^3}{3EI_0} + \bar{\zeta}_1 \frac{L}{EA_C} \right] + P_{2y} \left[-4v'_1(\bar{\zeta}_1, \bar{\zeta}_2)y_0^2 + (\bar{\zeta}_2 - \bar{\zeta}_1) \frac{L}{EA_C} \right] &= v'_0(\bar{\zeta}_1)y_0 \\ P_{1y} \left[-4v'_2(\bar{\zeta}_2, \bar{\zeta}_1)y_0^2 + \bar{\zeta}_1 \frac{L}{EA_C} \right] + P_{2y} \left[-4v'_1(\bar{\zeta}_2, \bar{\zeta}_2)y_0^2 + \frac{L_0^3}{3EI_0} + \bar{\zeta}_2 \frac{L}{EA_C} \right] &= v'_0(\bar{\zeta}_2)y_0 \end{aligned} \quad (5.21)$$

The first of equations (5.21) is the compatibility equation at the 1st level of outriggers (mid-height: $\bar{\zeta}_1 = 0.5$) while the second is written at the 2nd level of outriggers (top: $\bar{\zeta}_1 = 1$).

For the first compatibility equation, it is possible to recognize the following 6 contributions:

- $4 \cdot P_{1y} \cdot v'_1(\bar{\zeta}_1, \bar{\zeta}_1)y_0^2$ represents the displacement in the column at the 1st level of outriggers due to the rotation of the core given by the unknown bending moment $P_{1y} \cdot y_0$ deriving from the axial force at the 1st level of outriggers, assuming the outrigger as rigid. Note that the factor 4 is due to the presence of 4 outriggers at the outriggers level.
- $P_{1y} \cdot L_0^3/3EI_0$ is the displacement contribution given by the flexural deformability of the outrigger, assumed as a horizontal cantilever subjected to a vertical force at the free end.
- $P_{1y} \cdot \bar{\zeta}_1 \cdot L/EA_C$ is the displacement due to the axial deformability of the column at 1st level of outriggers, given by the axial force at the 1st level of outriggers.
- $4 \cdot P_{2y} \cdot v'_1(\bar{\zeta}_1, \bar{\zeta}_2)y_0^2$ represents the displacement in the column at 1st level of outriggers due to the rotation of the core given by the unknown bending moment $P_{2y} \cdot y_0$ deriving from the axial force at the 2nd level of outriggers, assuming the outrigger as rigid. Notice that the factor 4 is due to the presence of 4 outriggers at the outriggers level.
- $P_{1y} \cdot (\bar{\zeta}_2 - \bar{\zeta}_1) \cdot L/EA_C$ is the displacement due to axial deformability of the column at 1st level of outriggers, given by the axial force at the 2nd outriggers level.
- $v'_0(\bar{\zeta}_1)y_0$ is the displacement in the column due to the external triangular load, at 1st level of outriggers.

All contributions appearing in the second of equations (5.21) can be defined following the same path of reasoning.

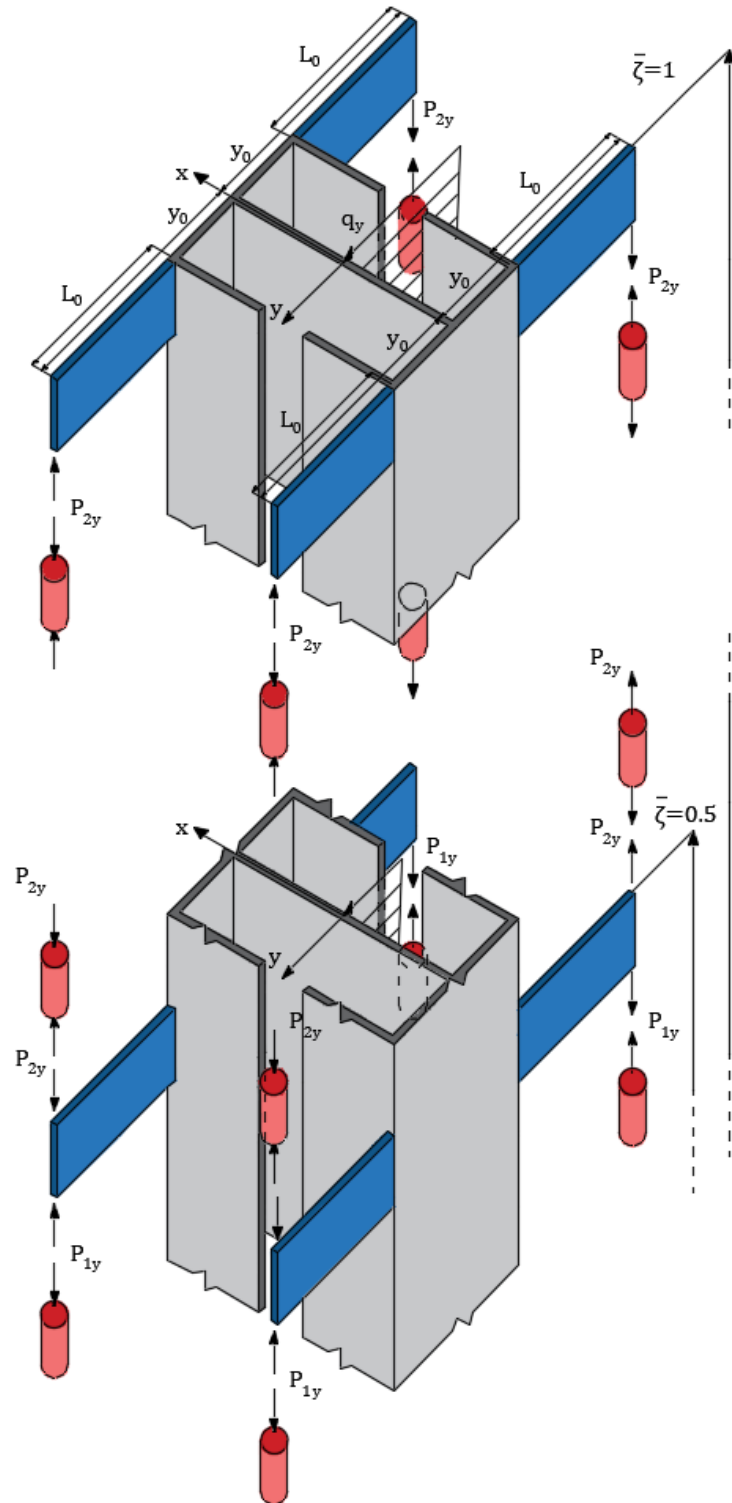


Figure 5.7: Core-outriggers interaction forces - Case: Two levels of outriggers

Computing the rotations $v'_1(\bar{\zeta}_1, \bar{\zeta}_1)$, $v'_1(\bar{\zeta}_1, \bar{\zeta}_2)$, $v'_1(\bar{\zeta}_2, \bar{\zeta}_2)$ and $v'_2(\bar{\zeta}_2, \bar{\zeta}_1)$ by deriving the corresponding *Green Functions* of Table 4.5 and $v'_0(\bar{\zeta})$ according to the second of equations (4.29), it is possible to explicit all the contributions of equations (5.21) as:

$$\begin{aligned}
 -4P_{1y}v'_1(\bar{\zeta}_1, \bar{\zeta}_1)y_0^2 &= 4P_{1y}\frac{L}{2EI_{yy}}y_0^2 \\
 P_{1y}\frac{L_0^3}{3EI_0} &= P_{1y}\frac{L_0^3}{3EI_0}; \quad P_{1y}\bar{\zeta}_1\frac{L}{EA_c} = P_{1y}\frac{L}{EA_c} \\
 -4P_{2y}v'_1(\bar{\zeta}_1, \bar{\zeta}_2)y_0^2 &= 4P_{2y}\frac{L}{2EI_{yy}}y_0^2 \\
 P_{1y}(\bar{\zeta}_2 - \bar{\zeta}_1)\frac{L}{EA_c} &= P_{1y}\frac{L}{2EA_c}
 \end{aligned} \tag{5.22}$$

$$v'_0(\bar{\zeta}_1)y_0 = \frac{41q_yL^3}{384EI_{yy}}y_0$$

$$\begin{aligned}
 -4P_{1y}v'_2(\bar{\zeta}_2, \bar{\zeta}_1)y_0^2 &= 4P_{1y}\frac{L}{2EI_{yy}}y_0^2 \\
 P_{1y}\bar{\zeta}_1\frac{L}{EA_c} &= P_{1y}\frac{L}{2EA_c} \\
 -4P_{2y}v'_1(\bar{\zeta}_2, \bar{\zeta}_2)y_0^2 &= 4P_{1y}\frac{L}{EI_{yy}}y_0^2 \\
 P_{2y}\frac{L_0^3}{3EI_0} &= P_{2y}\frac{L_0^3}{3EI_0}; \quad P_{2y}\bar{\zeta}_2\frac{L}{EA_c} = P_{2y}\frac{L}{EA_c}
 \end{aligned} \tag{5.23}$$

$$v'_0(\bar{\zeta}_2)y_0 = \frac{q_yL^3}{8EI_{yy}}y_0$$

The second block of terms in equations (5.22) and the first one in equations (5.23) are the coupling terms of the system (5.21) and, as we can see, they are equal. This is due to the symmetrical position of the outriggers at the two levels where they are introduced.

Substituting equations (5.22) and (5.23) in the system (5.21) yields the unknowns P_{1y} , P_{2y} and, in turn, the associated bending moments M_{1y} and M_{2y} acting on the core:

$$\begin{aligned}
 P_{1y} &= 0.2568 \cdot q_yL; \quad P_{2y} = 0.1385 \cdot q_yL \\
 M_{1y} &= 4P_{1y}L \cdot \frac{y_0}{L} = 0.0906 \cdot q_yL^2; \quad M_{2y} = 4P_{2y}L \cdot \frac{y_0}{L} = 0.0489 \cdot q_yL^2
 \end{aligned} \tag{5.24}$$

Once we know these quantities, it is possible to define the displacement v of the core by applying the principle of superposition between the displacement $v_0(\zeta)$ due to the external load, $v_1^{M_{1y}}(\zeta, 0.5)$ and $v_2^{M_{1y}}(\zeta, 0.5)$ due to the reaction of the column P_{1y} and $v_1^{M_{2y}}(\zeta, 1)$ due to the reaction of the column P_{2y} :

$$\begin{aligned}
 v(\zeta, \bar{\zeta}) &= v_0(\zeta) + v_1^{M_{1y}}(\zeta, \bar{\zeta}_1 = 0.5) + v_1^{M_{2y}}(\zeta, \bar{\zeta}_2 = 1) & 0 \leq \zeta \leq \bar{\zeta}_1 \\
 v(\zeta, \bar{\zeta}) &= v_0(\zeta) + v_2^{M_{1y}}(\zeta, \bar{\zeta}_1 = 0.5) + v_1^{M_{2y}}(\zeta, \bar{\zeta}_2 = 1) & \bar{\zeta}_1 \leq \zeta \leq \bar{\zeta}_2
 \end{aligned} \tag{5.25}$$

In particular, $v_0(\zeta)$ is defined by equation (4.29) while $v_1^{M_{1y}}(\zeta, 0.5)$, $v_2^{M_{1y}}(\zeta, 0.5)$ and $v_1^{M_{2y}}(\zeta, 1)$ are obtained, depending on the case, by multiplying $v_1(\zeta, \bar{\zeta})$ or $v_2(\zeta, \bar{\zeta})$ in Table 4.5 by M_{1y} or M_{2y} defined according to equations (5.24).

Given this, the rotation $v'(\zeta, \bar{\zeta})$ and the bending moment $M_y(\zeta, \bar{\zeta})$ can be defined by following the same path of reasoning, reading:

$$\begin{aligned} v'(\zeta, \bar{\zeta}) &= v'_0(\zeta) + v'_1^{M_{1y}}(\zeta, \bar{\zeta}_1 = 0.5) + v'_1^{M_{2y}}(\zeta, \bar{\zeta}_2 = 1) & 0 \leq \zeta \leq \bar{\zeta}_1 \\ v'(\zeta, \bar{\zeta}) &= v'_0(\zeta) + v'_2^{M_{1y}}(\zeta, \bar{\zeta}_1 = 0.5) + v'_1^{M_{2y}}(\zeta, \bar{\zeta}_2 = 1) & \bar{\zeta}_1 \leq \zeta \leq \bar{\zeta}_2 \end{aligned} \quad (5.26)$$

$$\begin{aligned} M_y(\zeta, \bar{\zeta}) &= M_{0y}(\zeta) + M_{1y} + M_{2y} & 0 \leq \zeta \leq \bar{\zeta}_1 \\ M_y(\zeta, \bar{\zeta}) &= M_{0y}(\zeta) + M_{2y} & \bar{\zeta}_1 \leq \zeta \leq \bar{\zeta}_2 \end{aligned} \quad (5.27)$$

5.2.3 Results

The vertical displacement, flexural rotation and bending moment are now reported for the cases of free-standing core, core with one level of outriggers and core with two levels of outriggers. Figure 5.8 shows the trend with ζ of the first of equations (4.29), equation (5.18) and equation (5.25), respectively represented by a yellow, red and blue line. Similarly, Figure 5.9 gives the variation of the second of equations (4.29), equation (5.19) and equation (5.26), while Figure 5.10 the third of equations (4.29), equation (5.20) and equation (5.27).

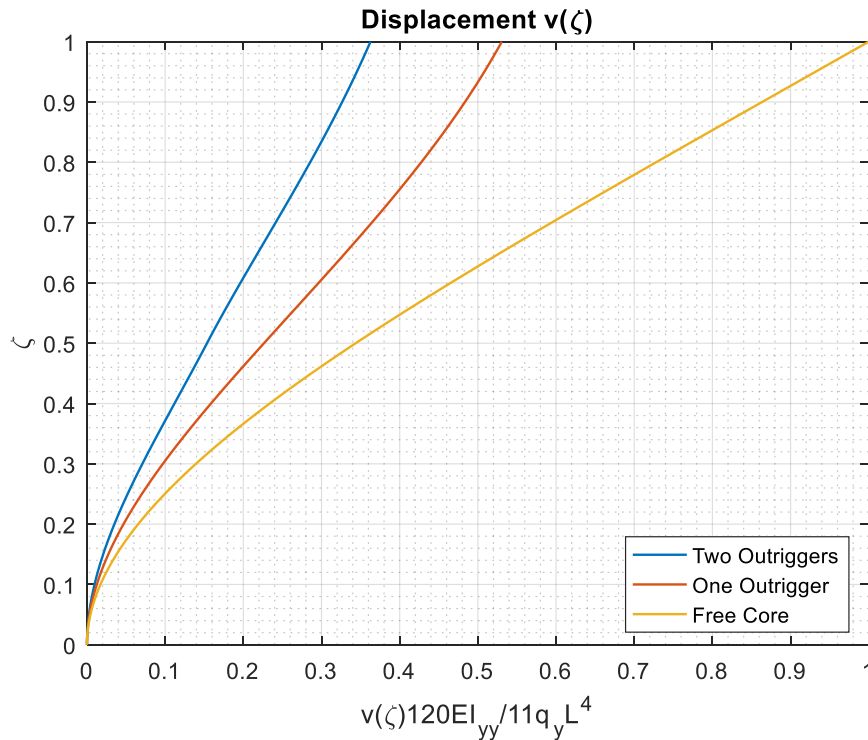


Figure 5.8: Core displacement under a triangular load distribution q_y

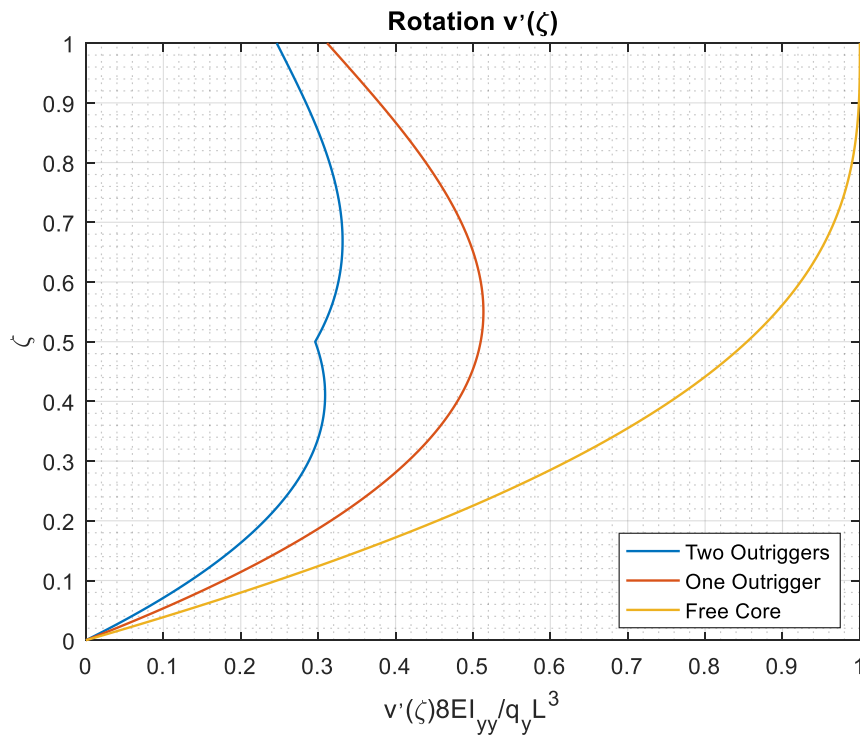


Figure 5.9: Core Rotation under a triangular load distribution q_y

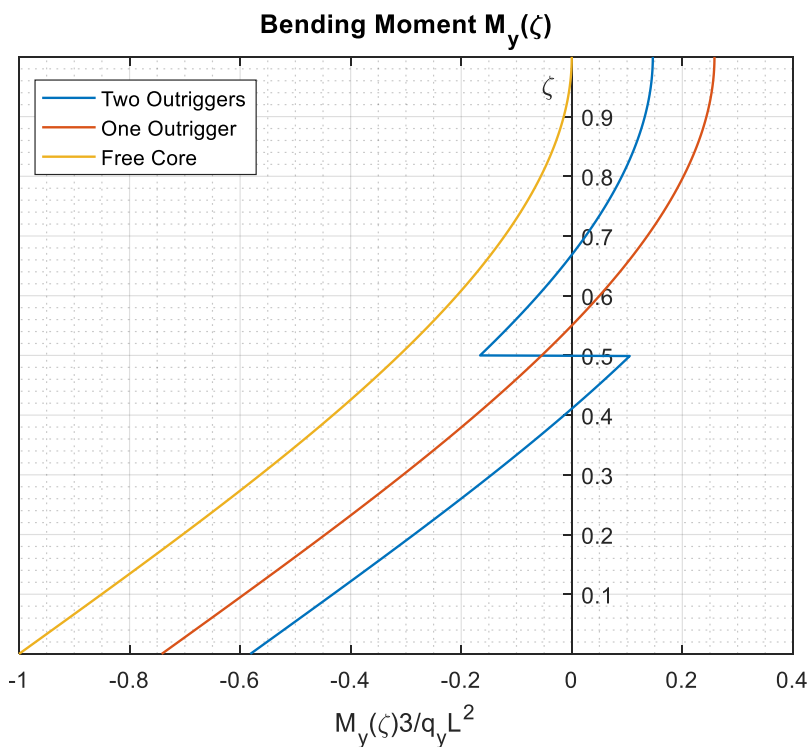


Figure 5.10: Bending moment in the core under a triangular load distribution q_y

As we can see from Figure 5.8, when outrigger structural systems are considered the displacement of the core significantly reduces; in particular, with one level of outriggers the

displacement reduction at the top of the structure reaches a value of 47 %, while with two levels of outriggers the reduction is even more pronounced, reaching a value at the top of 64 %. For what concerns the bending moment diagram, looking at Figure 5.10 it is evident that the main benefit induced by outrigger systems is their ability to effectively reduce the core's bending moment at the base, which is a favourable situation for the foundations, as already explained in §2.5.3. As a rule, beneficial effects achieved by introducing in the structure outrigger systems increase as the levels of outriggers increase but the rate decreases.

5.3 CORE-OUTRIGGERS INTERACTION: TORSIONAL BEHAVIOUR

5.3.1 *Structure with One Level of Outriggers*

Indicating by $P_{1\omega}$ the interaction forces between the outrigger and the column generated by the load q_ω , the system of equations (4.36) turns now into a single compatibility equation with the only $P_{1\omega}$ as unknown, having the form:

$$P_{1\omega} \left[-4\theta'_1(\bar{\zeta})\omega_B^2 + \frac{L_0^3}{3EI_0} + \bar{\zeta} \frac{L}{EA_C} \right] = \theta'_0(\bar{\zeta})\omega_B \quad (5.28)$$

where $\bar{\zeta} = 1$ represents the level of the outriggers, that is, in this case, the top of the structure.

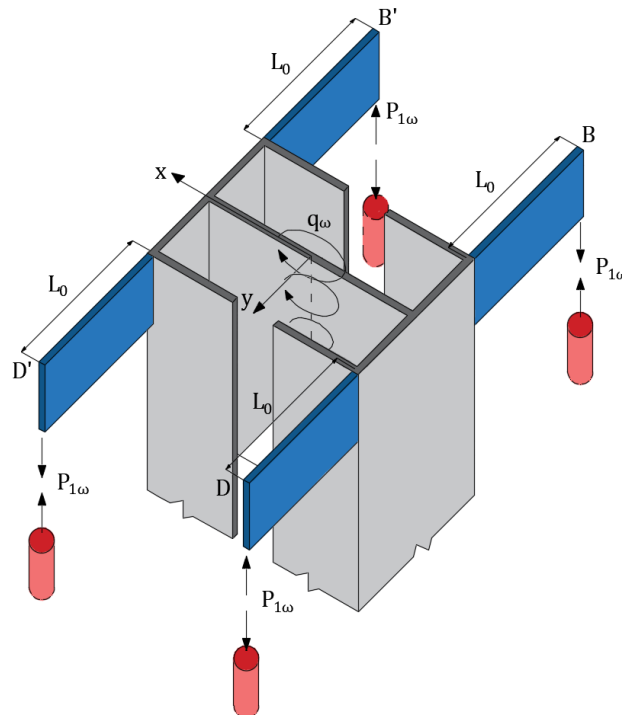


Figure 5.11: Core-outriggers interaction torsional forces - Case: One level of outriggers

In equation (5.28) it is possible to recognize 4 different contributions:

- $4 \cdot P_{1\omega} \cdot \theta'_1(\bar{\zeta}) \omega_B^2$ represents the displacement in the column due to the warping of the core given by the unknown bimoment $P_{1\omega} \cdot \omega_B$, assuming the outrigger as rigid. Note that the factor 4 is due to the presence of 4 outriggers at the outriggers level.
- $P_{1\omega} \cdot L_0^3/3EI_0$ is the displacement contribution given by the flexural deformability of the outrigger, assumed as a horizontal cantilever subjected to a vertical force at the free end.
- $P_{1\omega} \cdot \bar{\zeta} \cdot L/EA_C$ is the displacement due to axial deformability of the column.
- $\theta'_0(\bar{\zeta}) \omega_B$ is the displacement in the column due to the external triangular torque.

Computing the rotation $\theta'_1(\bar{\zeta})$ by deriving the corresponding *Green Function* of Table 4.5 and $\theta'_0(\bar{\zeta})$ according to the second of equations (4.35), it is possible to explicit all the contributions of equation (5.28) as:

$$\begin{aligned}
 -4P_{1\omega}\theta'_1(\bar{\zeta}, \bar{\zeta})\omega_B^2 &= 4P_{1\omega} \frac{L}{kEI_{\omega\omega}} \frac{\cosh(k)\cosh(k) - \sinh(k)\sinh(k)}{\cosh(k)} \sinh(k)\omega_B^2 \\
 P_{1\omega} \frac{L_0^3}{3EI_0} &= P_{1\omega} \frac{L_0^3}{3EI_0} \\
 P_{1\omega} \bar{\zeta} \frac{L}{EA_C} &= P_{1\omega} \frac{L}{EA_C}
 \end{aligned} \tag{5.29}$$

$$\theta'_0(\bar{\zeta})\omega_B = \frac{q_\omega L^3}{k^4 EI_{\omega\omega}} \left[F(k) \cdot \sinh(k) - \left(\frac{k^2}{2} - 1 \right) \cosh(k) + \left(\frac{k^2}{2} - 1 \right) - \frac{k^2}{2} \right] \omega_B$$

where:

$$F(k) = \frac{k^2 \sinh(k) - 2 \sinh(k) + 2k}{2 \cosh(k)}$$

Substituting equations (5.29) in the compatibility equation (5.28), yields the unknown $P_{1\omega}$ and the related bending moment M_{1y} acting on the core are:

$$\begin{aligned}
 P_{1\omega} &= 0.0224 \cdot q_\omega L \\
 M_{1\omega} &= 4P_{1\omega} L \cdot \frac{\omega_B}{L} = 0.0593 \cdot q_\omega L^2
 \end{aligned} \tag{5.30}$$

Once we know these quantities, it is possible to define the torsional rotation θ of the core by applying the principle of superposition between the torsional rotation $\theta_0(\zeta)$ due to the external torque load and the torsional rotation $\theta_1^{M_{1\omega}}(\zeta, 1)$ due to the reaction of the column:

$$\theta(\zeta, \bar{\zeta}) = \theta_0(\zeta) + \theta_1^{M_{1\omega}}(\zeta, \bar{\zeta} = 1) \tag{5.31}$$

In particular, $\theta_0(\zeta)$ is defined by equation (4.35) while $\theta_1^{M_{1\omega}}(\zeta, 1)$ is obtained by multiplying $\theta_1(\zeta)$ in Table 4.5 by $M_{1\omega}$ defined by equation (5.30).

Given this, the warping $\theta'(\zeta, \bar{\zeta})$ and the bimoment $M_\omega(\zeta, \bar{\zeta})$ can be defined by following the same path of reasoning, reading:

$$\theta'(\zeta, \bar{\zeta}) = \theta'_0(\zeta) + \theta'_1 M_{1\omega}(\zeta, \bar{\zeta} = 1) \quad (5.32)$$

$$M_\omega(\zeta, \bar{\zeta}) = M_{0\omega}(\zeta) + M_{1\omega} \quad (5.33)$$

For what concerns the axial displacements induced in the columns by the interaction force $P_{1\omega}$, they can be computed according to Table 4.5, by multiplying the corresponding *Green Function* by $P_{1\omega}$:

$$\begin{aligned} w_1(\zeta, \bar{\zeta}) &= P_{1\omega} \frac{L}{EA} \cdot \zeta & 0 \leq \zeta \leq \bar{\zeta}_1 \\ w_2(\zeta, \bar{\zeta}) &= P_{1\omega} \frac{L}{EA} \cdot \bar{\zeta} & \bar{\zeta}_1 \leq \zeta \leq \bar{\zeta}_2 \end{aligned} \quad (5.34)$$

5.3.2 *Structure with Two Levels of Outriggers*

Differently to the previous case, here we have two unknown axial forces, therefore two compatibility equations are needed, one for each level of outriggers. It is important to highlight that in this case the two equations are coupled because the effects of one level of outriggers are present on the other, and vice versa. This means that it is necessary to solve a system of two coupled equations in the unknowns $P_{1\omega}$ and $P_{2\omega}$:

$$\begin{aligned} P_{1\omega} \left[-4\theta'_1(\bar{\zeta}_1, \bar{\zeta}_1)\omega_B^2 + \frac{L_0^3}{3EI_0} + \bar{\zeta}_1 \frac{L}{EA_C} \right] + P_{2\omega} \left[-4\theta'_1(\bar{\zeta}_1, \bar{\zeta}_2)\omega_B^2 + (\bar{\zeta}_2 - \bar{\zeta}_1) \frac{L}{EA_C} \right] &= \theta'_0(\bar{\zeta}_1)\omega_B \\ P_{1\omega} \left[-4\theta'_2(\bar{\zeta}_2, \bar{\zeta}_1)\omega_B^2 + \bar{\zeta}_1 \frac{L}{EA_C} \right] + P_{2\omega} \left[-4\theta'_1(\bar{\zeta}_2, \bar{\zeta}_2)\omega_B^2 + \frac{L_0^3}{3EI_0} + \bar{\zeta}_2 \frac{L}{EA_C} \right] &= \theta'_0(\bar{\zeta}_2)\omega_B \end{aligned} \quad (5.35)$$

The first of equations (5.35) is the compatibility equation at the 1st level of outriggers (mid-height: $\bar{\zeta}_1 = 0.5$) while the second is written at the 2nd level of outriggers (top: $\bar{\zeta}_1 = 1$).

For the first compatibility equation, it is possible to recognize the following 6 contributions:

- $4 \cdot P_{1\omega} \cdot \theta'_1(\bar{\zeta}_1, \bar{\zeta}_1)\omega_B^2$ represents the displacement in the column at 1st outriggers level due to the warping of the core given by the unknown bimoment $P_{1\omega} \cdot \omega_B$ deriving from the axial force at the 1st outriggers level, assuming the outrigger as rigid. Note that the factor 4 is due to the presence of 4 outriggers at the outriggers level.
- $P_{1\omega} \cdot L_0^3/3EI_0$ is the displacement contribution given by the flexural deformability of the outrigger, assumed as a horizontal cantilever subjected to a vertical force at the free end.
- $P_{1\omega} \cdot \bar{\zeta}_1 \cdot L/EA_C$ is the displacement due to the axial deformability of the column at 1st outriggers level, given by the axial force at the 1st outriggers level.

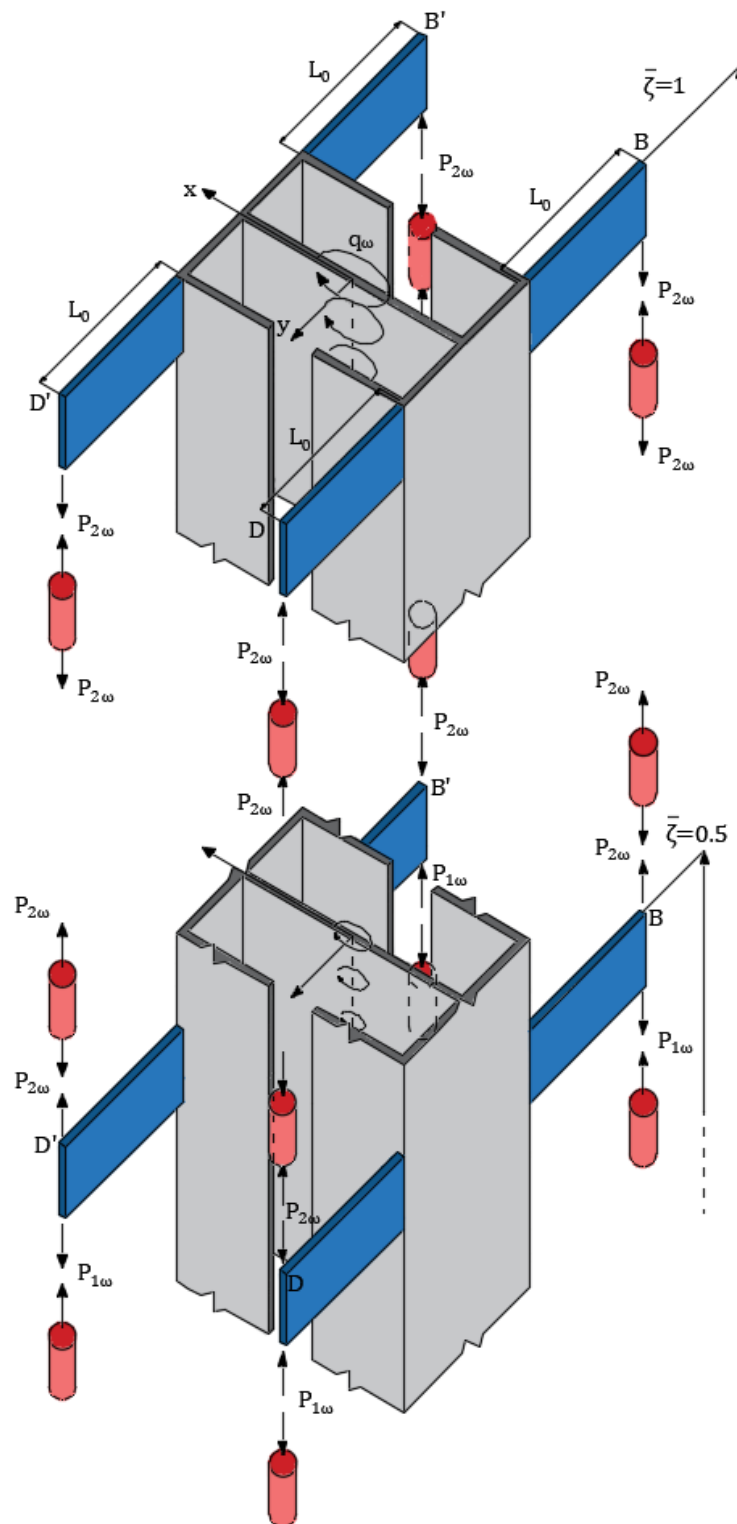


Figure 5.12: Core-outriggers interaction forces - Case: Two levels of outriggers

- $4 \cdot P_{2\omega} \cdot \theta'_1(\bar{\zeta}_1, \bar{\zeta}_2) \omega_B^2$ represents the displacement in the column at 1st outriggers level due to the warping of the core given by the unknown bimoment $P_{2\omega} \cdot \omega_B$ deriving from the axial force at the 2nd outriggers level, assuming the outrigger as

rigid. Notice that the factor 4 is due to the presence of 4 outriggers at the outriggers level.

- $P_{1\omega} \cdot (\bar{\zeta}_2 - \bar{\zeta}_1) \cdot L/E A_C$ is the displacement due to axial deformability of the column at 1st outriggers level, given by the axial force at the 2nd outriggers level.
- $\theta'_0(\bar{\zeta}_1)\omega_B$ is the displacement in the column due to the external distributed torque, at 1st outriggers level.

All contributions appearing in the second of equations (5.35) can be defined following the same path of reasoning.

Computing the warping deformations $\theta'_1(\bar{\zeta}_1, \bar{\zeta}_1)$, $\theta'_1(\bar{\zeta}_1, \bar{\zeta}_2)$, $\theta'_1(\bar{\zeta}_2, \bar{\zeta}_2)$ and $\theta'_2(\bar{\zeta}_2, \bar{\zeta}_1)$ by deriving the corresponding *Green Functions* of Table 4.5 and $\theta'_0(\bar{\zeta})$ according to the second of equations (4.35), it is possible to explicit all the contributions of equations (5.35) as:

$$\begin{aligned}
 -4P_{1\omega}\theta'_1(\bar{\zeta}_1, \bar{\zeta}_1)\omega_B^2 &= 4P_{1\omega} \frac{L}{kEI_{\omega\omega}} \frac{\cosh(k) \cosh(0.5k) - \sinh(k)\sinh(0.5k)}{\cosh(k)} \sinh(0.5k)\omega_B^2 \\
 P_{1y} \frac{L_0^3}{3EI_0} &= P_{1y} \frac{L_0^3}{3EI_0}; \quad P_{1\omega}\bar{\zeta}_1 \frac{L}{EA_C} = P_{1\omega} \frac{L}{EA_C} \\
 -4P_{2\omega}\theta'_1(\bar{\zeta}_1, \bar{\zeta}_2)\omega_B^2 &= 4P_{2\omega} \frac{L}{kEI_{\omega\omega}} \frac{\cosh(k) \cosh(k) - \sinh(k)\sinh(k)}{\cosh(k)} \sinh(0.5k)\omega_B^2 \\
 P_{1\omega}(\bar{\zeta}_2 - \bar{\zeta}_1) \frac{L}{EA_C} &= P_{1\omega} \frac{L}{2EA_C}
 \end{aligned} \tag{5.36}$$

$$\theta'_0(\bar{\zeta}_1)\omega_B = \frac{q_\omega L^3}{k^4 EI_{\omega\omega}} \left[F(k) \cdot \sinh(0.5k) - \left(\frac{k^2}{2} - 1 \right) \cosh(0.5k) + \left(\frac{k^2}{2} - 1 \right) - \frac{k^2}{2} 0.5^2 \right] \omega_B$$

$$\begin{aligned}
 -4P_{1\omega}\theta'_2(\bar{\zeta}_2, \bar{\zeta}_1)\omega_B^2 &= 4P_{1\omega} \frac{L}{kEI_{\omega\omega}} \frac{\cosh(k) \cosh(k) - \sinh(k)\sinh(k)}{\cosh(k)} \sinh(0.5k)\omega_B^2 \\
 P_{1\omega}\bar{\zeta}_1 \frac{L}{EA_C} &= P_{1\omega} \frac{L}{2EA_C} \\
 -4P_{2\omega}\theta'_1(\bar{\zeta}_2, \bar{\zeta}_2)\omega_B^2 &= 4 \cdot P_{1\omega} \cdot \frac{L}{kEI_{\omega\omega}} \frac{\cosh(k) \cosh(k) - \sinh(k)\sinh(k)}{\cosh(k)} \sinh(k)\omega_B^2 \\
 P_{1y} \frac{L_0^3}{3EI_0} &= P_{1y} \frac{L_0^3}{3EI_0}; \quad P_{2\omega}\bar{\zeta}_2 \frac{L}{EA_C} = P_{2\omega} \frac{L}{EA_C}
 \end{aligned} \tag{5.37}$$

$$\theta'_0(\bar{\zeta}_2)\omega_B = \frac{q_\omega L^3}{k^4 EI_{\omega\omega}} \left[F(k) \cdot \sinh(k) - \left(\frac{k^2}{2} - 1 \right) \cosh(k) + \left(\frac{k^2}{2} - 1 \right) - \frac{k^2}{2} \right] \omega_B$$

The second block of terms in equations (5.36) and the first one in equations (5.37) are the coupling terms of the system (5.35) and, as we can see, they are equal. This is due to the symmetrical position of the outriggers at the two levels where they are introduced.

Substituting equations (5.36) and (5.37) in the system (5.35) yields the unknowns $P_{1\omega}$, $P_{2\omega}$ and, in turn, the associated bimoments $M_{1\omega}$ and $M_{2\omega}$ acting on the core:

$$\begin{aligned} P_{1\omega} &= 0.0234 \cdot q_\omega L; & P_{2\omega} &= 0.0144 \cdot q_\omega L \\ M_{1\omega} &= 4P_{1\omega}L \cdot \frac{\omega_B}{L} = 0.0619 \cdot q_\omega L^2; & M_{2\omega} &= 4P_{2\omega}L \cdot \frac{\omega_B}{L} = 0.0382 \cdot \omega L^2 \end{aligned} \quad (5.38)$$

Once we know these quantities, it is possible to define the torsional rotation θ of the core by applying the principle of superposition between the torsional rotation $\theta_0(\zeta)$ due to the external load, $\theta_1^{M_{1\omega}}(\zeta, 0.5)$ and $\theta_2^{M_{1\omega}}(\zeta, 0.5)$ due to the reaction of the column $P_{1\omega}$ and $\theta_1^{M_{2\omega}}(\zeta, 1)$ due to the reaction of the column $P_{2\omega}$:

$$\begin{aligned} \theta(\zeta, \bar{\zeta}) &= \theta_0(\zeta) + \theta_1^{M_{1\omega}}(\zeta, \bar{\zeta}_1 = 0.5) + \theta_1^{M_{2\omega}}(\zeta, \bar{\zeta}_2 = 1) & 0 \leq \zeta \leq \bar{\zeta}_1 \\ \theta(\zeta, \bar{\zeta}) &= \theta_0(\zeta) + \theta_2^{M_{1\omega}}(\zeta, \bar{\zeta}_1 = 0.5) + \theta_1^{M_{2\omega}}(\zeta, \bar{\zeta}_2 = 1) & \bar{\zeta}_1 \leq \zeta \leq \bar{\zeta}_2 \end{aligned} \quad (5.39)$$

In particular, $\theta_0(\zeta)$ is defined by the first of equations (4.35) while $\theta_1^{M_{1\omega}}(\zeta, 0.5)$, $\theta_2^{M_{1\omega}}(\zeta, 0.5)$ and $\theta_1^{M_{2\omega}}(\zeta, 1)$ are obtained, depending on the case, by multiplying $\theta_1(\zeta, \bar{\zeta})$ or $\theta_2(\zeta, \bar{\zeta})$ in Table 4.5 by $M_{1\omega}$ or $M_{2\omega}$ defined according to equations (5.38).

Given this, the warping $\theta'(\zeta, \bar{\zeta})$ and the bimoment $M_\omega(\zeta, \bar{\zeta})$ can be defined by following the same path of reasoning, reading:

$$\begin{aligned} \theta'(\zeta, \bar{\zeta}) &= \theta'_0(\zeta) + \theta'_1^{M_{1\omega}}(\zeta, \bar{\zeta}_1 = 0.5) + \theta'_1^{M_{2\omega}}(\zeta, \bar{\zeta}_2 = 1) & 0 \leq \zeta \leq \bar{\zeta}_1 \\ \theta'(\zeta, \bar{\zeta}) &= \theta'_0(\zeta) + \theta'_2^{M_{1\omega}}(\zeta, \bar{\zeta}_1 = 0.5) + \theta'_1^{M_{2\omega}}(\zeta, \bar{\zeta}_2 = 1) & \bar{\zeta}_1 \leq \zeta \leq \bar{\zeta}_2 \end{aligned} \quad (5.40)$$

$$\begin{aligned} M_\omega(\zeta, \bar{\zeta}) &= M_{0\omega}(\zeta) + M_{1\omega} + M_{2\omega} & 0 \leq \zeta \leq \bar{\zeta}_1 \\ M_\omega(\zeta, \bar{\zeta}) &= M_{0\omega}(\zeta) + M_{2\omega} & \bar{\zeta}_1 \leq \zeta \leq \bar{\zeta}_2 \end{aligned} \quad (5.41)$$

For what concerns the axial displacements induced in the columns by the interaction forces $P_{1\omega}$ and $P_{2\omega}$, they can be computed according to Table 4.5, by multiplying the corresponding *Green Function* by $P_{1\omega}$ or $P_{2\omega}$:

$$\begin{aligned} w_1(\zeta, \bar{\zeta}) &= P_{1\omega} \frac{L}{EA} \cdot \zeta + P_{2\omega} \frac{L}{EA} \cdot \zeta & 0 \leq \zeta \leq \bar{\zeta}_1 \\ w_2(\zeta, \bar{\zeta}) &= P_{1\omega} \frac{L}{EA} \cdot \bar{\zeta} + P_{2\omega} \frac{L}{EA} \cdot \zeta & \bar{\zeta}_1 \leq \zeta \leq \bar{\zeta}_2 \end{aligned} \quad (5.42)$$

5.3.3 Results

The torsional rotation, the warping, the bimoment are now reported for the cases of free-standing core, core with one level of outriggers and core with two levels of outriggers. Figure 5.13 shows the trend with ζ of the first of equations (4.35), equation (5.31) and equation

(5.39), respectively represented by a yellow, red and blue line. Similarly, Figure 5.14 gives the variation of the second of equations (4.35), equation (5.32) and equation (5.40), while Figure 5.15 the third of equations (4.35), equation (5.33) and equation (5.41).

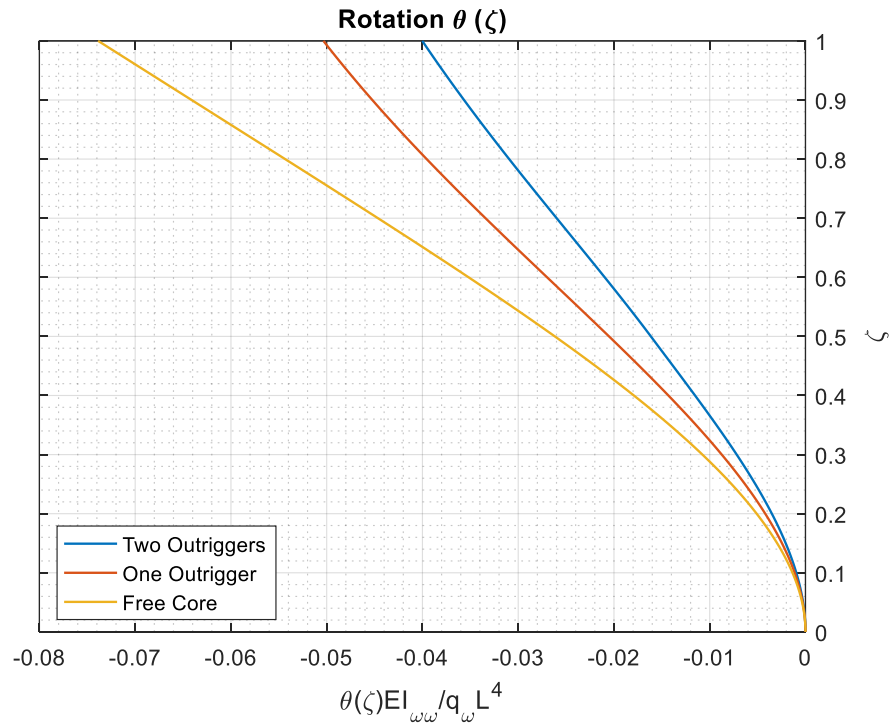


Figure 5.13: Torsional rotation in the core due to a triangular torque

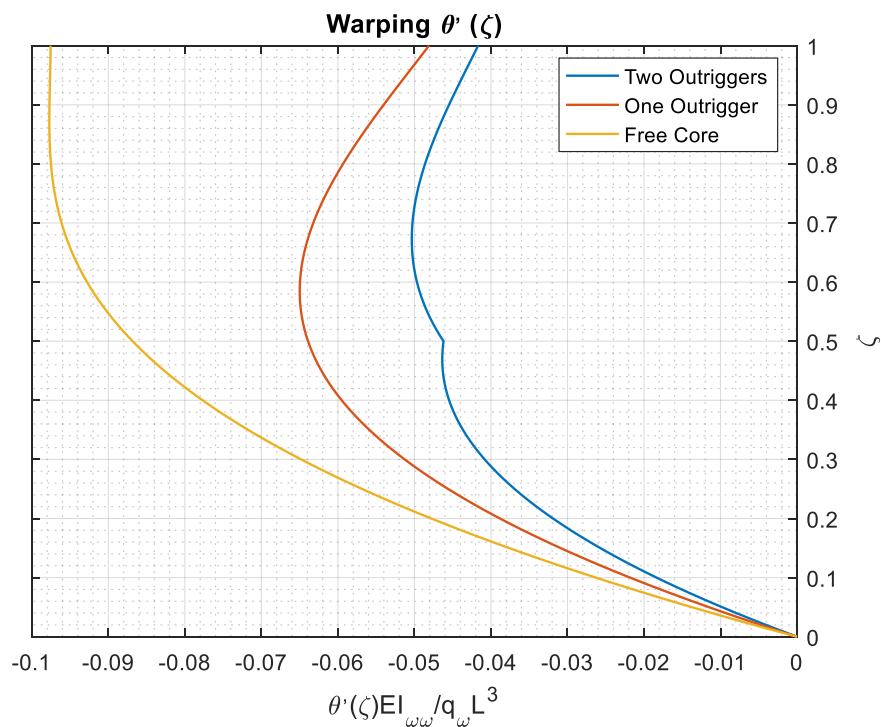


Figure 5.14: Warping of the core due to a triangular torque

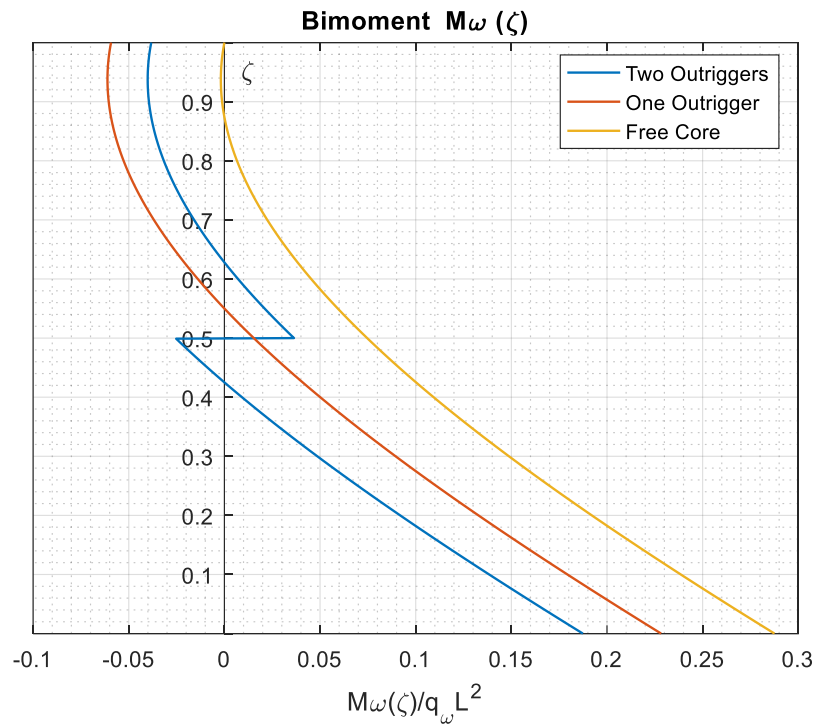


Figure 5.15: Bimoment in the core due to a triangular torque

As concerns the axial displacements, Figure 5.16 shows the trend with ζ of equations (5.34) for one level of outriggers and (5.42) for two levels of outriggers for Columns 2B (equivalent to 6D) and 2D (equivalent to 6B):

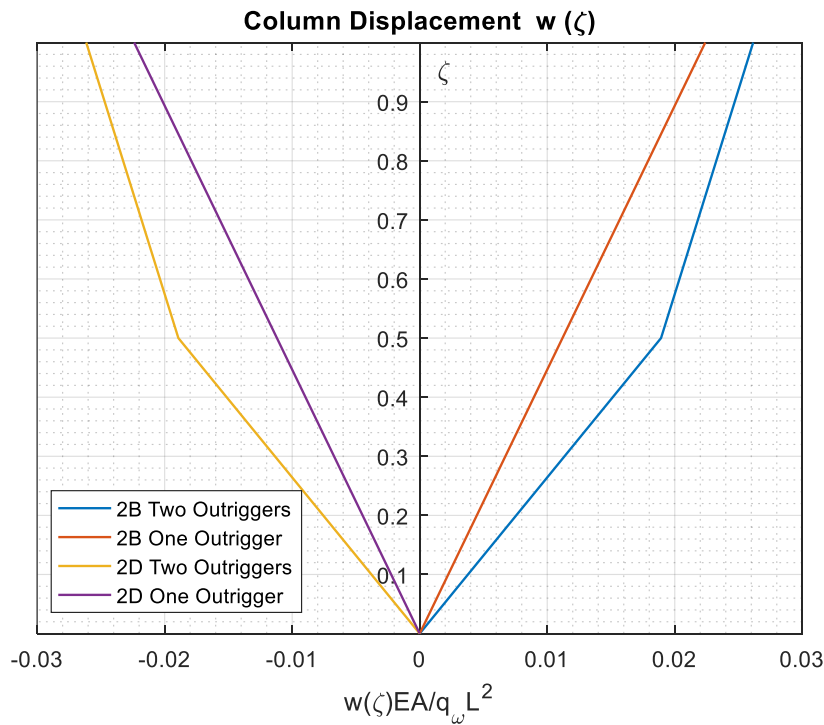


Figure 5.16: Column 2B and 2D displacements due to a triangular torque

As we can see from Figure 5.13 and Figure 5.14, when outrigger structural systems are considered torsional rotation and warping of the core significantly reduce; in particular, with one level of outriggers the rotation and warping reduction at the top of the structure reaches the values of 32% and 51% respectively, while with two levels of outriggers the reduction is even more pronounced, reaching the values of 45% and 57% at the top.

For what concerns the bimoment diagram, looking at Figure 5.15 it is evident that the main benefit induced by outrigger systems is their ability to effectively reduce the core's bimoment at the base, which is a favourable situation for the foundations, as already explained in §2.5.3.

Figure 5.16 shows that the displacements of columns 2B and 2D are equal but with opposite sign, this highlighting the warping of the structure. When one outrigger level is considered, their variation along the height of the building is linear, then becoming bilinear when dealing with two levels of outriggers, as a consequence of the concentrated outriggers reaction at mid-height.

As can be seen from figure 6.14, in case of free-standing core the maximum warping is at the top, whereas introducing one outriggers level the maximum shifts at almost mid height of the structure, being at almost 2/3 of the height when two levels are introduced.

5.3.4 *Structural Behaviour in Presence of Diaphragms*

We shall now analyse the behaviour of the core-outriggers structural system in presence of transversal diaphragms. Therefore, with reference to §3.4.1 it is possible to account for the presence of diaphragms by replacing the parameter k governing the torsional behaviour with its varied value:

$$k_{var} = \sqrt{\frac{G(I_d + \bar{I}_d)}{EI_{\omega\omega}}} \quad (5.43)$$

where \bar{I}_d represents the additional torsional stiffness given by the diaphragms, defined by equation (3.97) as:

$$\bar{I}_d = \frac{h^3 \Omega}{6b}$$

The solution of the torsional problem is thus the same as before except for k_{var} in place of k . For what concerns the bending behaviour, the presence of diaphragms does not give any contribution and the solution reported in §5.2.3 still holds true.

The effects induced by diaphragms with a thickness $h = 0.30 \text{ m}$ and distributed over the height of the building every 4.25 m are now shown in the following graphs. From the considered diaphragm dimensions $k_{var} = 0.9831$, that is the value of k is increased with respect to the case of simple core-outriggers structural system. As a consequence, we expect a lower efficiency of the outrigger system in reducing torsional rotations and warping deformations.

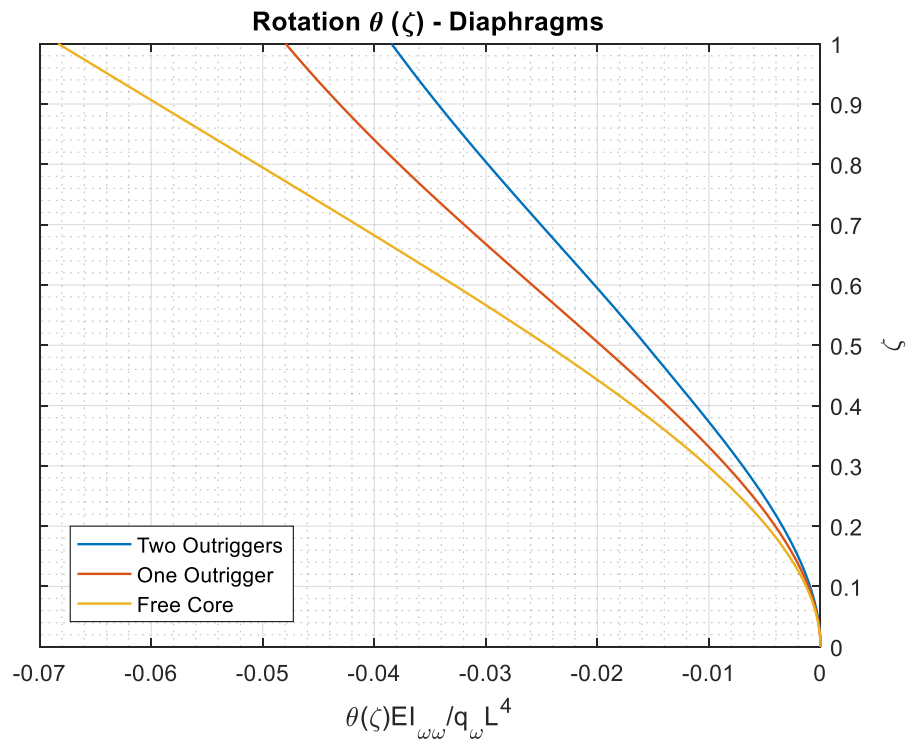


Figure 5.17: Core rotation in presence of diaphragm, due to a triangular torque

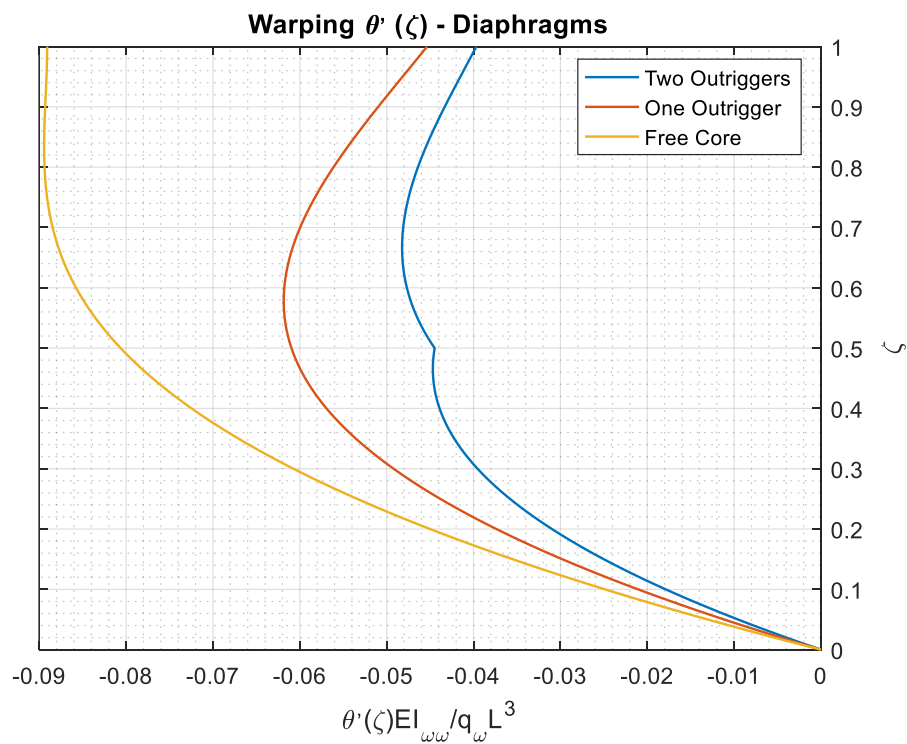


Figure 5.18: Core warping in presence of diaphragm, due to a triangular torque

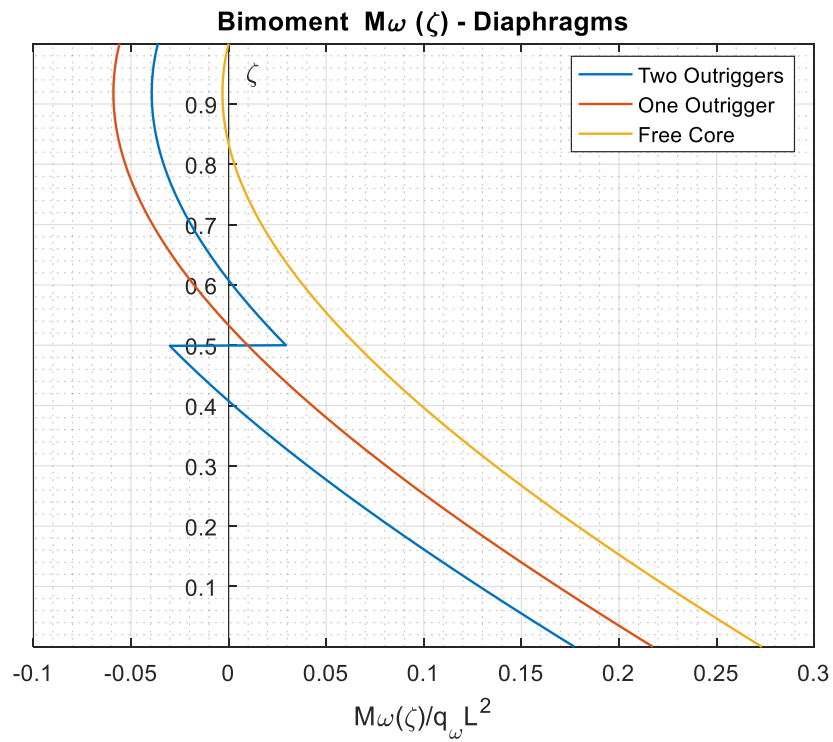


Figure 5.19: Core bimoment in presence of diaphragm, due to a triangular torque

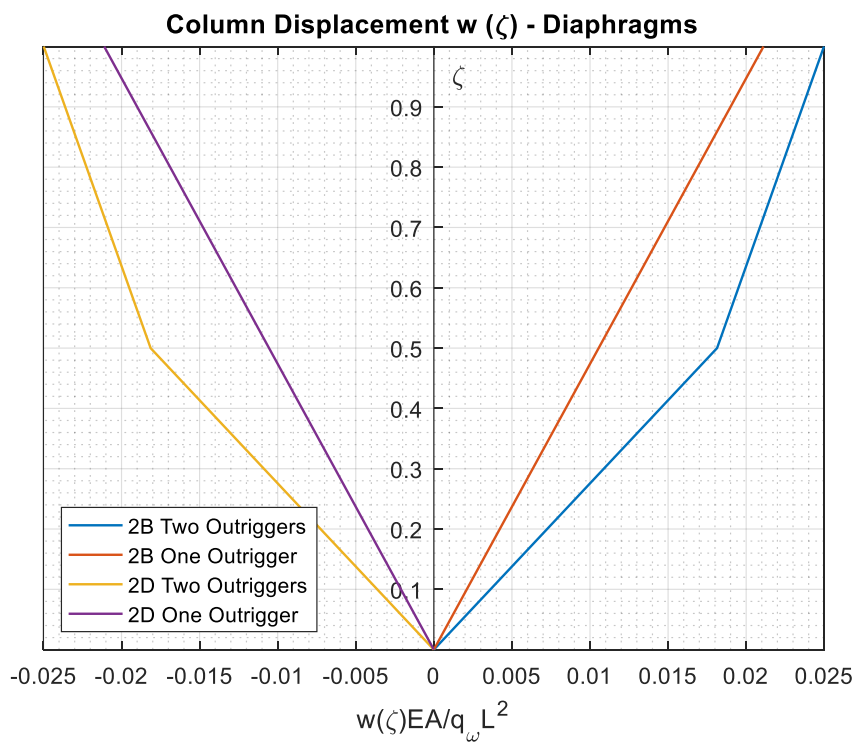


Figure 5.20: Column 2B and 2D displacements in presence of diaphragm due to a triangular torque

As can be noticed from the reported results, the torsion behaviour of the core is almost the same as in the case of simple core-outriggers system studied before, without diaphragms. This is because the parameter k is still in the range of the Vlasov's torsion (lower than 1, see Figure 4.19), therefore the warping of the core is still significant and the outrigger's effect is relevant. From Figure 5.17 it is possible to see the torsional rotation reduction given by the outrigger structural system, which is 29 % in case of one outriggers level and 43% in case of two outriggers levels, so almost similar to the value obtained in the case without diaphragms. Similarly, for the warping we have a reduction of 49 % with one outriggers level and 56% in case of two outriggers levels (see Figure 5.18). Also in this case, there is a reduction of bimoment at the base as we can see from Figure 5.19.

5.3.5 *Structural Behaviour in Presence of Lintels*

We shell now analyse the influence of lintels on the behaviour of the core, since these elements are often present in real structures. The approach used to consider lintels influence is the same used in the previous paragraph for diaphragms, with the only difference that in this case \bar{I}_d is defined by the equation (3.102) (see §3.4.2):

$$\bar{I}_d = \frac{\Omega^2}{\delta_T G} = \frac{\Omega^2}{ab} \cdot \frac{1}{\left(\frac{a^2 G}{12EI_{br}} + \frac{1.2}{A_{br}} \right)} \quad (5.44)$$

As for the case of diaphragms, the solution of the torsional problem can be simply obtained by changing the value of k in the one reported in paragraph §5.3. For the bending problem the solution is still the same as the one shown in §5.2.3.

In the following, we will consider lintels uniformly distributed along the height of the core, one each 4.25 m, having three different heights:

- 50 cm lintels
- 100 cm lintels
- 150 cm lintels

The geometrical properties of the lintels and the associated value of k_{var} are summarized in the following table:

Lintel	δ [m]	a [m]	d [m]	A_{br} [m ²]	I_{br} [m ⁴]	\bar{I}_d [m ⁴]	k_{var}
1	0.45	3.00	0.50	0.225	0.0047	105.2221	6.0855
2	0.45	3.00	1.00	0.450	0.0375	826.3198	16.9286
3	0.45	3.00	1.50	0.675	0.1266	2706	30.6116

Table 5.5: Geometrical properties of lintels and associate k_{var}

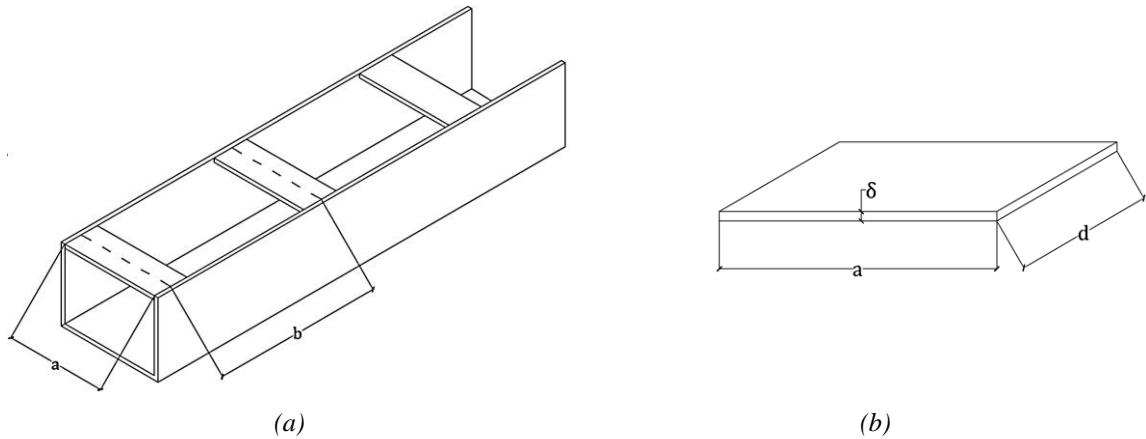


Figure 5.21: Lintels geometry

As we can see from Table 5.5 in presence of lintels the value of the parameter k highly increases with respect to the previous analysed cases. With such high values, the torsional behaviour of the core completely changes, since it works more as a thin-walled closed element rather than a thin-walled element with open profile. Indeed, looking at Figure 4.19 we can see that for values of k higher than 3, torsion is completely governed by the De Saint Venant Theory; therefore, the warping of the section is practically negligible. This means that in presence of lintels the outrigger system does not work and becomes much less effective from the point of view of the reduction of torsional effects, whereas it is still useful to reduce lateral displacements, since the bending behaviour is not influenced by lintels presence.

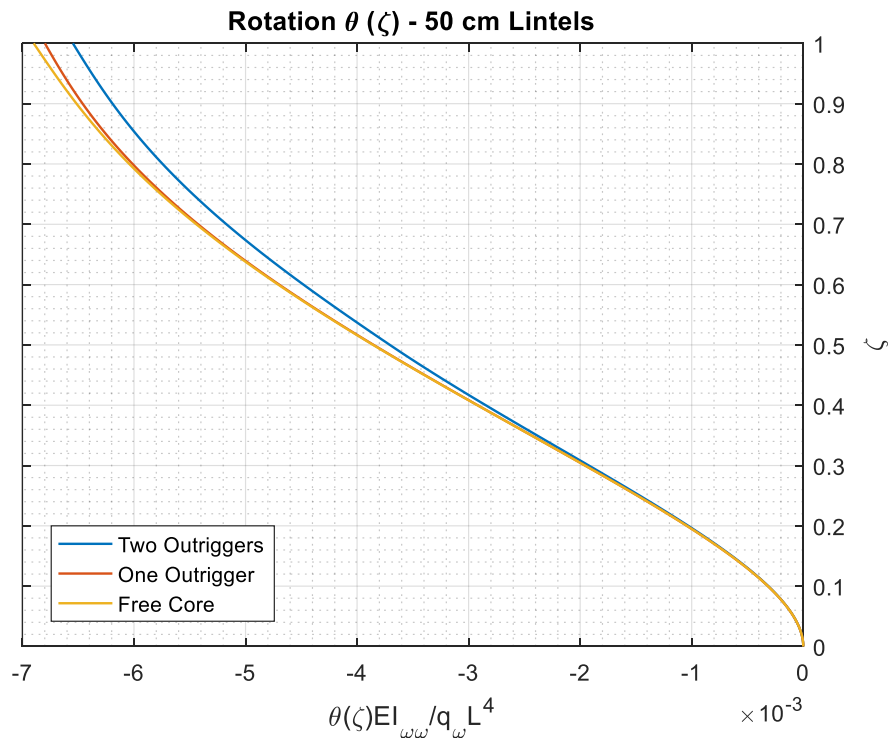


Figure 5.22: Core rotation in presence of 50 cm lintels, due to a triangular torque

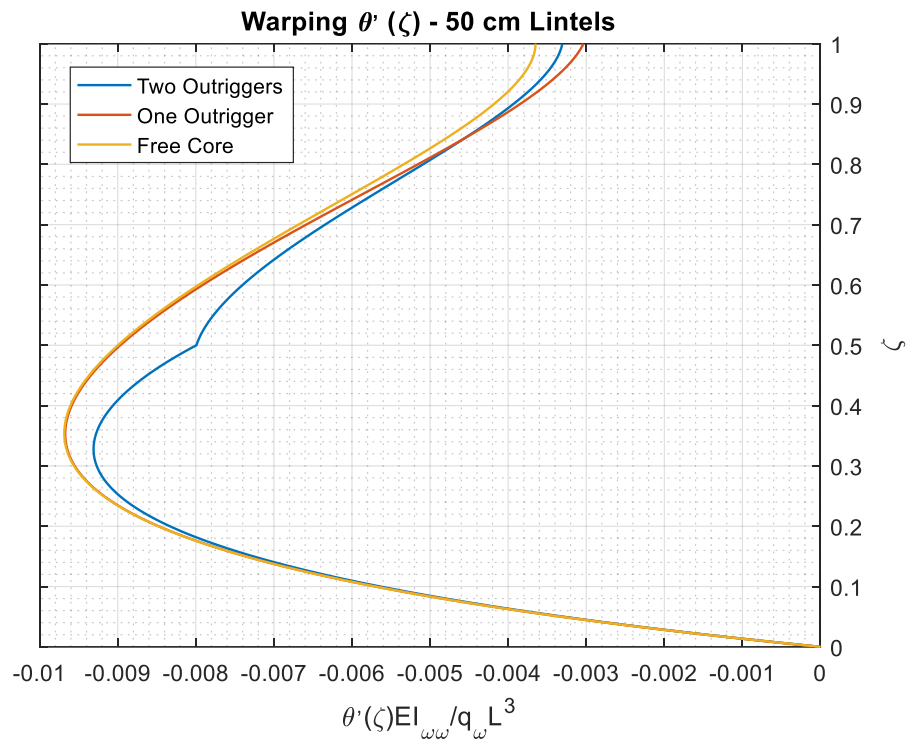


Figure 5.23: Core warping in presence of 50 cm lintels, due to a triangular torque

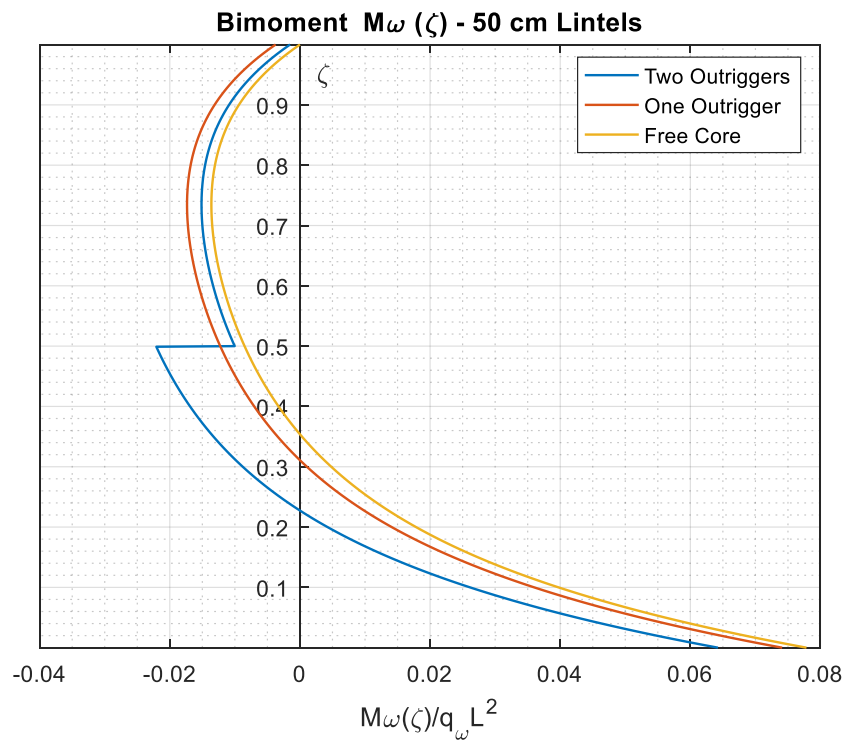


Figure 5.24: Core bimoment in presence of 50 cm lintels, due to a triangular torque

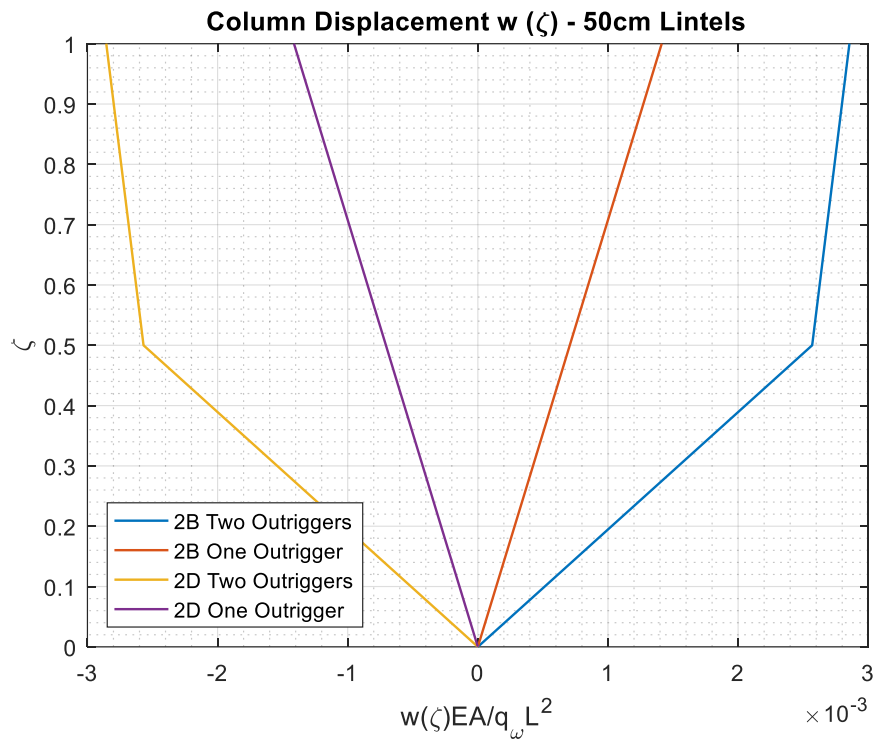


Figure 5.25: Column 2B and 2D displacements in presence of 50 cm lintels due to a triangular torque

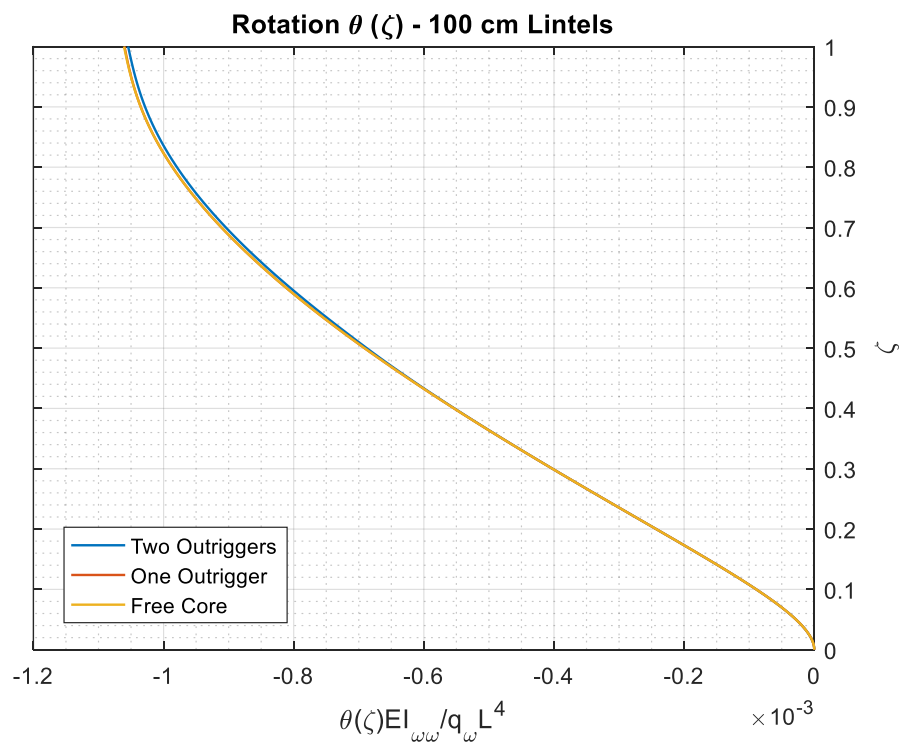


Figure 5.26: Core rotation in presence of 100 cm lintels, due to a triangular torque

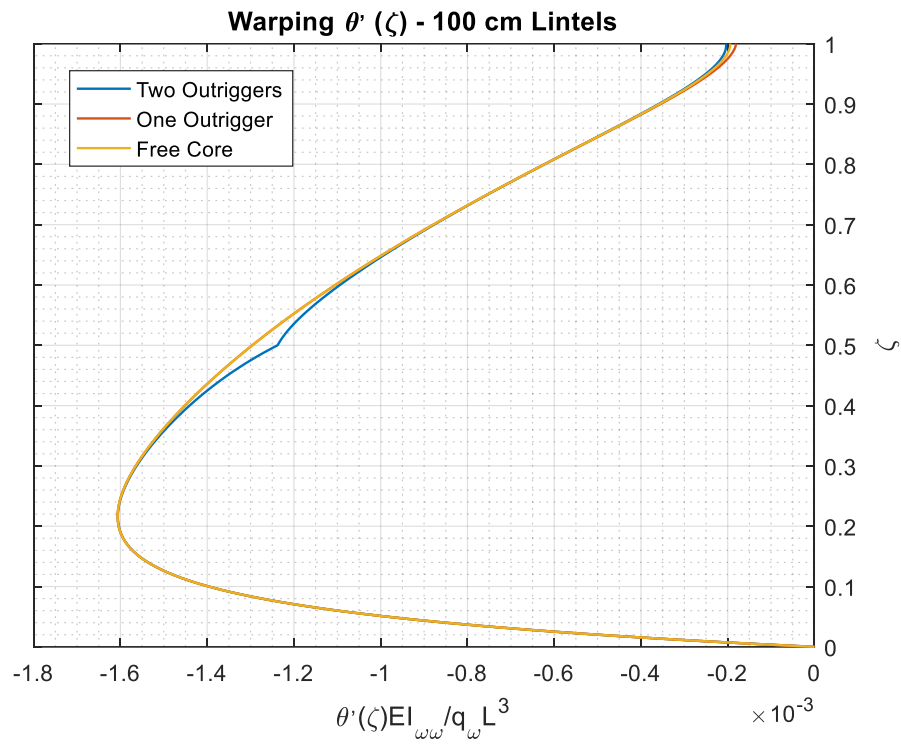


Figure 5.27: Core warping in presence of 100 cm lintels, due to a triangular torque

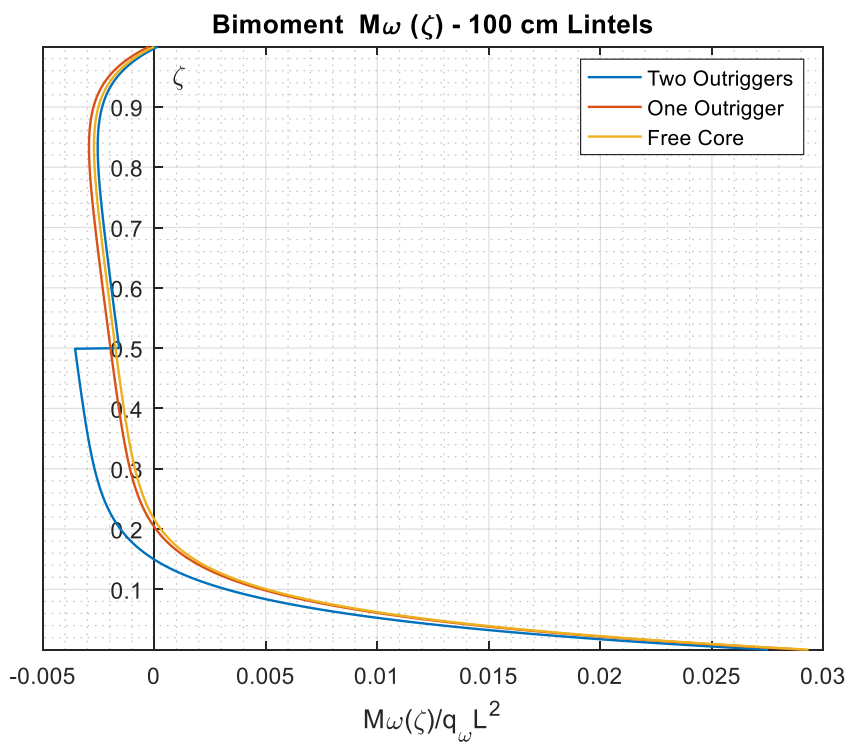


Figure 5.28: Core bimoment in presence of 100 cm lintels, due to a triangular torque

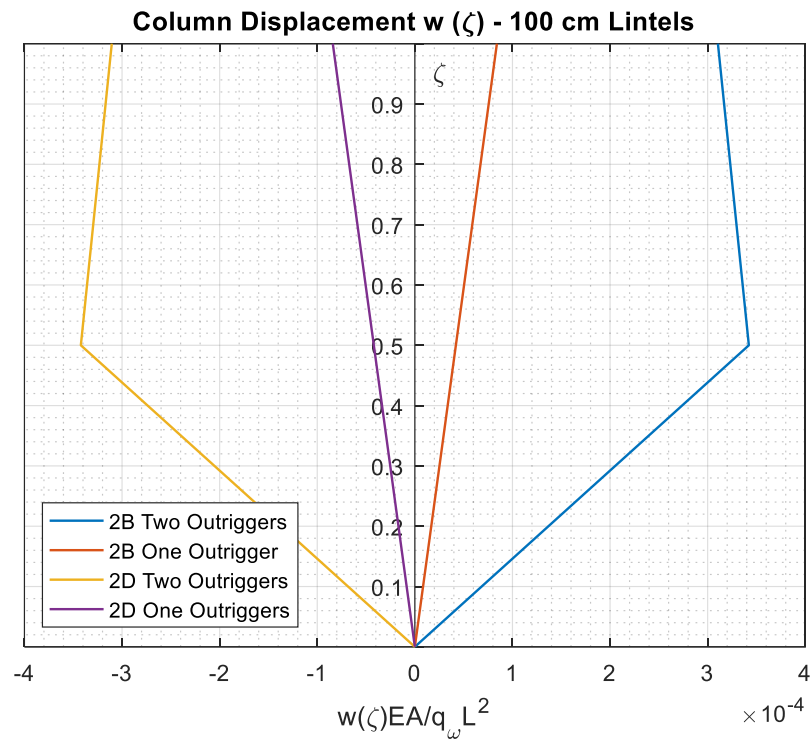


Figure 5.29: Column 2B and 2D displacements in presence of 100 cm lintels due to a triangular torque

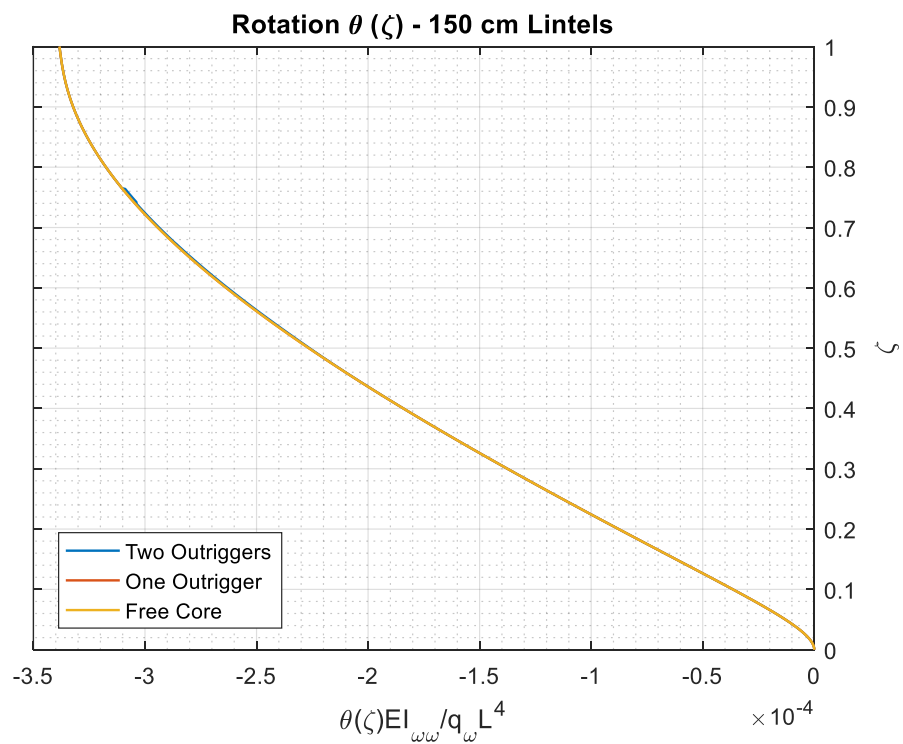


Figure 5.30: Core rotation in presence of 150 cm lintels, due to a triangular torque

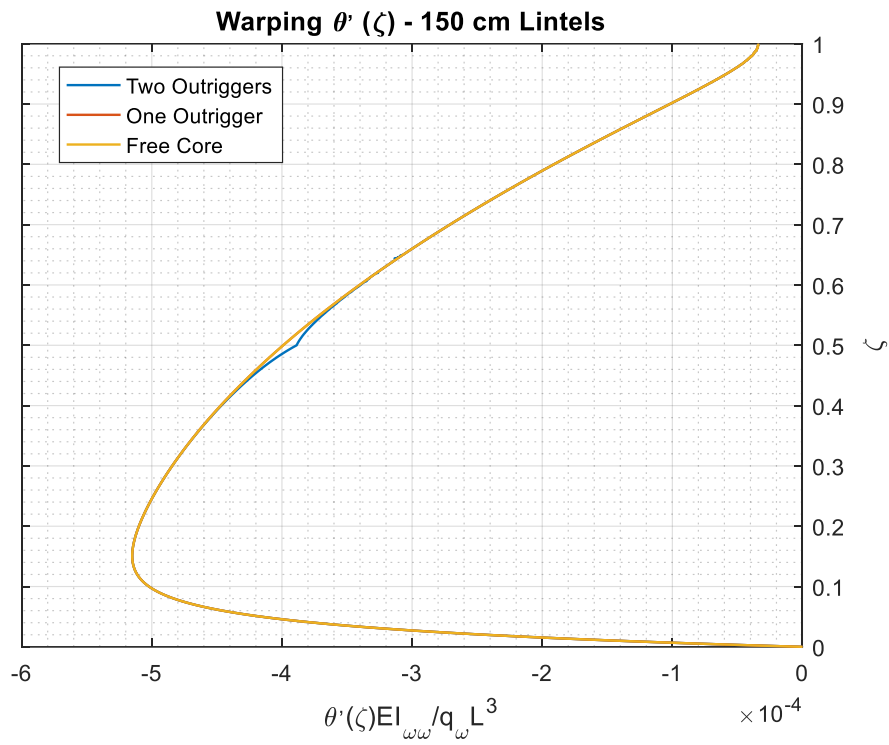


Figure 5.31: Core warping in presence of 150 cm lintels, due to a triangular torque

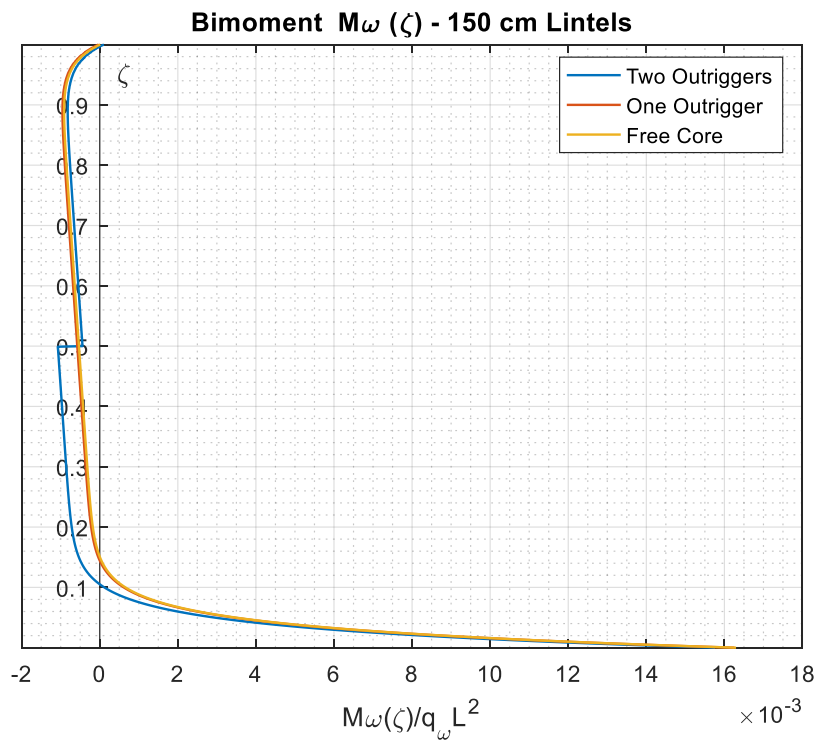


Figure 5.32: Core bimoment in presence of 150 cm lintels, due to a triangular torque

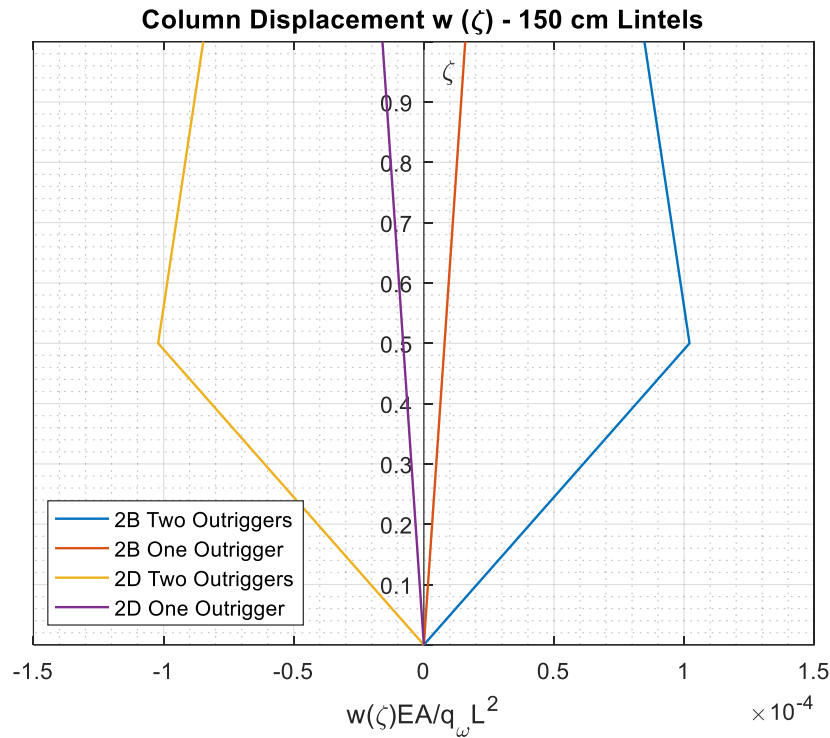


Figure 5.33: Column 2B and 2D displacements in presence of 100 cm lintels due to a triangular torque

As can be seen from the reported results, the effects of the outrigger system is almost negligible and it reduces as the dimensions of the lintels increase, leading to a behaviour almost identical to the free core case, in this case behaving as a thin-walled element of closed cross-section. The absence of warping is confirmed by the columns' displacement trends, as they reduce of two order of magnitude with respect to the case of diaphragms, where warping could still be detected. The bimoment along the height is almost zero but at the base it is much higher with respect to the global trend because of the presence of the clamp.

5.3.6 Long-Term Behaviour

The application of a lateral load constant in time generates a fairly pronounced delayed deformation due to creep depending on the rheological homogeneity of the whole structure. When the whole structure is rheologically homogeneous and subjected to loads constant in time, the basic theorems of linear viscoelasticity allow to express the stress and deformation states in the following way:

$$\begin{aligned} S(t) &= S_e \\ s(t) &= s_e \cdot [1 + \varphi(t, t_0)] \end{aligned} \quad (5.45)$$

where $S(t)$ represents the internal actions at time t while S_e are the initial ones at time t_0 evaluated assuming an elastic behaviour of the structure. In the same way, $s(t)$ and s_e are the displacements at time t and the elastic ones at time t_0 . $\varphi(t, t_0)$ is the creep coefficient,

expressing the ratio between the viscoelastic deformation and the elastic one, both considered for a unitary applied stress.

Equations (5.45) show that the stress state remains unchanged in time and can be computed by means of an elastic analysis, while the displacements increase in an affine way to the elastic ones. When rheological non-homogeneities are present, the problem becomes quite involved and the necessity of reaching a simple but well approximate solution is strongly convenient. For this reason, two limiting situations should be analysed by using algebraic procedures for creep analysis:

- Case a): Elastic behaviour for the outriggers and linear viscoelastic behaviour for the other parts, as it occurs for steel outriggers;
- Case b): Elastic behaviour for core and columns and viscoelastic behaviour for the outriggers. In this way we want to introduce, in an albeit approximate way, the non-homogeneity deriving from a different age of concrete. In other words, we are assuming that core and columns have been casted so early that they have already exhausted their viscoelastic deformations when outriggers are installed in the structure.

Regarding the procedure to be assumed for structural analysis, we shall introduce the Trost algebraic formulation, according to which equations (5.45) assume the following form:

$$\begin{aligned} S(t) &= S_e^{(1)}(t) \cdot (1 - \mu) + \mu \cdot S_e \\ s(t) &= s_e^{(1)}(t) \cdot (1 - \mu) + \mu \cdot s_e \end{aligned} \quad (5.46)$$

where $S_e^{(1)}$ and $s_e^{(1)}$ are the elastic quantities evaluated assuming the modified modulus for the viscoelastic parts:

$$E' = \frac{E}{1 + \chi\varphi} \quad (5.47)$$

Assuming for the aging factor χ a value of 0.8 and recalling that:

$$\mu = -\frac{1 - \chi}{\chi} \quad (5.48)$$

we obtain $\mu = -0.25$ and the use of equations (5.46) become straightforward.

The briefly summarized procedure here presented consists in increasing the deformability of the viscoelastic parts, so that when the outriggers are assumed as elastic, the interaction force increases in time, while for viscoelastic outriggers the reaction force decreases. Regarding

the displacements, they increase in the two cases but at a reduced rate with respect to equations (5.45). As done in the previous discussion, Case a) and Case b) are now applied to the considered structure by considering the cases of one level of outriggers only and two levels of outriggers.

➤ *Case a) - One Level of Outriggers*

According to the first of equations (5.46), to solve the problem it is necessary to compute the interaction forces $P_{1\omega,e}$ and $P_{1\omega,e}^{(1)}$. $P_{1\omega,e}$ coincides with the interaction force $P_{1\omega}$ already computed in §5.3.1 while $P_{1\omega,e}^{(1)}$ needs now to be computed accounting for the long-term behaviour of the viscoelastic parts (i.e. core and column) through the varied modulus of elasticity expressed by equation (5.47). According to this, the compatibility equation becomes:

$$P_{1\omega,e}^{(1)} \left[\left(-4\theta'_1(\bar{\zeta})\omega_B^2 + \bar{\zeta} \frac{L}{EA_C} \right) \cdot (1 + \chi\varphi) + \frac{L_0^3}{3EI_0} \right] = \theta'_0(\bar{\zeta})\omega_B \cdot (1 + \chi\varphi) \quad (5.49)$$

where $\bar{\zeta} = 1$ represents the level of the outriggers, that is, in this case, the top of the structure. All terms presented in equation (5.49) have the same meaning as those already defined in equation (5.28).

By combining the results of equations (5.28) and (5.49), the value in time of the interaction force $P_{1\omega}(t)$ and, in turn, the corresponding bimoment $M_{1\omega}(t)$ can be computed according to equations (5.46):

$$\begin{aligned} P_{1\omega}(t) &= P_{1\omega,e}^{(1)}(t) \cdot (1 - \mu) + \mu \cdot P_{1\omega,e} \\ M_{1\omega}(t) &= 4 \cdot P_{1\omega}(t) \cdot \omega_b \end{aligned} \quad (5.50)$$

Once we know these quantities, it is possible to define the time variation of the torsional rotation $\theta(\zeta, \bar{\zeta}, t)$ of the core by applying the second of equations (5.46):

$$\theta(\zeta, \bar{\zeta}, t) = \theta_e^{(1)} \cdot (1 - \mu) + \theta_e \cdot \mu \quad (5.51)$$

where θ_e is given by equation (5.31) and $\theta_e^{(1)}$ is given by equation (5.31) in which the elastic modulus has been replaced by the varied elastic modulus of equation (5.47). Thus:

$$\begin{aligned} \theta_e^{(1)}(\zeta, \bar{\zeta}, t) &= \theta_0(\zeta) \cdot (1 + \chi\varphi) + \theta_1^{M_{1\omega}(t)}(\zeta, \bar{\zeta} = 1) \cdot (1 + \chi\varphi) \\ \theta_e(\zeta, \bar{\zeta}, t) &= \theta_0(\zeta) + \theta_1^{M_{1\omega}}(\zeta, \bar{\zeta} = 1) \end{aligned} \quad (5.52)$$

where, analogously to §5.3.1, $\theta_0(\zeta)$ is the torsional rotation induced by the torque load and given by the first of equations (4.35), while $\theta_1^{M_{1\omega}(t)}$ and $\theta_1^{M_{1\omega}}$ are, respectively, the torsional

rotations induced by the interaction moments of equation (5.46) and (5.30), obtained by multiplying the corresponding *Green Function* in Table 4.5 by $M_{1\omega}(t)$ and $M_{1\omega}$.

Given this, the warping $\theta'(\zeta, \bar{\zeta}, t)$ and the bimoment $M_\omega(\zeta, \bar{\zeta}, t)$ can be defined by following the same path of reasoning, reading:

$$\theta'(\zeta, \bar{\zeta}, t) = \theta'_e{}^{(1)} \cdot (1 - \mu) + \theta'_e \cdot \mu \quad (5.53)$$

$$M_\omega(\zeta, \bar{\zeta}, t) = M_{\omega,e}{}^{(1)} \cdot (1 - \mu) + M_{\omega,e} \cdot \mu \quad (5.54)$$

where θ'_e and $M_{\omega,e}$ are given by equations (5.32) and (5.33), while $\theta'_e{}^{(1)}$ and $M_{\omega,e}{}^{(1)}$ are as follows:

$$\begin{aligned} \theta'_e{}^{(1)}(\zeta, \bar{\zeta}, t) &= \theta'_0(\zeta) \cdot (1 + \chi\varphi) + \theta'_1{}^{M_{1\omega}(t)}(\zeta, \bar{\zeta} = 1) \cdot (1 + \chi\varphi) \\ M_{\omega,e}{}^{(1)}(\zeta, \bar{\zeta}, t) &= M_{0\omega}(\zeta) + M_{1\omega}(t) \end{aligned} \quad (5.55)$$

➤ *Case a) - Two Levels of Outriggers*

In this case, the first of equations (5.46) makes necessary to calculate four interaction forces, that is $P_{1\omega,e}$, $P_{2\omega,e}$, $P_{1\omega,e}^{(1)}$ and $P_{2\omega,e}^{(1)}$. Aware of the fact that $P_{1\omega,e}$ and $P_{2\omega,e}$ are the elastic solutions according to equations (5.38), it now remains to compute $P_{1\omega,e}^{(1)}$ and $P_{2\omega,e}^{(1)}$. Thus, the system of compatibility equations becomes:

$$\begin{aligned} &P_{1\omega} \left[\left(-4\theta'_1(\bar{\zeta}_1, \bar{\zeta}_1)\omega_B^2 + \bar{\zeta}_1 \frac{L}{EA_C} \right) (1 + \chi\varphi) + \frac{L_0^3}{3EI_0} \right] + \\ &+ P_{2\omega} \left[-4\theta'_1(\bar{\zeta}_1, \bar{\zeta}_2)\omega_B^2 + (\bar{\zeta}_2 - \bar{\zeta}_1) \frac{L}{EA_C} \right] (1 + \chi\varphi) \\ &= \\ &\theta'_0(\bar{\zeta}_1)\omega_B(1 + \chi\varphi) \end{aligned} \quad (5.56)$$

$$\begin{aligned} &P_{1\omega} \left[-4\theta'_2(\bar{\zeta}_2, \bar{\zeta}_1)\omega_B^2 + \bar{\zeta}_1 \frac{L}{EA_C} \right] (1 + \chi\varphi) + \\ &+ P_{2\omega} \left[\left(-4\theta'_1(\bar{\zeta}_2, \bar{\zeta}_2)\omega_B^2 + \bar{\zeta}_2 \frac{L}{EA_C} \right) (1 + \chi\varphi) + \frac{L_0^3}{3EI_0} \right] \\ &= \\ &\theta'_0(\bar{\zeta}_2)\omega_B(1 + \chi\varphi) \end{aligned}$$

The first of equations (5.56) is the compatibility equation at the 1st level of outriggers (mid-height: $\bar{\zeta}_1 = 0.5$) while the second is written at the 2nd level of outriggers (top: $\bar{\zeta}_1 = 1$). All terms presented in equations (5.56) have the same meaning as those already defined in equations (5.35).

By combining the results of equations (5.35) and (5.56), the value in time of the interaction forces $P_{1\omega}(t)$, $P_{2\omega}(t)$ and, in turn, the corresponding bimoment $M_{1\omega}(t)$, $M_{2\omega}(t)$ can be computed according to equations (5.57):

$$\begin{aligned} P_{1\omega}(t) &= P_{1\omega,e}^{(1)}(t) \cdot (1 - \mu) + \mu \cdot P_{1\omega,e}; & P_{2\omega}(t) &= P_{2\omega,e}^{(1)}(t) \cdot (1 - \mu) + \mu \cdot P_{2\omega,e} \\ M_{1\omega}(t) &= 4 \cdot P_{1\omega}(t) \cdot \omega_B; & M_{2\omega}(t) &= 4 \cdot P_{2\omega}(t) \cdot \omega_B \end{aligned} \quad (5.57)$$

Once we know these quantities, it is possible to define the time variation of the torsional rotation $\theta(\zeta, \bar{\zeta}, t)$ of the core by applying the second of equations (5.46):

$$\theta(\zeta, \bar{\zeta}, t) = \theta_e^{(1)} \cdot (1 - \mu) + \theta_e \cdot \mu \quad (5.58)$$

where θ_e is given by equations (5.39) and $\theta_e^{(1)}$ is given by equations (5.39) in which the elastic modulus has been replaced by the varied elastic modulus of equation (5.47). Thus:

$$\begin{aligned} \theta_e(\zeta, \bar{\zeta}) &= \theta_0(\zeta) + \theta_1^{M_{1\omega}}(\zeta, \bar{\zeta}_1 = 0.5) + \theta_1^{M_{2\omega}}(\zeta, \bar{\zeta}_2 = 1) & 0 \leq \zeta \leq \bar{\zeta}_1 \\ \theta_e(\zeta, \bar{\zeta}) &= \theta_0(\zeta) + \theta_2^{M_{1\omega}}(\zeta, \bar{\zeta}_1 = 0.5) + \theta_1^{M_{2\omega}}(\zeta, \bar{\zeta}_2 = 1) & \bar{\zeta}_1 \leq \zeta \leq \bar{\zeta}_2 \end{aligned} \quad (5.59)$$

$$\begin{aligned} \theta_e^{(1)}(\zeta, \bar{\zeta}, t) &= [\theta_0(\zeta) + \theta_1^{M_{1\omega}(t)}(\zeta, \bar{\zeta}_1 = 0.5) + \theta_1^{M_{2\omega}(t)}(\zeta, \bar{\zeta}_2 = 1)](1 + \chi\varphi) & 0 \leq \zeta \leq \bar{\zeta}_1 \\ \theta_e^{(1)}(\zeta, \bar{\zeta}, t) &= [\theta_0(\zeta) + \theta_2^{M_{1\omega}(t)}(\zeta, \bar{\zeta}_1 = 0.5) + \theta_1^{M_{2\omega}(t)}(\zeta, \bar{\zeta}_2 = 1)](1 + \chi\varphi) & \bar{\zeta}_1 \leq \zeta \leq \bar{\zeta}_2 \end{aligned} \quad (5.60)$$

where, analogously to §5.3.2, $\theta_0(\zeta)$ is the torsional rotation induced by the torque load and given by the first of equations (4.35), while $\theta_1^{M_{1\omega}(t)}$, $\theta_1^{M_{2\omega}(t)}$, $\theta_2^{M_{1\omega}(t)}$ and $\theta_1^{M_{1\omega}}$, $\theta_1^{M_{2\omega}}$, $\theta_2^{M_{1\omega}}$ are, respectively, the torsional rotations induced by the interaction moments of equation (5.57) and (5.38), obtained by multiplying the corresponding *Green Function* in Table 4.5 by $M_{1\omega}(t)$, $M_{2\omega}(t)$ and $M_{1\omega}$, $M_{2\omega}$.

Given this, the warping $\theta'(\zeta, \bar{\zeta}, t)$ and the bimoment $M_\omega(\zeta, \bar{\zeta}, t)$ can be defined by following the same path of reasoning, reading:

$$\theta'(\zeta, \bar{\zeta}, t) = \theta_e'^{(1)} \cdot (1 - \mu) + \theta_e' \cdot \mu \quad (5.61)$$

$$M_\omega(\zeta, \bar{\zeta}, t) = M_{\omega,e}^{(1)} \cdot (1 - \mu) + M_{\omega,e} \cdot \mu \quad (5.62)$$

where θ_e' , $\theta_e'^{(1)}$ and $M_{\omega,e}$, $M_{\omega,e}^{(1)}$ are as follows:

$$\begin{aligned} \theta_e'(\zeta, \bar{\zeta}) &= \theta_0'(\zeta) + \theta_1^{M_{1\omega}}(\zeta, \bar{\zeta}_1 = 0.5) + \theta_1^{M_{2\omega}}(\zeta, \bar{\zeta}_2 = 1) & 0 \leq \zeta \leq \bar{\zeta}_1 \\ \theta_e'(\zeta, \bar{\zeta}) &= \theta_0'(\zeta) + \theta_2^{M_{1\omega}}(\zeta, \bar{\zeta}_1 = 0.5) + \theta_1^{M_{2\omega}}(\zeta, \bar{\zeta}_2 = 1) & \bar{\zeta}_1 \leq \zeta \leq \bar{\zeta}_2 \end{aligned} \quad (5.63)$$

$$\begin{aligned}\theta_e^{(1)}(\zeta, \bar{\zeta}, t) &= \left[\theta'_0(\zeta) + \theta'_1 M_{1\omega(t)}(\zeta, \bar{\zeta}_1 = 0.5) + \theta'_1 M_{2\omega(t)}(\zeta, \bar{\zeta}_2 = 1) \right] (1 + \chi\varphi) & 0 \leq \zeta \leq \bar{\zeta}_1 \\ \theta_e^{(1)}(\zeta, \bar{\zeta}, t) &= \left[\theta'_0(\zeta) + \theta'_2 M_{1\omega(t)}(\zeta, \bar{\zeta}_1 = 0.5) + \theta'_1 M_{2\omega(t)}(\zeta, \bar{\zeta}_2 = 1) \right] (1 + \chi\varphi) & \bar{\zeta}_1 \leq \zeta \leq \bar{\zeta}_2\end{aligned}\quad (5.64)$$

$$\begin{aligned}M_{\omega,e}(\zeta, \bar{\zeta}) &= M_{0\omega}(\zeta) + M_{1\omega} + M_{2\omega} & 0 \leq \zeta \leq \bar{\zeta}_1 \\ M_{\omega,e}(\zeta, \bar{\zeta}) &= M_{0\omega}(\zeta) + M_{2\omega} & \bar{\zeta}_1 \leq \zeta \leq \bar{\zeta}_2\end{aligned}\quad (5.65)$$

$$\begin{aligned}M_{\omega,e}^{(1)}(\zeta, \bar{\zeta}, t) &= M_{0\omega}(\zeta) + M_{1\omega}(t) + M_{2\omega}(t) & 0 \leq \zeta \leq \bar{\zeta}_1 \\ M_{\omega,e}^{(1)}(\zeta, \bar{\zeta}, t) &= M_{0\omega}(\zeta) + M_{2\omega}(t) & \bar{\zeta}_1 \leq \zeta \leq \bar{\zeta}_2\end{aligned}\quad (5.66)$$

➤ **Case b) - One Level of Outriggers**

According to the first of equations (5.46), to solve the problem it is necessary to compute the interaction forces $P_{1\omega,e}$ and $P_{1\omega,e}^{(1)}$. $P_{1\omega,e}$ coincides with the interaction force $P_{1\omega}$ already computed in §5.3.1 while $P_{1\omega,e}^{(1)}$ needs now to be computed accounting for the long-term behaviour of the viscoelastic parts (i.e. the outriggers) through the varied modulus of elasticity expressed by equation (5.47). According to this, the compatibility equation becomes:

$$P_{1\omega} \left[-4\theta'_1(\bar{\zeta})\omega_B^2 + \frac{L_0^3}{3EI_0}(1 + \chi\varphi) + \bar{\zeta} \frac{L}{EA_C} \right] = \theta'_0(\bar{\zeta})\omega_B \quad (5.67)$$

where $\bar{\zeta} = 1$ represents the level of the outriggers, that is, in this case, the top of the structure. All terms presented in equation (5.67) have the same meaning as those already defined in equation (5.28).

By combining the results of equations (5.28) and (5.67), the value in time of the interaction force $P_{1\omega}(t)$ and, in turn, the corresponding bimoment $M_{1\omega}(t)$ can be computed according to equations (5.46):

$$\begin{aligned}P_{1\omega}(t) &= P_{1\omega,e}^{(1)}(t) \cdot (1 - \mu) + \mu \cdot P_{1\omega,e} \\ M_{1\omega}(t) &= 4 \cdot P_{1\omega}(t) \cdot \omega_B\end{aligned}\quad (5.68)$$

Once we know these quantities, it is possible to define the time variation of the torsional rotation $\theta(\zeta, \bar{\zeta}, t)$ of the core by applying the second of equations (5.46):

$$\theta(\zeta, \bar{\zeta}, t) = \theta_e^{(1)} \cdot (1 - \mu) + \theta_e \cdot \mu \quad (5.69)$$

where θ_e is given by equation (5.31) and $\theta_e^{(1)}$ is given by equation (5.31) in which the interaction bimoment $M_{1\omega}(t)$ is taken into account. Thus:

$$\begin{aligned}\theta_e^{(1)}(\zeta, \bar{\zeta}, t) &= \theta_0(\zeta) + \theta_1^{M_{1\omega}(t)}(\zeta, \bar{\zeta} = 1) \\ \theta_e(\zeta, \bar{\zeta}) &= \theta_0(\zeta) + \theta_1^{M_{1\omega}}(\zeta, \bar{\zeta} = 1)\end{aligned}\quad (5.70)$$

where, analogously to §5.3.1, $\theta_0(\zeta)$ is the torsional rotation induced by the torque load and given by the first of equations (4.35), while $\theta_1^{M_{1\omega}(t)}$ and $\theta_1^{M_{1\omega}}$ are, respectively, the torsional rotations induced by the interaction moments of equation (5.68) and (5.30), obtained by multiplying the corresponding *Green Function* in Table 4.5 by $M_{1\omega}(t)$ and $M_{1\omega}$.

Given this, the warping $\theta'(\zeta, \bar{\zeta}, t)$ and the bimoment $M_\omega(\zeta, \bar{\zeta}, t)$ can be defined by following the same path of reasoning, reading:

$$\theta'(\zeta, \bar{\zeta}, t) = \theta_e'^{(1)} \cdot (1 - \mu) + \theta_e' \cdot \mu \quad (5.71)$$

$$M_\omega(\zeta, \bar{\zeta}, t) = M_{\omega,e}^{(1)} \cdot (1 - \mu) + M_{\omega,e} \cdot \mu \quad (5.72)$$

where θ_e' and $M_{\omega,e}$ are given by equations (5.32) and (5.33), while $\theta_e'^{(1)}$ and $M_{\omega,e}^{(1)}$ are as follows:

$$\begin{aligned}\theta_e'^{(1)}(\zeta, \bar{\zeta}, t) &= \theta_0'(\zeta) + \theta_1^{M_{1\omega}(t)}(\zeta, \bar{\zeta} = 1) \\ M_{\omega,e}^{(1)}(\zeta, \bar{\zeta}, t) &= M_{0\omega}(\zeta) + M_{1\omega}(t)\end{aligned}\quad (5.73)$$

➤ *Case b) - Two Levels of Outriggers*

In this case, the first of equations (5.46) makes necessary to calculate four interaction forces, that is $P_{1\omega,e}$, $P_{2\omega,e}$, $P_{1\omega,e}^{(1)}$ and $P_{2\omega,e}^{(1)}$. Aware of the fact that $P_{1\omega,e}$ and $P_{2\omega,e}$ are the elastic solutions according to equations (5.38), it now remains to compute $P_{1\omega,e}^{(1)}$ and $P_{2\omega,e}^{(1)}$. Thus, the system of compatibility equations becomes:

$$\begin{aligned}P_{1\omega} \left[-4\theta_1'(\bar{\zeta}_1, \bar{\zeta}_1)\omega_B^2 + \frac{L_0^3}{3EI_0}(1 + \chi\varphi) + \bar{\zeta}_1 \frac{L}{EA_C} \right] + \\ P_{2\omega} \left[-4\theta_1'(\bar{\zeta}_1, \bar{\zeta}_2)\omega_B^2 + (\bar{\zeta}_2 - \bar{\zeta}_1) \frac{L}{EA_C} \right] \\ = \\ \theta_0'(\bar{\zeta}_1)\omega_B \\ P_{1\omega} \left[-4\theta_2'(\bar{\zeta}_2, \bar{\zeta}_1)\omega_B^2 + \bar{\zeta}_1 \frac{L}{EA_C} \right] + \\ P_{2\omega} \left[-4\theta_1'(\bar{\zeta}_2, \bar{\zeta}_2)\omega_B^2 + \frac{L_0^3}{3EI_0}(1 + \chi\varphi) + \bar{\zeta}_2 \frac{L}{EA_C} \right] \\ = \\ \theta_0'(\bar{\zeta}_2)\omega_B\end{aligned}\quad (5.74)$$

The first of equations (5.74) is the compatibility equation at the 1st level of outriggers (mid-height: $\bar{\zeta}_1 = 0.5$) while the second is written at the 2nd level of outriggers (top: $\bar{\zeta}_1 = 1$). All terms presented in equations (5.74) have the same meaning as those already defined in equations (5.35).

By combining the results of equations (5.35) and (5.74), the value in time of the interaction forces $P_{1\omega}(t)$, $P_{2\omega}(t)$ and, in turn, the corresponding bimoment $M_{1\omega}(t)$, $M_{2\omega}(t)$ can be computed according to equations (5.57):

$$\begin{aligned} P_{1\omega}(t) &= P_{1\omega,e}^{(1)}(t) \cdot (1 - \mu) + \mu \cdot P_{1\omega,e}; & P_{2\omega}(t) &= P_{2\omega,e}^{(1)}(t) \cdot (1 - \mu) + \mu \cdot P_{2\omega,e} \\ M_{1\omega}(t) &= 4 \cdot P_{1\omega}(t) \cdot \omega_B; & M_{2\omega}(t) &= 4 \cdot P_{2\omega}(t) \cdot \omega_B \end{aligned} \quad (5.75)$$

Once we know these quantities, it is possible to define the time variation of the torsional rotation $\theta(\zeta, \bar{\zeta}, t)$ of the core by applying the second of equations (5.46):

$$\theta(\zeta, \bar{\zeta}, t) = \theta_e^{(1)} \cdot (1 - \mu) + \theta_e \cdot \mu \quad (5.76)$$

where θ_e is given by equations (5.39) and $\theta_e^{(1)}$ is given by equations (5.39) in which the elastic modulus has been replaced by the varied elastic modulus of equation (5.47). Thus:

$$\begin{aligned} \theta_e(\zeta, \bar{\zeta}) &= \theta_0(\zeta) + \theta_1^{M_{1\omega}}(\zeta, \bar{\zeta}_1 = 0.5) + \theta_1^{M_{2\omega}}(\zeta, \bar{\zeta}_2 = 1) & 0 \leq \zeta \leq \bar{\zeta}_1 \\ \theta_e(\zeta, \bar{\zeta}) &= \theta_0(\zeta) + \theta_2^{M_{1\omega}}(\zeta, \bar{\zeta}_1 = 0.5) + \theta_1^{M_{2\omega}}(\zeta, \bar{\zeta}_2 = 1) & \bar{\zeta}_1 \leq \zeta \leq \bar{\zeta}_2 \end{aligned} \quad (5.77)$$

$$\begin{aligned} \theta_e^{(1)}(\zeta, \bar{\zeta}, t) &= \theta_0(\zeta) + \theta_1^{M_{1\omega}(t)}(\zeta, \bar{\zeta}_1 = 0.5) + \theta_1^{M_{2\omega}(t)}(\zeta, \bar{\zeta}_2 = 1) & 0 \leq \zeta \leq \bar{\zeta}_1 \\ \theta_e^{(1)}(\zeta, \bar{\zeta}, t) &= \theta_0(\zeta) + \theta_2^{M_{1\omega}(t)}(\zeta, \bar{\zeta}_1 = 0.5) + \theta_1^{M_{2\omega}(t)}(\zeta, \bar{\zeta}_2 = 1) & \bar{\zeta}_1 \leq \zeta \leq \bar{\zeta}_2 \end{aligned} \quad (5.78)$$

where, analogously to §5.3.2, $\theta_0(\zeta)$ is the torsional rotation induced by the torque load and given by the first of equations (4.35), while $\theta_1^{M_{1\omega}(t)}$, $\theta_1^{M_{2\omega}(t)}$, $\theta_2^{M_{1\omega}(t)}$ and $\theta_1^{M_{1\omega}}$, $\theta_1^{M_{2\omega}}$, $\theta_2^{M_{1\omega}}$ are, respectively, the torsional rotations induced by the interaction moments of equation (5.75) and (5.38), obtained by multiplying the corresponding *Green Function* in Table 4.5 by $M_{1\omega}$, $M_{2\omega}$ and $M_{1\omega}(t)$, $M_{2\omega}(t)$.

Given this, the warping $\theta'(\zeta, \bar{\zeta}, t)$ and the bimoment $M_\omega(\zeta, \bar{\zeta}, t)$ can be defined by following the same path of reasoning, reading:

$$\theta'(\zeta, \bar{\zeta}, t) = \theta_e'^{(1)} \cdot (1 - \mu) + \theta_e' \cdot \mu \quad (5.79)$$

$$M_\omega(\zeta, \bar{\zeta}, t) = M_{\omega,e}^{(1)} \cdot (1 - \mu) + M_{\omega,e} \cdot \mu \quad (5.80)$$

where θ_e' , $\theta_e'^{(1)}$ and $M_{\omega,e}$, $M_{\omega,e}^{(1)}$ are as follows:

$$\begin{aligned}\theta'_e(\zeta, \bar{\zeta}) &= \theta'_0(\zeta) + \theta'_1 M_{1\omega}(\zeta, \bar{\zeta}_1 = 0.5) + \theta'_1 M_{2\omega}(\zeta, \bar{\zeta}_2 = 1) & 0 \leq \zeta \leq \bar{\zeta}_1 \\ \theta'_e(\zeta, \bar{\zeta}) &= \theta'_0(\zeta) + \theta'_2 M_{1\omega}(\zeta, \bar{\zeta}_1 = 0.5) + \theta'_1 M_{2\omega}(\zeta, \bar{\zeta}_2 = 1) & \bar{\zeta}_1 \leq \zeta \leq \bar{\zeta}_2\end{aligned}\quad (5.81)$$

$$\begin{aligned}\theta_e^{(1)}(\zeta, \bar{\zeta}, t) &= \theta'_0(\zeta) + \theta'_1 M_{1\omega(t)}(\zeta, \bar{\zeta}_1 = 0.5) + \theta'_1 M_{2\omega(t)}(\zeta, \bar{\zeta}_2 = 1) & 0 \leq \zeta \leq \bar{\zeta}_1 \\ \theta_e^{(1)}(\zeta, \bar{\zeta}, t) &= \theta'_0(\zeta) + \theta'_2 M_{1\omega(t)}(\zeta, \bar{\zeta}_1 = 0.5) + \theta'_1 M_{2\omega(t)}(\zeta, \bar{\zeta}_2 = 1) & \bar{\zeta}_1 \leq \zeta \leq \bar{\zeta}_2\end{aligned}\quad (5.82)$$

$$\begin{aligned}M_{\omega,e}(\zeta, \bar{\zeta}) &= M_{0\omega}(\zeta) + M_{1\omega} + M_{2\omega} & 0 \leq \zeta \leq \bar{\zeta}_1 \\ M_{\omega,e}(\zeta, \bar{\zeta}) &= M_{0\omega}(\zeta) + M_{2\omega} & \bar{\zeta}_1 \leq \zeta \leq \bar{\zeta}_2\end{aligned}\quad (5.83)$$

$$\begin{aligned}M_{\omega,e}^{(1)}(\zeta, \bar{\zeta}, t) &= M_{0\omega}(\zeta) + M_{1\omega}(t) + M_{2\omega}(t) & 0 \leq \zeta \leq \bar{\zeta}_1 \\ M_{\omega,e}^{(1)}(\zeta, \bar{\zeta}, t) &= M_{0\omega}(\zeta) + M_{2\omega}(t) & \bar{\zeta}_1 \leq \zeta \leq \bar{\zeta}_2\end{aligned}\quad (5.84)$$

➤ Plots

In the following, torsional rotations, warping deformations and bimoments for Case a) and b) are plotted for both the situations of one and two outriggers levels. Results are also compared to those coming from analysing a pure elastic structure (Elastic Solution) and a homogenous viscoelastic structure (First Theorem of Viscoelasticity).

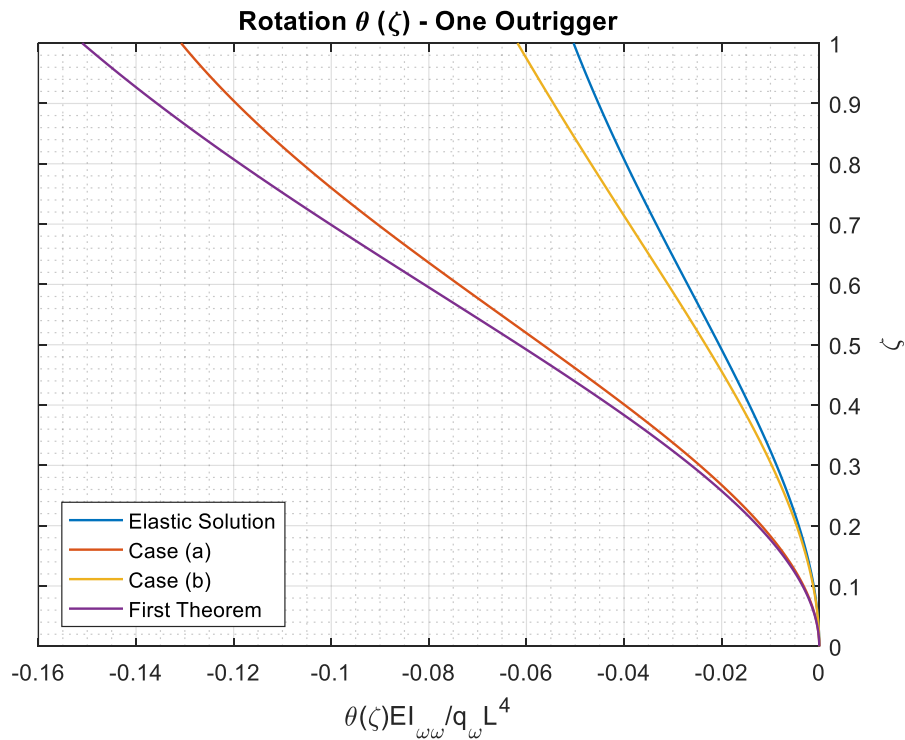


Figure 5.34: Viscoelastic behaviour - Rotation in case of one outriggers level

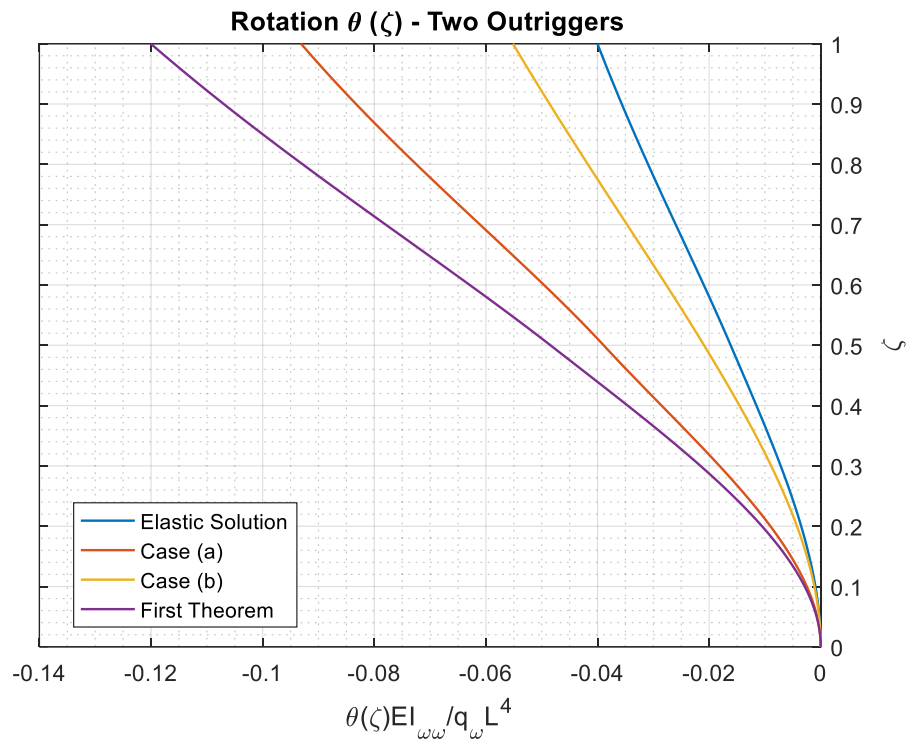


Figure 5.35: Viscoelastic behaviour - Rotation in case of two outriggers levels

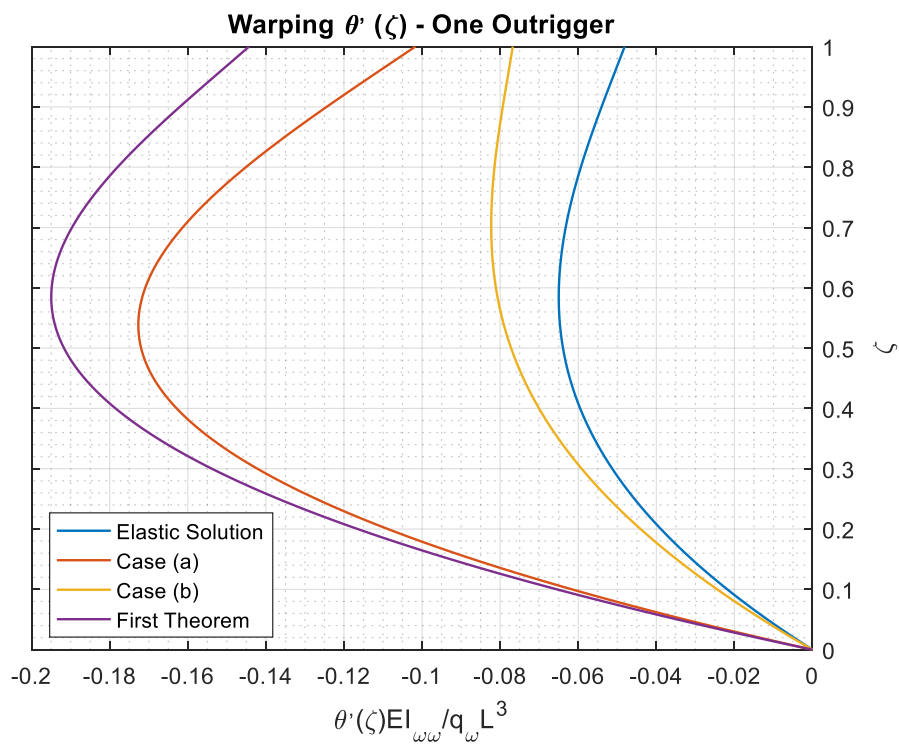


Figure 5.36: Viscoelastic behaviour - Warping in case of one outriggers level

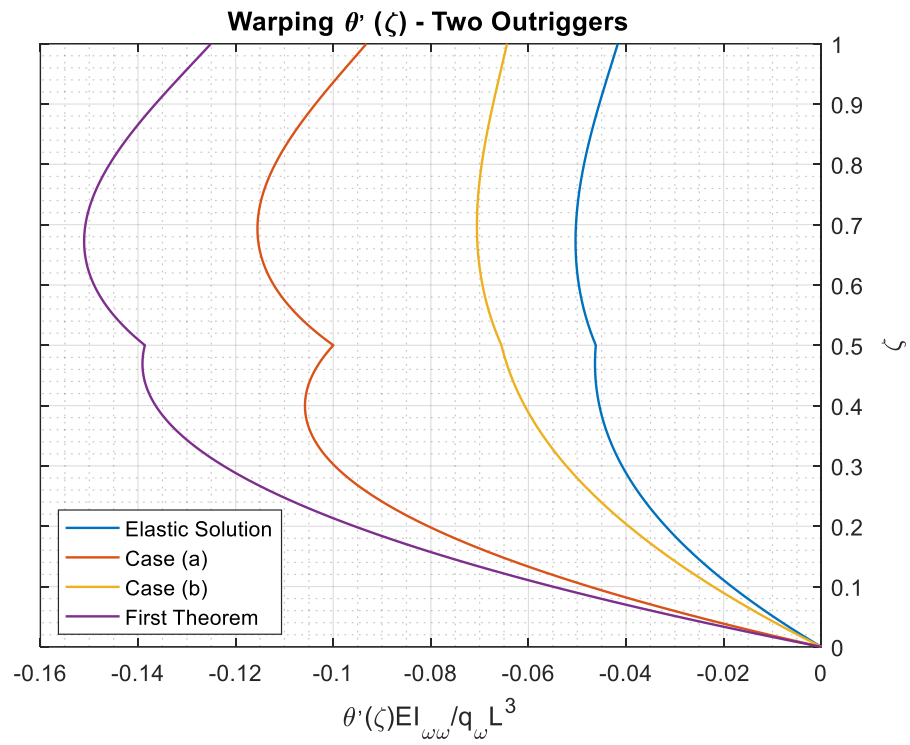


Figure 5.37: Viscoelastic behaviour - Warping in case of two outriggers levels

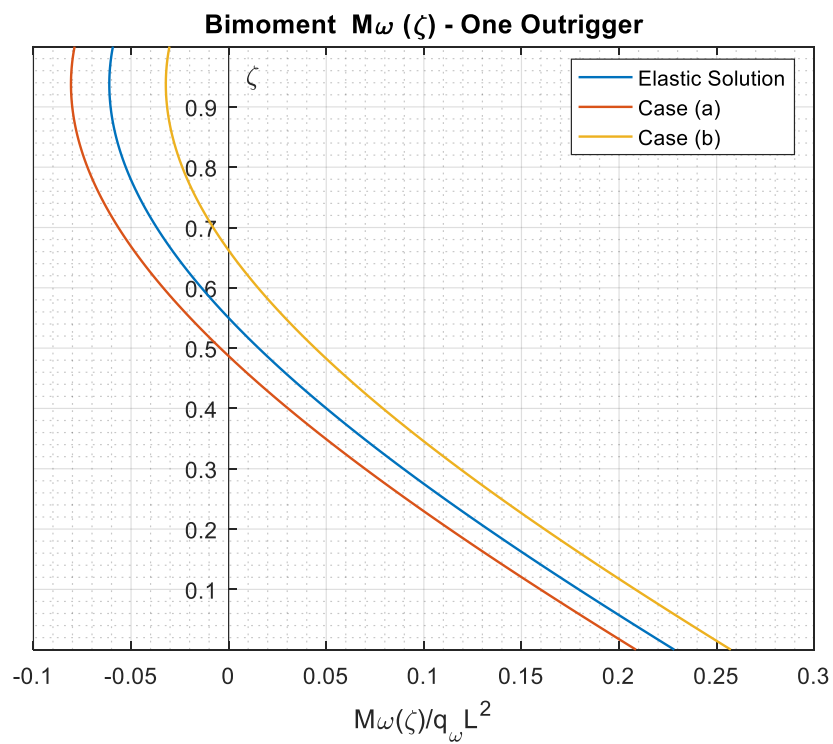


Figure 5.38: Viscoelastic behaviour - Bimoment in case of one outriggers level

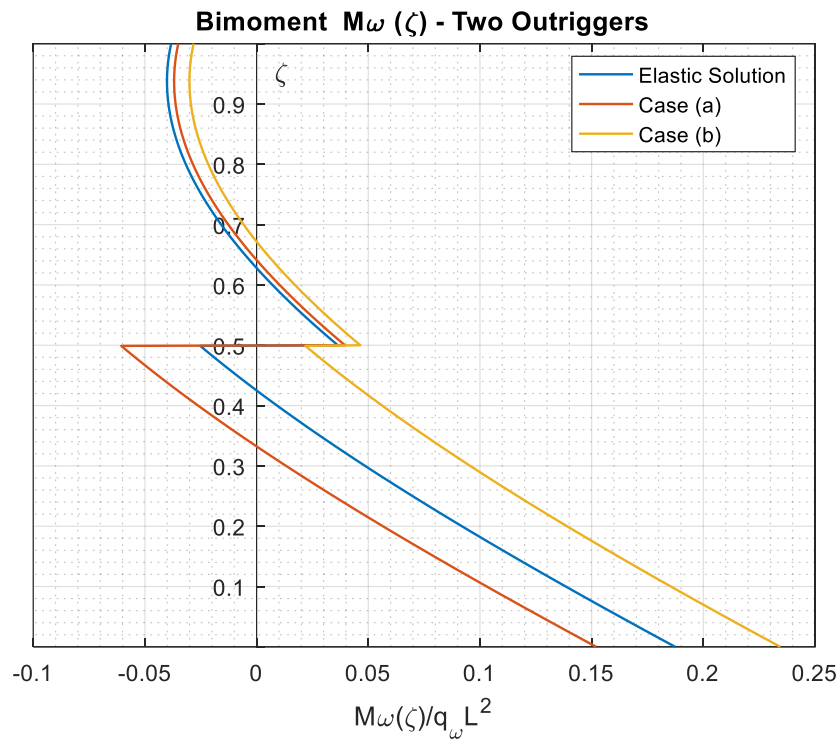


Figure 5.39: Viscoelastic behaviour - Bimoment in case of two outriggers levels

As it is possible to observe from Figure 5.34, Figure 5.35, Figure 5.36 and Figure 5.37 the solution provided by Case a) is close to the solution provided by the First Theorem of Viscoelasticity, since most of the structure (core and columns) is viscoelastic. Nevertheless, torsional rotation and warping deformation take on lower values than those suggested by the First Theorem because of the presence of elastic restraints (outriggers) applied to a viscoelastic structure. Following conceptually the same reasoning, the solution provided by Case b) is close to the Elastic Solution but torsional rotation and warping take on higher values than those suggested by the Elastic Solution since the outriggers are now viscoelastic and they are subjected to a progressive deformation in time due to relaxation, this reducing the restraining action on the elastic part (core and columns).

Furthermore, comparing the rotation for one and two levels of outriggers, it can be observed that the distance between the curve associated to Case a) and the First Theorem is higher when two levels of outriggers rather than only one are considered because of the presence of two elastic restraints (outriggers) which work together to reduce the rotation. In the same way, in Case b) the distance with respect to the Elastic Curve is higher when two levels of outriggers are considered since there are two viscoelastic restraints that are reducing their effects contemporary, this leading to a more pronounced increase of torsional rotation than the one achieved when one level of outriggers only is disposed.

As concerns the bimoment, from Figure 5.38 and Figure 5.39 it can be observed the following: when one level of outriggers is considered, the bimoment at the top for Case a) is higher than the one suggested by the elastic solution because the viscoelastic structure

increases its deformation in time, leading to an increasing reaction of the elastic restraint (outrigger). On the contrary, in Case b) the reaction provided by the viscoelastic outrigger at the top reduces in time due to relaxation and, therefore, the curve is now lower than the one provided by the Elastic Solution. The same path of reasoning can be adopted for the cases of two outriggers, at the top and at mid-height.

5.4 BENDING – TORSION INTERACTION

Despite the triangular prismatic volumes of the considered structure are disposed in a way that their effect on the building is of pure torsion, different structural configurations, as the one reported in Figure 5.40, may lead to a combination of flexure and torsion. In such circumstances, understanding whether one effect prevails or not on the other is of fundamental importance.



Figure 5.40: *Bending-torsion interaction*

To illustrate the features of the bending-torsion interaction which may characterize specific problems, in the following we will study the effects induced by a single sloping outward triangular volume when it is progressively moved towards the right from its initial position. One level of outriggers is considered only, located at the top of the building.

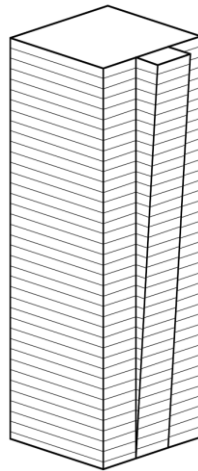


Figure 5.41: General 3D view of the problem for bending-torsion interaction

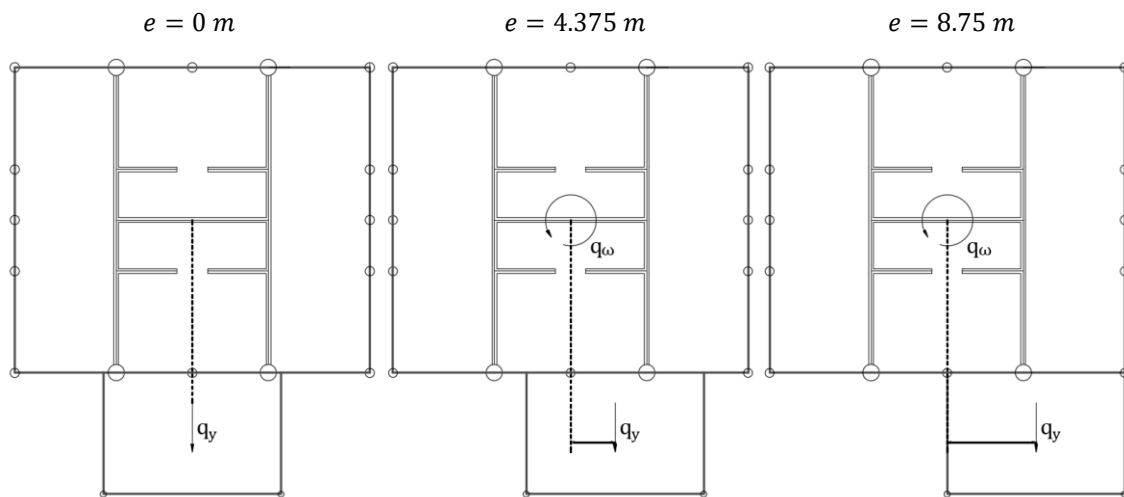


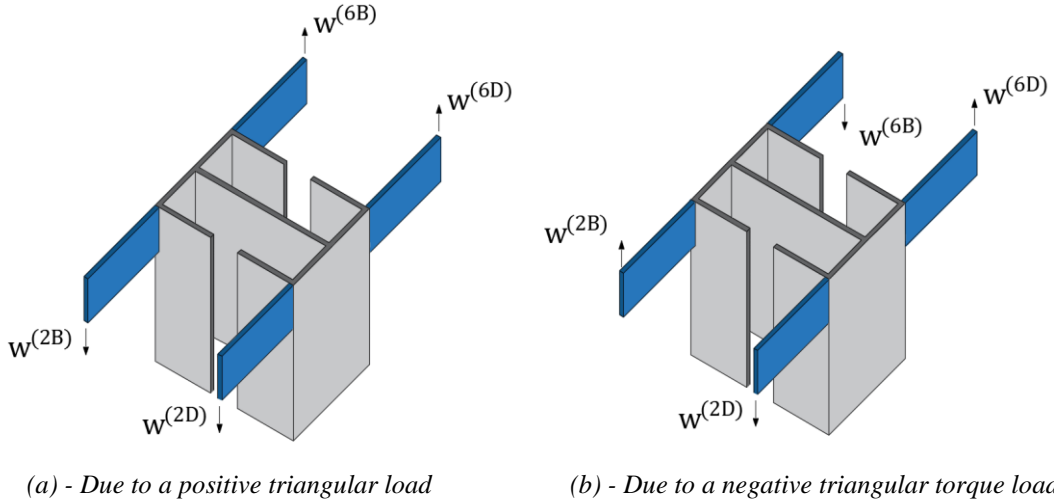
Figure 5.42: Sloping volume with varying eccentricity

In particular, when the triangular volume is centred with respect to the axis of the structure where it is introduced ($e = 0 \text{ m}$), its effect is purely flexural and equivalent to a triangularly distributed load $q_y(z)$. On the contrary, when the eccentricity between the centroids of the structure and the triangular volume increases, that is when the triangular volume is moved toward the right, a torsional effect $q_\omega(z)$, again with triangular distribution, is generated in addition to the flexural effect $q_y(z)$, which is always the same. By calling:

$$q_\omega(z) = e \cdot q_y(z) \quad (5.85)$$

the problem can be studied as a function of the eccentricity e of the volume.

Keeping in mind the column displacements in the two limit situations, that is pure bending (Figure 5.43 (a)) and pure torsion (Figure 5.43 (b)), we are now intended to show first the column displacement variation with height of columns 6D, 6B, 2D and 2B for three given eccentricities, i.e. $e = 0$; $e = 4.3725 \text{ m}$ and $e = 8.75 \text{ m}$.



(a) - Due to a positive triangular load

(b) - Due to a negative triangular torque load

Figure 5.43: Column displacements in case of pure bending (a) and pure torsion (b)

To solve the problem, we first compute the interaction forces according to equations (5.14) and (5.28), here recalled:

$$P_{1y} \left[-4v'_1(\bar{\zeta})y_0^2 + \frac{L_0^3}{3EI_0} + \bar{\zeta} \frac{L}{EA_C} \right] = v'_0(\bar{\zeta})y_0 \quad (5.86)$$

$$P_{1\omega} \left[-4\theta'_1(\bar{\zeta})\omega_B^2 + \frac{L_0^3}{3EI_0} + \bar{\zeta} \frac{L}{EA_C} \right] = \theta'_0(\bar{\zeta})\omega_B \quad (5.87)$$

where $\theta'_0(\bar{\zeta})$ is now computed according to the second of equations (4.35), in which q_ω is replaced by equation (5.85) to explicit the dependency on the eccentricity.

Once the interaction forces are known, the bending and torsion component of the column displacements can be obtained through equations (4.11) as:

Bending Component	Torsion Component	
$w_1(\zeta, \bar{\zeta}) = P_{1y} \frac{L}{EA} \cdot \zeta$	$w_1(\zeta, \bar{\zeta}) = P_{1\omega} \frac{L}{EA} \cdot \zeta$	$0 \leq \zeta \leq \bar{\zeta}$
$w_2(\zeta, \bar{\zeta}) = P_{1y} \frac{L}{EA} \cdot \bar{\zeta}$	$w_2(\zeta, \bar{\zeta}) = P_{1\omega} \frac{L}{EA} \cdot \bar{\zeta}$	$\bar{\zeta} \leq \zeta \leq 1$

(5.88)

The overall displacement can be obtained by performing the sum with sign of equations (5.88) according to Figure 5.43. Results are reported in the following graphs.

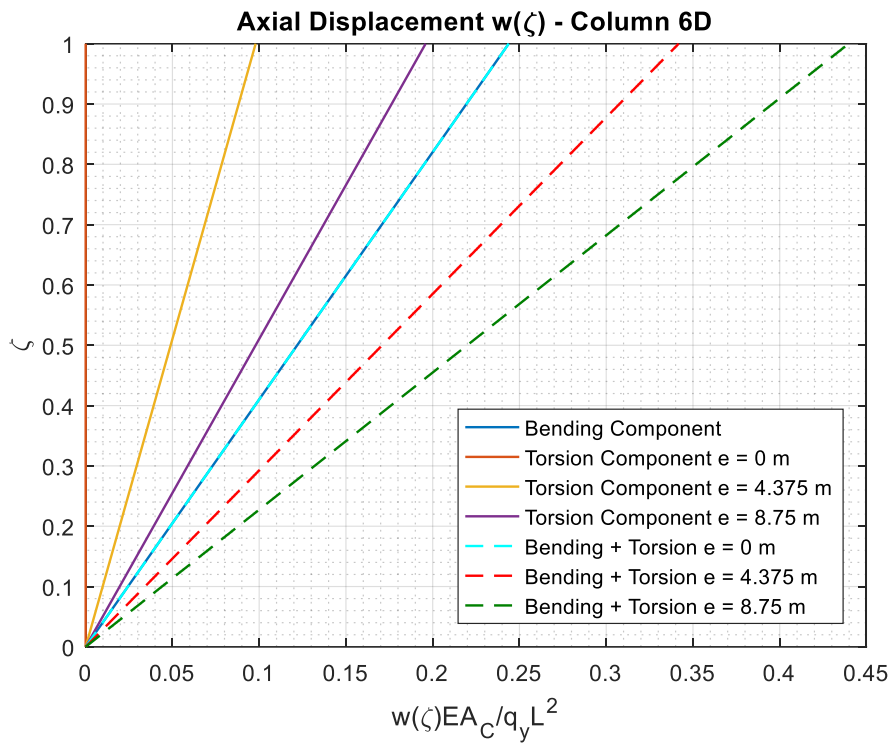


Figure 5.44: Column Displacement for fixed eccentricities - Column 6D

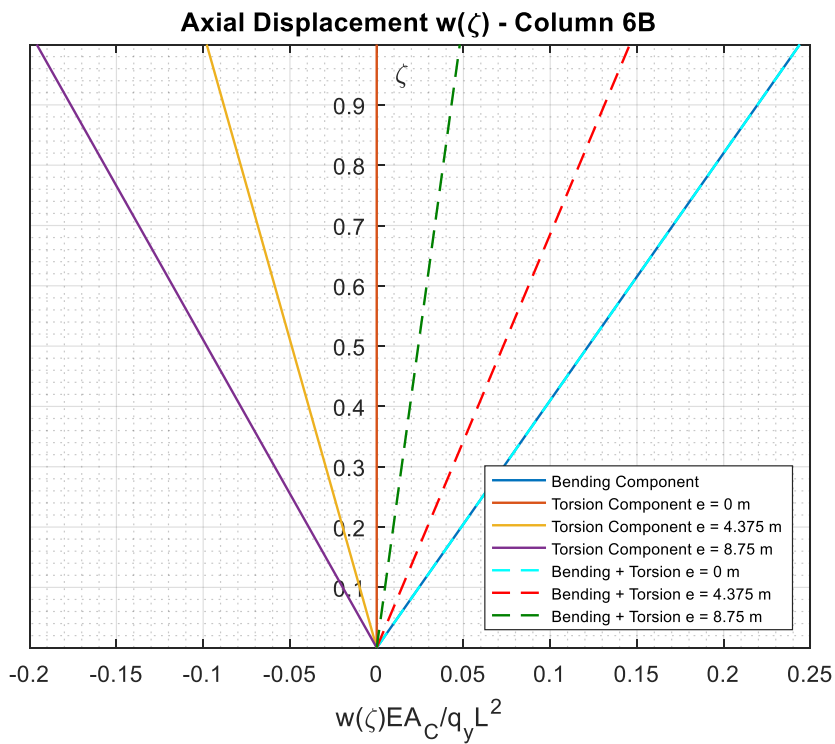


Figure 5.45: Column Displacement for fixed eccentricities - Column 6B

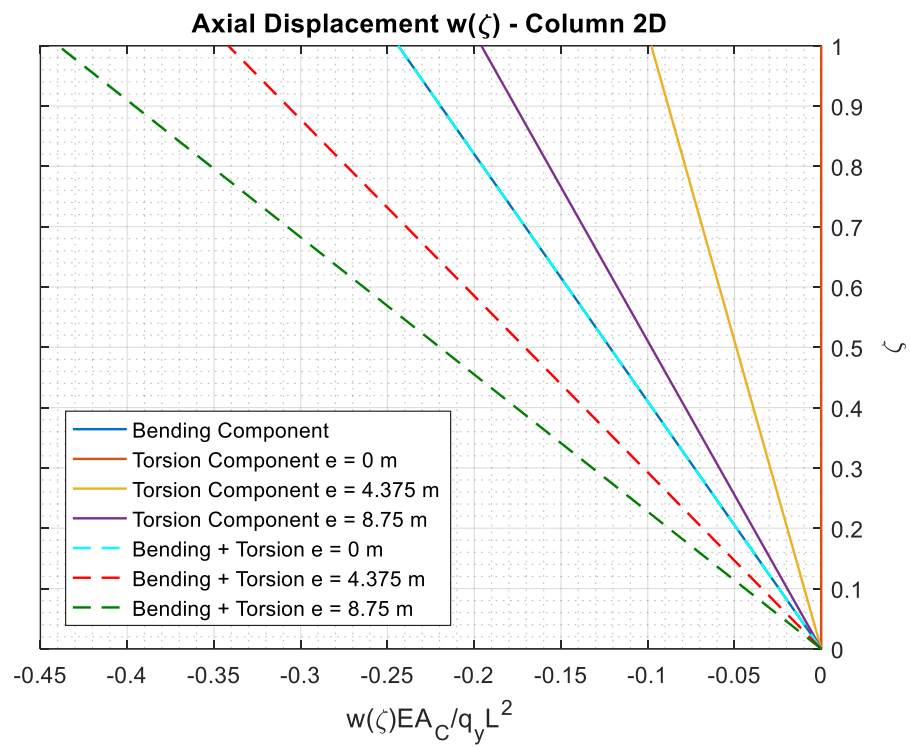


Figure 5.46: Column Displacement for fixed eccentricities - Column 2D

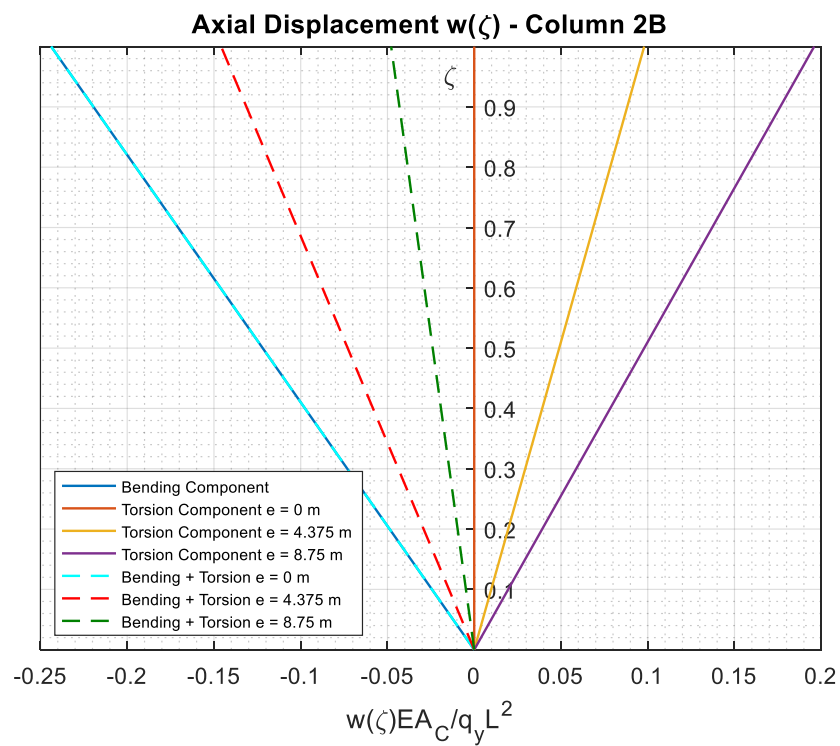


Figure 5.47: Column Displacement for fixed eccentricities - Column 2B

As it can be observed, when $e = 0$ the torsion component is always zero and the total column displacements are given by the bending component only. As the eccentricity increases, the torsion component increases too and the total column displacement depends on this. From the reported figures, it is also possible to observe that while for columns 6D and 2D the torsion component is summing up with the bending component, thus leading to a final displacement increment, in columns 6B and 2B the two contributions have different signs, thus leading to a final column displacement reduction. Nevertheless, for the considered structure, the torsion component is never so high to determine a sign inversion of the final displacements, which have the following verse when $e = 8.75$:

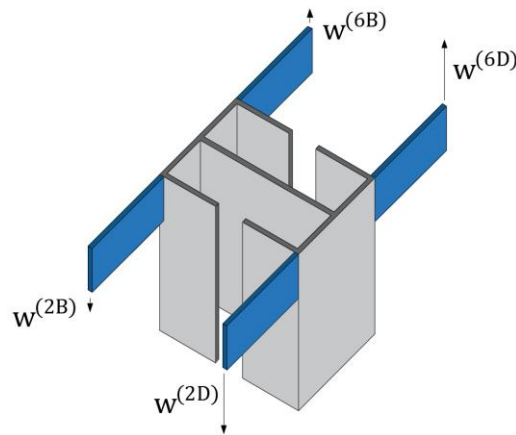


Figure 5.48: Bending plus torsion column displacements for $e = 8.75$

To better appreciate what happens to column displacements at varying eccentricity, reference can be made to the following graphs.

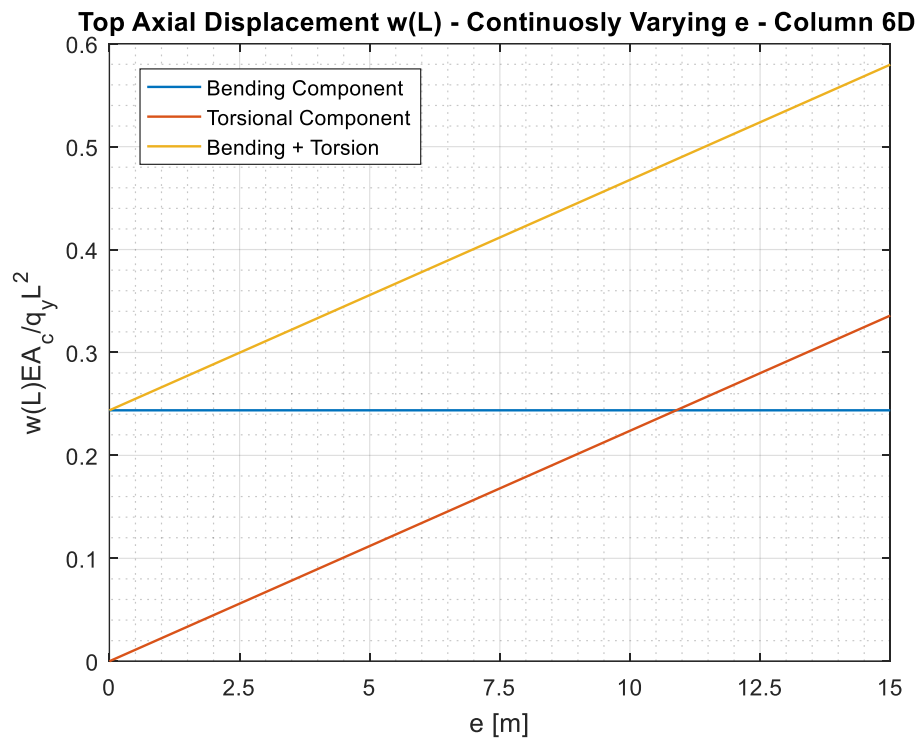


Figure 5.49: Column displacement variation with e - Column 6D

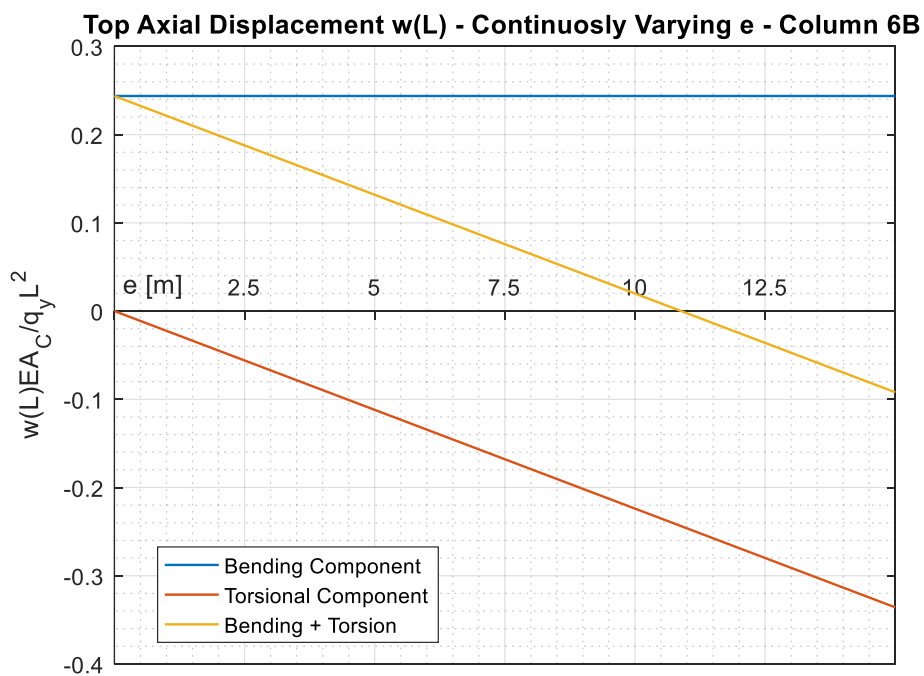


Figure 5.50: Column displacement variation with e - Column 6B

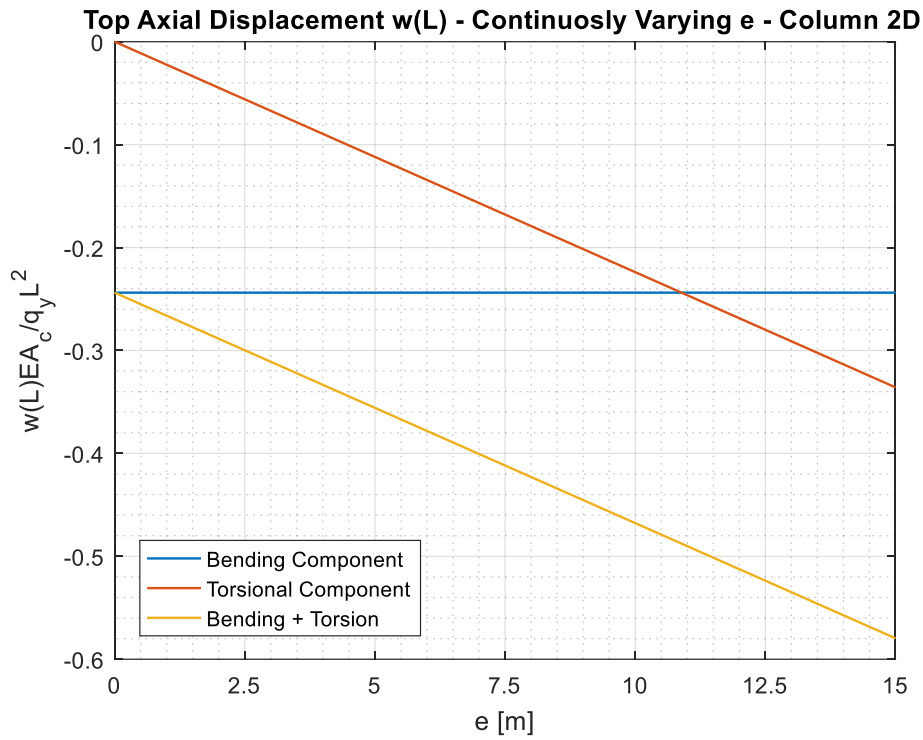


Figure 5.51: Column displacement variation with e - Column 2D

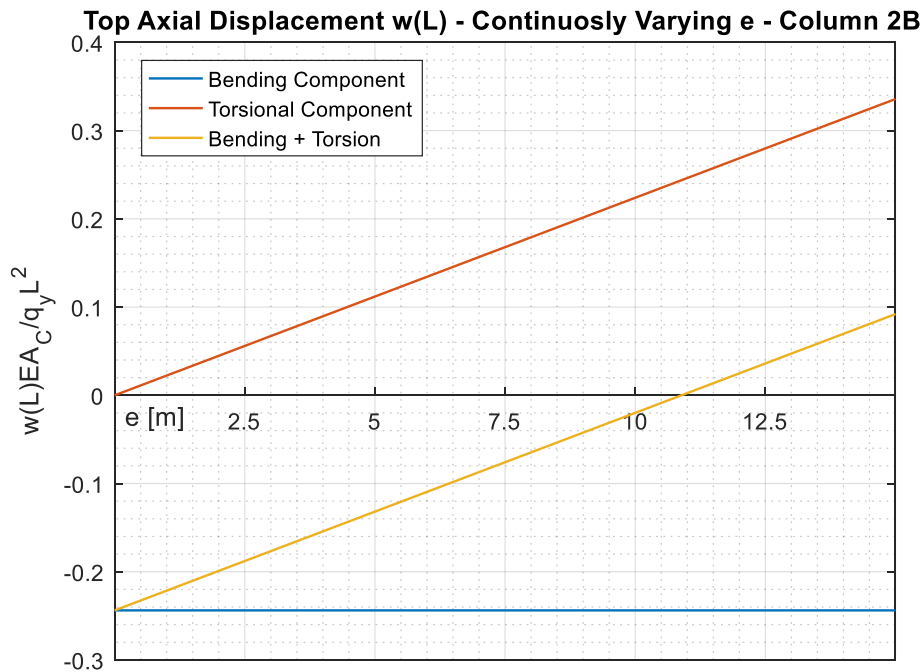


Figure 5.52: Column displacement variation with e - Column 2B

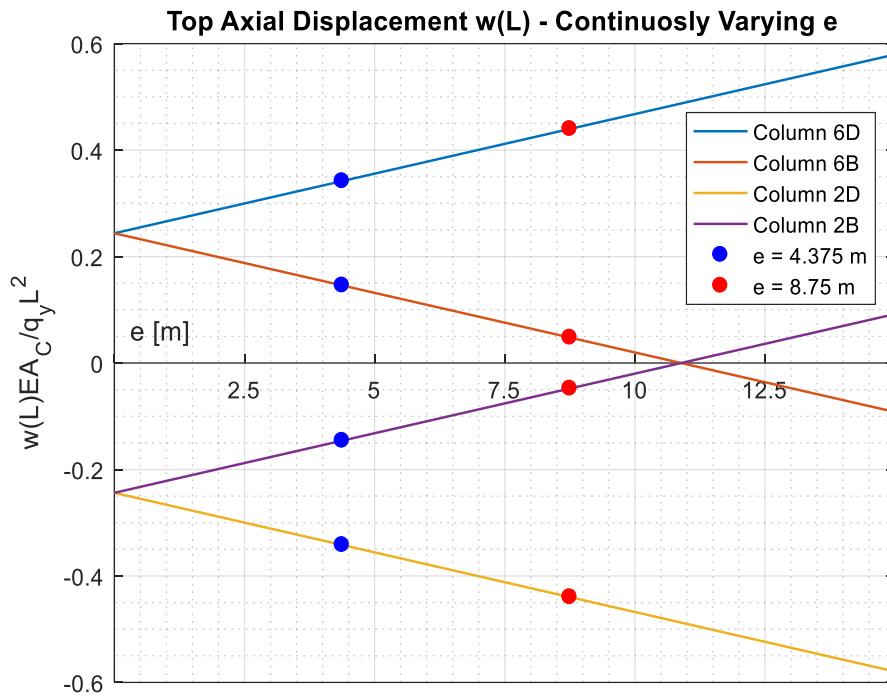


Figure 5.53: Top column displacement variation with e - Columns 6D, 6B, 2D, 2B

5.5 NUMERICAL MODEL

5.5.1 *Midas GEN: Background*

The structure has been analysed by means of Midas GEN, a powerful software for structural analysis commonly used in practice and in particular for the analysis of tall buildings like Burj Khalifa in Dubai or The Spire in Chicago. The MIDAS/Gen element library consists of the following elements:

- Truss Element;
- Tension-only Element (Hook and Cable function included);
- Compression-only Element (Gap function included);
- Beam Element/Tapered Beam Element;
- Plane Stress Element;
- Plate Element;
- Two-dimensional Plane Strain Element;
- Two-dimensional Axisymmetric Element;
- Solid Element;
- Wall Element.

In modelling the structure “BEAM” and “PLATE” element have been used and their characteristics are reported in the following.

➤ **Beam Element**

Two nodes define a Prismatic/Non-prismatic, three-dimensional beam element. Its formulation is founded on the Timoshenko Beam theory taking into account the stiffness effects of tension/compression, shear, bending and torsional deformations. However, it is possible to neglect shear deformability, according to Euler-Bernoulli Beam theory. MIDAS/Gen assumes linear variations for cross-sectional areas, effective shear areas and torsional stiffness along the length of a non-prismatic element. For moments of inertia about the major and minor axes, a linear, parabolic or cubic variation may be selected

Each node retains three translational and three rotational d.o.f. irrespective of the ECS (Element Coordinate System) or GCS (Global Coordinate System). MIDAS/Gen uses the Beta Angle (β) conventions to identify the orientation of each cross-section. The Beta Angle relates the ECS to the GCS. The ECS x -axis starts from node N1 and passes through node N2 for all line elements (Figure 5.54). The ECS z -axis is defined to be parallel with the direction of the height of cross-sections, that is, the y -axis is in the strong axis direction. The use of the right-hand rule prevails in the process.

The sign convention for beam element forces is shown in Figure 5.54. The arrows represent the positive (+) directions. Element stresses follow the same sign convention. However, stresses due to bending moments are denoted by ‘+’ for tension and ‘-’ for compression. The displacement sign is defined with reference to the GCS, following the right-hand rule for the rotations.

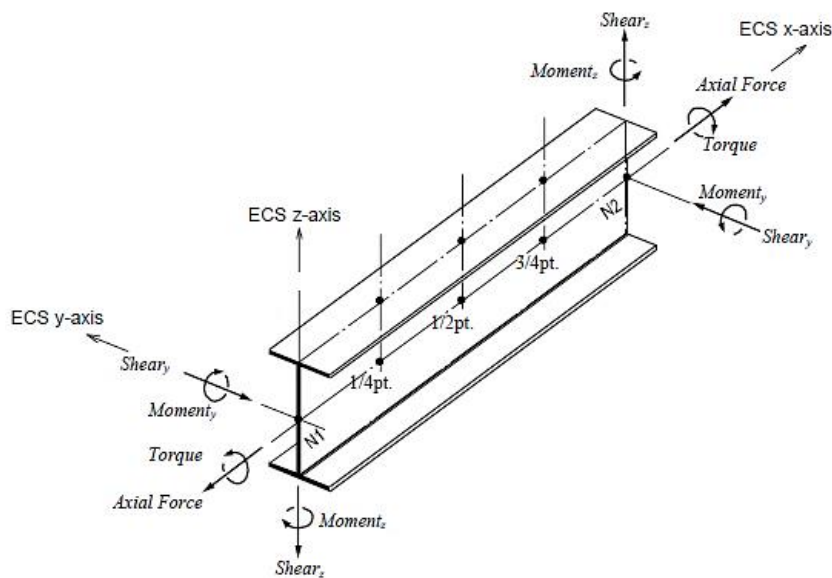
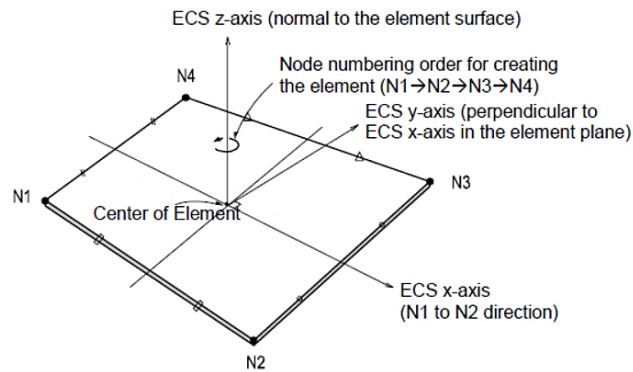


Figure 5.54: Sign convention for ECS and element forces (or stresses) of a beam element

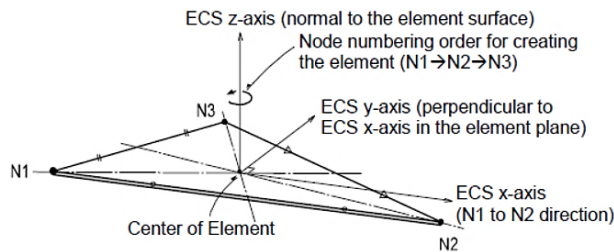
➤ Plate Element

Three or four nodes placed in the same plane define a plate element. The element is capable of accounting for in-plane tension/compression, in-plane/out-of-plane shear and out-of-plane bending behaviours.

The out-of-plane stiffness used in MIDAS/Gen includes two types, DKT/DKQ (Discrete Kirchhoff element) and DKMT/DKMQ (Discrete Kirchhoff-Mindlin element). DKT and DKQ are developed on the basis of a thin plate theory, Kirchhoff Plate theory. Whereas, DKMT and DKMQ are developed on the basis of a thick plate theory, Mindlin-Reissner Plate theory.



(a) ECS for a quadrilateral element



(b) ECS for a triangular element

Figure 5.55: Arrangement of plate elements and their ECS

The ECS for plate elements is used when the program calculates the element stiffness matrices. The directions of the ECS axes are defined as presented in Figure 5.55. In the case of a quadrilateral (4-node) element, the thumb direction signifies the ECS z-axis.

At a connecting node, multiplying each nodal displacement component by the corresponding stiffness component of the element produces the element forces. In order to calculate element forces per unit length at a connecting node or an element centre, the stresses are separately calculated for in-plane and out-of-plane behaviours and integrated in the direction of the thickness.

MIDAS/Gen is formulated on the basis of linear analysis, but it is also capable of carrying out geometric nonlinear analyses. MIDAS/Gen implements nonlinear elements (tension or compression-only), P-Delta and large displacement analyses, etc. The structural analysis features of MIDAS/Gen include basic linear analysis and nonlinear analysis in addition to various analysis capabilities required in practice.

The following outlines some of the highlights of the analysis features:

- Linear Static Analysis;
- Linear Dynamic Analysis;
- Eigenvalue Analysis;
- Response Spectrum Analysis;
- Time History Analysis;
- Linear Buckling Analysis;
- Nonlinear Static Analysis;
- P-Delta Analysis;
- Large Displacement Analysis;
- Nonlinear Analysis with Nonlinear Elements;
- Construction Sequence Analysis;
- Steel Box Bridge Analysis reflecting Pre- and Post-composite Action;
- Analysis of Unknown Loads Using Optimization Technique.

The structure subject of this work has been analysed by means of the *Linear Static* type of analysis. The basic equation adopted in MIDAS/Gen for linear static analysis is as follows:

$$[K]\{U\} = \{P\}$$

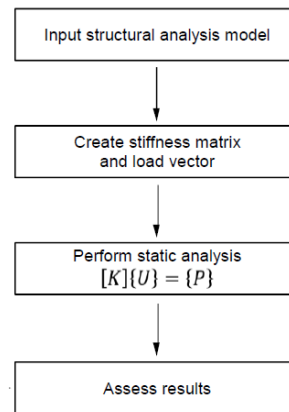


Figure 5.56: Flow chart of linear static analysis in MidasGen

where $[K]$ is the stiffness matrix, $\{U\}$ is the displacement vector; $\{P\}$ is the load vector.

5.5.2 *Numerical Model*

The structure has been modelled using BEAM elements for columns and PLATE elements for the core, the outriggers and floors. In Figure 5.57 and Figure 5.58 some representations of the model are reported.

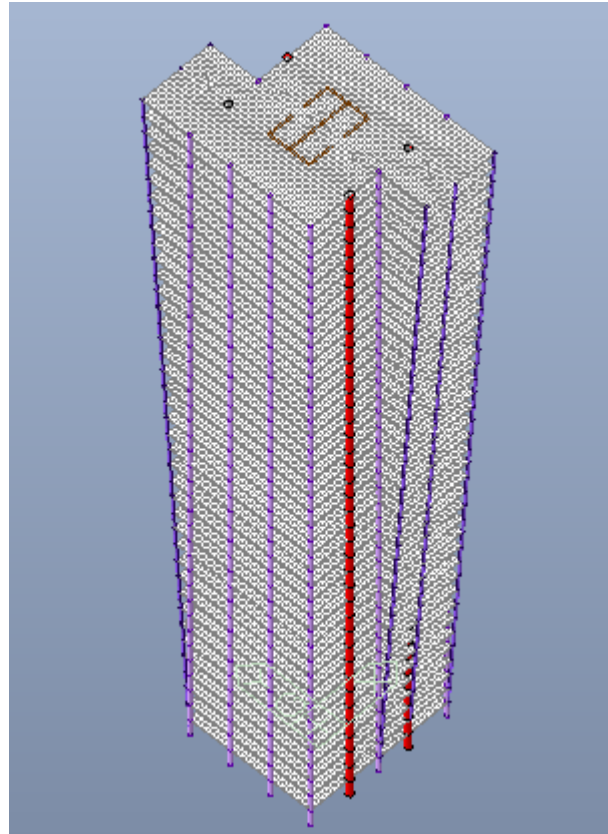


Figure 5.57: *Numerical Model - Global View*

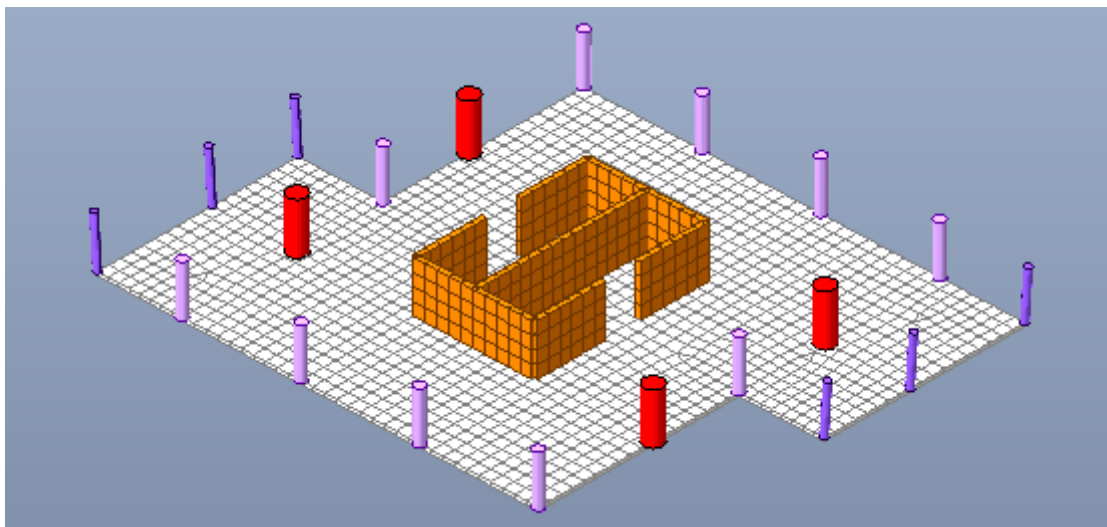


Figure 5.58: *Numerical Model – Floor Detail*

The structure has been analysed first without outriggers, then with outriggers structural system at Floor 40 (top of the building) and outriggers both at Floor 40 and Floor 20 (half of the building). In Figure 5.59 is represented the modelled outrigger structural system. Notice that plate elements has been used to model outriggers instead of beam elements, to better reproduce the interaction between core and reinforcing system. In red, it is possible to recognize the megacolumns, with diameter 1.60 m, supporting the outriggers.

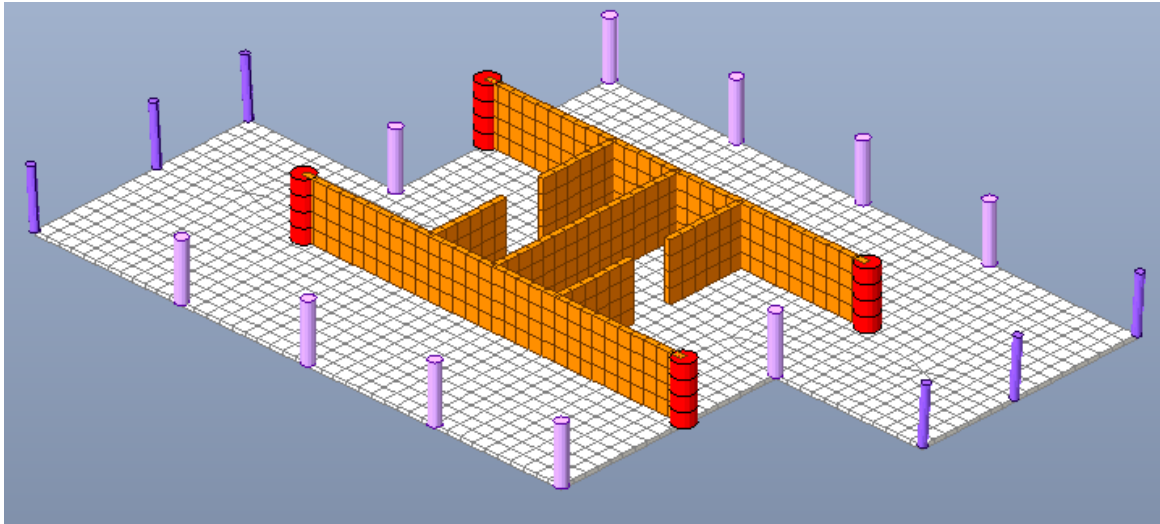


Figure 5.59: Numerical Model – Outriggers Detail

To better highlight the effect of torsion on the structure, the self-weight has been neglected and the action induced by the triangular external volumes has been simulated through horizontal forces according to what specified in §5.1, using the influence areas of Figure 5.60 for columns 7A, 7B, 7C, 1C, 1D and 1E.

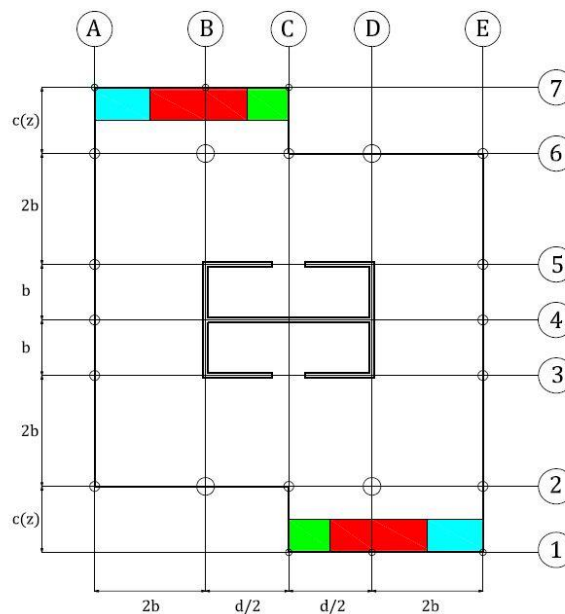


Figure 5.60: Influence areas for definition of horizontal forces

Level [m]	c [m]	C1 - C7			D1 - B7			A1 - E7		
		A [m ²]	P [kN]	H [kN]	A [m ²]	P [kN]	H [kN]	A [m ²]	P [kN]	H [kN]
0.00	0.00	0.00	0.00	0.00	0.00	0.00	0.00	0.00	0.0	0.0
4.25	0.15	0.56	34.30	2.40	1.30	39.88	2.79	0.74	35.69	2.50
8.50	0.30	1.12	38.48	2.69	2.60	49.64	3.47	1.49	41.27	2.89
12.75	0.45	1.67	42.67	2.98	3.90	59.40	4.15	2.23	46.85	3.28
17.00	0.60	2.23	46.85	3.28	5.21	69.16	4.84	2.98	52.43	3.67
21.25	0.74	2.79	51.03	3.57	6.51	78.92	5.52	3.72	58.01	4.06
25.50	0.89	3.35	55.22	3.86	7.81	88.69	6.20	4.46	63.58	4.45
29.75	1.04	3.90	59.40	4.15	9.11	98.45	6.88	5.21	69.16	4.84
34.00	1.19	4.46	63.58	4.45	10.41	108.21	7.57	5.95	74.74	5.23
38.25	1.34	5.02	67.77	4.74	11.71	117.97	8.25	6.69	80.32	5.62
42.50	1.49	5.58	71.95	5.03	13.02	127.73	8.93	7.44	85.90	6.01
46.75	1.64	6.14	76.13	5.32	14.32	137.49	9.61	8.18	91.47	6.40
51.00	1.79	6.69	80.32	5.62	15.62	147.26	10.30	8.93	97.05	6.79
55.25	1.93	7.25	84.50	5.91	16.92	157.02	10.98	9.67	102.63	7.18
59.50	2.08	7.81	88.69	6.20	18.22	166.78	11.66	10.41	108.21	7.57
63.75	2.23	8.37	92.87	6.49	19.52	176.54	12.34	11.16	113.79	7.96
68.00	2.38	8.93	97.05	6.79	20.83	186.30	13.03	11.90	119.36	8.35
72.25	2.53	9.48	101.24	7.08	22.13	196.06	13.71	12.64	124.94	8.74
76.50	2.68	10.04	105.42	7.37	23.43	205.83	14.39	13.39	130.52	9.13
80.75	2.83	10.60	109.60	7.66	24.73	215.59	15.08	14.13	136.10	9.52
85.00	2.98	11.16	113.79	7.96	26.03	225.35	15.76	14.88	141.68	9.91
89.25	3.12	11.71	117.97	8.25	27.33	235.11	16.44	15.62	147.26	10.30
93.50	3.27	12.27	122.15	8.54	28.63	244.87	17.12	16.36	152.83	10.69
97.75	3.42	12.83	126.34	8.83	29.94	254.63	17.81	17.11	158.41	11.08
102.00	3.57	13.39	130.52	9.13	31.24	264.40	18.49	17.85	163.99	11.47
106.25	3.72	13.95	134.70	9.42	32.54	274.16	19.17	18.59	169.57	11.86
110.50	3.87	14.50	138.89	9.71	33.84	283.92	19.85	19.34	175.15	12.25
114.75	4.02	15.06	143.07	10.00	35.14	293.68	20.54	20.08	180.72	12.64
119.00	4.17	15.62	147.26	10.30	36.44	303.44	21.22	20.83	186.30	13.03
123.25	4.31	16.18	151.44	10.59	37.75	313.20	21.90	21.57	191.88	13.42
127.50	4.46	16.73	155.62	10.88	39.05	322.97	22.58	22.31	197.46	13.81
131.75	4.61	17.29	159.81	11.17	40.35	332.73	23.27	23.06	203.04	14.20
136.00	4.76	17.85	163.99	11.47	41.65	342.49	23.95	23.80	208.61	14.59
140.25	4.91	18.41	168.17	11.76	42.95	352.25	24.63	24.54	214.19	14.98
144.50	5.06	18.97	172.36	12.05	44.25	362.01	25.31	25.29	219.77	15.37
148.75	5.21	19.52	176.54	12.34	45.55	371.77	26.00	26.03	225.35	15.76
153.00	5.36	20.08	180.72	12.64	46.86	381.54	26.68	26.78	230.93	16.15
157.25	5.50	20.64	184.91	12.93	48.16	391.30	27.36	27.52	236.51	16.54
161.50	5.65	21.20	189.09	13.22	49.46	401.06	28.04	28.26	242.08	16.93
165.75	5.80	21.75	193.27	13.52	50.76	410.82	28.73	29.01	247.66	17.32
170.00	5.95	22.31	182.40	12.75	52.06	405.53	28.36	29.75	238.18	16.66

Table 5.6: Applied horizontal forces

In Table 5.6 are reported the computed forces, where P is the vertical force deriving from the self-weight of slab and column at each level, and H is the horizontal force deriving from the inclination of the columns.

Figure 5.61 shows how the computed horizontal forces of Table 5.2 have been applied to the structure.

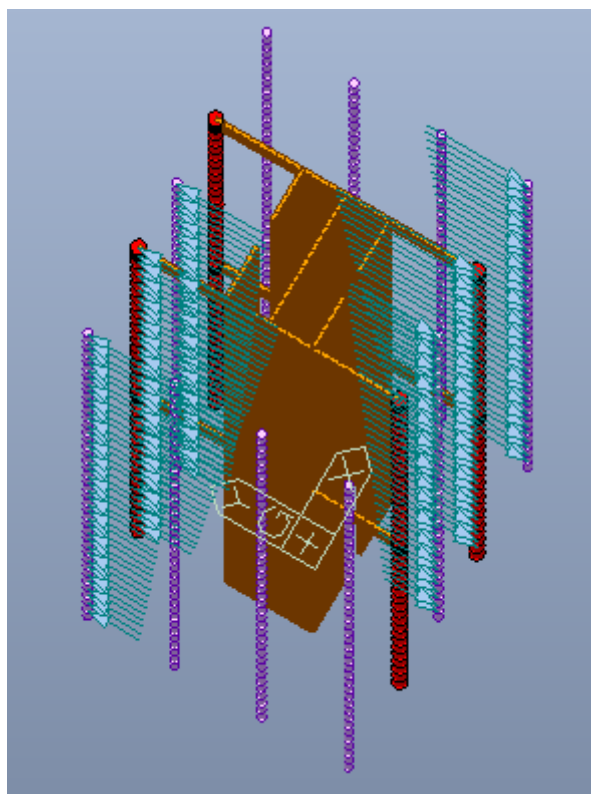


Figure 5.61: Numerical Model – Applied horizontal forces

As specified in §5.1 the wind action is simplified by a triangular distribution with maximum value at the top. The wind action is applied in the positive y direction and its value at the top of the structure, defined according to NTC 2018 assuming that the structure is located in Milan, is $55,96 \text{ kN/m}$.

5.5.3 Model I: Rigid Diaphragm Floors

First the structure has been analysed assuming floor as diaphragms infinitely rigid in their plane and infinitely deformable out of plane.

In Figure 5.62 the torsional rotation of the core is reported. As we can see, the outrigger system has good efficiency in reducing torsional rotation of the core: with one outriggers level the rotation is reduced of almost 33% whereas with two outriggers levels, the reduction reaches 50%. As we can see, results are really similar to those of the theoretical analysis because the hypothesis of section non-deformable in its plane, which is at the basis of the Vlasov's theory, is fairly well simulated by the floor diaphragms used in the numerical model.

Figure 5.63 shows the axial displacement of megacolumns 2B and 2D due to the warping of the section. The displacement variation through the height of the other two megacolumns 6B and 6D is the same as 2D and 2B respectively.

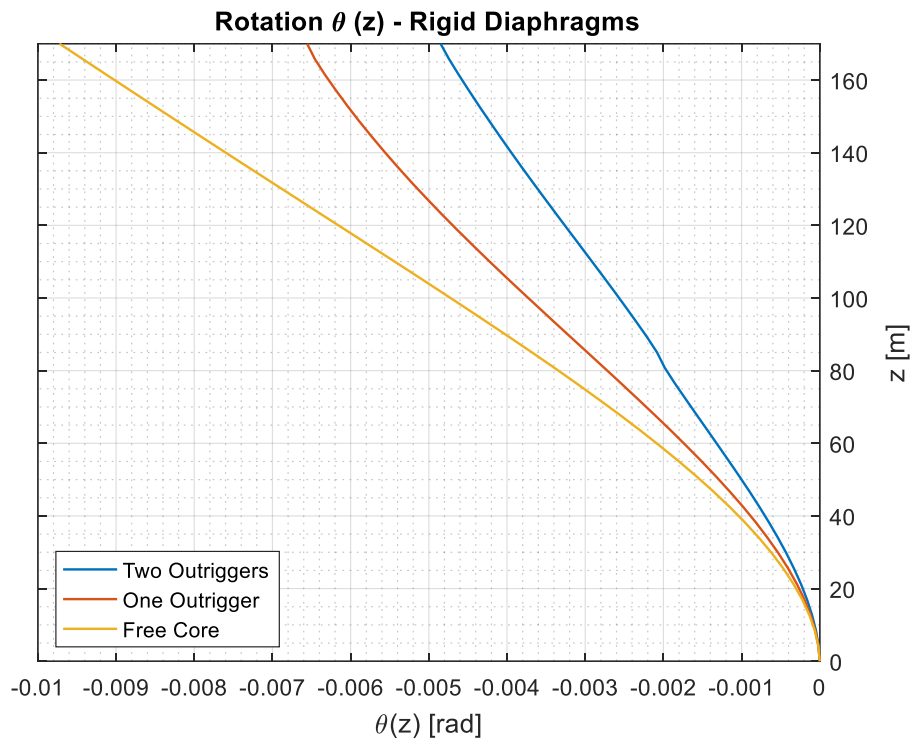


Figure 5.62: Model I – Torsional Rotation

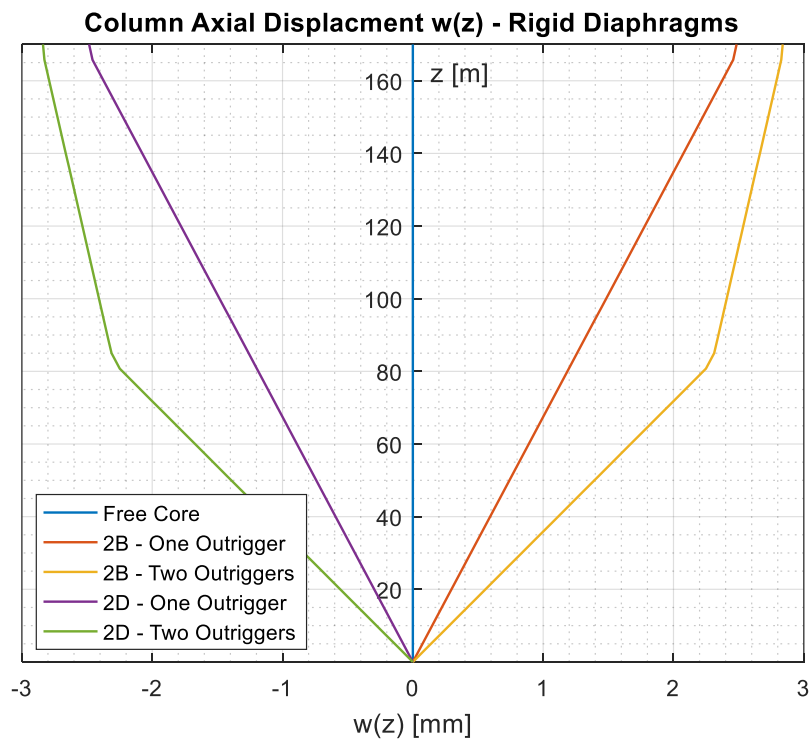


Figure 5.63: Model I – Column Axial Displacement

For what concerns the column axial displacement, from Figure 5.63 it is evident that in the structure without outriggers the axial displacement due to torsion is zero. On the contrary, in presence of outrigger systems the displacement increases along the height and is higher in case of two outriggers levels. As we can see, the displacements of columns B2 and D2 differ only for the sign, because of the warping of the core section: in B2 it is upward whereas in D2 it is downward. Moreover, it can be highlighted that in case of one outriggers level the development is linear, whereas in case of two it is bilinear, due to the presence of the column reaction at mid-height of the building (first outriggers level).

Let's analyse now the behaviour of the structure under the action of the wind load. In Figure 5.64 is reported the lateral flexural displacement of the core in the three usual different cases: free core, one and two outriggers levels.

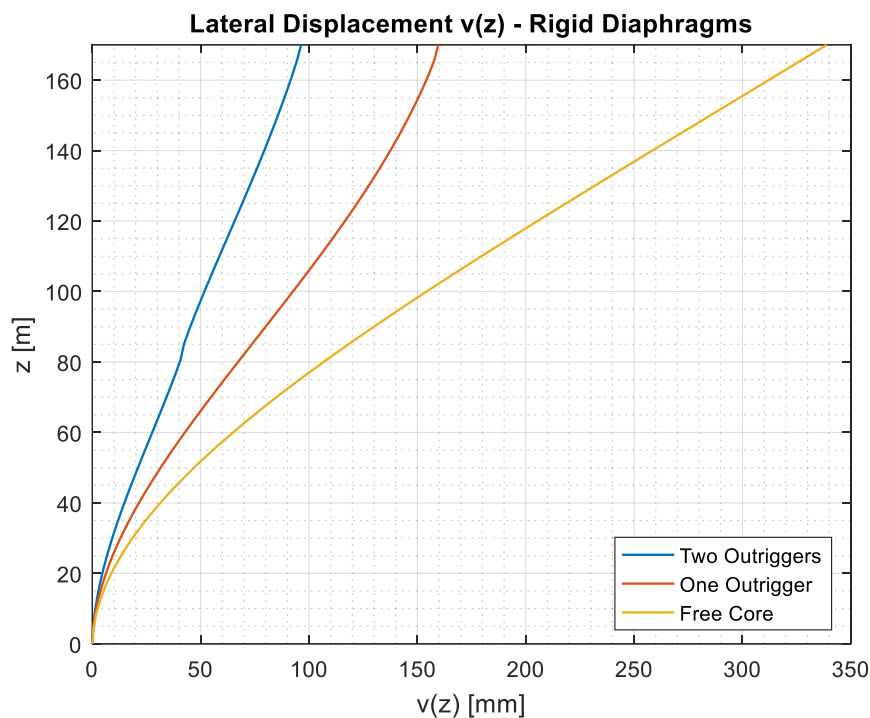


Figure 5.64: Model I – Lateral Displacement due to wind load

As we can see from Figure 5.64 the lateral displacement is reduced by outrigger systems, respectively of 53% and 72% in case of one and two outriggers levels. It is evident that the efficiency of the outrigger structural system is higher for bending with respect to torsion, as predicted in the theoretical analysis.

5.5.4 Model II: Real Slabs

In this case floors are modelled with PLATE DKT element (Kirchhoff Theory), with thickness of 0.30 m. This makes the model different than previous case because now the out-of-plane deformability is not negligible.

In Figure 5.65 is reported the torsional rotation of the core and in Figure 5.66 the axial displacement of megacolumns B2 and D2 due to the warping of the section. The displacements of the other two megacolumns B6 and D6 is the same of D2 and B2 respectively.

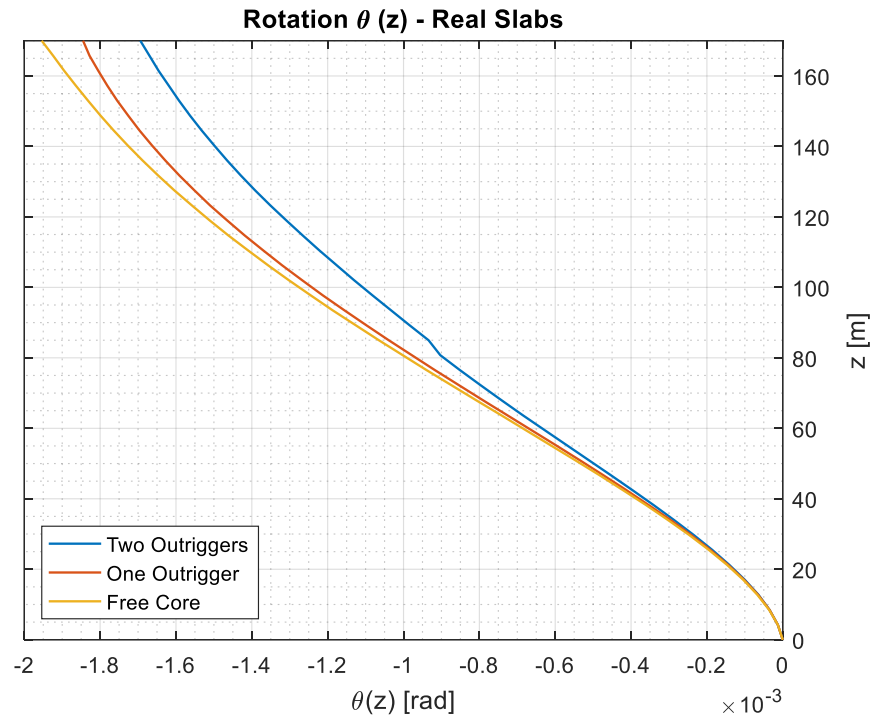


Figure 5.65: Model II – Torsional Rotation

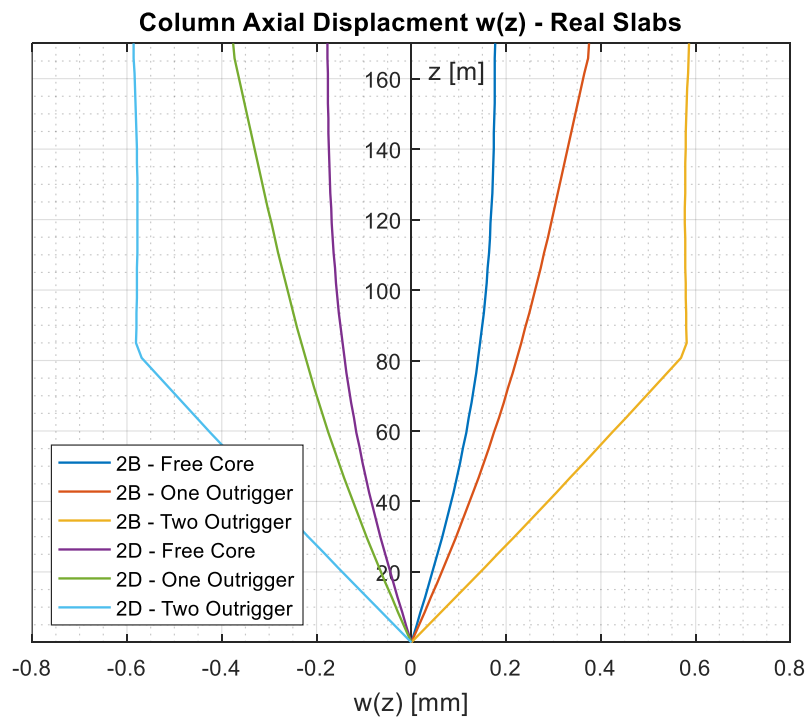


Figure 5.66: Model II – Column Axial Displacement

As we can see from Figure 5.65, the torsional rotation drastically reduces in presence of floors and therefore also the outriggers efficiency, which decreases to 6% and 13% in case of one and two outriggers respectively. This is completely different from the theoretical analysis, where the presence of diaphragms doesn't influence a lot the torsion behaviour of the core. This can be explained considering that in the numerical model, slabs are connected to external columns, giving a sort of additional "outrigger effect" which is not taken into account in the theoretical analysis, which reduces the outriggers efficiency.

As a consequence of the increased stiffness of the structure, the warping of the section is reduced and therefore the axial displacement in the columns dramatically reduces, as we can see from Figure 5.66. We can highlight that, different than the previous case, the displacement in columns in case of core with no outriggers is not zero, because the presence of slabs connecting the core to the columns lead columns to move according to the warping of the core section.

For what concerns the bending behaviour of the core under the action of wind load, it is represented in Figure 5.67.

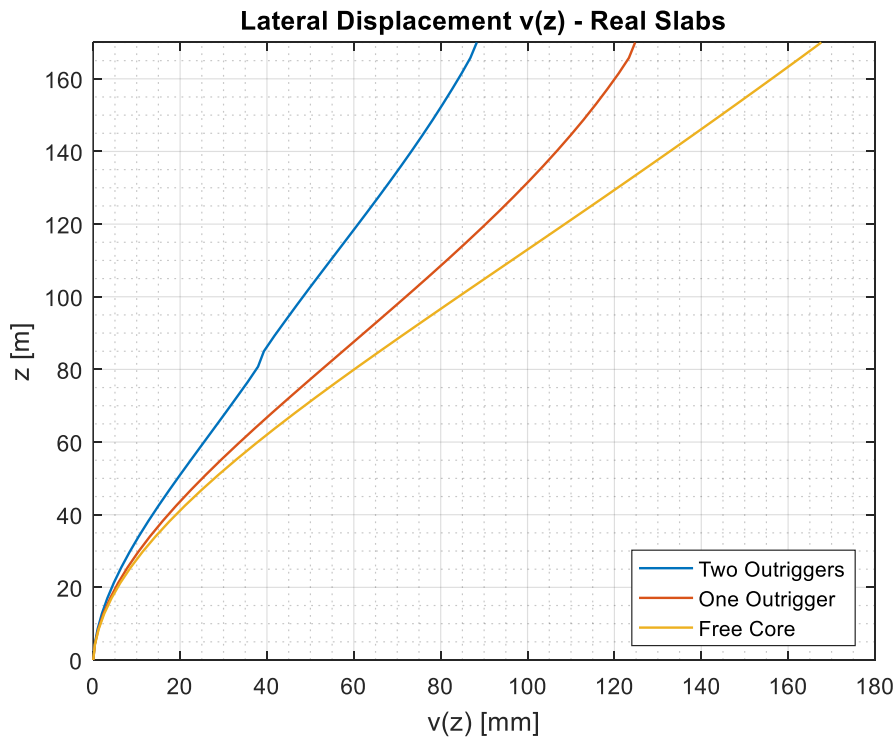


Figure 5.67: Model II – Lateral Displacement due to wind load

It is possible to notice that the lateral displacement reduces with respect to the case of floors as rigid diaphragms due to the presence of slabs which increase the global stiffness of the structure and gives an additional outrigger effects at each level. From the outrigger's efficiency point of view, it decreases compared to rigid diaphragms case to 26% and 47% in case of one and two outriggers levels respectively. This is due to increased stiffness of the

structure, which lead to a lower displacement in the megacolumns with consequent reduced column reaction acting again core deflection.

5.5.5 *Model III: Core with Lintels*

The structure has been analysed introducing lintels at each floor in the core, considering different dimensions for the lintel's height: 50 cm, 100 cm and 150 cm. In Figure 5.68 is reported a detail of the numerical model realised.

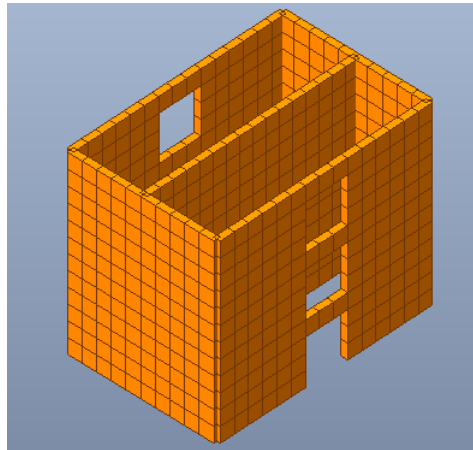


Figure 5.68: *Model III – Numerical model of core with lintels*

In the following results of core torsional rotation and column axial displacement are reported

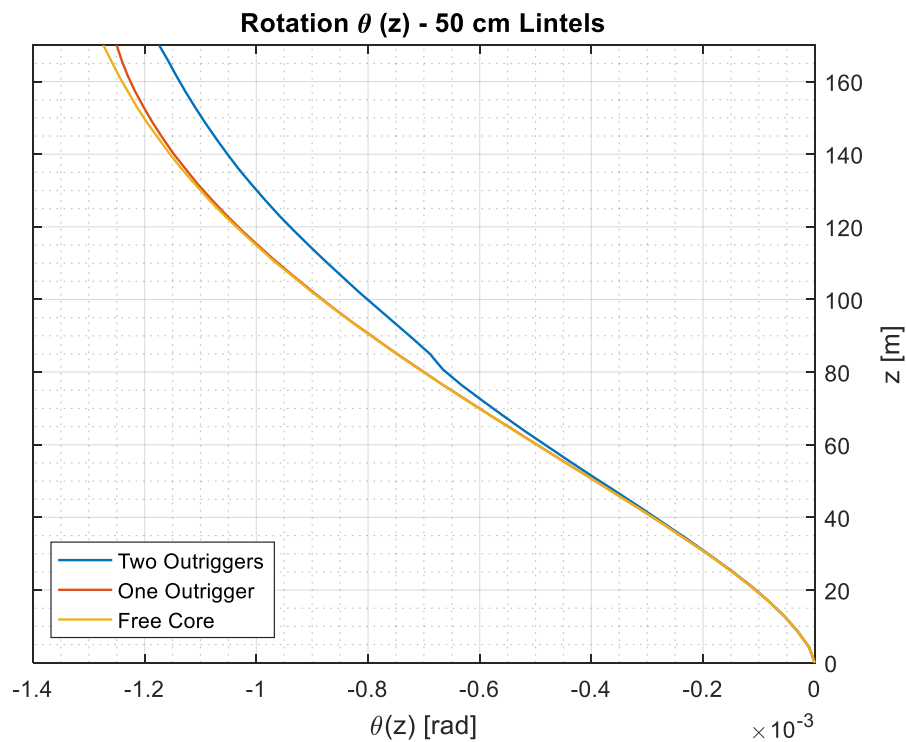


Figure 5.69: *Model III – Torsional Rotation with 50 cm lintels*

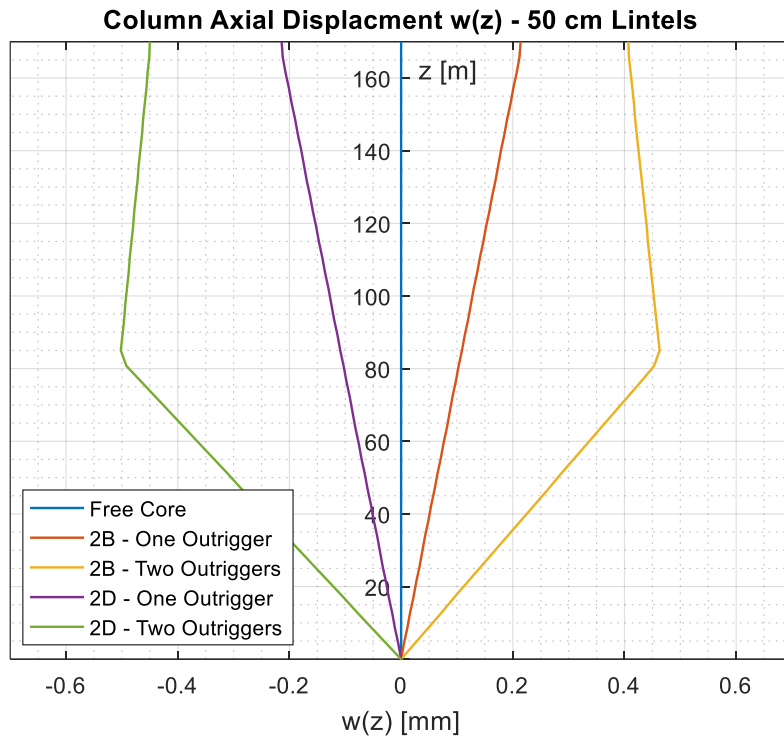


Figure 5.70: Model III – Column Axial Displacement with 50 cm lintels

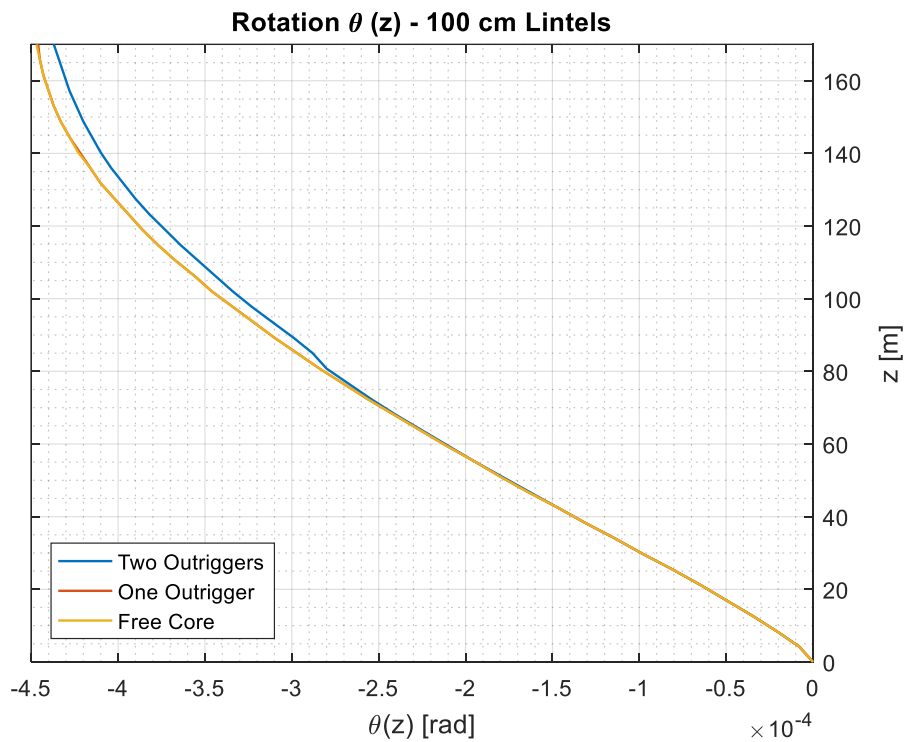


Figure 5.71: Model III – Torsional Rotation with 100 cm lintels

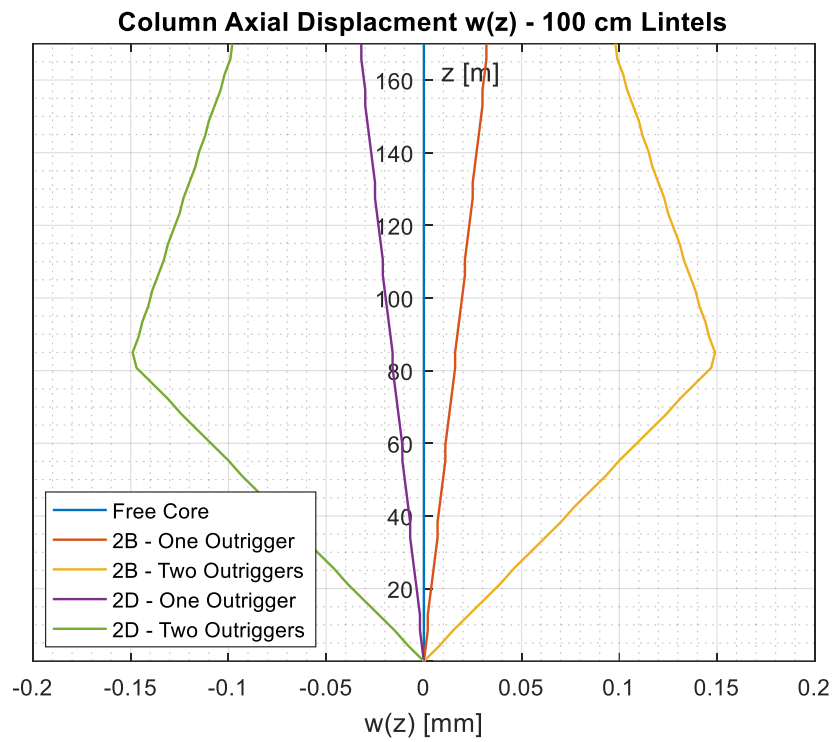


Figure 5.72: Model III – Column Axial Displacement with 100 cm lintels

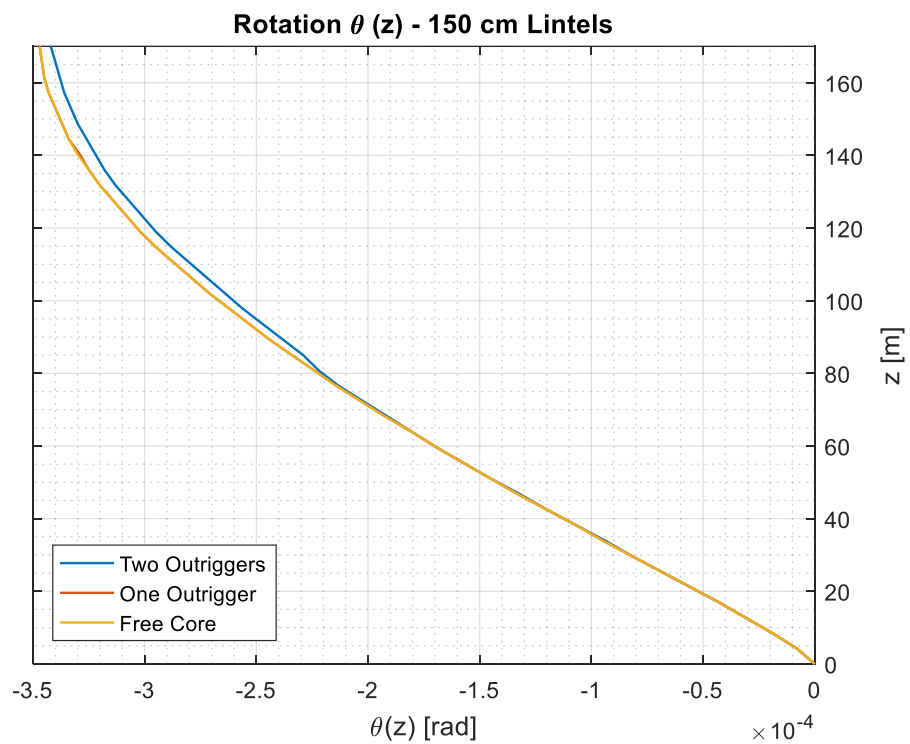


Figure 5.73: Model III – Torsional Rotation with 150 cm lintels

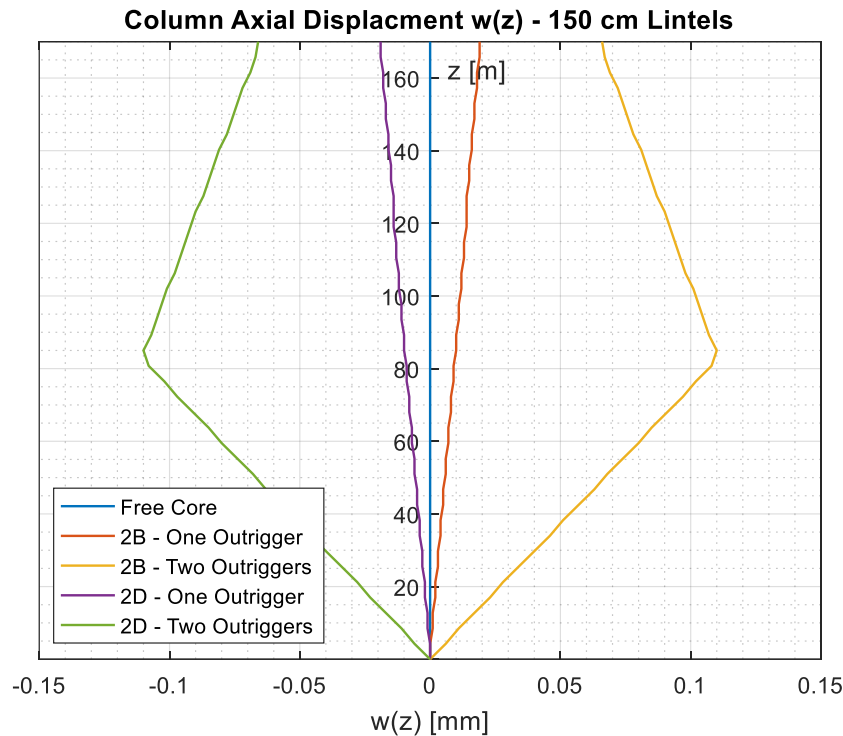


Figure 5.74: Model III – Column Axial Displacement with 150 cm lintels

As we can see from the reported graphs, increasing the height of lintels the torsional rotation progressively reduces and so the column axial displacement, because the warping of the section is more and more low due to the increasing increment of core stiffness given by lintels. Obviously, this lead to a non effectiveness of the outriggers because basically they are not activated, as can be noticed from the column axial displacement which is practically null.

5.5.6 Bending – Torsion Interaction

The bending-torsion interaction has been analysed for the case of structure with one outriggers level through a numerical structural analysis, realizing different models with different eccentricity of the additional triangular volume, considering the same cases analysed theoretically in §5.4. As done in the previous analysis, the self-weight has been neglected to better put in evidence the phenomenon studied and the forces deriving from the triangular volume have been applied directly to the core. The horizontal forces have been computed with the usual procedure, but in this case we have applied the resultant at each level, without considering the division between the three columns of the triangular volume. Then, a torsional moment has been applied, computed as the product between horizontal force and eccentricity considered in each case. The applied forces are summarized in Table 5.7.

				e = 0 m	e = 4.375 m	e = 8.75 m
Level [m]	c [m]	P [kN]	H [kN]	M _t [kN*m]	M _t [kN*m]	M _t [kN*m]
0.00	0.00	0.00	0.00	0.00	0.00	0.00
4.25	0.15	109.87	7.68	0.00	33.61	67.22
8.50	0.30	129.39	9.05	0.00	39.58	79.17
12.75	0.45	148.91	10.41	0.00	45.56	91.11
17.00	0.60	168.44	11.78	0.00	51.53	103.06
21.25	0.74	187.96	13.14	0.00	57.50	115.01
25.50	0.89	207.49	14.51	0.00	63.48	126.95
29.75	1.04	227.01	15.87	0.00	69.45	138.90
34.00	1.19	246.53	17.24	0.00	75.42	150.84
38.25	1.34	266.06	18.60	0.00	81.39	162.79
42.50	1.49	285.58	19.97	0.00	87.37	174.73
46.75	1.64	305.10	21.33	0.00	93.34	186.68
51.00	1.79	324.63	22.70	0.00	99.31	198.63
55.25	1.93	344.15	24.07	0.00	105.29	210.57
59.50	2.08	363.67	25.43	0.00	111.26	222.52
63.75	2.23	383.20	26.80	0.00	117.23	234.46
68.00	2.38	402.72	28.16	0.00	123.20	246.41
72.25	2.53	422.24	29.53	0.00	129.18	258.35
76.50	2.68	441.77	30.89	0.00	135.15	270.30
80.75	2.83	461.29	32.26	0.00	141.12	282.24
85.00	2.98	480.81	33.62	0.00	147.10	294.19
89.25	3.12	500.34	34.99	0.00	153.07	306.14
93.50	3.27	519.86	36.35	0.00	159.04	318.08
97.75	3.42	539.38	37.72	0.00	165.01	330.03
102.00	3.57	558.91	39.08	0.00	170.99	341.97
106.25	3.72	578.43	40.45	0.00	176.96	353.92
110.50	3.87	597.95	41.81	0.00	182.93	365.86
114.75	4.02	617.48	43.18	0.00	188.90	377.81
119.00	4.17	637.00	44.54	0.00	194.88	389.76
123.25	4.31	656.52	45.91	0.00	200.85	401.70
127.50	4.46	676.05	47.27	0.00	206.82	413.65
131.75	4.61	695.57	48.64	0.00	212.80	425.59
136.00	4.76	715.09	50.00	0.00	218.77	437.54
140.25	4.91	734.62	51.37	0.00	224.74	449.48
144.50	5.06	754.14	52.73	0.00	230.71	461.43
148.75	5.21	773.66	54.10	0.00	236.69	473.37
153.00	5.36	793.19	55.47	0.00	242.66	485.32
157.25	5.50	812.71	56.83	0.00	248.63	497.27
161.50	5.65	832.24	58.20	0.00	254.61	509.21
165.75	5.80	851.76	59.56	0.00	260.58	521.16
170.00	5.95	826.11	57.77	0.00	252.73	505.46

Table 5.7: Applied forces

The parameters monitored to study the interaction between the two behaviours are the megacolumns axial displacements, in particular columns 2B, 2D, 6B and 6D, represented in the following graphs.

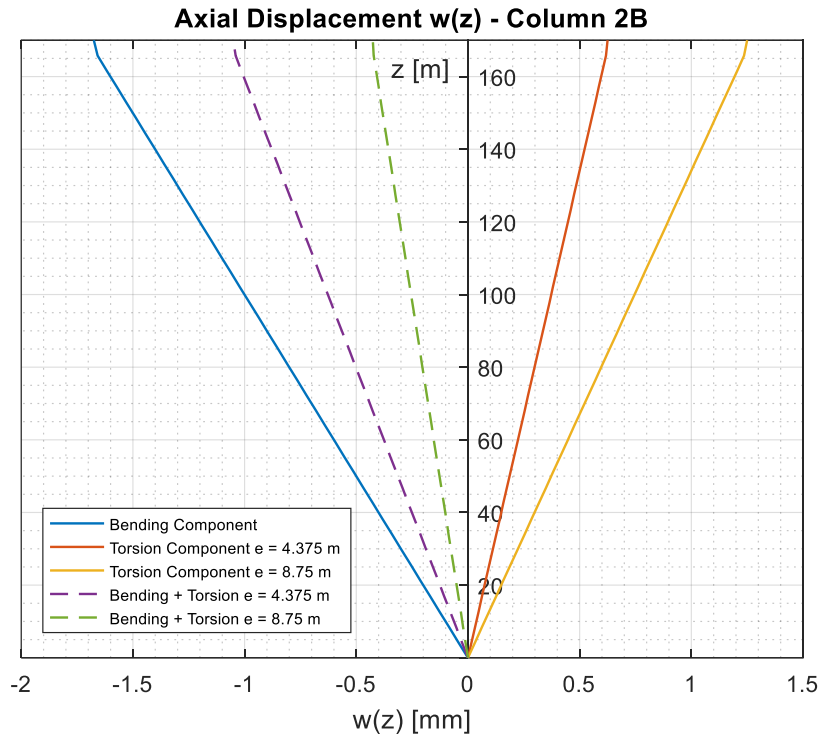


Figure 5.75: Bending – Torsion Interaction: Axial Displacement Column 2B

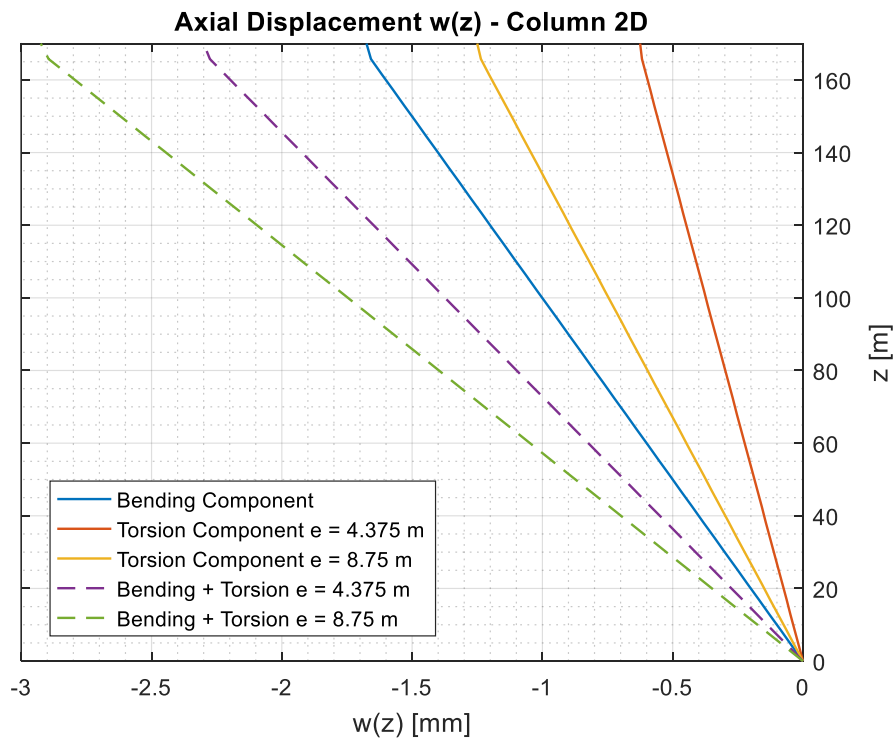


Figure 5.76: Bending – Torsion Interaction: Axial Displacement Column 2D

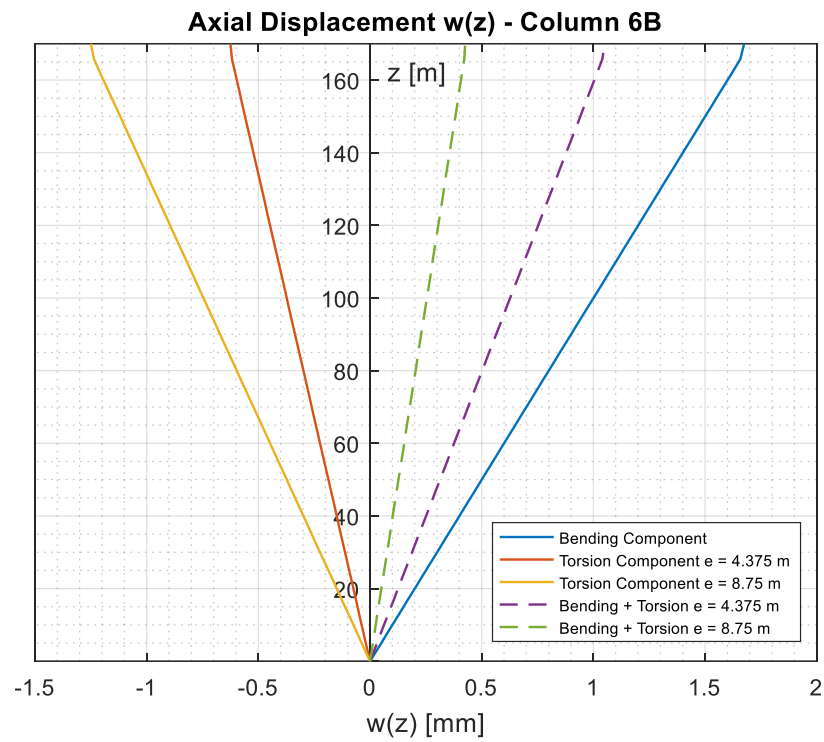


Figure 5.77: Bending – Torsion Interaction: Axial Displacement Column 6B

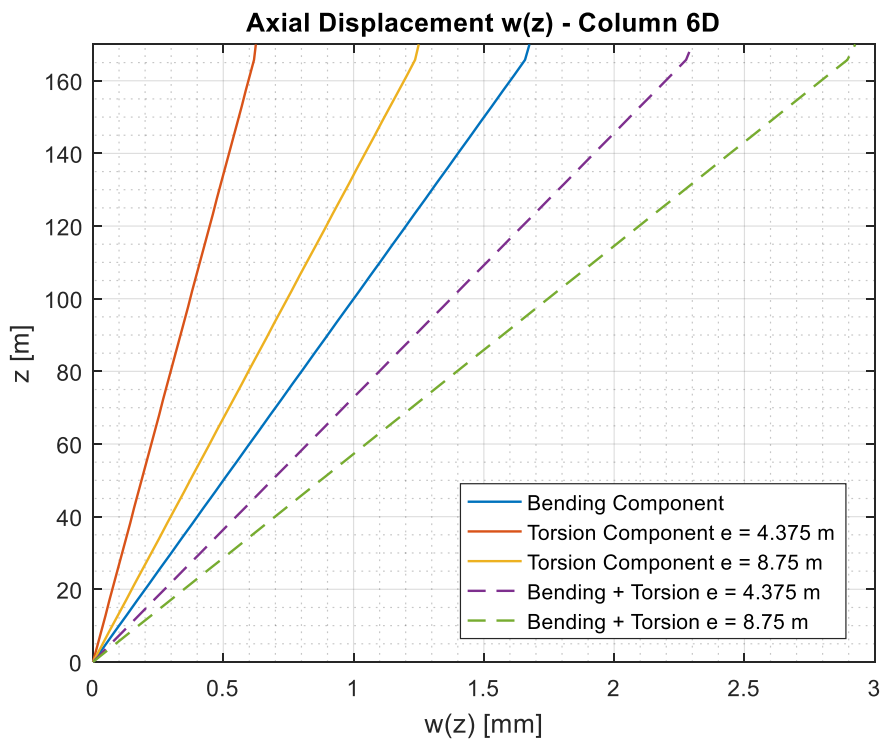


Figure 5.78: Bending – Torsion Interaction: Axial Displacement Column 6D

The numerical results confirm what expected from the theory. Indeed, for zero eccentricity there is no displacement due to torsion and columns move according to the bending behaviour: 2D and 6D moves upward, whereas 2B and 6B moves downward. Increasing the eccentricity, the torsional moment on the structure rises up, leading to a higher warping of the core cross section. Due to warping, columns 2B and 6D move upward whereas 2D and 6B move downward. Superimposing these effects to the bending's ones (same for all eccentricities), we can see that the downward displacement of column 2B and upward displacement of column 6B decrease with increasing eccentricity; on the contrary the downward displacement of column 2D and upward displacement of column 6D increase.

6 CONCLUSIONS AND FUTURE RESEARCH

Outrigger systems are a convenient solution to ensure an adequate transverse stiffness of shear-resistant elements in tall buildings. The use of such systems, in spatial configurations, has been extensively studied in literature, by analysing the static interaction between outriggers, peripheral columns and cores subjected to displacement states deriving from biaxial bending. In complex architectural configurations, the rotational effects deriving from the warping generated by the application of torsional moments to the core, increases the vertical displacements of the outriggers which, in addition to their primary function of limiting flexural displacements, also act as torsional rotation reducers. This functionality is even more pronounced when the core warping deformations are higher, as occurs in the case of cores having a thin-walled open section.

The theoretical analysis conducted were based on classic formulations of the elastic and viscoelastic problem, allowing to derive compatibility relations of simple solution and excellent approximation.

Theoretical analysis has shown that outriggers placed at top and mid height have great efficiency in reducing the torsional rotation of the core, also with regard to delayed concrete deformations, evaluated in the two extreme cases of viscoelastic structure with elastic outriggers and vice versa. This is true when there are no other reinforcing systems: indeed, in presence of lintels the core behaves like a thin-walled closed section with reduced warping, therefore the outrigger effects are practically negligible, because of they are not activated.

Numerical analysis confirmed what found by theory, except for the case of diaphragms. As a matter of fact, diaphragms were theoretically analysed without accounting for the additional “outrigger” effects that real floor slabs, which connect the core to the external megacolumns and perimeter columns, are able to develop. This fact highly decreases the warping of the core cross section, with consequent reduced efficiency of the outriggers structural systems. From the point of view of flexural displacements, the efficiency of outrigger systems is higher than that for torsional displacements in all the studied cases.

We can conclude that outrigger systems are generally efficient in reducing lateral displacements, whereas their contribution in limiting torsional rotation is not so evident, because the presence of floor slabs limits warping and torsional rotation of the core cross

section even when there are no other reinforcing systems (e.g. lintels), leading to low efficiency of outriggers.

In this work the interaction between torsion and bending has also been analysed, showing that for high eccentricity of external volumes giving torsion on the core, warping effects can prevail on bending ones, leading to an inversion of the displacement in megacolumns supporting the outriggers.

A possible future research could be to analyse outriggered structures taking into account the effects of lateral loads, like wind and earthquakes, insisting in on the eccentric external volumes in more directions, giving in this way additional torsional contributions. Moreover, in this work, it has been studied a structure with double symmetric core, allowing for decoupling of torsional and flexural behaviour. An interesting suggestion could be to analyse non-symmetric core structures where there a complete interaction between the two phenomena can be observed. Finally, the long-term behaviour of the structure has been studied only for limit cases, therefore a detailed construction stage analysis could be developed to better understand the evolution of the structural behaviour in time and the role of outriggers in counteracting delayed deformations.

INDEX OF FIGURES

Figure 2.1: <i>Tour Eiffel, Paris (1889); Chrysler Building, NY (1930); Empire State Building, NY (1931)</i>	25
Figure 2.2: <i>Ingalls Building, Cincinnati (1903); Woolworth Building, NY (1913)</i>	26
Figure 2.3: <i>Petronas Twin Towers, Kuala Lumpur (1996); Burj Khalifa, Dubai (2010)</i> ...	27
Figure 2.4: <i>Piacentini Tower, Genova (1940); Velasca Tower, Milan (1958)</i>	27
Figure 2.5: <i>Pirelli Tower, Milan (1960)</i>	28
Figure 2.6: <i>Palazzo Lombardia, Milan (2010); Unicredit Tower, Milan (2012)</i>	28
Figure 2.7: <i>City Life neighbourhood, Milan</i>	30
Figure 2.8: <i>Il Dritto, Milan (2015); Lo Storto, Milan (2017); Il Curvo, Milan (2019)</i>	30
Figure 2.9: <i>Intesa Sanpaolo Skyscraper, Turin (2015); Regione Piemonte Skyscraper, Turin (2019)</i>	31
Figure 2.10: <i>High-rise buildings and their evolution</i>	33
Figure 2.11: <i>Lever House (Rigid Frame); North Riverside (Shear Walls); World Trade Centre (Outriggers)</i>	34
Figure 2.12: <i>Aon Centre (Framed Tube); Hancock Centre (Trussed Tube); Bank of China (Space Truss)</i>	34
Figure 2.13: <i>Hearst Tower (Diagrid systems); Burj Khalifa plant (Y footprint structure)</i> .	34
Figure 2.14: <i>Concrete static efficiency</i>	35
Figure 2.15: <i>Samoan outrigger canoe</i>	37
Figure 2.16: <i>Bending and torsional effects of outriggers</i>	38
Figure 2.17: <i>Interaction of core and outrigger</i>	38
Figure 2.18: <i>Resisting system with belts</i>	39
Figure 3.1: <i>Example of thin-walled beams</i>	45
Figure 3.2: <i>Geometrical characterization of the problem</i>	46
Figure 3.3: <i>In-plane displacements</i>	47
Figure 3.4: <i>Geometrical characterization for the transverse tangent displacement</i>	49
Figure 3.5: <i>Geometrical characterization for the perpendiculars $h(s)$ and $t(s)$</i>	49
Figure 3.6: <i>Tangential displacements of an elementary rectangle</i>	50
Figure 3.7: <i>Geometrical characterization for the longitudinal displacement</i>	51
Figure 3.8: <i>Definition of sectorial area</i>	51
Figure 3.9: <i>(a) normal stresses, (b) tangential stresses, (c) shear force, (d) pure torsional moments</i>	53
Figure 3.10: <i>Sign convention for the stress components</i>	53
Figure 3.11: <i>Equilibrium in the longitudinal direction</i>	55
Figure 3.12: <i>Forces on an elementary transverse strip</i>	56

Figure 3.13: *Bending moments induced by a positive elementary force (left-hand side rule)* 58

Figure 3.14: *Section under a longitudinal force transmitted to it through a rigid arm* 63

Figure 3.15: *Involved longitudinal displacements* 64

Figure 3.16: *Rotation of the rigid arm* 64

Figure 3.17: *Bimoment induced by a longitudinal force applied outside the section* 66

Figure 3.18: *Elastic reduced orthotropic plate equivalent to the transverse connections*.. 67

Figure 3.19: *Analysis model for the transverse connections*..... 67

Figure 3.20: *Structural scheme for diaphragms*..... 71

Figure 3.21: *Lintels geometry*..... 75

Figure 3.22: *Structural scheme for lintels; Internal actions in lintels* 76

Figure 4.1: *Outrigger-thin-walled core and reference axes* 79

Figure 4.2: *Displacement induced by a uniformly distributed load q_x* 88

Figure 4.3: *Rotation induced by a uniformly distributed load q_x* 88

Figure 4.4: *Bending moment induced by a uniformly distributed load q_x* 89

Figure 4.5: *Shear force induced by a uniformly distributed load q_x* 89

Figure 4.6: *Displacement induced by a triangular load with maximum value q_x at the top*91

Figure 4.7: *Rotation induced by a triangular load with maximum value q_x at the top* 91

Figure 4.8: *Bending moment induced by a triangular load with maximum value q_x at the top* 92

Figure 4.9: *Shear force induced by a triangular load with maximum value q_x at the top* .. 92

Figure 4.10: *Torsional rotation for a uniform torque load q_ω* 94

Figure 4.11: *Warping for a uniform torque load q_ω* 95

Figure 4.12: *Bimoment for a uniform torque load q_ω* 95

Figure 4.13: *Torsional moments for a uniform torque load q_ω* 96

Figure 4.14: *Torsional rotation for a triangular torque load q_ω* 98

Figure 4.15: *Warping for a triangular torque load q_ω* 98

Figure 4.16: *Bimoment for a triangular torque load q_ω* 99

Figure 4.17: *Torsional moments for a triangular torque load q_ω* 99

Figure 4.18: *Scheme for structural analysis*..... 100

Figure 4.19: *Torsional rotation and warping due to a constant distributed torque in free core* 101

Figure 5.1: *Case Study – General 3D view* 103

Figure 5.2: *(a) Top floor; (b) Mid-height floor; (c) Mid-height floor; (d) Core-Outriggers system* 104

Figure 5.3: *(a) Horizontal actions due to the inclined volumes; (b) Acting loads*..... 105

Figure 5.4: *Scheme for the computation of the inertia moments*..... 107

Figure 5.5: *Diagram of sectorial areas - Blue: positive; Red: negative - Dimensions: m^2* 108

Figure 5.6: *Core-outriggers interaction flexural forces - Case: One level of outriggers*. 110

Figure 5.7: <i>Core-outriggers interaction forces - Case: Two levels of outriggers</i>	113
Figure 5.8: <i>Core displacement under a triangular load distribution q_y</i>	115
Figure 5.9: <i>Core Rotation under a triangular load distribution q_y</i>	116
Figure 5.10: <i>Bending moment in the core under a triangular load distribution q_y</i>	116
Figure 5.11: <i>Core-outriggers interaction torsional forces - Case: One level of outriggers</i>	117
Figure 5.12: <i>Core-outriggers interaction forces - Case: Two levels of outriggers</i>	120
Figure 5.13: <i>Torsional rotation in the core due to a triangular torque</i>	123
Figure 5.14: <i>Warping of the core due to a triangular torque</i>	123
Figure 5.15: <i>Bimoment in the core due to a triangular torque</i>	124
Figure 5.16: <i>Column 2B and 2D displacements due to a triangular torque</i>	124
Figure 5.17: <i>Core rotation in presence of diaphragm, due to a triangular torque</i>	126
Figure 5.18: <i>Core warping in presence of diaphragm, due to a triangular torque</i>	126
Figure 5.19: <i>Core bimoment in presence of diaphragm, due to a triangular torque</i>	127
Figure 5.20: <i>Column 2B and 2D displacements in presence of diaphragm due to a triangular torque</i>	127
Figure 5.21: <i>Lintels geometry</i>	129
Figure 5.22: <i>Core rotation in presence of 50 cm lintels, due to a triangular torque</i>	129
Figure 5.23: <i>Core warping in presence of 50 cm lintels, due to a triangular torque</i>	130
Figure 5.24: <i>Core bimoment in presence of 50 cm lintels, due to a triangular torque</i>	130
Figure 5.25: <i>Column 2B and 2D displacements in presence of 50 cm lintels due to a triangular torque</i>	131
Figure 5.26: <i>Core rotation in presence of 100 cm lintels, due to a triangular torque</i>	131
Figure 5.27: <i>Core warping in presence of 100 cm lintels, due to a triangular torque</i>	132
Figure 5.28: <i>Core bimoment in presence of 100 cm lintels, due to a triangular torque</i> ...	132
Figure 5.29: <i>Column 2B and 2D displacements in presence of 100 cm lintels due to a triangular torque</i>	133
Figure 5.30: <i>Core rotation in presence of 150 cm lintels, due to a triangular torque</i>	133
Figure 5.31: <i>Core warping in presence of 150 cm lintels, due to a triangular torque</i>	134
Figure 5.32: <i>Core bimoment in presence of 150 cm lintels, due to a triangular torque</i> ...	134
Figure 5.33: <i>Column 2B and 2D displacements in presence of 100 cm lintels due to a triangular torque</i>	135
Figure 5.34: <i>Viscoelastic behaviour - Rotation in case of one outriggers level</i>	143
Figure 5.35: <i>Viscoelastic behaviour - Rotation in case of two outriggers levels</i>	144
Figure 5.36: <i>Viscoelastic behaviour - Warping in case of one outriggers level</i>	144
Figure 5.37: <i>Viscoelastic behaviour - Warping in case of two outriggers levels</i>	145
Figure 5.38: <i>Viscoelastic behaviour - Bimoment in case of one outriggers level</i>	145
Figure 5.39: <i>Viscoelastic behaviour - Bimoment in case of two outriggers levels</i>	146
Figure 5.40: <i>Bending-torsion interaction</i>	147
Figure 5.41: <i>General 3D view of the problem for bending-torsion interaction</i>	148

Figure 5.42: <i>Sloping volume with varying eccentricity</i>	148
Figure 5.43: <i>Column displacements in case of pure bending (a) and pure torsion (b)</i>	149
Figure 5.44: <i>Column Displacement for fixed eccentricities - Column 6D</i>	150
Figure 5.45: <i>Column Displacement for fixed eccentricities - Column 6B</i>	150
Figure 5.46: <i>Column Displacement for fixed eccentricities - Column 2D</i>	151
Figure 5.47: <i>Column Displacement for fixed eccentricities - Column 2B</i>	151
Figure 5.48: <i>Bending plus torsion column displacements for $e = 8.75$</i>	152
Figure 5.49: <i>Column displacement variation with e - Column 6D</i>	153
Figure 5.50: <i>Column displacement variation with e - Column 6B</i>	153
Figure 5.51: <i>Column displacement variation with e - Column 2D</i>	154
Figure 5.52: <i>Column displacement variation with e - Column 2B</i>	154
Figure 5.53: <i>Top column displacement variation with e - Columns 6D, 6B,2D,2B</i>	155
Figure 5.54: <i>Sign convention for ECS and element forces (or stresses) of a beam element</i>	156
Figure 5.55: <i>Arrangement of plate elements and their ECS</i>	157
Figure 5.56: <i>Flow chart of linear static analysis in MidasGen</i>	158
Figure 5.57: <i>Numerical Model - Global View</i>	159
Figure 5.58: <i>Numerical Model – Floor Detail</i>	159
Figure 5.59: <i>Numerical Model – Outriggers Detail</i>	160
Figure 5.60: <i>Influence areas for definition of horizontal forces</i>	160
Figure 5.61: <i>Numerical Model – Applied horizontal forces</i>	162
Figure 5.62: <i>Model I – Torsional Rotation</i>	163
Figure 5.63: <i>Model I – Column Axial Displacement</i>	163
Figure 5.64: <i>Model I – Lateral Displacement due to wind load</i>	164
Figure 5.65: <i>Model II – Torsional Rotation</i>	165
Figure 5.66: <i>Model II – Column Axial Displacement</i>	165
Figure 5.68: <i>Model II – Lateral Displacement due to wind load</i>	166
Figure 5.69: <i>Model III – Numerical model of core with lintels</i>	167
Figure 5.70: <i>Model III – Torsional Rotation with 50 cm lintels</i>	167
Figure 5.71: <i>Model III – Column Axial Displacement with 50 cm lintels</i>	168
Figure 5.72: <i>Model III – Torsional Rotation with 100 cm lintels</i>	168
Figure 5.73: <i>Model III – Column Axial Displacement with 100 cm lintels</i>	169
Figure 5.74: <i>Model III – Torsional Rotation with 150 cm lintels</i>	169
Figure 5.75: <i>Model III – Column Axial Displacement with 150 cm lintels</i>	170
Figure 5.76: <i>Bending – Torsion Interaction: Axial Displacement Column 2B</i>	172
Figure 5.77: <i>Bending – Torsion Interaction: Axial Displacement Column 2D</i>	172
Figure 5.78: <i>Bending – Torsion Interaction: Axial Displacement Column 6B</i>	173
Figure 5.79: <i>Bending – Torsion Interaction: Axial Displacement Column 6D</i>	173

INDEX OF TABLES

Table 4.1: <i>Green Functions – Axial load P</i>	81
Table 4.2: <i>Green Functions – Bending Moment M_x</i>	82
Table 4.3: <i>Green Functions – Bending Moment M_y</i>	83
Table 4.4: <i>Green Functions – Bimoment M_ω – Method of initial parameters</i>	84
Table 4.5: <i>Green Functions</i>	86
Table 4.6: <i>External load effects – distributed load q_x</i>	87
Table 4.7: <i>External load effects – Linearly distributed load with maximum value q_x at the top</i>	90
Table 4.8: <i>Green Functions – Bimoment M_ω – Method of initial parameters</i>	93
Table 4.9: <i>Green Functions – Bimoment M_ω – Method of initial parameters</i>	97
Table 5.1: <i>General data of the building</i>	106
Table 5.2: <i>Central core's properties</i>	106
Table 5.3: <i>Outriggers' properties</i>	106
Table 5.4: <i>Triangular prismatic volumes' properties</i>	106
Table 5.5: <i>Geometrical properties of lintels and associate k_{var}</i>	128
Table 5.6: <i>Applied horizontal forces</i>	161
Table 5.7: <i>Applied forces</i>	171

BIBLIOGRAPHY

- [1] Smith, B.S., Coull, A., Tall Building Structures – Analysis and Design, Wiley – Interscience Publication London, 1991.
- [2] Choi, H.S., Ho, G., Mathias, L.J., Mathias, N., Outrigger Design for High-Rise Buildings, Council of Tall Buildings and Human Habitat (CTBUH), Chicago, 2012.
- [3] Choi, H., Ho, G., Joseph, L. & Mathias, N., Outrigger Design for High-Rise Buildings 2nd Edition: An output of the CTBUH Outrigger Working Group, Council of Tall Buildings and Human Habitat (CTBUH), Chicago, 2017.
- [4] Kolbrunner, C.F., Basler, K., Torsion in Structures, Springer Verlag Berlin, 1969.
- [5] Leone, Corradi, Dell' Acqua, Meccanica delle strutture: le teorie strutturali e il metodo degli elementi finiti, McGraw-Hill Education, 2010.
- [6] Vlasov, V.Z, Thin-Walled Elastic Beams, Israel Program for Scientific Translations, Jerusalem, 1961.
- [7] Stafford Smith, B. and Taranath, B.S., Analysis of Tall Core-Supported Structures Subject to Torsion, Proc. Inst. Civ. Engineers, 1972.
- [8] Stafford Smith, B., Nawaka, I. O., Behaviour of Multioutrigger Braced Tall Buildings, ACI Special Publication, 1980.
- [9] Stafford Smith, B., Salim, I., Parameter Study of Outrigger-Braced Tall Buildings Structures, Proceedings ASCE 107, 1981.
- [10] Po, S. & Siahaan, F., The Use of Outrigger and Belt Truss System for High-Rise Concrete Buildings, Dimensi Teknik Sipil, Vol.3, no.1, 2001.
- [11] Bayati, Z., Mahdikhani, M., and Rahaei, A., Optimized use of multi outriggers system to stiffen tall buildings, The 14th world conference on earthquake engineering-Beijing, 2008.

- [12] Gatti, M.A., Mola, F., Ishak, N., Structural behaviour of tall buildings stiffened by outriggered thin walled cores, Proc, of 3rd Int. Conf. on “Conquest of Vertical Space in the 21st Century”, Concrete Society, E & FN Spon, London, 1997.
- [13] Trost, H., Auswirkungen des Superpositionprinzips auf Kriech und Relaxation Probleme bei Belton und Spannbeton, Beton und Stahlbetonbau, 1967.
- [14] Mola, F., Problemi di deformazione a lungo termine negli edifici alti, Terzo Convegno Italiano SEWC Italian Group, Novembre 2013.
- [15] Mola, F., Introduzione all’approccio concettuale nella progettazione degli edifici alti, Ottobre 2012.
- [16] Mola, F., New Theoretical Aspects in Linear Viscoelastic Analysis of Concrete Structures, 32nd Conference on “Our World in Concrete and Structures, Singapore, 2007.
- [17] Mola, F., Mola, E., Pellegrini, L.M., Antelo, A.E., Interaction Problems in Outriggered Structural Systems Subjected to Torsional Effects, 43rd Conference on “Our World in Concrete & Structures, Singapore, 2018.
- [18] Zaknic, I., 100 of the World’s Tallest Buildings, P. O. Remainder, 1998.
- [19] Midas GEN, Analysis Manual.
- [20] D.M. 17/01/2018 - NTC2018: Norme Tecniche per le Costruzioni.
- [21] Eurocode 2, UNI EN 1992 - 1 - 1, 2010.